



**FACULTY OF SCIENCE**

**DEPARTMENT OF EARTH SCIENCE**

**Analysis of monthly MOD16 evapotranspiration rates at sites with different climatic characteristics; Heuningnes and Letaba catchments in South Africa**

**UNIVERSITY of the  
WESTERN CAPE**

*A thesis submitted in partial fulfilment of the requirements for the degree of  
Magister Scientiae in Environmental and Water Sciences*

**By**

**Nolusindiso Ndara**

**Supervisor : Prof D. Mazvimavi**

**Co-supervisor : Prof N. Jovanovic**

**January 2017**

## **Key words**

Actual Evapotranspiration

Eddy covariance

Land cover types

Land uses

MOD 16

Remote sensing

Seasonality

Scintillometer



## Abstract

*Analysis of monthly MOD16 evapotranspiration rates at sites with different climatic characteristics; Heuningnes and Letaba catchments in South Africa*

N.Ndara

*MSc Environmental and Water Science Thesis, Department of Earth Science, University of the Western Cape*

Evapotranspiration (ET) is an important component of the water cycle that is estimated to return about 60% of precipitation back to the atmosphere. Actual ET can be estimated using remote sensing techniques and ground-based measurements. In recent years, a remote sensing product MOD 16 ET has been developed. The limited validation of this product done in South Africa showed that ET was underestimated at some sites. A comprehensive analysis of historic and seasonal trends in MOD 16 ET data in different climatic regions of South Africa has not been done.

This study has the objective of evaluating if MOD 16 evapotranspiration estimates realistically represent the seasonal variations of ET on different land cover types in two different climatic regions; Mediterranean (Heuningnes catchment in Western Cape) and Sub-tropical (Letaba catchment in Limpopo) regions. Monthly MOD 16 ET maps for 2000-2012 for the Letaba catchment and Heuningnes catchment were created using ArcGIS. The results suggested that during the 2000 – 2012 period, ET was 438 - 753 mm/ year in the Letaba catchment and 432 – 458 mm/year in the Heuningnes catchment.

The accuracy of MOD 16 ET was evaluated using estimates of actual ET from scintillometer data in Elandsberg (Western Cape) and flux tower data in Malopeni (Limpopo) and Skukuza (Limpopo). Monthly ET estimated using scintillometer and flux tower were calculated to coincide with the monthly MOD 16 ET data for a period of 1 year from Nov 2012- Oct 2013 in Elandsberg, 1 year 1 month from Mar 2009- Mar 2010 in Malopeni and 13 years from 2000-2012 in Skukuza. In Elandsberg, the results showed that MOD 16 underestimated ET ( $R^2 = 0.16$ , RMSE = 28.30 mm/month). In Malopeni, the results suggested that there is a strong relationship between ET estimated from flux tower data and MOD 16 ET ( $R^2 = 0.77$ ), but MOD 16 slightly overestimate ET (RMSE = 8.6 mm/month). MODIS ET estimates for Elandsberg had a poorer comparison with the results obtained at Malopeni and Skukuza. Thus, it is evident that MOD 16

underestimates ET in the Mediterranean region and slightly overestimates in the Sub-tropical region.

The second objective was to establish whether the performance of MOD 16 is influenced by spatial variation of ET in the Heuningnes catchment and the Letaba catchment, in relation to different land cover types. It was found that forest had highest ET (603 mm) during summer and cultivated dry land had lowest ET (367 mm) during winter in Heuningnes. In Letaba, forest had highest ET (1204 mm) during summer wet season, and cultivated dry land had lowest ET (330 mm) during summer wet season. MOD 16 was found to be applicable in applications like mapping shallow groundwater areas, as it was successfully used to identify areas with shallow groundwater in the Heuningnes catchment and Molototsi in Letaba catchment.

**January 2017**



## Declaration

I declare that *Analysis of monthly MOD16 evapotranspiration rates at sites with different climatic characteristics; Heuningnes and Letaba catchments in South Africa* is my own work, that it has not been submitted for any degree or examination in any other University, and that all the sources I have used or quoted have been indicated and acknowledged by complete references.

Full name..... Date.....

Signed.....



## Acknowledgements

Firstly, I would like to thank God who has granted me life, strength and courage to accomplish all that I have.

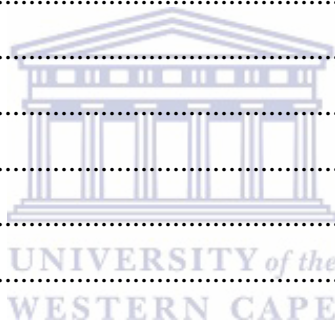
I would like to thank my supervisor, Prof. D. Mazvimavi, for his valuable guidance and, critical input in my work. His constant motivation to deliver my best is gratefully acknowledged. I am much grateful to my co-supervisor, Prof. N. Jovanovic, without his assistance this thesis would not have been possible. I am also grateful for the support and motivation of my parents and my siblings (Siyabonga Ndara, Refiloe Ndara, and Mbuyiselo Ndara) who have been much patient with me, not forgetting my friends who always believed in me. Lastly I'm sincerely grateful to the Applied Centre for Climate and Earth Systems Science (ACCESS) for funding my studies and granting me the opportunity to advance myself.



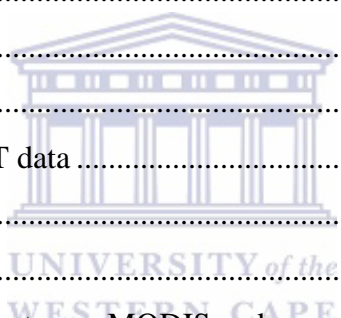
*This thesis is dedicated to my parents Zamukwakha Ndara and Lydia Ndara for their passion and love for education; it also serves as motivation to my dearest first born son Alunamda Ndara*

## Contents

<b>Key words</b> .....	<i>i</i>
<b>Abstract</b> .....	<i>ii</i>
<b>Declaration</b> .....	<i>iv</i>
<b>Acknowledgements</b> .....	<i>v</i>
<b>List of figures</b> .....	<i>ix</i>
<b>List of tables</b> .....	<i>xii</i>
<b>Chapter 1: General Introduction</b> .....	<i>1</i>
1.1 Background to the study.....	1
1.2 Problem Statement .....	4
1.3 Research Questions .....	5
1.4 General Objective.....	5
1.5 Specific Objectives.....	5
1.6 Significance of the study .....	5
1.7 Outline of the study .....	6
<b>Chapter 2: Literature review</b> .....	7
2.1 Introduction .....	7
2.2 Remote sensing techniques .....	7
2.2.1 Surface Energy Balance System (SEBS) .....	7
2.2.2 Surface Energy Balance Algorithm over Land (SEBAL) .....	9
2.2.3 Mapping EvapoTranspiration at high Resolution with Internalized Calibration (METRIC) .....	11
2.2.4 Moderate Resolution Imaging Spectroradiometer (MOD 16) .....	13
2.3 Ground based measurement techniques .....	15
2.3.1 Scintillometer .....	15
2.3.2 Eddy Covariance method .....	16
2.3.3 Lysimeters .....	18
2.4 Review of the performance of remote sensing and ground measured techniques .....	19
2.4.1 Validation of MOD 16 ET product .....	19



2.4.2 Influence of Land cover .....	20
2.4.3 Validation of METRIC and SEBAL .....	20
2.4.4 Temporal and spatial variation of actual ET .....	21
2.5 Summarized gaps in knowledge and practice .....	22
<b>Chapter 3: Methodology</b> .....	<b>23</b>
3.1 Introduction .....	23
3.2 Selection of study sites .....	23
3.2.1 Elandsberg site .....	23
3.2.2 Skukuza and Malopeni sites.....	25
3.2.3 Heuningnes Catchment .....	26
3.2.4 Letaba Catchment.....	29
3.3 Data collection.....	33
3.3.1 MODIS ET data .....	34
3.3.2 Rainfall data .....	34
3.3.3 Ground measured actual ET data .....	34
3.3.3 Ground-truthing.....	35
3.4 Data analysis method .....	35
3.4.1 Assessment of similarities between MODIS and ground based estimate of ET .....	35
3.4.2 Assessment of the influence of land uses on MODIS ET .....	37
<b>Chapter 4: Validation of MOD 16 ET</b> .....	<b>39</b>
4.1 Introduction .....	39
4.2 Validation of MOD 16 product .....	39
4.2.1 The effect of weather factors on ground measured actual ET and MOD 16 ET at Elandsberg.....	39
4.2.2 Relationship between scintillometer ET and MOD 16 ET at Elandsberg.....	46
4.2.3 The effect of weather factors on ground measured actual ET and MODIS ET at Malopeni .....	49
4.2.4 Relationship between Flux tower ET and MOD 16 ET at Malopeni.....	50
4.2.5 The effect of weather factors on ground measured actual ET and MODIS ET at Skukuza .....	51
4.2.6 Relationship between Flux tower ET and MOD 16 ET at Skukuza .....	54





4.3 Seasonal and interannual variation of MOD 16 ET .....	59
4.3.1 Letaba catchment.....	59
4.3.2 Heuningnes catchment .....	64
<b>Chapter 5: Variations of ET with land cover</b> .....	<b>70</b>
5.1 Introduction .....	70
5.2 Spatial variation of MOD 16 ET in different land cover types.....	70
5.2.1 Letaba catchment.....	70
5.2.2 Heuningnes Catchment .....	73
5.3 Ground-truthing and mapping of shallow groundwater areas.....	75
5.3.1 Ground-truthing in Letaba catchment .....	75
5.3.2 Mapping of shallow groundwater areas in the Letaba catchment.....	78
5.3.3 Ground-truthing in the Heuningnes catchment .....	87
5.3.4 Mapping of shallow groundwater areas in the Heuningnes catchment.....	89
<b>Chapter 6: Conclusion and Recommendations</b> .....	<b>96</b>
<b>List of References</b> .....	<b>xiii</b>
<b>Appendices</b> .....	<b>xx</b>
Appendix A: Monthly MOD 16 ET in the Letaba catchment.....	xx
Appendix B: Monthly MOD 16 ET in the Heuningnes catchment.....	xlvi
Appendix C: The sites visited during the recognisance trip in October 2015 in the Molototsi catchment .....	lxxii
Appendix D: The sites visited during the field trip on 26 February 2016 in the Heuningnes catchment .....	lxxxiii

## List of figures

Figure 2.1: Flowchart of MODIS Evapotranspiration (ET) algorithm (Mu <i>et al.</i> , 2011).....	14
Figure 3.1: Vegetation types of Elandsberg Nature Reserve (Jovanovic <i>et al.</i> , 2013) based on the mapping and classification developed by Rebelo <i>et al.</i> , (2006). .....	24
Figure 3.2: Land cover types in Elandsberg Nature Reserve and the position of the transmitter and receiver (Jovanovic <i>et al.</i> , 2013). .....	25
Figure 3.3: Heuningnes Catchment, Western Cape Province, South Africa .....	26
Figure 3.4: Geology of the Heuningnes Catchment.....	27
Figure 3.5: Land cover and land use of the Heuningnes Catchment .....	29
Figure 3.6: Letaba Catchment, Limpopo Province, South Africa .....	30
Figure 3.7: Geology of the Letaba Catchment.....	31
Figure 3.8: Land cover and land use of the Letaba catchment .....	33
Figure 4.1: MOD 16 pixels numbered at Elandsberg site, Scintillometer was installed at pixel number 67 .....	40
Figure 4.2: The relationship between weather factors and actual ET derived from scintillometer and MODIS ET at Elandsberg (pixel 67) .....	42
Figure 4.3: The relationship between weather factors and actual ET derived from scintillometer and MODIS ET at Elandsberg (pixel 62) .....	43
Figure 4.4: The relationship between weather factors and actual ET derived from scintillometer and MODIS ET at Elandsberg (pixel 63) .....	45
Figure 4.5: The relationship between scintillometer ET and MOD 16 ET (mm/month) at Elandsberg (pixel 67).....	46
Figure 4.6: The relationship between scintillometer ET and MOD 16 ET (mm/month) at Elandsberg (pixel 62).....	47
Figure 4.7: The relationship between scintillometer ET and MOD 16 ET (mm/month) at Elandsberg (pixel 63).....	48
Figure 4.8: The relationship between weather factors and actual ET derived from a flux tower and MODIS ET (mm/month) at Malopeni.....	50
Figure 4.9: The relationship between flux tower ET and MOD 16 ET (mm/month) at Malopeni.....	51
Figure 4.10: The relationship between weather factors and actual ET derived from flux tower and MODIS ET at Skukuza (2009) .....	52

Figure 4.11: The relationship between weather factors and actual ET derived from flux tower and MODIS ET at Skukuza (2011) .....	53
Figure 4.12: The relationship between flux tower ET and MOD 16 ET (mm/month) from 2001-2011 at Skukuza.....	56
Figure 4.13: MOD 16 monthly evapotranspiration rates for Jan (top left), Feb (top right), Aug (bottom left) and Sep (bottom right) in 2000 for Letaba catchment at a pixel resolution of approximately 1 km. ....	59
Figure 4.14: MOD 16 monthly evapotranspiration rates for Jan (top left), Feb (top right), Aug (bottom left) and Sep (bottom right) in 2003 for Letaba catchment at a pixel resolution of approximately 1 km. ....	61
Figure 4.15: Monthly average evapotranspiration rates from 2000-2012 in the Letaba catchment estimated from MOD 16 .....	62
Figure 4.16: MOD 16 annual average evapotranspiration and annual rainfall from 2000-2012 in the Letaba catchment. ....	63
Figure 4.17: MOD 16 monthly evapotranspiration rates for January (top left), February (top right), August (bottom left) and September (bottom right) in 2004 for the Heuningnes catchment at a pixel resolution of approximately 1 km. ....	65
Figure 4.18: MOD 16 monthly evapotranspiration rates for January (top left), February (top right), August (bottom left) and September (bottom right) in 2008 for the Heuningnes catchment at a pixel resolution of approximately 1 km. ....	66
Figure 4.19: MOD16 monthly average evapotranspiration from 2000-2012 in the Heuningnes catchment .....	67
Figure 4.20: MOD 16 annual average evapotranspiration and annual average rainfall from 2000-2012 in the Heuningnes catchment .....	68
Figure 5.1: MOD 16 ET (mm/year) for different land cover types in 2000 (wet year), 2003 (dry year) and 2004 (average year) in the Letaba catchment .....	71
Figure 5.2: The box plots of MOD 16 ET data for different land cover types in 2000 (wet year), 2003 (dry year) and 2004 (average year) in the Letaba catchment.....	72
Figure 5.3: MOD 16 ET (mm/year) for different land cover types in 2008 (wet year), 2004 (dry year) and 2009 (average year) in the Heuningnes catchment .....	73

Figure 5.4: The box plots of MOD 16 ET data for different land cover types in 2004 (dry year), 2008 (wet year) and 2009 (average year) in the Heuningnes catchment.....	74
Figure 5.5: Sites visited during the recognisance trip in the Molototsi river catchment, starting from the East (source) to the West (confluence) on a Google Earth map. Source: (www.google earth, Date 04/10/2013) .....	76
Figure 5.6: Groundwater monitoring points from GRIP database for the Molototsi river catchment. ....	78
Figure 5.7: Groundwater depths interpolated with inverse distance weighting with a power factor of 0.5 (top left), 1 (top right), 1.5 (bottom left) and 2 (bottom right), all with default cell size...	79
Figure 5.8: Wetland map for the Molototsi river catchment with categories and descriptions according to NFEPA (National Freshwater Ecosystem Priority Areas). ....	82
Figure 5.9: Digital elevation model (DEM) for the Molototsi river catchment.....	83
Figure 5.10: Annual average rainfall measured at weather stations of the Agricultural Research Council (ARC) in Limpopo. ....	84
Figure 5.11: MOD16 annual evapotranspiration (ET) for the Molototsi river catchment during a dry year (2003).....	84
Figure 5.12: Land cover map from 2009 (top) and 2014 (bottom) for the Molototsi river catchment. ....	86
Figure 5.13: Final map of shallow groundwater for the Molototsi River overlaying interpolated groundwater depths with inverse distance weighting (IDW GWL), NFEPA wetlands and MOD16 pixels of high annual evapotranspiration (ET) during a dry year.....	87
Figure 5.14: Sites visited in the Heuningnes catchment. Source: (www.google earth, Date 02/07/2014).....	88
Figure 5.15: Groundwater monitoring points for the Heuningnes catchment. ....	90
Figure 5.16: Groundwater depths interpolated with inverse distance weighting with a power factor of 0.5 (top left), 1 (top right), 1.5 (bottom left) and 2 (bottom right), all with default cell size. ....	91
Figure 5.17: Wetland map for the Heuningnes catchment with categories and descriptions according to NFEPA (National Freshwater Ecosystem Priority Areas). ....	92
Figure 5.18: Annual average rainfall measured at weather stations (Prinskraal and Agulhas) in the Heuningnes Catchment. ....	93

Figure 5.19: MOD16 annual evapotranspiration (ET) for the Heuningnes catchment during an average rainfall year (2004). ..... 93

Figure 5.20: Final map of shallow groundwater for the Heuningnes catchment overlaying interpolated groundwater depths with inverse distance weighting (IDW GWL), NFEPA wetlands and MOD16 pixels of high annual evapotranspiration (ET) during an average rainfall year. .... 95

**List of tables**

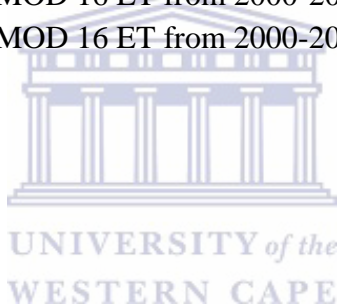
Table 4.1: t-test variables used to test the similarities between MODIS and ground based estimates of ET at Malopeni site..... 57

Table 4.2: t-test variables used to test the similarities between MOD 16 ET and ground based estimates of ET at Skukuza site. .... 57

Table 4.3: t-test variables used to test the similarities between MOD 16 ET and ground based estimates of ET at Elandsberg site. .... 58

Table 4.4: Descriptive statistics of MOD 16 ET from 2000-2012 in the Letaba catchment ..... 63

Table 4.5: Descriptive statistics of MOD 16 ET from 2000-2012 in the Heuningnes catchment 68



## Chapter 1: General Introduction

### 1.1 Background to the study

Evapotranspiration (ET), is defined as the sum of water transferred to the atmosphere from water bodies, soil surface through evaporation, and from plant tissues via transpiration (Mu *et al.*, 2007). Evapotranspiration is the second largest component after precipitation in the terrestrial water cycle at the global scale, since it returns more than 60% of precipitation back to the atmosphere and therefore determines the availability of water at the land surface (Mu *et al.*, 2011).

In plant leaves the most important pathway for ET is the stomata. There is a high correlation between stomatal conductance and the rate of carbon assimilation for a wide range of plant species (Mu *et al.*, 2007). Stomatal conductance controls the rate of water and carbon exchange between vegetation and the atmosphere (Mu *et al.*, 2007). In general, high stomatal conductance leads to high transpiration and high photosynthesis, resulting in lowering of soil moisture assuming there is no additional input of water, which in turn reduces the stomatal conductance.

ET rates differ between warm wet regions and cold dry regions. Brown (2000), states that in cold dry regions the rate of ET is low due to limited available water and solar radiation. In arid areas ET and soil water content are the most critical variables, where ET may reach nearly 100% of rainfall (Jovanovic *et al.*, 2014). In warm wet regions the rate of ET is high due to high levels of available water and solar radiation (Brown 2000).

There are possibly three different evapotranspiration rates, namely actual ET, reference ET and potential ET in the water cycle. Potential ET is the rate at which ET will occur from a large area uniformly and completely covered with growing vegetation which has access to an unlimited supply of soil water (McMahon *et al.*, 2013). The assumptions of no advection and no heating effects refer to water-advected energy and to heat storage effects, which will be valid for water bodies but may not be so for vegetation surfaces. In nature, potential ET rarely occurs, especially in semi-arid areas. Stomata close and ET rates are below potential rates when water is a limiting factor (Jovanovic & Israel 2012). Reference ET is the evapotranspiration rate from a reference surface, not short of water (Allen *et al.*, 1998). The reference surface is assumed to be a grass reference crop with specific characteristics; such as crop height of 0.12 m, fixed surface resistance of  $70 \text{ s m}^{-1}$  and an albedo of 0.23. Reference ET does not consider the crop

characteristics and soil factors; it is only affected by climatic parameters such as temperature, radiation, wind speed, sunshine hours and air humidity and can be computed from weather data (Allen *et al.*, 1998). Actual ET is the rate at which water is transformed into water vapor under the prevailing meteorological, soil water and plant conditions (McMahon *et al.*, 2013). Actual ET is the major component in the water balance of a catchment, reservoir or lake, irrigation region and some groundwater systems. Thus it is important to have knowledge of actual ET rates and how these affect availability of water.

Actual ET is the most difficult component to determine, especially in arid and semi-arid areas where a large proportion of low and sporadic precipitation is returned to atmosphere via ET (Jovanovic *et al.*, 2015). In these areas, vegetation is often subject to water stress and plant species adapt in different ways to prolonged drought conditions. Actual ET as part of the hydrologic cycle is affected by a multitude of processes at the interface between soil, vegetation and atmosphere (Mauser & Schadlich 1998). Actual ET therefore varies depending on the heterogeneity of the landscape and topography, climate, type of vegetation and soil properties (Mu *et al.*, 2007). This makes actual ET very dynamic over time and variable in space.

Actual ET is important in managing and monitoring ecosystems. For instance, sustainable management of water resources within the water cycle requires monitoring of both the quality and quantity of water (Jovanovic *et al.*, 2011). Monitoring actual ET has important implications in modeling the hydrological cycle at regional and global scales (Kustas & Norman 1996). For many land surfaces even those containing sparse vegetation cover, ET rates are closely related to the need for plants to assimilate carbon for their maintenance and growth (Kustas & Norman 1996). Therefore, significant deviation from a potential or optimal ET rate for different vegetated surfaces has been related to plant stress indicators, which in turn have been related to vegetation temperature. Actual ET can thus be estimated using the remote sensing techniques or ground based measurements.

Remote sensing techniques have advantages over ground based measurements. The remote sensing techniques inherently have the ability to provide spatial and temporal information of the land surface (Chen *et al.*, 2005). The remote sensing imagery is directly used to identify phenomena such as flooded areas and snow cover (Chen *et al.*, 2005). Bastiaanssen *et al.*, (1998), state that remote sensing data from satellites provide consistent and frequent observation of spectral reflectance and emittance of radiation of the land surface at micro and macro scales.

Remote sensing data are used to estimate precipitation and soil moisture. Various remote sensing algorithms are used to estimate actual ET. These include; SEBAL, METRIC, SEBS, and MODIS. The Surface Energy Balance Algorithm over Land (SEBAL) uses remote sensing imagery, empirical relationships and physical modules to calculate the terms of the energy balance equation and estimate ET (Bastiaanssen *et al.*, 1998). The Mapping EvapoTranspiration at high Resolution with Internalized Calibration (METRIC) uses LandSat data to estimate ET at high resolution (Allen *et al.*, 2007). The Surface Energy Balance System (SEBS) is an energy balance algorithm for the estimation of ET that works on similar principles as SEBAL and METRIC (Courault *et al.*, 2005). The Moderate Resolution Imaging Spectroradiometer (MODIS) is based on the physical sound theory of the Penman-Monteith method and estimates both canopy conductance and ET (Mu *et al.*, 2007).

The MOD 16 ET algorithm estimates ET using global daily temperature, actual vapour pressure and incoming solar radiation, and remotely-sensed Leaf Area Index, fraction of Photosynthetically Active Radiation (fPAR), albedo and land cover (Mu *et al.*, 2007). MOD 16 ET is a sum of three components;

$$ET = T_c + E_s + E_i \quad (1.1)$$

where:  $T_c$  is the canopy transpiration,  $E_s$  is soil evaporation and  $E_i$  is interception evaporation (Mu *et al.*, 2007). The MOD 16 ET product estimates global ET from ground-based meteorological observations and remote-sensing data from the Moderate Resolution Imaging Spectroradiometer (MODIS) located on NASA's Terra and Aqua satellites (Mu *et al.*, 2007). The MODIS sensor works on spatial resolution of approximately 1 km, suitable for application in water resources management (Mu *et al.*, 2007). Actual ET rates estimated using MODIS are freely available. However the accuracy of actual ET rates estimated using MODIS needs to be evaluated in arid and semi-arid areas (Jovanovic *et al.* 2013).

There are various techniques used to measure actual ET in the field namely; Bowen ratio, Eddy correlation systems, soil water balance. Courault et al (2005), state that the main problem with the field techniques is that they do not allow estimating the fluxes when dealing with large spatial scales. The other disadvantage with in situ techniques is that measurements are taken across a specific distance, 1-5 km (eg. when using the scintillometer), that result in a small area being covered. The ground based methods are also relatively time consuming and require expensive equipment.



The current study will therefore validate MOD 16 ET estimates using ground based measurements, evaluate if actual ET rates estimated by MOD 16 effectively represent the seasonal and interannual variations of actual ET at the catchment scale and examine if actual ET rates estimated by MOD 16 capture the variations of actual ET with land cover or land use types on selected catchments.

## 1.2 Problem Statement

Jovanovic et al. (2015) analysed yearly temporal and spatial variation of MOD16 ET in South Africa and concluded that MOD16 may underestimate ET at national scale (15%). However, a comprehensive analysis of seasonal and interannual variation of MOD 16 ET data in different climatic regions of South Africa has not been done. An understanding of temporal and spatial ET variation for different climatic regions, e.g. Mediterranean (Heuningnes catchment in Western Cape) and Sub-tropical (Letaba catchment in Limpopo) of South Africa, can contribute to accurate mapping and comparing historic changes in land cover types in these regions.

Land cover types are generally very important in ecosystem; therefore the variation of actual ET rates in different land cover types needs to be examined. Land cover types are beneficial in the ecosystem in different ways. Forests, for example, provide food and shelter for some animal species and also reduce soil erosion. Wetlands can reduce flooding by holding back peak flows when water levels are high and in some cases, storing water within the wetland. They can also produce a number of valuable plants and animals, which can be harvested on a sustainable basis to provide an economic return. Shallow groundwater can contribute water for irrigation purposes. Application of MODIS would therefore examine if actual ET rates by MOD 16 capture the variation of ET with different land cover or land use types. Therefore the analysis of MOD 16 ET data is very crucial in the Heuningnes catchment (Western Cape) and the Letaba catchment (Limpopo) in order to identify the effects of historic changes in land cover types on the water consumption in catchments. The Heuningnes catchment (Western Cape) and Letaba catchment (Limpopo) were selected as examples because of the marked differences in climatic and environmental conditions.

### 1.3 Research Questions

1. Can MOD 16 accurately represent the seasonal and interannual variations of ET at the catchment scale?
2. Can actual ET rates estimated by MOD 16 capture the variations of ET with land cover or land use types on selected catchments?

### 1.4 General Objective

The general objective of this study is to evaluate whether MOD 16 realistically represents the seasonal and interannual variations of actual ET rates in two different climatic regions of South Africa; Mediterranean (Heuningnes catchment in Western Cape) and Sub-tropical (Letaba catchment in Limpopo) regions.

### 1.5 Specific Objectives

1. To evaluate if ET rates estimated by MOD 16 adequately represent the seasonal and interannual variations of actual ET at the catchment scale.
2. To examine whether ET rates estimated by MOD 16 capture the variations of actual ET with land cover or land use types on selected catchments.
3. To evaluate whether MOD 16 can be used to identify areas with shallow groundwater

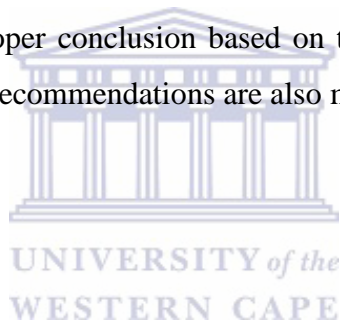
### 1.6 Significance of the study

Validation of the accuracy of MOD 16 ET products is very crucial. This enables proper conclusions to be drawn based on the MOD 16 ET product. MOD 16 was developed in recent years and its accuracy is therefore not well known in South Africa. Therefore, it is crucial to validate its accuracy in different climatic regions of South Africa. It is also important to analyse the seasonal and interannual MOD 16 ET in different climatic regions in order to evaluate whether MOD 16 adequately represent the seasonal and interannual variations of ET and also to examine if actual ET rates estimated by MOD 16 capture the variations of actual ET with land cover or land use types on selected catchments. The MOD 16 ET data can possibly contribute in determining water use from different land cover types such as forest and shrub land, lakes, rivers, wetlands, crop lands, shallow groundwater. These land cover types in turn each play a significant role on earth ecosystems. The wetlands for instance are essential components of the water cycle and many are a link between surface and groundwater. They are very important in the ecosystem

as they provide food, shelter, breeding and resting places for many species of plants, and animals. Wetlands improve water quality as they act like a filter to remove sediments, absorb nutrients and biologically change many chemicals into less harmful forms. Shallow groundwater is widely used for agricultural purposes, and mostly used in areas that are likely to have drought. Appropriate knowledge about land cover types can therefore be used in proper management of water and ecosystem.

### **1.7 Outline of the study**

Chapter 1 represents the background of the study, problem statement, research questions, objectives of the study, and the significance of the study. Chapter 2 presents the review from previous studies that are similar to the current study with the aim of identifying the gap in knowledge and practice including methods. Chapter 3 describes the research design and explains the methods that are going to be used in this study. Chapter 4 represents and discusses the results found in validation of MOD 16 ET. Chapter 5 illustrates and discusses the variations of ET with land cover. Chapter 6 draws a proper conclusion based on the objectives of this study, results found and discussed. Appropriate recommendations are also made in this chapter.



## Chapter 2: Literature review

### 2.1 Introduction

This chapter will firstly examine the principles upon which methods for establishing ET using remote sensing data are based. Secondly the principles upon which methods for establishing ET using ground measured data will be examined. In the last section the assessment of the performance of these methods will be reviewed.

### 2.2 Remote sensing techniques

The methods for estimating ET using remote sensing data are grouped into; vegetation index models and energy balance models. These models are distinguished based on how they calculate ET and their inputs. The vegetation index models are useful for calculating ET in arid and semiarid regions because ET is dominated by transpiration (Senay *et al.*, 2011). These models are based on the observation that foliage density on the ground, as measured by satellite vegetation index, often is strongly correlated with ET. Vegetation index methods must be combined with meteorological data to estimate atmospheric water demand and the energy available to evaporate water. However the vegetation index models are not examined in detail, as the main focus of the study is on the energy balance models. The energy balance models for ET estimation are driven by the land surface temperature (Senay *et al.*, 2011). Critical information on the partitioning of the net radiation among latent heat, sensible and ground heat flux is provided by the spatial or temporal variation in land surface temperature. Based on these general principles several methods can be used to estimate ET. These methods include Surface Energy Balance System (SEBS), Surface Energy Balance Algorithm over Land (SEBAL), Mapping EvapoTranspiration at high Resolution with Internalized Calibration (METRIC) and MOD 16.

#### 2.2.1 Surface Energy Balance System (SEBS)

The Surface Energy Balance System (SEBS) uses remote sensing and meteorological data to estimate sensible and latent heat fluxes (Su., 2002). SEBS estimates the evaporative fraction from land surfaces and consists of the following components; the computations of land surface physical parameters, calculation of roughness length for heat transfer, and estimation of the evaporative fraction based on energy balance for limiting cases (Liou & Kar 2014). The algorithm of SEBS calculates ET as a residual of the energy balance (Su., 2002):

$$\lambda E = R_n - H - G \quad (2.1)$$

where:  $R_n$  ( $\text{MJ.m}^{-2} \cdot \text{day}^{-1}$ ) is the net radiation,  $G$  ( $\text{MJ.m}^{-2} \cdot \text{day}^{-1}$ ) is the soil heat flux,  $H$  ( $\text{MJ.m}^{-2} \cdot \text{day}^{-1}$ ) is the sensible heat flux,  $\lambda E$  ( $\text{mm. day}^{-1}$ ) is the turbulent latent heat flux,  $\lambda$  ( $\text{MJ.kg}^{-1}$ ) is the latent heat of vaporization and  $E$  ( $\text{mm. day}^{-1}$ ) is the actual evapotranspiration.

Net radiation ( $R_n$ ) is the total amount of radiation that reaches the earth's surface.  $R_n$  is estimated from downward solar radiation ( $R_{swd}$ ) and emitted long wave radiation ( $R_{lwd}$ ) as shown in Equation (2.2):

$$R_n = (1 - \alpha) * R_{swd} + \varepsilon * R_{lwd} - \varepsilon * \sigma * T_o^4 \quad (2.2)$$

where:  $\alpha$  is albedo,  $\varepsilon$  is emissivity of the surface,  $\sigma$  is the Stefan-Boltzmann constant and  $T_o$  ( $^{\circ}\text{C}$ ) is the surface temperature.

Soil heat flux ( $G$ ) is determined as:

$$G = R_n(T_c + (1 - F_c)(T_s - T_c)) \quad (2.3)$$

where:  $T_c$  is the ratio of soil heat flux to net radiation for full vegetation canopy,  $T_s$  is the ratio of soil heat flux to net radiation for bare soils,  $F_c$  is the fractional vegetation coverage. Sensible and latent heat flux are derived using similarity theory. A distinction is made between the atmosphere or planetary boundary layer and the atmospheric surface layer.

Su (2002) conducted a study to assess the reliabilities of SEBS. The results indicated that SEBS can be used to estimate turbulent heat fluxes at different scales with acceptable accuracy. The application of SEBS does not require any prior knowledge of the actual turbulent heat fluxes, which indicates that SEBS is a credible and independent approach. The advantages of SEBS include; a) consideration of the energy balance at the limiting cases which minimizes the uncertainty involved in surface temperature or meteorological variables, b) new formulation of the roughness height for heat transfer instead of using constant values, c) characterizing actual turbulent heat fluxes without any prior knowledge, and d) representativeness of parameters associated with surface resistance (Liou & Kar 2014). SEBS has been widely applied over large heterogeneous areas using MODIS data for the thermal band information of 1 km (Liou & Kar 2014). However, relatively complex solution of the turbulent heat fluxes and too many required parameters can often cause more or less inconveniences in SEBS when data are not readily available.

### 2.2.2 Surface Energy Balance Algorithm over Land (SEBAL)

The Surface Energy Balance Algorithm over Land (SEBAL) is an algorithm that uses remote sensing data, empirical relationships and physical modules to calculate the terms of the energy balance equation and estimate ET (Bastiaanssen *et al.*, 1998). SEBAL is suitable for visible, near-infrared and thermal infrared input data obtained from satellite sensors.

Net radiation is calculated as follows for each pixel of the satellite image:

$$R_n = (1 - r_0)R_s + L_i - L_o \quad (2.4)$$

where:  $r_0$  is the hemispherical surface reflectance,  $R_s$  is the incoming solar radiation ( $\text{W m}^{-2}$ ),  $L_i$  is the incoming long wave radiation ( $\text{W m}^{-2}$ ), and  $L_o$  is the outgoing long wave radiation ( $\text{W m}^{-2}$ ).

$r_0$  can be obtained from the broadband directional planetary reflectance and atmospheric transmittance, whereas  $R_s$  can be calculated from incoming extra-terrestrial radiation and atmospheric transmittance for cloudless conditions.  $L_i$  can be calculated with the Stephan-Boltzmann formula as a function of the apparent thermal infrared emissivity of the atmosphere and air temperature.  $L_o$  can be calculated with the Stephan-Boltzmann formula as a function of surface emissivity and temperature.

UNIVERSITY of the  
WESTERN CAPE

Soil heat flux for the whole day is calculated with the following empirical equation:

$$G = R_n \frac{T_0}{r_0} \left( 0.0032 r_0^{avg} + 0.0062 r_0^{avg2} \right) \left( 1 - 0.98 NDVI^4 \right) \quad (2.5)$$

where:  $T_0$  ( $^{\circ}\text{C}$ ) is the surface temperature and  $r_0$  is the daytime hemispherical surface resistance,  $r_0^{avg}$  is the average daytime hemispherical resistance and  $NDVI$  is Normalized Difference Vegetation Index.

In the calculation of  $H$  both wet and dry surface pixels are required because these represent extreme pixels in the studied domain at the specific time when the satellite images are taken. The sensible heat flux is controlled by a dry limit (surface with latent heat flux  $\lambda E = 0$ ; sensible heat flux  $H = R_n - G$ ) and wet limit (surface with sensible heat flux  $H = 0$ ; near-surface vertical difference in air temperature  $\delta T_a = 0$ ). The near-surface vertical difference in air temperature

value ( $\delta T_a$ ) is assigned to all other pixels assuming it varies linearly between the dry and wet ranges.  $H$  is then calculated for each pixel of the satellite image as follows:

$$H = \frac{\rho_a C_p}{r_{ahsur}} \delta T_a \quad (2.6)$$

where  $\rho_a$  ( $\text{kg m}^{-3}$ ) is the moist air density,  $C_p$  ( $\text{Jkg}^{-1} \text{K}^{-1}$ ) is the air specific heat at constant pressure,  $r_{ahsur}$  ( $\text{s m}^{-1}$ ) is the distributed air resistance to heat transport and  $\delta T_a$  ( $^{\circ}\text{C}$ ) is the near-surface vertical air temperature difference.

$r_{ahsur}$  is calculated as a function of friction velocity.  $\delta T_a$  ( $^{\circ}\text{C}$ ) is obtained from radiometric surface temperature ( $T_0$  in K) as follows:

$$\delta T_a = c_4 T_k - c_5 \quad (2.7)$$

Where  $c_4$  and  $c_5$  are linear regression coefficients valid for one particular moment and landscape (a given satellite image) for the function that relates dry and wet pixels.

$\lambda E$  is finally computed from Equation (2.1) as residual. Instantaneous  $\lambda E$  values are extrapolated over time assuming that the instantaneous evaporative fraction in Equation (2.1) is stable, where the evaporative fraction  $EF$  is:

$$EF = \frac{\lambda E}{R_n - G} \quad (2.8)$$

$\lambda E$  is converted into mm and provides directly a measure of actual ET.

The advantages of this algorithm are; a) the algorithm is a physical concept, and thus applicable to various climates, b) there is no need for land use classification, c) the method is suitable for all visible, near-infrared and thermal-infrared radiometers, which indicates that it can be applied at different spatial and temporal resolutions, d) minimum ground-based data are required, e) it does not require a strict correction of atmospheric effects on surface temperature due to its automatic internal calibration, and f) internal calibration can be done with each analyzed image (Bala *et al.*, 2013). On the other hand the disadvantages of this algorithm are; a) it requires cloud-free conditions, b) presence of wetlands and dry lands is required, c) subjective specifications of representative hot or dry and wet or cool pixels within the image are required to determine model parameters. The resulting  $H$  flux and ET estimates from SEBAL can vary with differing extreme

pixels selected by the operator, domain size and spatial resolution of satellite sensors (Liou & Kar 2014), and d) estimated H is greatly affected by the errors in surface air temperature differences or surface temperature measurements.

### 2.2.3 Mapping EvapoTranspiration at high Resolution with Internalized Calibration (METRIC)

Mapping EvapoTranspiration at high Resolution with Internalized Calibration (METRIC) is a satellite-based image-processing tool for mapping ET as a residual of the energy balance at the Earth's surface (Equation 2.1) (Allen *et al.*, 2007a and b). The primary inputs for the model are short-wave and long wave images from a satellite (e.g. LandSat), a digital elevation model and ground-based weather data measured within or near the area of interest. These ET images (i.e. maps) provide the means to quantify ET on a field by field basis in terms of both rates and spatial distribution (Allen *et al.*, 2007a and b).

METRIC calculates  $R_n$  using Equation (2.4). METRIC uses a bi-directional reflectance at the top of the atmosphere instead of  $r_0$ . Soil heat flux (G) is calculated using the following equation:

$$G = R_n (T_0 - 273.15) (0.0038 + 0.0074\alpha) (1 - 0.98 NDVI^4) \quad (2.9)$$

Where:  $\alpha$  is the albedo. METRIC uses Equation (2.6) to calculate  $\delta T_a$  ( $^{\circ}\text{C}$ ) from sensible heat flux (H) by inversion. When calibrating the ET model for the wet and dry surface pixels, METRIC considers all the assumption  $\lambda E = R_n - G$  for the wet limit (wet pixel) may not necessarily be true because advection may occur as an additional source of energy to  $R_n$ .  $\lambda E$  for the wet pixel is therefore estimated as:

$$\lambda E = F ET_r \quad (2.10)$$

where:  $ET_r$  is the reference evapotranspiration of an alfalfa (lucerne) crop and  $F$  is a factor.  $ET_r$  is calculated for each satellite image using ground-based weather stations.  $F$  is usually taken as 1.05 based on the assumption that agricultural fields that are at full cover have ET rates that are typically about 5% greater than  $ET_r$  (some fields have a wet soil surface beneath a full vegetation canopy that tends to increase the total ET rate to about 5% above that of the  $ET_r$ ).  $H$  can then be estimated as a residual from  $H = R_n - G - \lambda E$ . In this way, an independent estimate of  $\lambda E$  is built into the calibration (Equation 2.7) and the value of  $\lambda E$  is freed from being expressed as an evaporative fraction dependent on  $R_n$  (Allen *et al.*, 2007a).



Once  $H$  is calculated for each pixel using Equation (2.6),  $\lambda E$  can be calculated for each pixel as residual of the energy balance (Equation 2.1). Instantaneous  $\lambda E$  is converted into hourly  $ET_h$  using the following equation:

$$ET_h = 3,600 \frac{\lambda E}{\lambda \rho_w} \quad (2.11)$$

where  $\lambda$  is the latent heat of vapourization ( $\text{MJ kg}^{-1}$ ), 3,600 is the conversion factor from seconds to hours and  $\rho_w$  is the density of water ( $1,000 \text{ kg m}^{-3}$ ). Latent heat of vaporization ( $\lambda$ ) is given by:

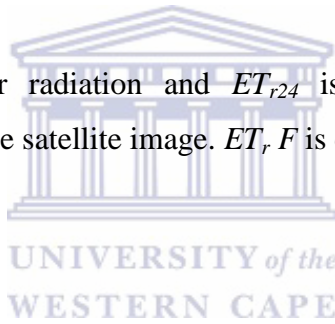
$$\lambda = [2.501 - 0.00236(T_0 - 273.15)]10^6 \quad (2.12)$$

Daily evapotranspiration  $ET_{24h}$  is calculated as:

$$ET_{24h} = C_{rad} (ET_r F) ET_{r24} \quad (2.13)$$

where:  $C_{rad}$  is a clear-sky solar radiation and  $ET_{r24}$  is the cumulative 24 h reference evapotranspiration for the day of the satellite image.  $ET_r F$  is calculated as:

$$ET_r F = \frac{ET_h}{ET_r} \quad (2.14)$$



In Equation (2.14) METRIC assumes that the ratio  $ET_h / ET_r$  is constant during the day (the ratio is the same at both the observation time and for the 24 h period).  $ET$  for periods longer than 1 day can be obtained by cumulating daily  $ET_r$  values multiplied by the corresponding  $ET_r F$ :

$$ET = \sum_{i=m}^n [(ET_r F_i)(ET_{r24i})] \quad (2.15)$$

The use of an independently calculated reference evapotranspiration  $ET_r$  (from ground-based weather data) in the extrapolation of instantaneous  $ET$  and  $ET_h$  to periods of 24 h and longer accounts better for regional advection effects compared to the use of the evaporative fraction to net radiation, because  $ET$  can exceed daily net radiation in many arid or semi-arid locations and  $ET_r$  incorporates advection effects (Allen *et al.*, 2007a).

The advantage of METRIC is that the use of reference ET in calibration of METRIC and the use of  $ET_r$   $F$  in extrapolation to 24 h ET provide general equivalency and congruency. METRIC estimates actual ET rather than potential ET and does not require knowledge of crop types (no satellite-based crop classification is needed). METRIC relies on theoretical and physical relationships but, provides for the introduction and automated calibration of empirical coefficients and relationships to make process operational and accurate (Allen *et al.*, 2007a).

#### 2.2.4 Moderate Resolution Imaging Spectroradiometer (MOD 16)

MOD 16 was developed by Mu *et al.*, (2007) and improved by Mu *et al.*, (2011).

MOD 16 is based on the Penman-Monteith equation:

$$\lambda ET = \frac{S \cdot A + p \cdot C_p \cdot \frac{e_{sat} - e}{r_a}}{s + \gamma \cdot \left(1 + \frac{r_s}{r_a}\right)} \quad (2.16)$$

where:

$\lambda ET$  is the latent heat flux;  $\lambda$  is the latent heat of vaporization;  $s = d(e_{sat})/dT$ , the slope of the curve relating saturated water vapour pressure ( $e_{sat}$ ) to temperature;  $e$  is actual vapour pressure;  $A$  is available energy partitioned between sensible heat, latent heat and soil heat fluxes on land surface;  $p$  is air density;  $C_p$  is the specific heat capacity of air; and  $r_a$  is the aerodynamic resistance;  $\gamma$  is the psychrometric constant and  $r_s$  is the surface resistance (Mu *et al.*, 2011).

MOD 16 has a spatial resolution of approximately 1 km and a temporal resolution of 8-day, monthly and annual intervals. The MOD 16 ET algorithm estimates ET using 8- day remote sensing data (Land cover, Leaf Area Index (LAI), Fraction of Photosynthetically Active Radiation (fPAR), and albedo) and daily in situ data (air temperature, air pressure, humidity, and solar radiation) (Mu *et al.*, 2011). MOD 16 ET algorithm estimates both plant evapotranspiration and soil evaporation (Figure 2.1). Plant evapotranspiration is the evaporation of water intercepted by the canopy before reaching the ground and transpiration through stomata on plant leaves and stems. Plant evapotranspiration is estimated using both remote sensing data (land cover, LAI, albedo and fPAR) and in situ data (air pressure, air temperature, humidity and radiation). Moreover, soil evaporation includes the potential evaporation from the saturated soil surface and evaporation from the moist soil surface. Soil evaporation is estimated using remote sensing data (albedo, fPAR, and land cover) and in situ data (radiation and air temperature). Soil evaporation is important in areas with a sparse canopy. ET is given as  $T_c + E_s + E_i$  where  $T_c$  is the canopy

transpiration,  $E_s$  is the soil evaporation and  $E_i$  is the interception evaporation. The combination of plant evapotranspiration and soil evaporation result to actual evapotranspiration (Figure 2.1).

The uncertainties about MOD 16 include the misclassification of land type in the given pixel as that would result in misinterpretation of results (Kim *et al.*, 2012). A large number of physical factors are involved in soil surface evaporation and plant transpiration processes, including microclimate, plant biophysics for site specific species and landscape heterogeneity, making accurate assessment of ET a challenge (Mu *et al.*, 2011). Uncertainties from MODIS LAI/FPAR and daily meteorological data can introduce biases to ET estimates. Ramoelo *et al.*, (2014) validated the MOD 16 ET product using flux tower data in the African Savanna, South Africa. The flux tower results achieved a poorer comparison with MOD 16 ET. These results may be due to a number of factors, including the parameterization (input data) of the Penman-Monteith model, flux tower measurement error, and flux tower footprint versus MODIS pixel size. The input data parameters of MODIS ET are coarse scale products, generally poorly or not validated in the semi-arid conditions of South Africa, which are likely to generate significant ET prediction errors (Ramoelo *et al.*, 2014). For instance MODIS global land cover is a relatively coarse product (500 m) which inadequately captures the heterogeneity of Savanna ecosystems.

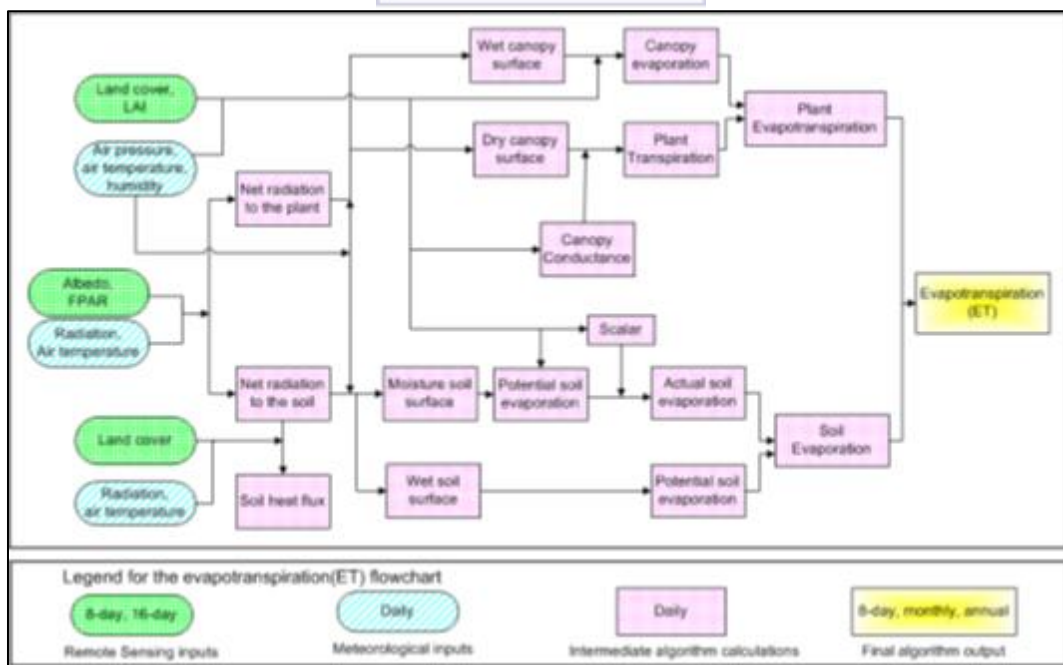


Figure 2.1: Flowchart of MODIS Evapotranspiration (ET) algorithm (Mu *et al.*, 2011)

## 2.3 Ground based measurement techniques

Actual ET is estimated using various methods such as a scintillometer, eddy covariance and lysimeters. Ground based measurement techniques are important for the evaluation of ET estimates obtained by remote sensing techniques. A review of each mentioned method is given below.

### 2.3.1 Scintillometer

This method is based on the physical principle of the propagation of electromagnetic waves in the atmosphere and their disturbance by atmospheric turbulence. A scintillometer measures the variation of radiation intensity fluctuations (Petropoulos *et al.*, 2013). These variations in the refraction index are caused by fluctuations in temperature, pressure, and humidity as well as their interactions. A scintillometer measures a parameter of the refractive index of air ( $Cn^2$ ) over a horizontal path, caused by air temperature fluctuations that represent the atmospheric turbulence structure. The  $Cn^2$  and ET are determined over a distance of 500 m to 5 km (Jovanovic *et al.*, 2014). An area-averaged heat flux can be derived from the changes in the refractive index of the air between a transmitter and a receiver (Petropoulos *et al.*, 2013). Estimates of total evaporation are spatially averaged over the area between the transmitter and receiver.

The advantage of scintillometers is that they can provide representative estimates of the latent heat fluxes (LE) over large areas with the use of a single instrument, due to the extended spatial averaging of those instruments (Petropoulos *et al.*, 2013). Furthermore, as the scintillometer measurement principle is based on evaluations of relative intensity statistics, the system is free of long term drift and does not require calibration prior to use. However a major disadvantage is that they are affected by strong turbulence that is referred to as saturation, which occurs at path lengths of about 250 m (Petropoulos *et al.*, 2013).

Savage *et al.*, (2010), contrasted various methods used for estimating evaporation rates as a residual of the shortened energy balance in mesic grassland in South Africa. Bowen ratio systems (BR) were used to measure water vapour pressure and air temperature profile differences between heights of 1.55 m and 2.96 m above the soil surface. Eddy covariance system (EC) was used to measure sensible heat flux at a height of 1.45 m above the soil surface and later the height was increased to 2.12 m above the soil surface. Surface-layer scintillometer (SLS) was used to estimate sensible heat flux (H) for a path lengths of either 50 or 101, for more than 30 months. From the sensible heat flux (H) estimates, using surface-layer scintillometer (SLS) and measurements of soil heat flux and net irradiance, evaporation rates were calculated as

a residual of the shortened energy balance equation and compared with grass reference evaporation rates (ET<sub>o</sub>).

The results showed inconsistent hourly ET<sub>o</sub> values in the late afternoon due to the incorrect assumption that the soil heat flux is 10% of net irradiance. The surface-layer scintillometer (SLS) estimates of sensible heat flux (H) and the estimates of evaporation rates as a residual compared favorably with those obtained using Bowen ratio (BR) and eddy covariance (EC) methods for cloudless days, cloudy days and days with variable cloud. There was no evidence for eddy covariance (EC) measurements of sensible heat flux (H) being underestimated in comparison to the Bowen ratio (BR) and surface-layer scintillometer (SLS) measurements. It was concluded that the surface-layer scintillometer (SLS) method is a robust method allowing long-term and continuous evaporation rate measurements that represent a larger measurement footprint than may be the case for the Bowen ratio (BR) and eddy covariance (EC) methods.

Scintillometer performs well in areas with uniform and natural vegetation and does not perform well in areas with heterogeneous vegetation. The areas with heterogeneous vegetation bring uncertainties about the scintillometer as the measured refractive index of air is not the same throughout the horizontal path. For instance, Jovanovic *et al.*, (2013) conducted a study to collect ground measured data derived from Scintillometer in Elandsberg Nature Reserve, Western Cape. The data collected was intended to ground-truth satellite remote sensing estimates of ET from MOD 16 product. The site where scintillometer was installed was selected based on the extent and uniformity of the natural vegetation.

### **2.3.2 Eddy Covariance method**

This is one of the most widely used direct methods for collecting data for the purpose of estimating energy fluxes above a canopy. The eddy covariance method explicitly measures the turbulent components of momentum, heat, and moisture, theoretically providing a direct estimate of surface fluxes (Petropoulos *et al.*, 2013). The method estimates rate of evaporation from measurements of upwind velocity and vapour fluxes of the air at a single point above the evaporation surface.

The advantage of this method is that it provides a direct means of measuring the fluxes without making any kind of assumptions regarding diffusivities or about parameter values, the shape of the vertical profile, atmospheric stability, or the nature of the surface cover (Petropoulos *et al.*, 2013). Furthermore, as a direct measurement method, the eddy covariance method allows direct

checking of the fluxes estimated. The disadvantages of the method include the need for complex, fragile, and expensive instrumentation, and well-trained personnel to obtain accurate results.

Eddy covariance measurements of evapotranspiration, are used to determine local, regional and global water budgets, calibrate and validate land surface models, and acquire understanding of ecosystem processes. Scott (2010) evaluated the accuracy of eddy covariance evaporation measurements for three semiarid ecosystems using catchment water balance. The aim of the study was to assess the accuracy of eddy covariance evaporation measurements by comparing them with those derived from small catchment water balances. Thirteen years of data from shrub land, grassland and savanna sites in southern Arizona USA were compared. The results showed that the two independent measurements agreed to within an average of 3% annually and differed from -10 to +17% in any given year, when an assumed 5% underestimation in precipitation due to gauge under catch was considered. The two measurements generally agreed better in drier years and at less topographically complex sites.

Ding *et al.*, (2010), validated eddy covariance method (EC) by large-scale weighing lysimeter in a maize field of northwest China. The study compared ET measured by EC ( $ET_{EC}$ ) with that measured by large-scale weighing lysimeter ( $ET_L$ ) during the whole growing season of maize in 2009. A lack of energy balance closure occurred, and so the day time  $ET_{EC}$  was then adjusted by Bowen-ratio forced closure method. The half-hourly daytime  $ET_{EC}$  was underestimated by 21.8% without the adjustment and 4.8% with the adjustment, when compared to the corresponding  $ET_L$ . Furthermore, nighttime  $ET_{EC}$  was adjusted using filtering method. The results then showed that the mean error between half-hourly night time  $ET_{EC}$  and  $ET_L$  decreased from 30.2% without the adjustment to 10.3% with the adjustment. After such adjustment of day and night measurements, daily  $ET_{EC}$  was underestimated by 6.2% compared to  $ET_L$ . Moreover, the inconsistency of adjusted total  $ET_{EC}$  and  $ET_L$  was decreased to 3.2% after subtracting the overestimated ET by lysimeter resulting from irrigation and heavy rainfall events. Therefore, after appropriate adjustments of observations, eddy covariance method was accurate in estimating maize ET in the arid region of northwest China.

Eddy covariance method is most accurate when atmospheric conditions (wind, temperature, and humidity) are stable, the underlying vegetation type is homogeneous and the site is located on a flat terrain for an extended distance upwind (Baldocchi, 2003). Methodology for selection of homogeneous sites for validation of MOD 16 ET using flux tower data was done by Jovanovic *et*

*al.*, (2013). The selected sites were Berg River in the Western Cape and Letaba catchment in the Limpopo Province. The eddy covariance flux tower sites were selected based on several criteria; including land cover homogeneity, vegetation height, topographic variability and atmospheric stability. The two sites were successfully selected based on the above mentioned criteria's.

### 2.3.3 Lysimeters

Lysimeters are used in water balance analysis. The amount of water lost to ET can be calculated by recording the amount of precipitation that an area receives and amount lost through the soil (Seyfried *et al.*, 2001). Lysimeters are divided into two types; the weighing and the nonweighing lysimeters. The nonweighing lysimeters determine the changes in soil water content indirectly, whereas the weighing lysimeters measures the changes in soil water within a constructed container (Seyfried *et al.*, 2001). In weighing lysimeters ET for a specified time period is calculated based on the following equation

$$ET = P - \frac{V_l + V_r + \Delta V_s}{A} \quad (2.17)$$

where;  $P$  is the precipitation (millimeters),  $V_l$  is the volume drainage loss  $m^3$ ,  $V_r$  is volume of net surface run on or runoff  $m^3$ ,  $\Delta V_s$  is the change in the volume of soil water in the lysimeters and  $A$  is the area of the lysimeters  $m^2$ .  $V_l$  and  $V_r$  are said to be zero if the lysimeters is well sealed and overland flow is prevented. Thus ET can be calculated from measured values of  $P$ ,  $A$ , and  $\Delta V_s$  (Seyfried *et al.*, 2001). The weighing lysimeters is further divided into two types; the mechanical and hydraulic weighing lysimeters (Johnson & Odin., 1978). The soil sample is placed directly on the balance in the mechanical weighing lysimeters, therefore the sensitivity will be high, if friction can be reduced using advanced support construction. In the hydraulic weighing lysimeters the soil sample is placed in a tank floating on a fluid (Johnson & Odin., 1978). The changes in level reflect weight changes in the sample.

Some of the limitations of lysimeters include that the values measured are only valid for a single position and results may not be transferred to large areas (Johnson & Odin., 1978). To guarantee comparable vegetation, hydrological and micro-climatic conditions the lysimeters surface should be as high as possible representative of the field in which the vessel is installed (Lanthaler 2004). The vegetation has to be of the same on the vessel as in the surrounding field, and the adjacent soil has to correspond to the soil in the lysimeters (Lanthaler 2004). The bypass fluxes can hardly be determined in lysimeters containers, as the lateral water transport is suppressed in a closed

vessel. In lysimeters less amount of water is sampled than really occurs and they are also expensive to construct.

## **2.4 Review of the performance of remote sensing and ground measured techniques**

### **2.4.1 Validation of MOD 16 ET product**

The most promising tool for estimation of ET over a large spatial scale is considered to be remote sensing. Sun et al. (2007), evaluated the MOD 16 algorithm using MODIS and ground observational data in a winter wheat field in North China Plain. The purpose of the study was to analyse and find the potential problems of the MOD 16 algorithm and evaluate it in winter wheat fields by using MODIS land products, MOD 11-land surface temperature and MOD 13-standard normalized difference vegetation index (NDVI), as well as observations at the Yuchens Experimental Station, China in 2002. The study used two kinds of data: MODIS data and ground measured data from eddy covariance flux tower. For MODIS, two data products were used: MOD 11-land surface temperature and emissivity, and MOD13-standard normalized difference vegetation index with 1 km spatial resolution. Ground based data was collected from the eddy covariance flux tower from day of year (DOY) 97 to 162 of 2002. The data set included air temperature, humidity, soil heat flux, sensible heat flux, wind speed and components of radiation balance at half hour intervals measured by eddy covariance system. The other ground measured data from DOY 1-161, were also collected from a micrometeorological station near the flux tower, except for the latent heat flux and sensible heat flux.

Actual ET and Evaporative fraction (EF) were then calculated using Penman-Monteith method. Actual ET and Evaporative fraction (EF) for vegetation estimated with the modified algorithm were found consistent with the observations of an eddy covariance system. A radiation budget sub-model was analyzed and it was found that the estimate for solar radiation was acceptable only on cloud-free days. When the sky was cloud-free, the downward shortwave radiation was consistent with the observed data. In the original MOD 16 it was found that the seasonal variations of minimum canopy resistance and physiological temperatures were not considered, which results in overestimation of canopy resistance when leaf area index was less than 2.5. The original MOD 16 estimated Evaporative fraction (EF) for vegetation was compared with the Evaporative fraction (EF) calculated with the Penman-Monteith method, which was consistent with the eddy covariance measurements. It was found that its mean absolute error was 0.13 mm, mean relative error was 40%, and the correlation coefficient was 0.62. The original MOD 16 algorithm was then modified and its comparison with the Penman-Monteith calculated



Evaporative fraction (EF) showed that its mean absolute error was 0.1 mm, mean relative error was 26% and the correlation coefficient was 0.88. The results show that both EF and ET for vegetation are consistent with both observations of an eddy covariance system and the calculations using the Penman-Monteith method. The current study will therefore also compare MOD 16 ET data with ground based data to evaluate the accuracy of MOD 16.

#### **2.4.2 Influence of Land cover**

Regional ET is vital to understanding interactions between land-atmosphere surface energy and water balances. Kim *et al.*, (2012), validated MODIS 16 global terrestrial ET products in various climates and land cover types in Asia. The performance of the MOD 16 ET algorithm was fully examined through the comparison of data sets collected from 17 flux tower sites across Asia. The validation studies were conducted from 2000 to 2006. MOD 16 ET estimates were averaged over the surrounding 1 km<sup>2</sup> MODIS pixels at each site and compared to the ET measured at the tower.

It was found that global MOD 16 terrestrial ET overestimated ground ET measurements at nine flux tower sites. In eight of these sites the land cover types were forest and only in one site it was cropland. The climate was continental at five sites and equatorial for three sites and one site was warm temperature. MOD 16 ET underestimates were observed at sites where the land cover was rice paddy cropland and the climate was warm temperature. The MODIS ET algorithm performance was found poor at sites with grassland cover and it was found to have the best performance at sites with forest land cover. Among the climate conditions it was difficult to determine any trends that could clearly explain the connectivity between ground measurements of ET and MOD 16 ET. It was then concluded that MODIS global terrestrial ET product can estimate actual ET with reasonable accuracy in Asia. Based on this study similar approach will be adopted in the current study, whereby MOD 16 ET data will be compared with ground measurement ET data to test its accuracy in different climatic regions and detect the ET changes with different land uses and land cover.

#### **2.4.3 Validation of METRIC and SEBAL**

Information about surface ET over a range of spatial and temporal scales is required by many water resources, agricultural and forest management applications. There are several satellite remote sensing methods that can be used to estimate ET. Mkhwanazi and Chaves (2013) carried out a study to compare the remote sensing ET algorithms METRIC and SEBAL under advective and non-advective conditions. The accuracy of the two algorithms was assessed by comparing the estimated ET values with measured ET values using a weighing lysimeter. A total of nine

Landsat 7 ETM+ images (2010-2012) were processed using both algorithms (METRIC and SEBAL) and ET were estimated for former alfalfa and latter alfalfa fields. Both fields were equipped with weighing lysimeters. The remote sensing estimated daily ET was compared with lysimeter-based ET measurements. The model error was determined for each data, to measure the performance of these models under varying advective conditions. The results showed that there were larger errors in SEBAL than in METRIC, with errors up to 45% for the former and up to 25% for the latter. The largest errors occurred on windy and hot days when there was no advection. In general the METRIC performed better than SEBAL, although both underestimated ET in all cases, with the latter underestimating significantly under windy and warm conditions which indicated advection. The current study will also follow the similar approach to compare the MOD 16 ET data with the ground based data obtained from scintillometers and eddy covariance.

#### **2.4.4 Temporal and spatial variation of actual ET**

Frank and Richard (1994), investigated the temporal variation in actual ET of terrestrial ecosystems: the patterns and ecological implications. The water balance was compared among the earth's major terrestrial ecosystems. The 25 year climate records (1965-1989) at ninety four sites around the world representing eleven biomes were used. Actual ET, potential ET and deficit were derived for each month and year from the 25 year climate records. The main objective of the study was to examine temporal variation in actual ET. The results indicated that the standard deviation of annual actual ET, an absolute measure of interannual variability, was highest for grassland (71) and lowest for tundra (34) and taiga (43). Coefficient of variation of annual actual ET was negatively related to mean actual ET and was higher for non-forested than for forested ecosystems. Monthly variation, an index of seasonality and interannual variation of actual ET were positively related for forested ecosystems and negatively related for non-forested ecosystems. Also there was a positive relationship between interannual variability and variation among sites within a biome. Furthermore, the results indicated a link between temperature variability and spatial heterogeneity among biomes.

Temporal and spatial variability of the water budget components within the Limpopo River basin were investigated using a modeling study of atmospheric and terrestrial hydrological processes (Alemaw *et al.*, no date). The spatio-temporal climatology database was created from a network of 66 gauging stations in the basin with monthly average records of rainfall and potential ET. A GIS-based simple water balance model called Limpopo Water Balance (LIMWAB) model was

developed in order to understand the water balances which include: surface runoff, actual ET, and soil moisture. LIMWAB model simulated water balance components by taking rainfall-runoff processes in the basin including soil texture controlled moisture in the terrestrial system, and the vertical integrated moisture convergence that accounts for the net water vapor flux from the basin in order to close the hydrologic water budget. The results indicated that actual ET was highly variable both spatially and temporally. The actual ET varied from 400 to 1100 mm/ year with high seasonal variability. Additionally, the central sub-catchment of the Limpopo basin experienced much less runoff with an average of 30 mm/ year. About 60% of the whole catchment areas had an average total runoff of about 100 mm/ year. Soil moisture was found to range between 50 and 450 mm/ year.

## **2.5 Summarized gaps in knowledge and practice**

Although ET can be estimated using various satellite and ground based methods as shown in the reviewed studies, it is important to understand these existing ET estimation methods in order to improve ET estimation for different environments in South Africa. The current study will use MOD 16 to estimate ET in two different climatic regions of South Africa. Knowledge about the accuracy of ET estimated by MOD 16 is lacking, thus this study aims to fill this gap. Accurate and consistent estimation and mapping of ET is critical for understanding plant water use which is an important component of managing ecosystems. MOD 16 has freely readily available data from 2000-2012, whereas other remote sensing techniques do not have historical available data for South Africa and are also not readily available, they need to be purchased and run on a complex software.

Previous studies showed that remote sensing techniques are widely used to estimate ET; however they are still prone to errors in the estimation of ET in some areas nationwide. The main reason for errors is the misinterpretation of land type, which results in misinterpretation of results. Also the inaccuracy in remote sensing inputs such as LAI, albedo and land cover is an issue that results in errors in estimation of ET by the remote sensing techniques.

## Chapter 3: Methodology

### 3.1 Introduction

This chapter presents the approach to the study. The first part describes the selected sites; their locations, geology, climate, vegetation and topography. The second part explains the types of data required. The ET derived from MOD 16 will be used and compared with ground measured ET on catchments differing in climate and topography. The last section explains statistical methods used to analyse data.

### 3.2 Selection of study sites

Study sites were selected based on two reasons: (i) the availability of ground measured ET data derived from flux towers and scintillometer, and (ii) catchments with contrasting climate and topography. The Elandsberg in the Western Cape was selected because of readily available ET data derived from scintillometer. Skukuza and Malopeni in the Limpopo Province were selected because they have readily available ground measured ET data derived from flux towers. These sites were selected to validate the accuracy of MOD 16. The Heuningnes catchment in the Western Cape Province and the Letaba catchment in the Limpopo Province were selected as the study sites. The study sites were selected because they have contrasting climatic regions (Mediterranean and Sub-tropical climatic regions) in South Africa. These sites were selected to evaluate if MOD 16 can adequately represent the seasonal and interannual variations of ET in different climatic regions.

#### 3.2.1 Elandsberg site

The Elandsberg site is situated on the west-facing footslopes of the Elandskloof mountain range,  $\pm$  2 km south of the small town Hermon and  $\pm$  13 km east of Riebeek kasteel (Jovanovic *et al.*, 2013). Malmersbury is the underlying geology with some sandstone talus from adjacent mountain slopes and extensive areas of gravelly soils derived from ferricrete formed on old terraces. According to the vegetation map compiled by Rebelo *et al.*, (2006), the dominant vegetation types are Swartland Alluvium Fynbos (SAF), with patches of Swartland Shale Renosterveld scattered within, and to the west of the fynbos (Figure 3.1). The adjacent slopes have Hawequas Sandstone fynbos. According to the 2000 Land cover type map produced by Jovanovic *et al.*, (2013), the natural vegetation in the area is dominated by two classes; shrubland and low fynbos and thicket, bushland, bush clumps and high fynbos which are distinguished primarily on the degree of canopy cover features such as image texture which indicate taller vegetation. Although the 2000 land cover map is old, there have not been significant changes in

the land cover since then (Jovanovic *et al.*, 2013). The scintillometer was installed at 33.47404°S, 19.0629°E transmitter and 33.47029°S, 19.05796°E receiver and falls entirely within the SAF and crosses a seasonal stream (Figure 3.1).

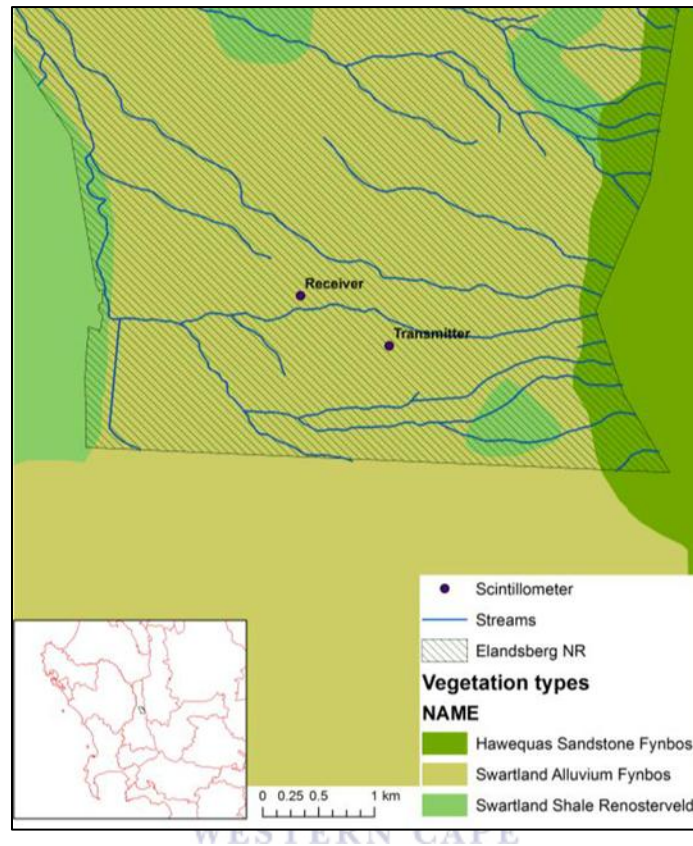


Figure 3.1: Vegetation types of Elandsberg Nature Reserve (Jovanovic *et al.*, 2013) based on the mapping and classification developed by Rebelo *et al.*, (2006).

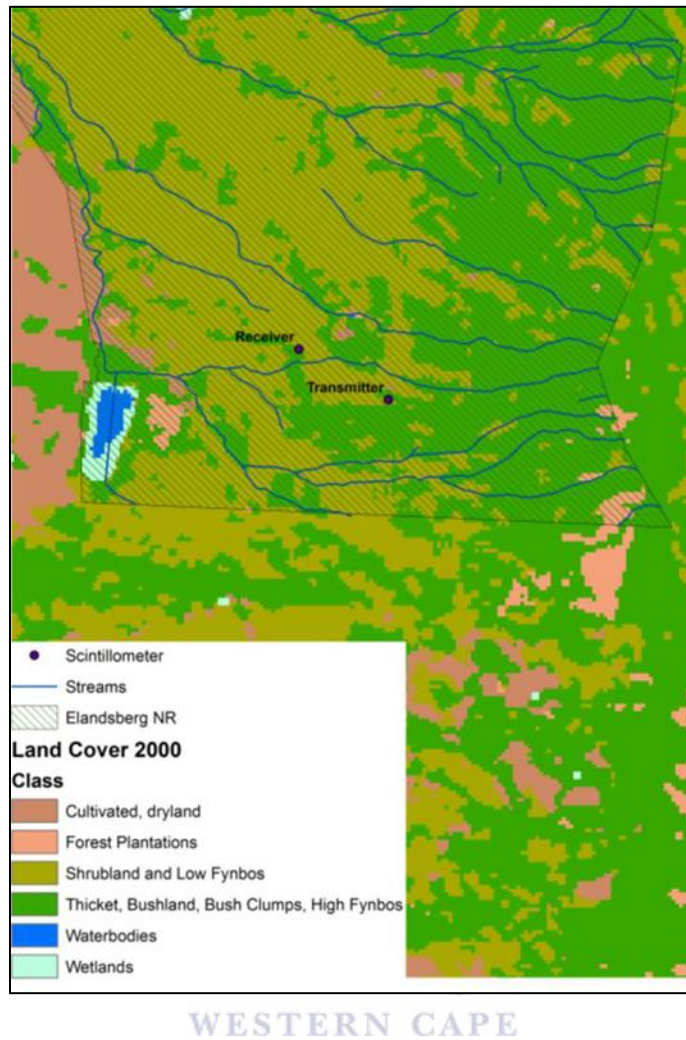


Figure 3.2: Land cover types in Elandsberg Nature Reserve and the position of the transmitter and receiver (Jovanovic *et al.*, 2013).

### 3.2.2 Skukuza and Malopeni sites

The Skukuza and Malopeni sites are located in the Kruger National Park (KNP). The Skukuza flux tower is located in two distinct savanna types (25.01184°S, 31.29813°E), a broad-leafed *Combretum* savanna and fine-leafed *Acacia* savanna. These contrasting savanna types occur on soils of differing textures, water holding capacities and nutrient levels and are characterized by different physical structure, physiology and phenology (Scholes *et al.*, 2001). The Skukuza site lies at 365 m above the sea level with 547 mm/year of mean annual rainfall and the temperatures range between 14.5 and 29.5°C (Scholes *et al.*, 2001). The Malopeni flux tower is located on the northern part of KNP (23.495714°S, 31.125170°E) along the broad-leaf Mopane savanna, which is a hot and dry savanna. The Malopeni site is situated 384 m above the sea level, with mean annual rainfall of 473 mm/year and temperatures range between 12.4 and 30.5°C (Kirton and Scholes 2012).

### 3.2.3 Heuningnes Catchment

The Heuningnes catchment is located at the southern tip of the African continent (Figure 3.3). The Heuningnes catchment drains into the Indian Ocean, and has the southernmost estuary in South Africa, situated near the Cape Agulhas. The catchment covers an area of 1401 km<sup>2</sup> and lies within the Cape Agulhas Municipality in the Overberg District (Heydorn & Grindley, 1984). The Heuningnes River has two major tributaries, the Kars River which rises in the Bredasdorpberge and runs for 75 km to its confluence with Soetendalsvlei, and the Nuwejaars River that rises primarily in the Bredasdorpberge, Koueberge and Soetangsberg and runs for some 55 km to the Soetendalsvlei (Heydorn & Grindley, 1984). Wetlands occur from upstream of the Nuwejaars River-Soetendalsvlei confluence to the mouth of the Heuningnes River. The Soetendalsvlei is a 3 km by 8 km lake that overflows into the Heuningnes River which feeds an estuary (Hoekstra & Waller, 2014).

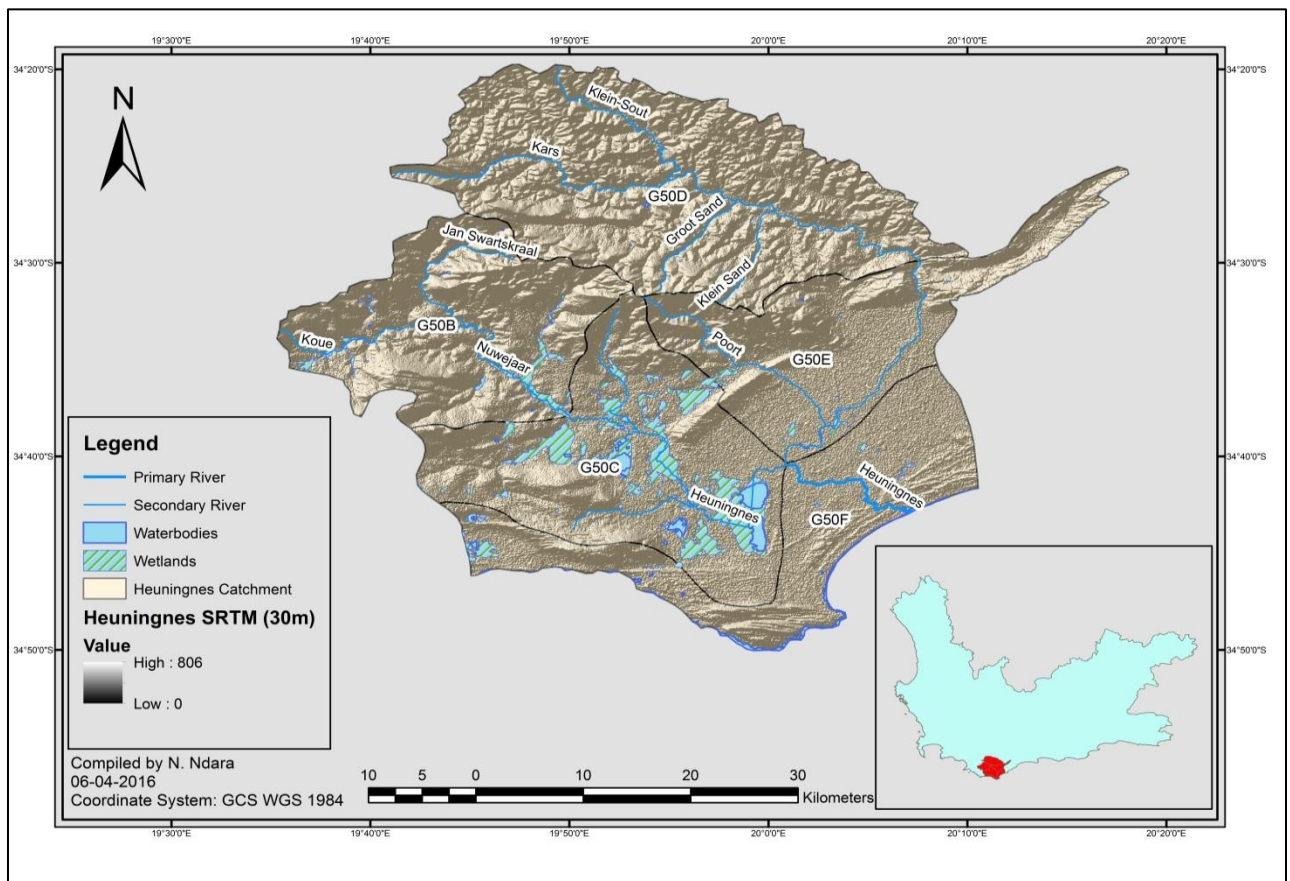


Figure 3.3: Heuningnes Catchment, Western Cape Province, South Africa

## Geology

The Heuningnes catchment is underlain by the Bredasdorp Beds which comprise calcified dune sand (Figure 3.4). These occur along the coast up to the Potberg Mountain in a band varying from three to twenty kilometers in width (Heydorn & Grindley, 1984). The geology of the upper catchment of Kars River is dominated by Table Mountain Group sandstones, quartzite and shale of the Bredasdorpberge in the southern parts, and Bokkeveld shale in the undulating northern parts. Further downstream, east of Bredasdorp, the Kars River crosses calcified dune sand and coastal limestone of the Bredasdorp beds. The geology of the upper catchment of the Nuwejaars River is dominated by sandstones, quartzite and shale of the Table Mountain Group (Hoekstra & Waller, 2014). Additional downstream near Elim, the Nuwejaars River traverses shale and sandy shale of the Bokkeveld Group which continues eastwards almost to where the Nuwejaars River enters Soetendalsvlei (Hoekstra & Waller, 2014).

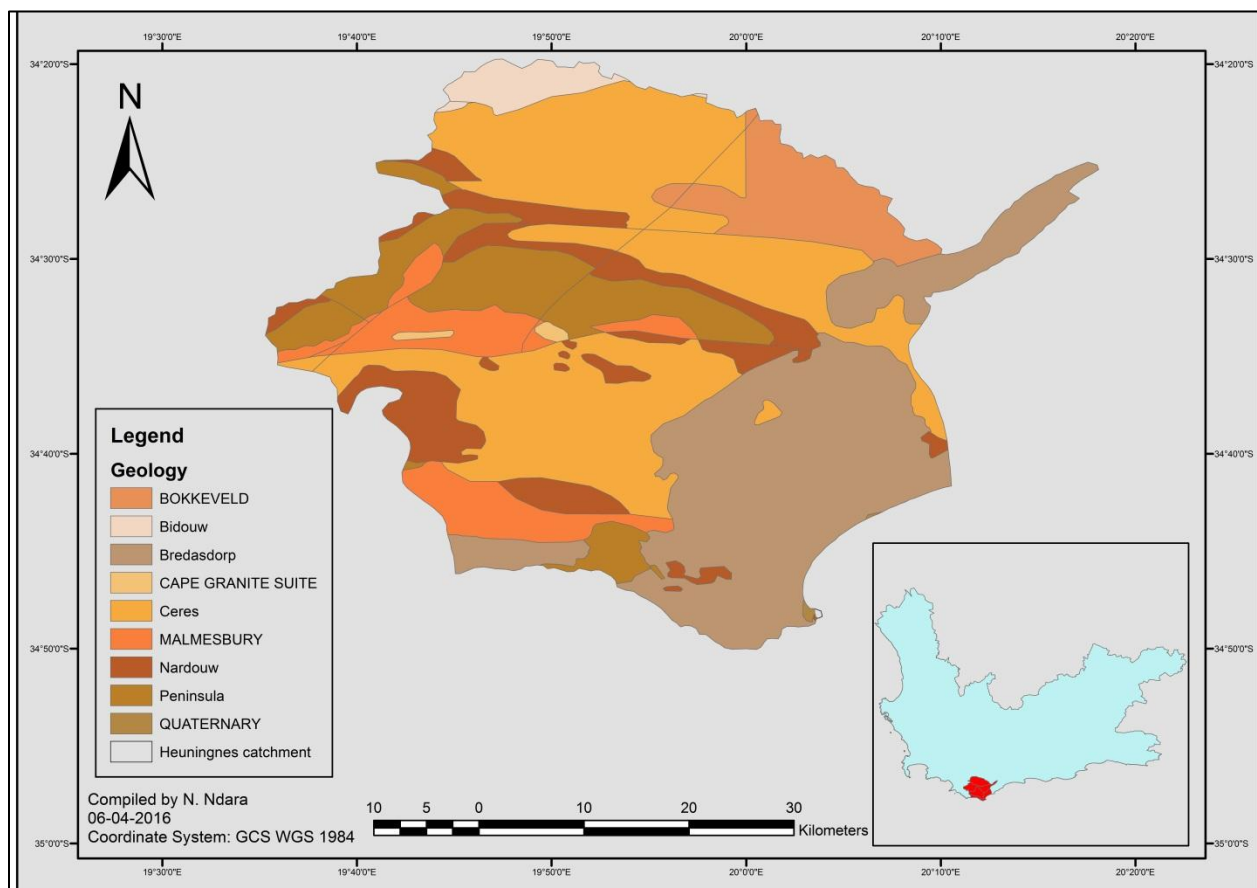


Figure 3.4: Geology of the Heuningnes Catchment



## *Climate*

The Heuningnes catchment has a Mediterranean climate receiving most of its rainfall in winter and is characterized by a warm to hot and dry summer (Heydorn & Grindley, 1984). The mean annual rainfall over most of the catchment varies from 400mm/year to 600 mm/year (Heydorn & Grindley, 1984). The rainfall is mostly of cyclonic origin with some orographic rainfall occurring in the upper reaches of the catchment. Rain-bearing winds are mostly from the west or south-west. Rainfall is more on the southern faces of the mountains than on the north facing slopes. During the summer months easterly winds predominate.

## *Vegetation*

The vegetation of the Heuningnes catchment belongs to the fynbos biome. The fynbos biome is divided into various types such as; mountain fynbos, proteoid fynbos, restioid fynbos and asteraceous fynbos (ODM, 2004). Mountain fynbos occurs in mountainous areas on shallow, sandy, acid soils, most of which are derived from sandstones of the Table Mountain Group and are highly infertile. The mountain fynbos is found extensively in moister areas on the steep south-facing slopes of the mountains and also occurs in small patches on seaward-facing coastal slopes (ODM, 2004). The proteoid fynbos are usually taller than the surrounding vegetation. This type of vegetation is divided into various kinds; including *Protea compacta* veld, *Protea susannae* veld and limestone fynbos. The *Protea compacta* veld is the dominant species in the Proteoid fynbos and is found mainly on deep, leached sands and is restricted to low-lying areas. The *Protea susannae* veld occurs on deep, more fertile sands, often at the base of major outcrops of limestones of the Bredasdorp formation. The limestone fynbos is rich in species and most of the vegetation is relatively intact, although invasion by rooikrans is increasing (ODM, 2004).

The restioid fynbos is dominated by tall reeds and is confined to low lying areas. This vegetation type is closely associated with vleis and may be flooded during winter rainfall season. It is mostly found along the coast and the east of Soetendalsvlei. The Asteraceous fynbos is distinguished into two types, namely Elim and dune fynbos. The Elim fynbos is characterized by the absence or sparse cover of a tall proteoid shrub layer. It occurs on dry, gravelly soils, usually overlying Bokkeveld Shales or sand stones of the Table Mountain Group and occurs on low lying areas. The dune fynbos on the other hand occurs on coastal sands that are subject to severe winds (ODM, 2004). Dune fynbos has very few local endemics and reasonably large tracts of this vegetation type remain.

## *Land cover and Land use*

According to the 2013-2014 land cover map classified by Agricultural Research Council (Figure 3.5), the Heuningnes catchment has various land cover types such as; woodland or open bush, wetlands, open water bodies, urban built-up, thicket or dense bush, shrubland fynbos, forest plantations, mines water, low shrubland, grassland, cultivated land and bare none vegetated land. Cultivated land is dominating along the mountains and there is also shrubland fynbos and small patches of thicket or dense bush. In the central part of the catchment shrubland fynbos, thicket or dense bush, cultivated land, woodland, and wetlands are found. Further down the catchment there are wetlands, open water bodies, thicket or dense bush and urban built-up. The entire catchment is generally dominated by cultivated land and shrubland fynbos.

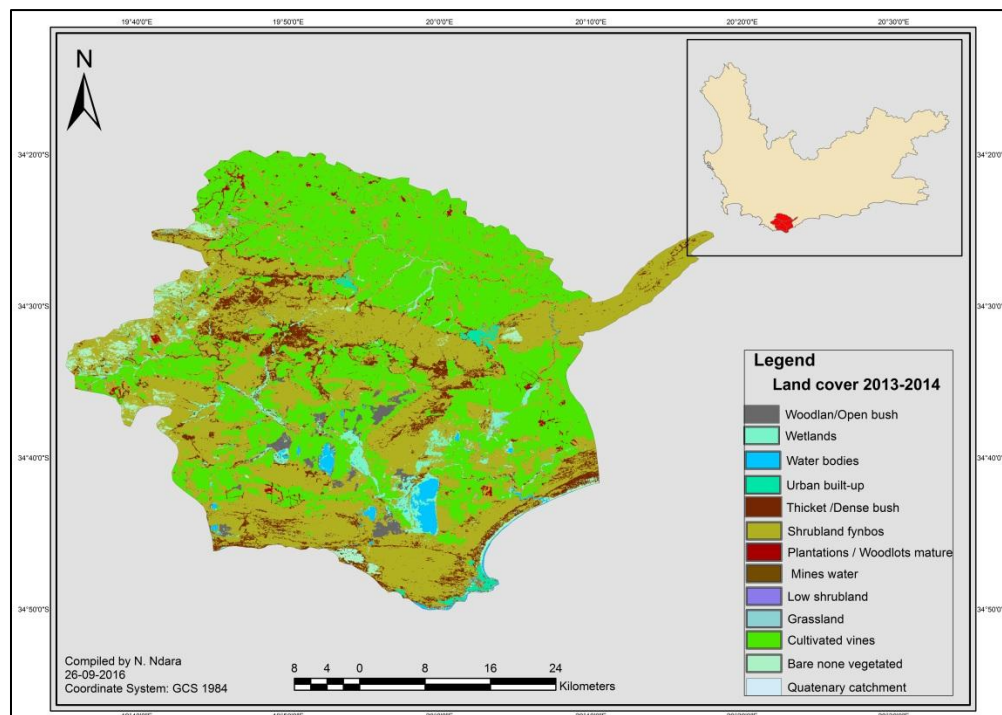


Figure 3.5: Land cover and land use of the Heuningnes Catchment

### **3.2.4 Letaba Catchment**

The Letaba River flows through the Kruger National Park and into Mozambique before discharging into the Limpopo River (Figure 3.6). The Letaba River catchment covers an area of 13 400 km<sup>2</sup>. The two main tributaries of the Letaba River are the Groot Letaba River and Klein Letaba River. The Groot Letaba River originates in the Drakensberg escarpment, descending in long runs with infrequent riffles or pools, mostly in the Limpopo Province of South Africa. At the high levels the Broederstroom River, Politsi River, Debengeni River Letsitele River, and

Thabina River, join the Groot Letaba (DWAF, 2001). Lower down the Molototsi River (a seasonal stream) and Nsama River join before the Nsami Dam, just before the Kruger National Park and Klein Letaba River flows into the Groot Letaba River.

The topography of the Letaba varies from mountains in the west to low lying plains in the east (DWAF, 2001). The mountainous zone includes the northern portion of the Drakensberg mountain range and the eastern Southpansberg, which both spread to the western parts of the Letaba water management area. The highest peaks have an elevation of more than 2 000 m above mean sea level (SARHP, 2001). This zone is deeply incised by the major tributaries. The low lying plains cover most of the area and have gentle to flat slopes.

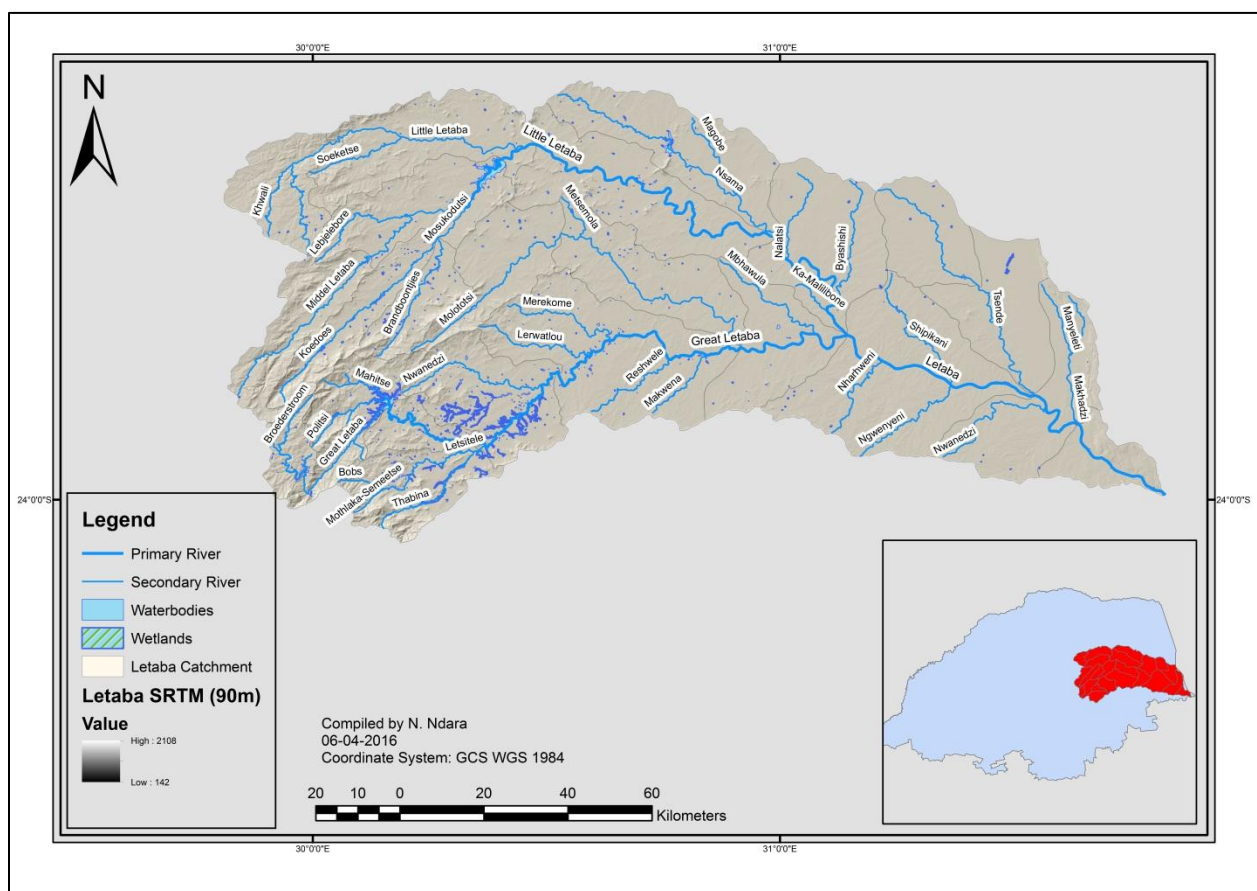


Figure 3.6: Letaba Catchment, Limpopo Province, South Africa

## Geology

The Letaba Catchment consists mainly of sedimentary rocks in the north, and metamorphic and igneous rocks in the south (Figure 3.7) (DWAF, 2004). High quality coal deposits are found near Tshikondeni and in the northern part of the Kruger National Park, whilst the eastern limb of the mineral rich Bushveld igneous complex are found on the southern parts of the water management area (DWAF, 2004). The Letaba Catchment consists of granite and gneiss with dolerite intrusions, quartzite, sandstone and shale in the west part and basalt, rhyolite and granophyre, and granite and gneiss with dolerite intrusions in the east part (DWAF, 2001).

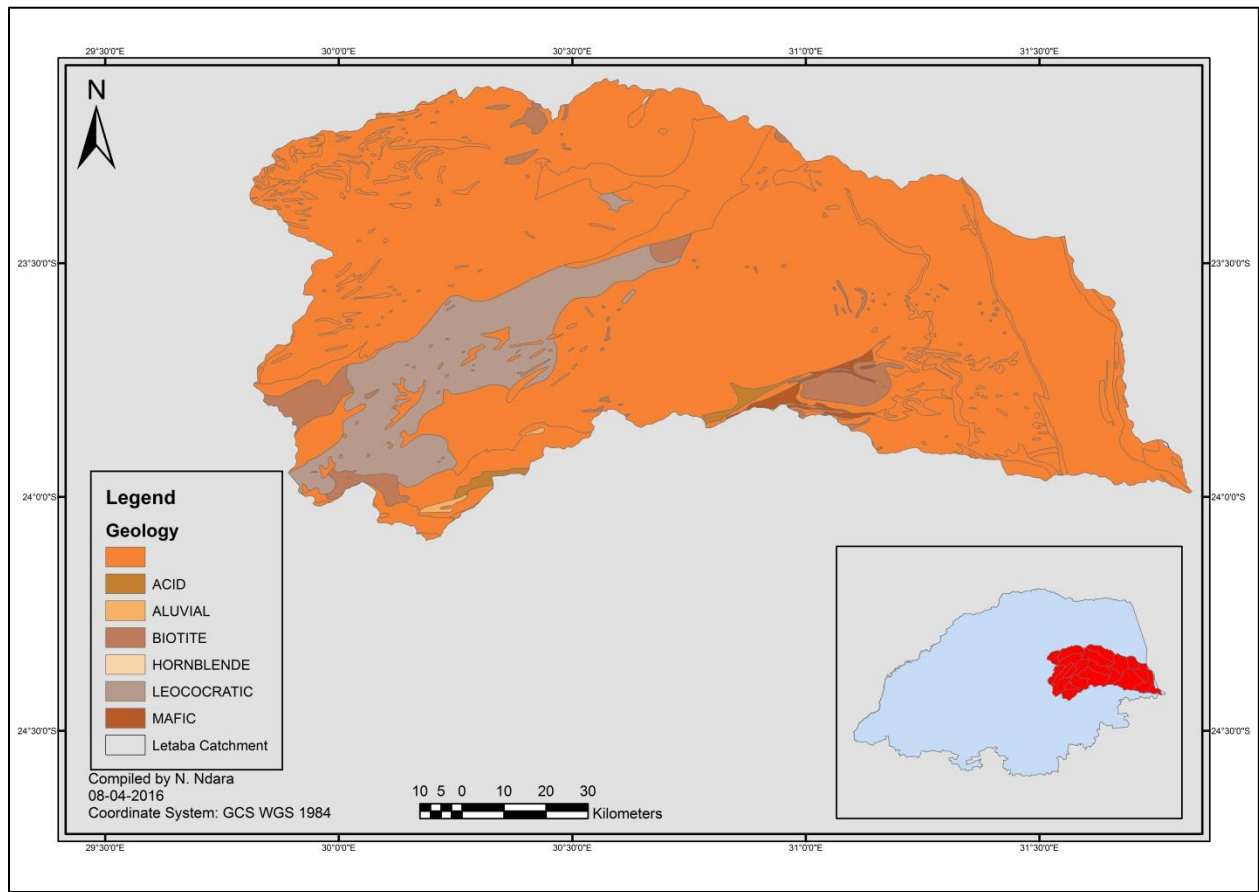


Figure 3.7: Geology of the Letaba Catchment

## *Climate*

The change in topography (altitude and relief) gives rise to different climatic characteristics. The mountain zone receives about 2000 mm/year of rainfall and the lowland receives 400 mm/year (DWAF, 2001). More than 85% of the rain falls during the summer months. Relative humidity is high during the wet months ranging from about 70% in the west to above 72 % in the east of the catchment (DWA, 2004). The summers (Oct-Mar) are very hot and the winters (Apr-Sep) are mild with frost as exceptions in the bottomlands (DWAF, 2001). The mean annual temperature ranges from 18°C in the mountainous regions to more than 28°C in the eastern parts of the catchment with an average of about 25.5°C. High and low temperatures occur in the month of January and July respectively (DWA, 2004).

## *Vegetation*

The Letaba catchment falls within the Savanna biome and the types of vegetation that occur in this catchment differ according to the geology and soil types in a specific region (Siebert *et al.*, 2010). The various types of vegetations are northern Sandveld, Mopane veld, savanna grasslands, mixed broad leaf woodland, thorn thickets and riverine bush. The northern Sandveld has sandy, well-drained soils that support a range of vegetation with no particular dominant species and it is mostly found in mountainous areas. The Mopane tree known as *Colophospermum* Mopane is found in three main forms; Mopane woodlands (mostly in the north-west) which are generally found on granite and gneiss, mopane shrubveld (mostly the central northern plains and the north-east) and Mopane thicket which are on ecca shales (Siebert *et al.*, 2010). The savanna grasslands are found dominating the eastern low-land plains. This type of vegetation is divided into various kinds such as; blue buffalo grass, finger grass and stinking grass. The mixed broad leaf woodland is another type of vegetation and is divided into various kinds; the bushwillow, russet bushwillow, large-fruited bushwillow and the leadwood. The mixed broad leaf woodland is found in low lying areas. The thorn thickets type of vegetation is found within the mixed broad leaf woodlands. The thorn thickets are almost impenetrable in some areas and are the favored habitat of the rare black rhino (Siebert *et al.*, 2010). The riverine bush forests are found in varying degrees of intensity along the river. They mainly occur on the banks of the perennial rivers.

## *Land cover and Land uses*

According to the 2013-2014 land cover map classified by Agricultural Research Council (Figure 3.8), the Letaba catchment has various land cover types namely; cultivated land, grassland, bare none vegetated land, indigenous forest, low shrubland, mines water, forest plantations, thicket or dense bush, urban built-up, open water bodies, wetlands and woodland. The western part of the catchment is dominated by thicket or dense bush and the eastern part is dominated by grassland and woodland. The urban built-up is found dominating the central part of the catchment and open water bodies are found in the west and north part of the catchment. A lot of cultivation is done in the western part and indigenous forests and forest plantations are also found in the western part spreading to the middle of the catchment. Small patches of low shrubland are found in the edges of eastern part of the catchment.

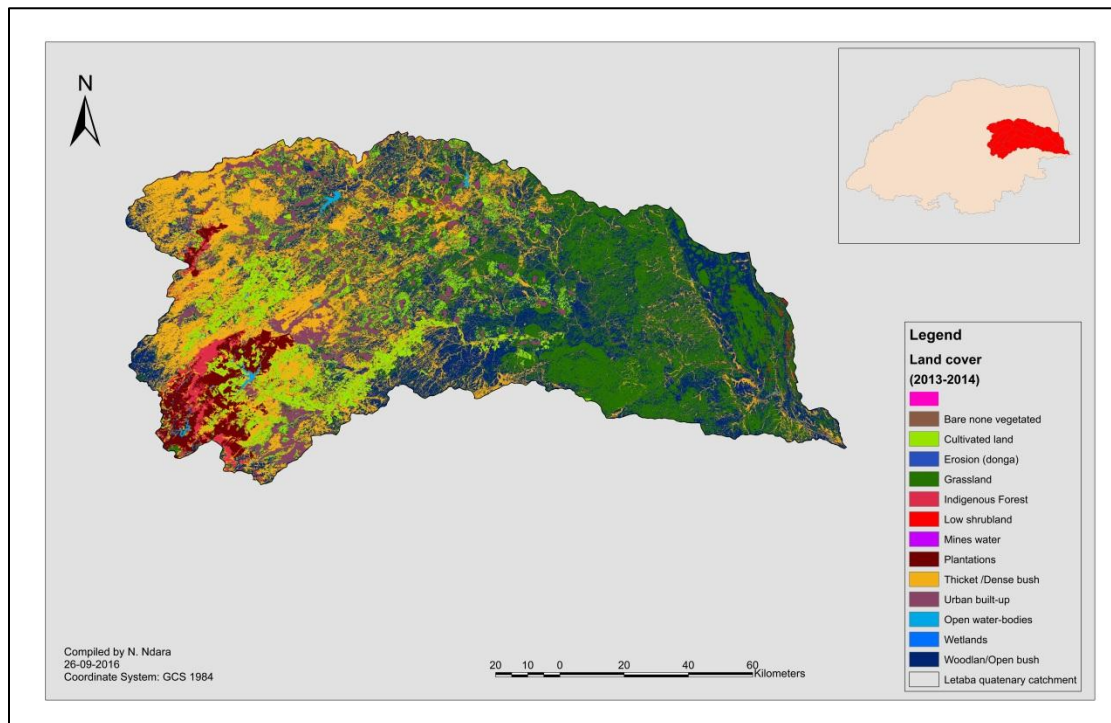


Figure 3.8: Land cover and land use of the Letaba catchment

### **3.3 Data collection**

The types of data that were required for this study were satellite derived ET data from MOD 16, ground measured actual ET and rainfall data. MOD 16 ET data have a spatial resolution of 1 km pixels and a temporal resolution of 8 day, monthly and annual intervals. However this study was interested in working on monthly intervals for which the data has not been previously analysed. The thirteen years duration (2000-2012) was analysed, because by the time the research started

(March 2015) the data was available only from 2000-2012. In contrast, other satellite derived products such as SEBAL and SEBS were not used in this study because they do not have readily available data and cannot be accessed free. Ground measured ET data derived from scintillometer and eddy covariance flux towers were required for the purpose of validating the accuracy of MOD 16 ET. The rainfall data for (2000-2012) duration were obtained from weather stations of Agricultural Research Council. The rainfall data were required for the purpose of interpreting variability in ET in relation with the wetness conditions in the investigated years.

### **3.3.1 MODIS ET data**

The MOD 16 ET data were acquired for free from the University of Montana's Numerical Terradynamic Simulation group (<http://www.ntsug.umt.edu/project/mod16>, accessed on June 2015). The data for areas of interest; Heuningnes Catchment in Western Cape and Letaba Catchment in Limpopo were extracted. Monthly MOD 16 ET maps were created for (2000-2012) for both catchments to determine the seasonal and interannual variation of ET over this period. From the monthly MOD 16 ET maps that were created for each catchment, three years were selected; one that was relatively wet, dry, and average. From each year, each month was overlaid with the land cover and land use map to clip out the ET for different land cover and land use types. Actual ET was separated for different land cover and land use types to examine if actual ET rates estimated by MOD 16 capture the variations of ET with land cover and land use types.

### **3.3.2 Rainfall data**

For the purpose of identifying the possible causes of variations in ET from the period 2000-2012; rainfall recorded by the network of weather stations in the Letaba catchment and in the Heuningnes catchment was used. Rainfall recorded at Citimba, Pietersburg, Brits-AGR, Lephalale, Dendron and Polokwane stations were used in the Letaba catchment, Limpopo Province. Rainfall recorded at Prinskraal and Agulhas stations was used in the Heuningnes catchment, Western Cape. Rainfall data were used to interpret variability in ET in relation with the wetness conditions in the landscape and the response of land cover types and vegetation.

### **3.3.3 Ground measured actual ET data**

The ground measured actual ET derived from scintillometer and eddy covariance flux towers was collected by CSIR and this research obtained the data from CSIR. The ground measured ET data for Elandsberg, Skukuza and Malopeni sites were used. The sites are described in detail at the beginning of Chapter 3. For Elandsberg site actual ET was derived from a scintillometer for a period of 1 year (Nov 2012- Oct 2013). For the Malopeni site the actual ET was derived from an

eddy covariance flux tower for a period of 1 year and 1 month (Feb 2009-Mar 2010). For the Skukuza site the actual ET was derived from an eddy covariance flux tower for a period of 13 years (2000-2012). However the years 2000, 2002, 2006 and 2012 were excluded from analyses because they have a lot of missing data. The duration of ground measured ET data varies at three sites, because the instruments at these sites were installed in different years. The actual ET estimated using ground measurement of meteorological variables was compared with the MOD 16 ET estimates, to establish how accurate is remote sensing technique (MOD 16) compared to ground based methods.

### 3.3.3 Ground-truthing

Ground-truthing was done in the Letaba catchment and Heuningnes catchment to validate the ET data that was produced by MOD 16. The ground-truthing was not done in the entire catchment but instead the focus was on the areas that had high ET according to the MOD 16 ET maps. In each catchment pictures of land cover or land use types and vegetation were taken. Ground-truthing supports the interpretation and analysis of MOD 16 ET data.

### 3.4 Data analysis method

This section explains the statistical methods that were used to answer the research questions. The appropriate statistical methods that were used are t-test, correlation coefficient, analysis of variances and box and whisker plots. These methods are commonly used because they are suitable to investigate the research questions.

#### 3.4.1 Assessment of similarities between MODIS and ground based estimate of ET

To assess the similarities between MODIS and ground based estimates of ET, a t-test at 5% significance level was used. The t-test is a statistical model used for testing the significance of differences between averages of two samples (Equation 3.1). A t-test is a parametric method that was used to compare the means of estimated and measured ET. The null hypothesis states that there is no difference between the means and the alternative hypothesis states that there is a difference between the means. A t-test assumes that the sets of data are continuous, follow a normal distribution, and that the two samples are independent (Wackerly *et al.*, 2008). A t-test is calculated as:

$$t = (\bar{x}_1 + \bar{x}_2) / sp \sqrt{\frac{1}{n_1} + \frac{1}{n_2}}, sp = \frac{\sqrt{n_1 s_1^2 + n_2 s_2^2}}{n_1 + n_2 - 2} \quad (3.1)$$



where:  $\bar{x}_1$  and  $\bar{x}_2$  represents the first and second sample mean respectively,  $n$  is the number of samples,  $s$  is the sample standard deviation and  $S_p$  represents the pool standard deviation.

This study used coefficient of determination ( $R^2$ ), root mean square error (RMSE) (Equation (3.2)), bias (Equation (3.3)) and percent bias (PBias) (Equation (3.4)) to assess the relationship between MOD 16 ET products and ground based estimates of ET, and the strength of the relationship.

The coefficient of determination was used to determine the strength of the relationship between ground measured ET and MOD 16 ET. Bias is a measure of how a modeled value (MOD 16 ET value) deviates from the true value (ground measured ET value), and indicates whether there is under or overestimation, while the percent bias is a percent of bias relative to observed mean. The equations for RMSE, Bias and PBias are

$$RMSE = \sqrt{\frac{\sum(GET - MET)^2}{N}} \quad (3.2)$$

$$BIAS = \frac{\sum MET - GET}{N} \quad (3.3)$$

$$PBIAS = \left( \frac{BIAS}{\frac{1}{N}} * \sum GET \right) * 100 \quad (3.4)$$



Where  $GET$  is ground ET,  $MET$  is MOD 16 ET and  $N$  number of measurements. Bias and RMSE values close to zero (0.1-0.7) signify that MOD 16 is considered accurate, while higher values of these statistics metric indicate inaccuracy (Kim *et al.*, 2011). A negative value of bias signifies underestimation while positive value shows overestimation by MOD 16.

The  $R^2$ , RMSE, BIAS and PBIAS were used in this study because they are suitable to answer the research question. Kim *et al.*, (2011), used  $R^2$ , RMSE, BIAS and PBIAS to validate the accuracy of MOD 16 at 17 flux towers located in Asia. The results showed a linear relationship between MOD 16 ET and ET measured at the flux towers ( $r^2 = 0.5-0.76$ , bias = -1.42-1.99 mm/ 8 day, RMSE = 1.99-8.96 mm/ 8 day). A study by Ramoelo *et al.*, (2014), also used these methods to do the validation of MOD 16 product using flux tower data in the African Savanna, South Africa. The  $R^2$ , RMSE, BIAS and PBIAS were successfully applied and produced meaningful results. The results generally showed overestimation of ET by MOD 16 (BIAS = 1.18, and PBIAS = 21%).

### 3.4.2 Assessment of the influence of land uses on MODIS ET

The current study used ANOVA to test the difference between the means of MOD 16 ET for different land cover types (dry land, bush land, irrigation, forest, grass land, wetland etc.) in two different climatic regions. Testing the difference between the means was done as the study wished to determine whether MOD 16 has the ability to distinguish differences in the actual ET rates on different land cover types.

Analysis of variance (ANOVA) is a parametric method that is used to test difference between two or more means. ANOVA is used to test overall rather than exact difference among means. This test groups the samples using one factor (e.g. land cover type), with the purpose of determining whether samples drawn from different groups have meaningfully different means (Wackerly *et al.*, 2008). In this study the null hypothesis states that MOD 16 cannot differentiate actual ET rates on different land cover types ( $\bar{x}_1 = \bar{x}_2$ ). The alternative hypothesis states that MOD 16 has the ability to distinguish differences in the actual ET rates on different land cover types ( $\bar{x}_1 \neq \bar{x}_2$ ). The null hypothesis is rejected, when at least one sample mean is different from at least one other mean. The alternative hypothesis is not rejected if the variation between groups is greater than the variation within groups. ANOVA offers less specific information than the Tukey HSD test, since it does not tell which means are different from which. However the ANOVA is more appropriate to use than the Tukey test because it allows complex types of analyses to be done which is not the case with the Tukey test (Wackerly *et al.*, 2008). ANOVA is also the most commonly used technique for comparing means.

Other studies have used ANOVA to achieve the similar objective as the current study. Ibrahim *et al.*, (2016), undertook a study to analyse the impact of land surface temperature on land cover types. The results showed that there is a significant difference in the temperature variation on land cover types. A study about the effects of land use change on land degradation reflected by soil properties along Mara River, Kenya and Tanzania was done by Matano *et al.*, (2015). Using the ANOVA test, the objective of the study was to determine the effect of land use change on the physic-chemical properties of soil along the course of the Mara River. The results indicated that the land use types affected land degradation differently along the Mara River, while adjacent land degradation affected water physic-chemical properties.

Descriptive statistics such as the average, standard deviations, maximum, minimum, and median were calculated for each sample of data. ArcGIS was used for processing of layers such as MOD

16 ET maps, land use and land cover maps, topography map, wetlands maps, and groundwater data. All these maps were overlaid with the purpose of identifying areas of water use, such as irrigated land, land invaded by alien species, shallow groundwater areas and wetlands in the Letaba catchment and Heuningnes catchment.



## Chapter 4: Validation of MOD 16 ET

### 4.1 Introduction

This chapter illustrates and discusses the results of the first objective, which is to evaluate whether actual ET rates estimated by MOD 16 adequately represent the seasonal and interannual variations of actual ET at the catchment scale. Firstly the MOD 16 product was validated at three sites; Elandsberg, Malopeni, and Skukuza sites, and the findings of validation of MOD 16 product are presented. Secondly the seasonal and interannual variation of MOD 16 ET in the Heuningnes catchment and in the Letaba catchment is presented.

### 4.2 Validation of MOD 16 product

Firstly each weather factor such as relative humidity, solar radiation, air temperature and wind speed was compared with ground measured ET and MOD 16 ET for each site. This was done to investigate the effect of each weather factor on ground measured ET and MOD 16 ET. Secondly ground measured ET was correlated with MOD 16 ET for each site, to evaluate the accuracy of MOD 16.

#### 4.2.1 The effect of weather factors on ground measured actual ET and MOD 16 ET at Elandsberg

Ground measured actual ET data were collected using a scintillometer for a period of 1 year (Nov 2012- Oct 2013). The scintillometer receiver was located approximately 900 m away from the transmitter at Elandsberg Nature Reserve at pixel 67. Monthly MOD 16 ET data for this period were downloaded from (<http://www.ntsug.umt.edu/project/mod16>, accessed on 21 March 2016). The weather factors such as solar radiation, temperature, relative humidity and wind speed were measured from the weather station installed in Elandsberg Nature Reserve on the 26 October 2012. The ground measured actual ET and MOD 16 ET were compared with the weather factors that mostly affect actual ET, to investigate the relations between variables. The comparison was first done at pixel 67 where the scintillometer was installed. The results showed a weak relationship between weather factors and scintillometer ET and MOD 16 ET, therefore further comparison was done with the pixels surrounding pixel 67 (Figure 4.1). From those pixels only pixel 62 and pixel 63 showed a better relationship.

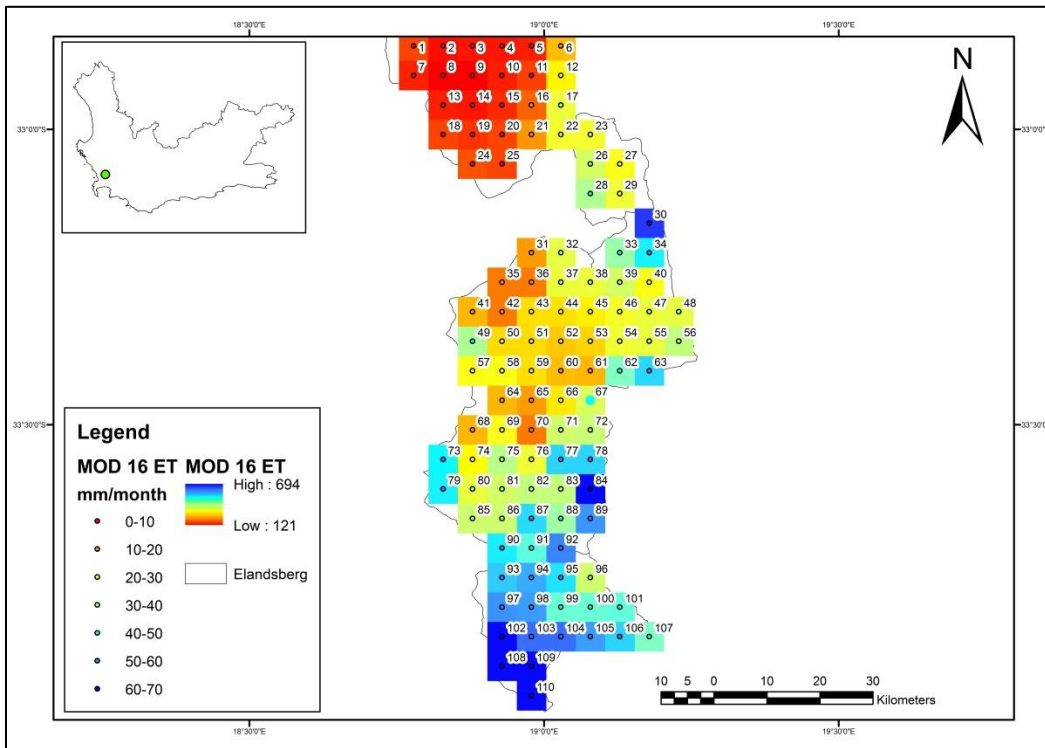
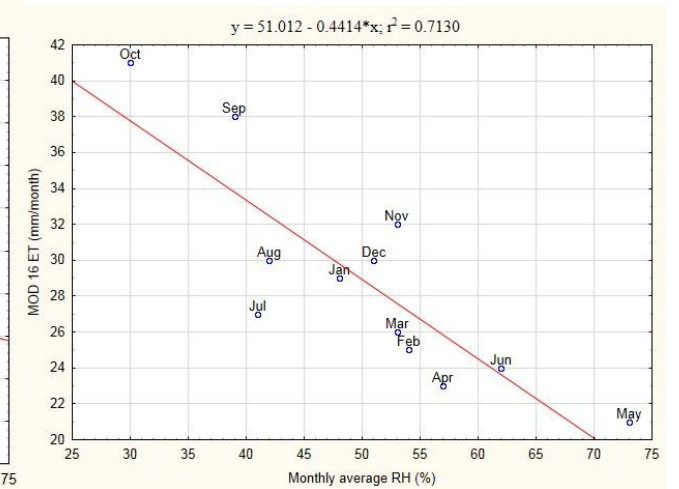
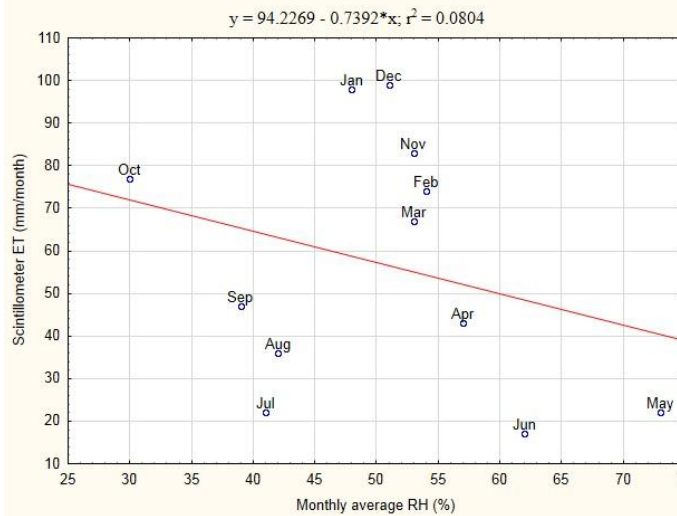
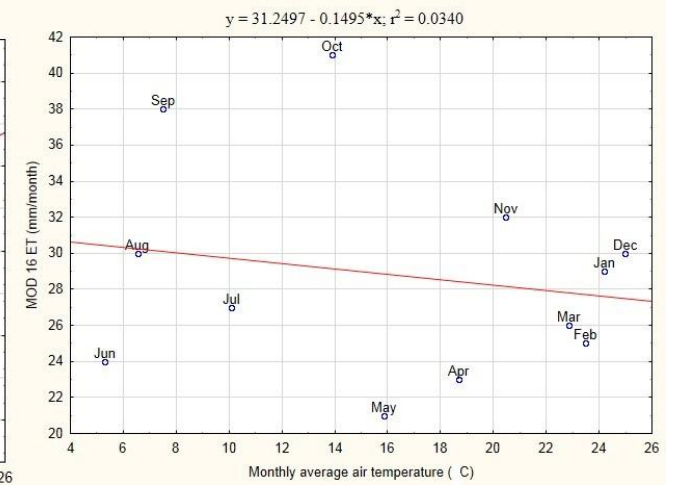
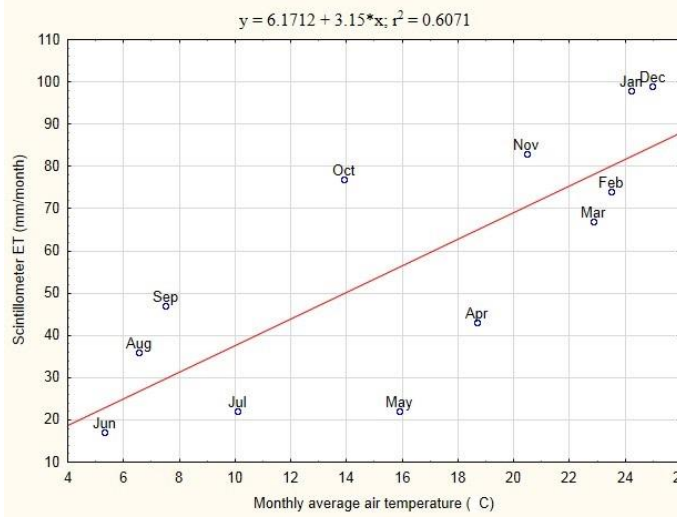
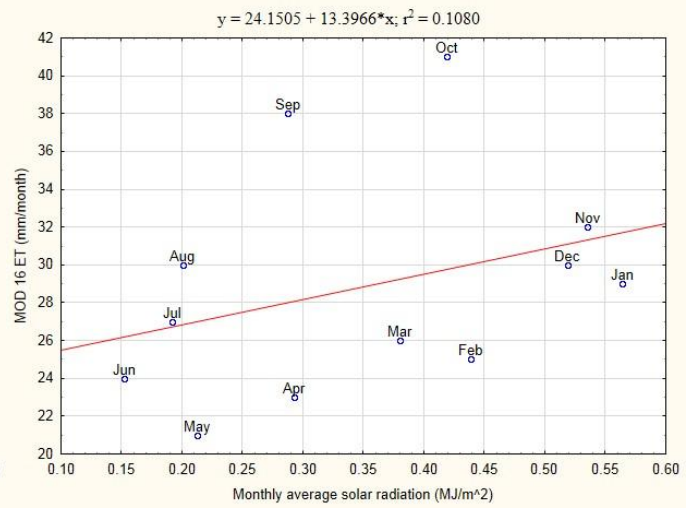
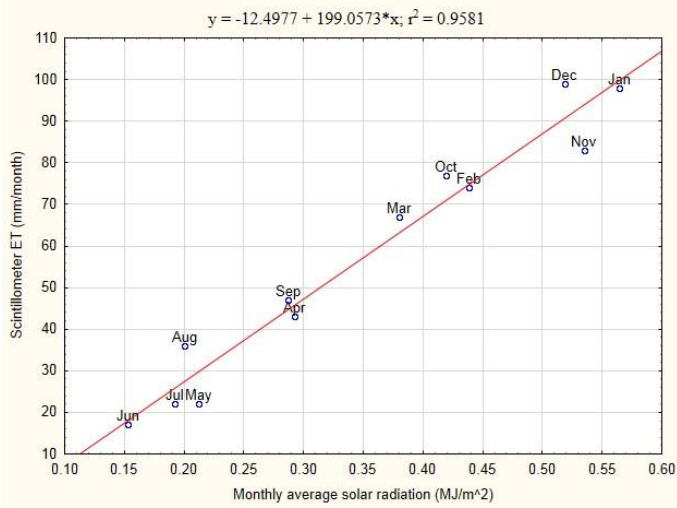


Figure 4.1: MOD 16 pixels numbered at Elandsberg site, Scintillometer was installed at pixel number 67

The weather factors were compared with scintillometer ET and MOD 16 ET for pixel 67 (Figure 4.2). The results showed that there is a strong relationship between scintillometer ET and solar radiation ( $R^2 = 0.95$ ), moderate relationship between scintillometer ET air temperature ( $R^2 = 0.61$ ) and wind speed ( $R^2 = 0.71$ ) compared to relative humidity ( $R^2 = 0.08$ ). The results showed that there is a moderate relationship between MOD 16 ET and relative humidity ( $R^2 = 0.72$ ) compared to wind speed ( $R^2 = 0.19$ ) and solar radiation ( $R^2 = 0.10$ ) where there is a weak relationship and air temperature ( $R^2 = 0.03$ ).



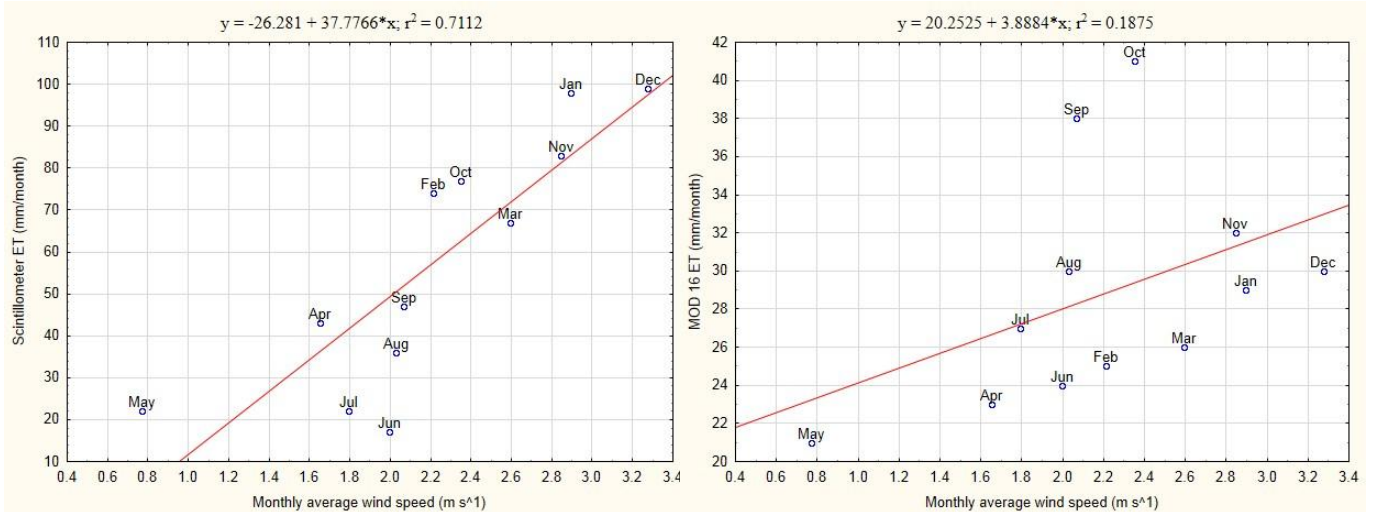
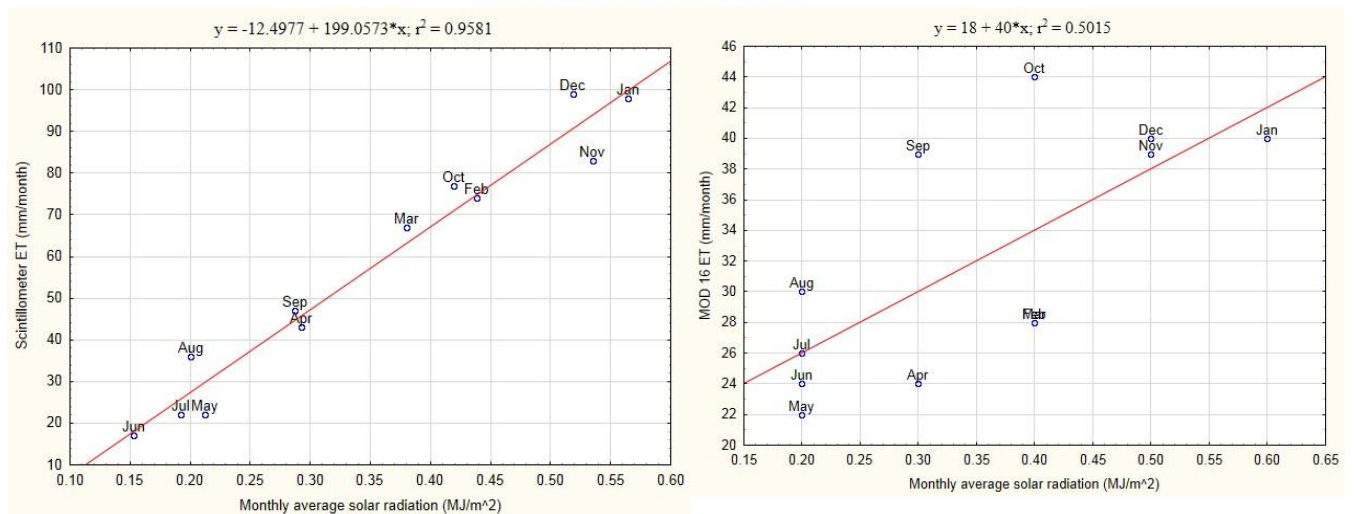
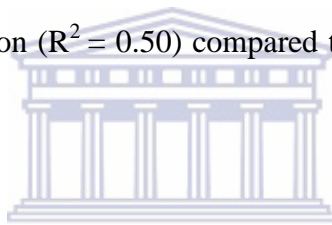


Figure 4.2: The relationship between weather factors and actual ET derived from scintillometer and MODIS ET at Elandsberg (pixel 67)

The weather factors were compared with scintillometer ET and MOD 16 ET for pixel 62 (Figure 4.3). The results showed that there is a moderate relationship between MOD 16 ET and wind speed ( $R^2 = 0.51$ ) and solar radiation ( $R^2 = 0.50$ ) compared to relative humidity ( $R^2 = 0.43$ ) and air temperature ( $R^2 = 0.05$ ).



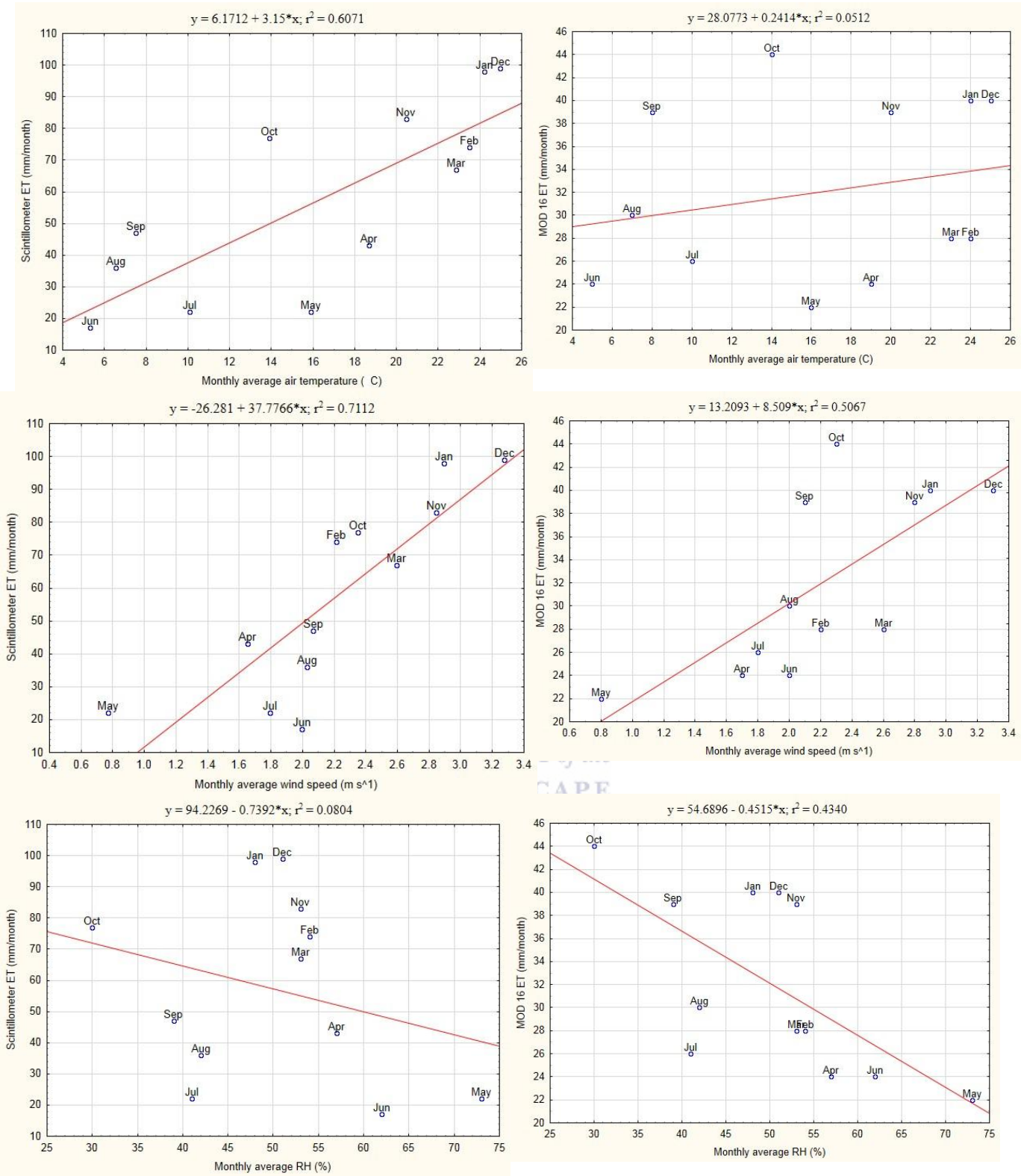
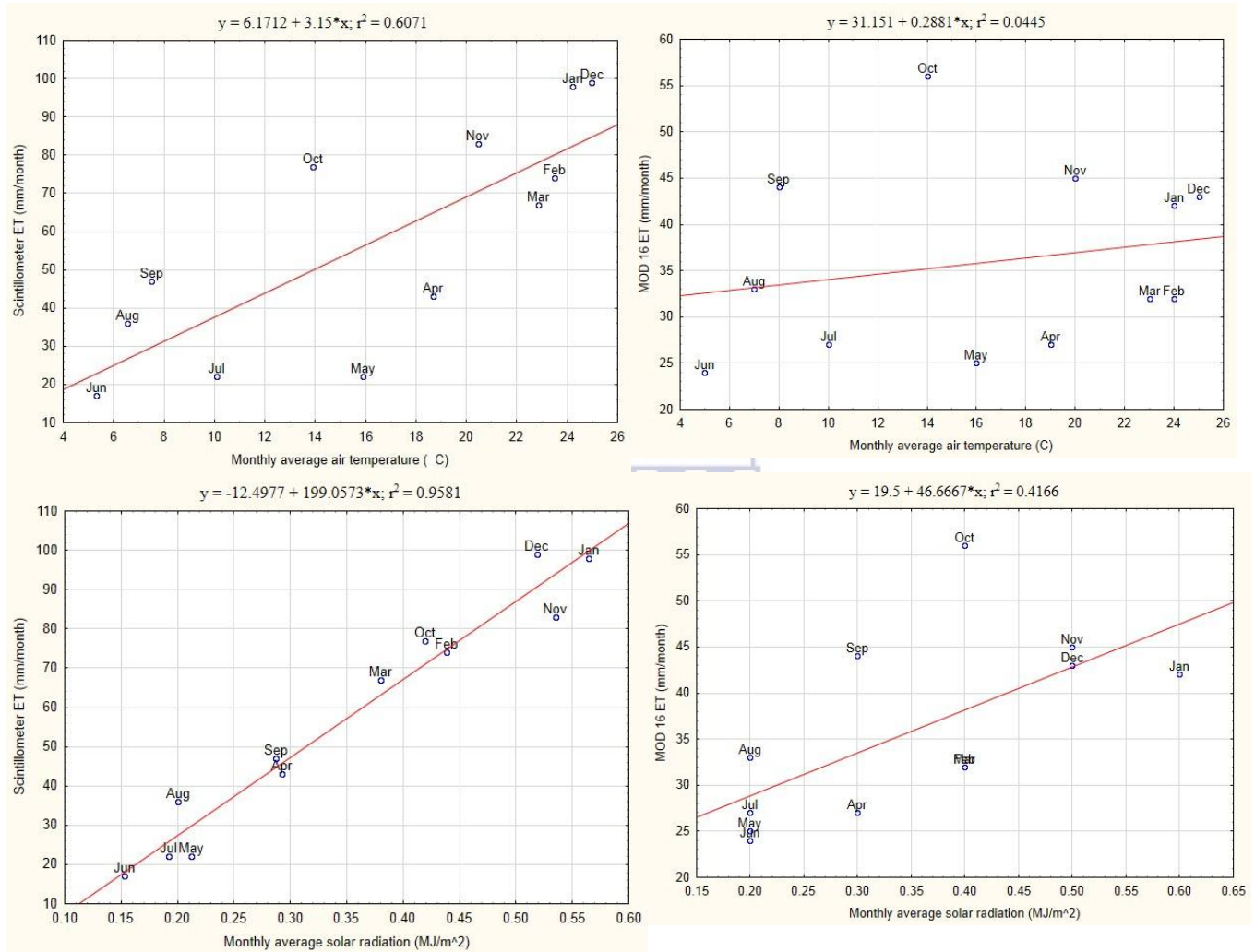


Figure 4.3: The relationship between weather factors and actual ET derived from scintillometer and MODIS ET at Elandsberg (pixel 62)



The weather factors were compared with scintillometer ET and MOD 16 ET for pixel 63 (Figure 4.4). The results showed that there is a weak relationship between MOD 16 ET and relative humidity ( $R^2 = 0.46$ ), solar radiation ( $R^2 = 0.42$ ) and wind speed ( $R^2 = 0.36$ ) compared to air temperature ( $R^2 = 0.04$ ).



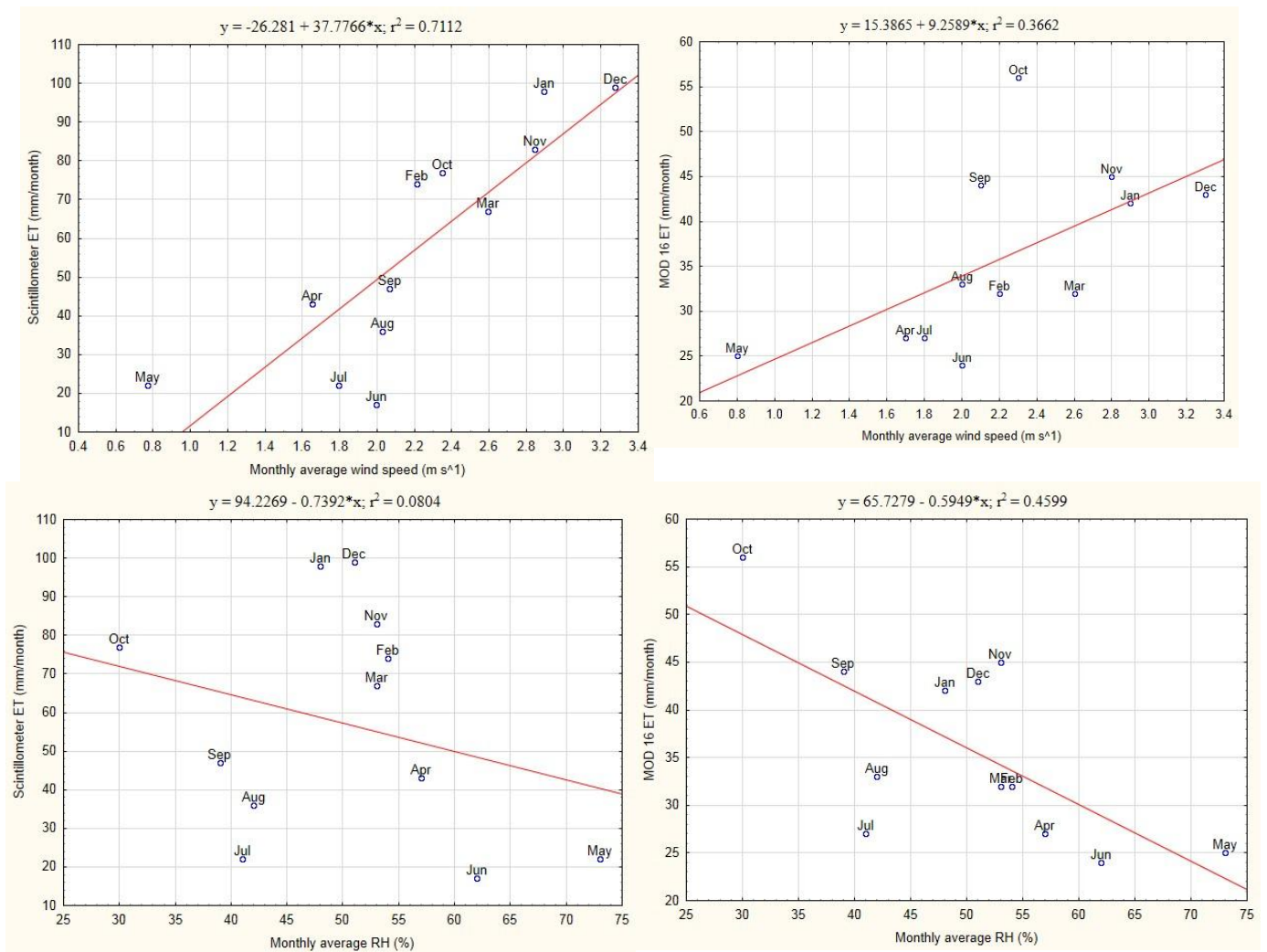


Figure 4.4: The relationship between weather factors and actual ET derived from scintillometer and MODIS ET at Elandsberg (pixel 63)

A moderate and strong relationship between ground measured ET and solar radiation, air temperature and wind speed is expected because actual ET is influenced by these weather factors. According to Allen *et al.*, (1998) ET is influenced by solar radiation in a way that during winter months (May, Jun and Jul) when there is less amount of energy coming from the solar radiation, ET becomes low and during summer months (Oct, Nov, Dec and Jan) when there is high amount of energy coming from solar radiation, ET is high (Figures 4.2, 4.3 and 4.4). High temperatures also occurred during summer months and low temperatures occurred during winter months; therefore the relationship between air temperature and ET derived from scintillometer is positive, as an increase in temperature resulted in an increase in actual ET. However this is not the case between air temperature and MOD 16 ET, in the studied pixels (67, 62 and 63) when air temperature increased MOD 16 ET decreased.

The high humidity of the air reduces the ET demand (Allen *et al.*, 1998). During summer months in Elandsberg when the soil conditions are dry and there is high energy coming from solar radiation, relative humidity is low therefore ET is high. However during winter months when the soil conditions are moist and there is low amount of solar radiation, relative humidity is high thus ET is low. Relative humidity is therefore inversely proportional to ET. A moderate relationship is observed between wind speed and ET derived from scintillometer. The continuous replacement of air above evaporative surface with dry air increases the rate of ET, thus an increase in wind speed results in an increase in ET.

#### 4.2.2 Relationship between scintillometer ET and MOD 16 ET at Elandsberg

The scintillometer ET was compared with MOD 16 ET for pixel 67 where scintillometer was installed and the surrounding pixels 62 and 63. The results suggested that at pixel 67 there is a very weak relationship between scintillometer ET and MOD 16 ET ( $R^2 = 0.16$ ) (Figure 4.5). Based on RMSE = 28.30 mm/month, Bias = -28.30 mm/month and PBias = -49.53%, MOD 16 underestimated ET. High values of Bias and RMSE indicate a high level of inaccuracy of the MOD 16 ET and a negative value of Bias indicates underestimation.

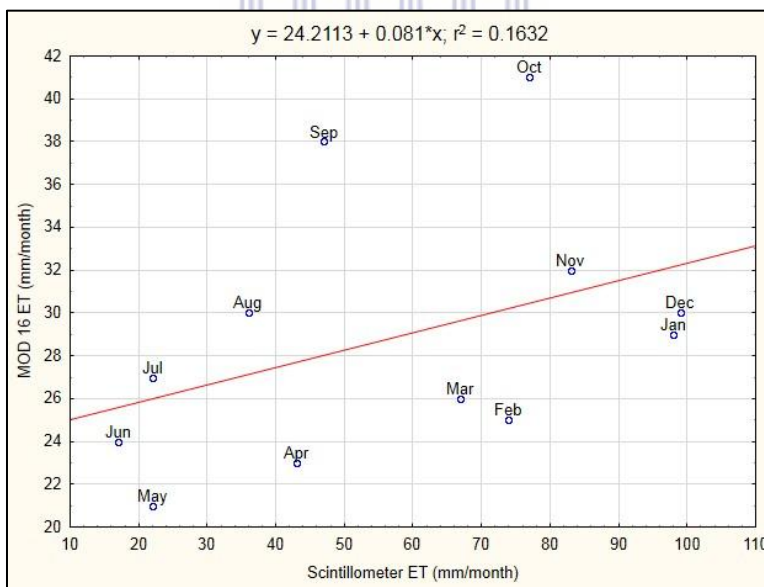


Figure 4.5: The relationship between scintillometer ET and MOD 16 ET (mm/month) at Elandsberg (pixel 67)

The scintillometer ET was compared with MOD 16 ET for pixel 62. The results showed that there is moderate relationship between scintillometer ET and MOD 16 ET ( $R^2=0.58$ ) (Figure 4.6). Pixel 62 achieved the highest values of RMSE = 25 mm/month, Bias = -25 mm/month and PBias = -43.99%, which indicates inaccuracy of the MOD 16 ET product.

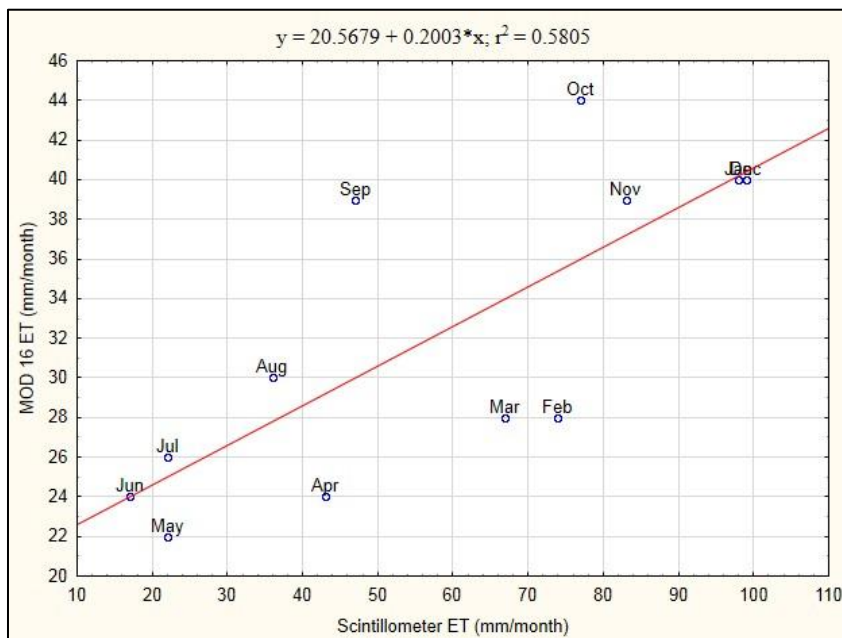


Figure 4.6: The relationship between scintillometer ET and MOD 16 ET (mm/month) at Elandsberg (pixel 62)

The monthly Scintillometer ET was compared with monthly MOD 16 ET for pixel 63. The results showed that there is moderate relationship between scintillometer ET and MOD 16 ET ( $R^2 = 0.52$ ) (Figure 4.7). Based on RMSE = 21 mm/month, Bias = -21 mm/month and PBias = -37.28%, pixel 63 achieved the highest values which indicates inaccuracy of the MOD 16 ET product.

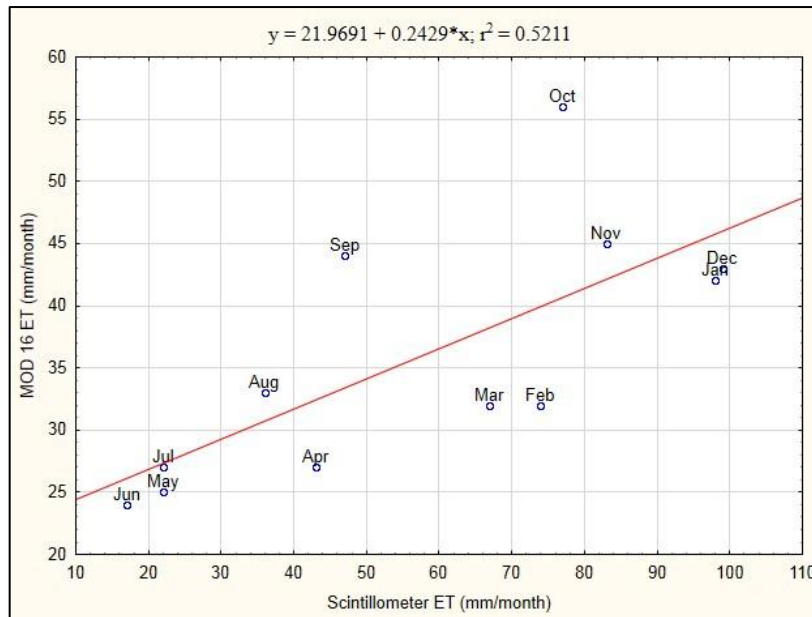


Figure 4.7: The relationship between scintillometer ET and MOD 16 ET (mm/month) at Elandsberg (pixel 63)

In summary, the Elandsberg results showed that MOD 16 ET underestimated actual ET in the Mediterranean climate of the Western Cape. It is apparent that the ET values derived from scintillometer are higher than MOD 16 ET values in summer months (Nov- Feb) and are closely related during winter months (May- Aug). This means that ET is mostly underestimated by MOD 16 during summer season. These results rather match with the results found by Ramoelo *et al.*, (2014). It is argued that the differences between MOD 16 ET and ground measured ET can originate from a number of factors, such as scintillometer or flux tower footprints versus MOD 16 pixel size, remote sensing data and in situ data. The pixel 67 was chosen to be in a homogeneity area of natural vegetation for installation of scintillometer. However pixel 67 was found to have a weak relationship with MOD 16 ET, and the surrounding pixels (62 and 63) had a moderate relationship with MOD 16 ET. The remote sensing input parameters include 8 day land cover, albedo, leaf area index, fraction of photosynthetic absorbed radiation and have a spatial resolution of approximately 1 km<sup>2</sup>. The in situ data parameters include daily air temperature, humidity and solar radiation. The findings suggest that the remote sensing parameters are generally poorly or not validated in Mediterranean region of South Africa, therefore they are likely to generate ET prediction errors (Ramoelo *et al.*, 2014).

### 4.2.3 The effect of weather factors on ground measured actual ET and MODIS ET at Malopeni

In Malopeni actual ET was measured using an eddy covariance flux tower for a period of 1 year and 1 month (March 2009- March 2010). The eddy covariance flux tower was installed at 23.495714°S, 31.125170°E and monthly MOD 16 ET data for this period was downloaded from (<http://www.ntsg.umat.edu/project/mod16>, accessed on the 28 March 2016). The ground measured actual ET and MOD 16 ET were compared with the weather factors that mostly affect actual ET, to investigate the possible causes of errors in estimating actual ET. The temperature and relative humidity were excluded from comparison because they had a lot of missing values. There is no relationship between flux tower ET and solar radiation ( $R^2 = 0.09$ ) and wind speed ( $R^2 = 0.004$ ). The results also showed that MOD 16 ET was not related to solar radiation ( $R^2 = 0.003$ ) and wind speed ( $R^2 = 0.004$ ) (Figure 4.8). There is generally a poor relationship between weather factors and MOD 16 ET and ET derived from flux tower in Malopeni.



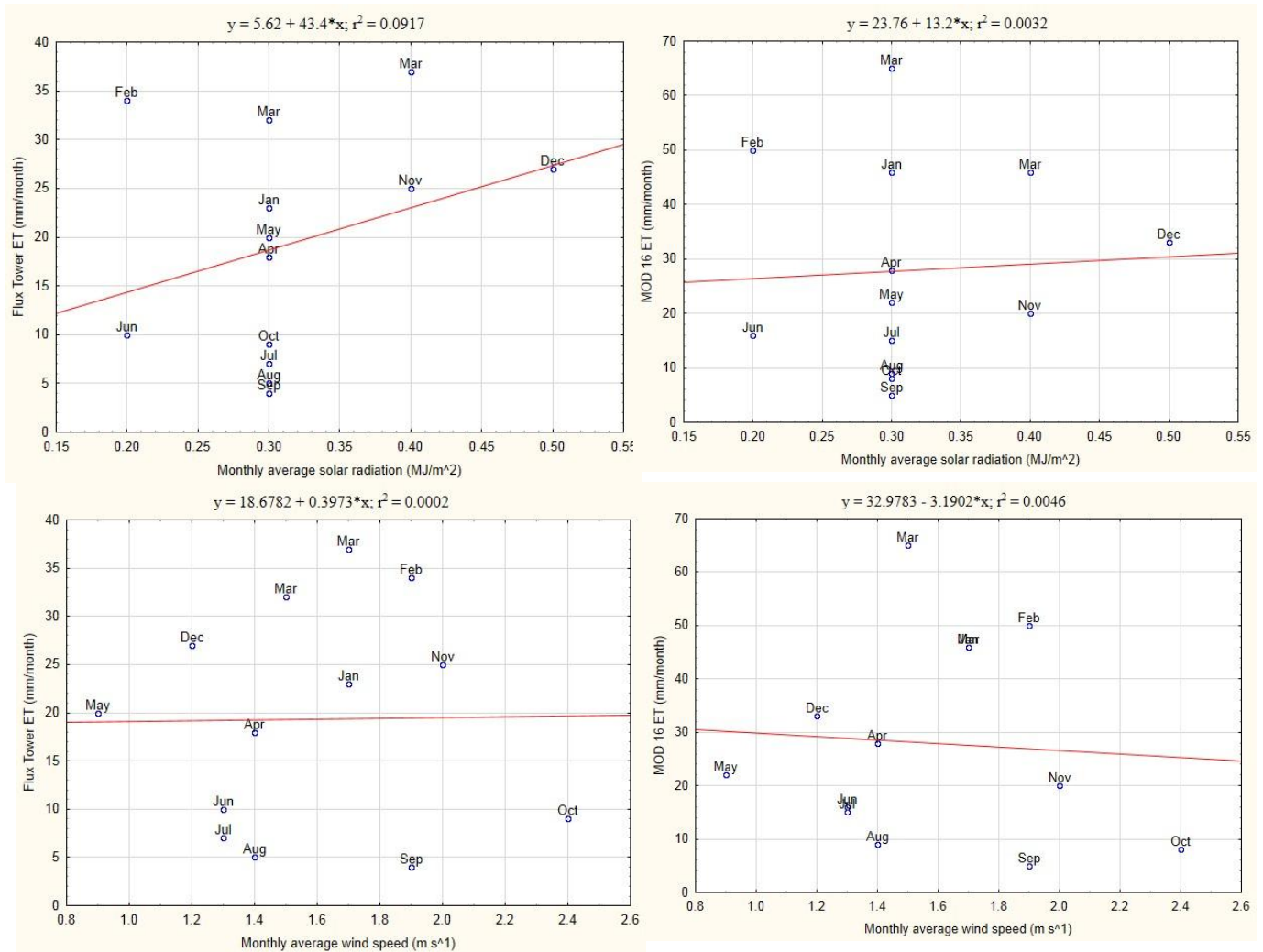


Figure 4.8: The relationship between weather factors and actual ET derived from a flux tower and MODIS ET (mm/month) at Malopeni

#### 4.2.4 Relationship between Flux tower ET and MOD 16 ET at Malopeni

There is a moderate relationship between flux tower ET and MOD 16 ET ( $R^2 = 0.76$ ), but MOD 16 slightly overestimated ET (RMSE = 8.6 mm/month) (Figure 4.9). The ET values are closely related throughout the year, but MOD 16 slightly overestimated during summer months.

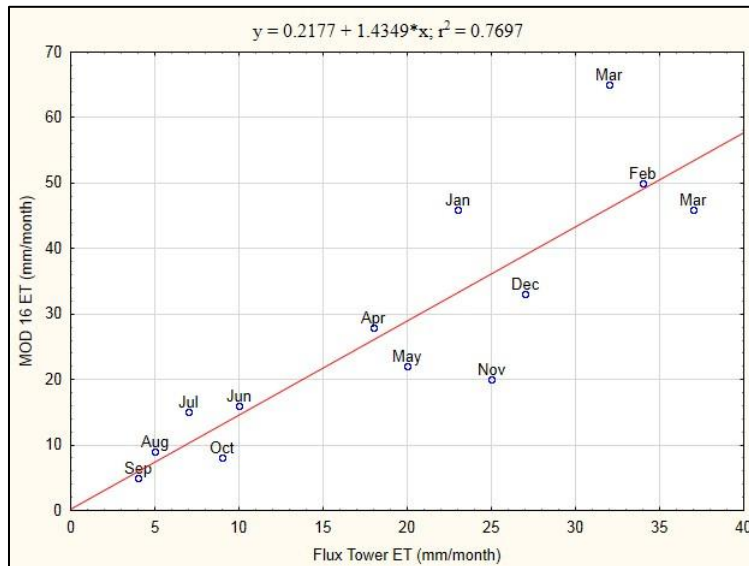


Figure 4.9: The relationship between flux tower ET and MOD 16 ET (mm/month) at Malopeni

#### 4.2.5 The effect of weather factors on ground measured actual ET and MODIS ET at Skukuza

In Skukuza actual ET was measured using an eddy covariance flux tower from 2000-2012. The eddy covariance flux tower was installed at 25.01184°S, 31.29813°E and the monthly MOD 16 ET data for this period was downloaded from <http://www.ntsg.umn.edu/project/mod16>, accessed on 28 March 2016). The weather data obtained from CSIR for the Skukuza site are in years (2009 and 2011), therefore for the Skukuza site the comparison was done in years. In 2009 there was a weak relationship between flux tower ET and relative humidity ( $R^2 = 0.41$ ) and air temperature ( $R^2 = 0.37$ ). Furthermore there is a weak relationship between MOD 16 ET and relative humidity ( $R^2 = 0.47$ ) and air temperature ( $R^2 = 0.36$ ) (Figure 4.10).



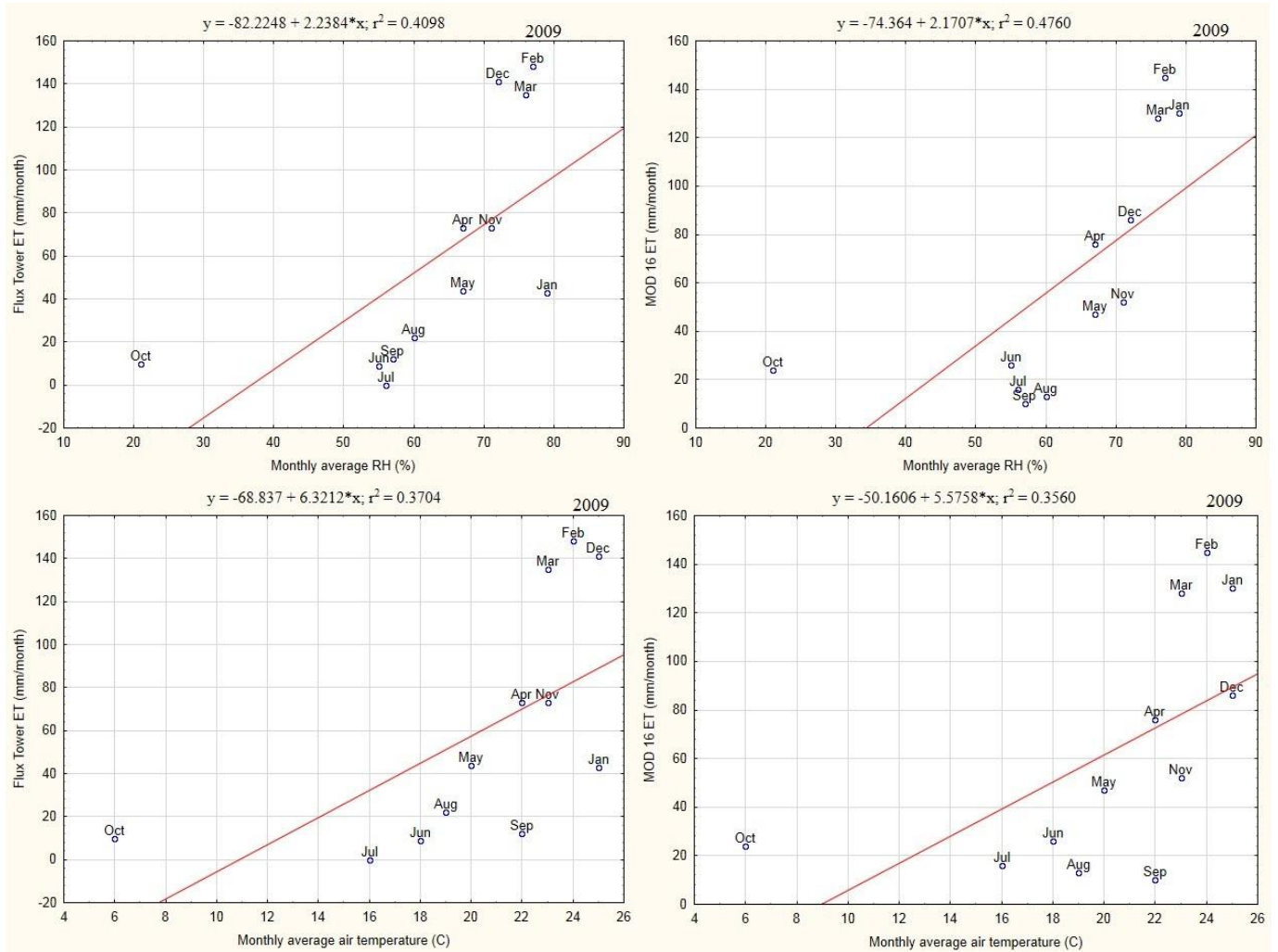


Figure 4.10: The relationship between weather factors and actual ET derived from flux tower and MODIS ET at Skukuza (2009)

In 2011 there is a moderate relationship between flux tower ET and relative humidity ( $R^2 = 0.63$ ) and air temperature ( $R^2 = 0.54$ ). Moreover there is a moderate relationship between MOD 16 ET and relative humidity ( $R^2 = 0.69$ ) and air temperature ( $R^2 = 0.57$ ) (Figure 4.11).

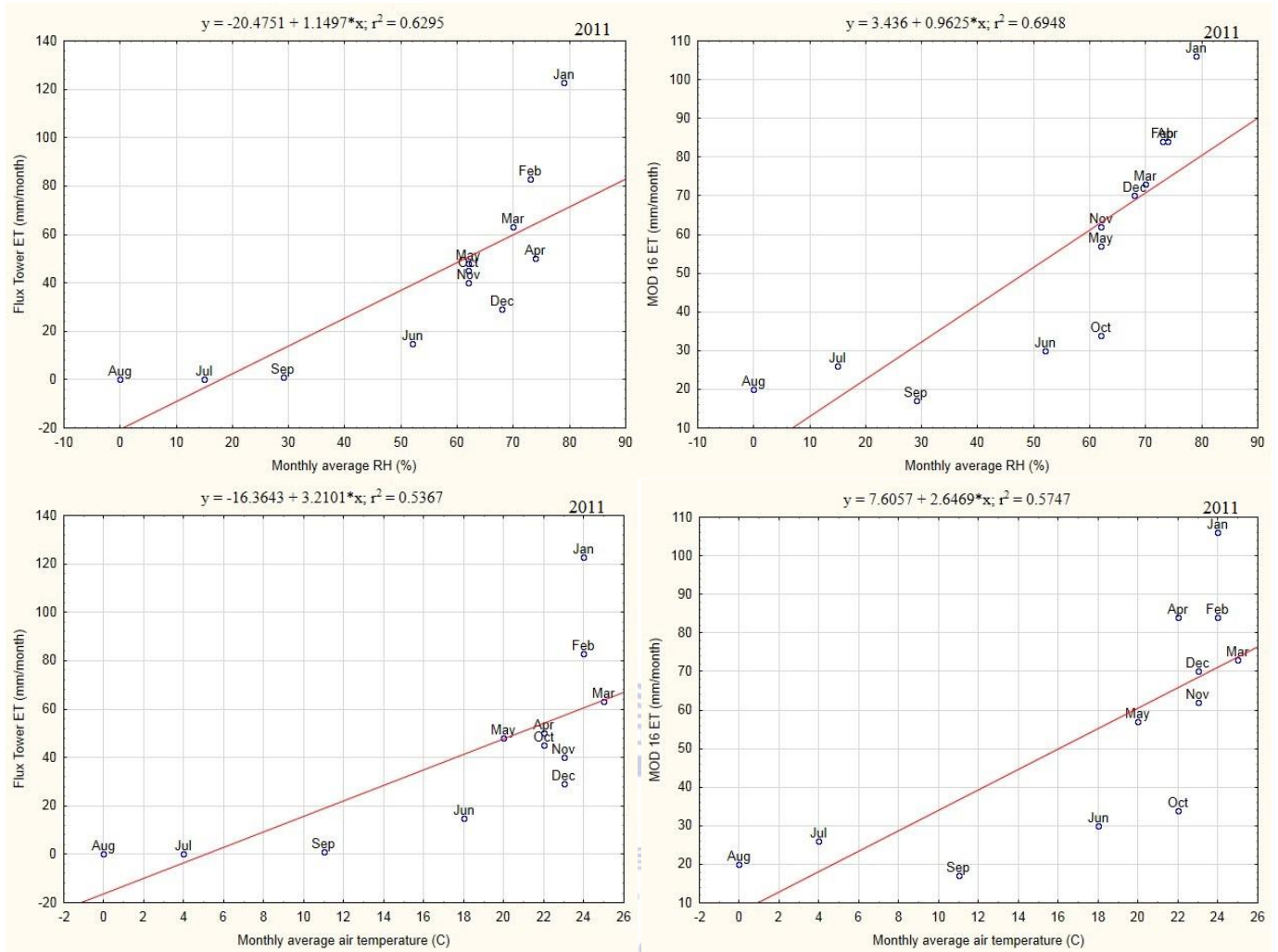


Figure 4.11: The relationship between weather factors and actual ET derived from flux tower and MODIS ET at Skukuza (2011)

In comparison, 2009 achieved the weak relationship between weather factors and ET derived from flux tower and MOD 16 ET, whereas 2011 achieved the moderate relationship between weather factors and ET derived from flux tower and MOD 16 ET. Issues like malfunction of equipment and change in climatic conditions have an impact in the results of these years. Generally, there was a moderate relationship between weather factors such as solar radiation, air temperature and relative humidity and ET derived from flux towers and MOD 16 ET at Skukuza. These weather factors are therefore important in predicting actual ET.

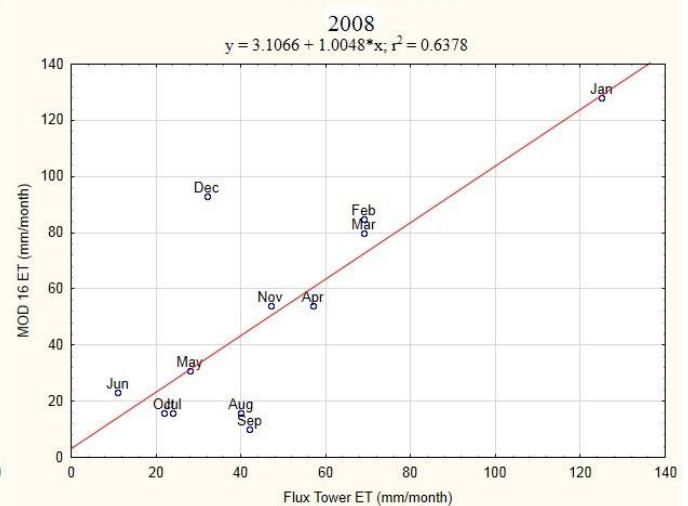
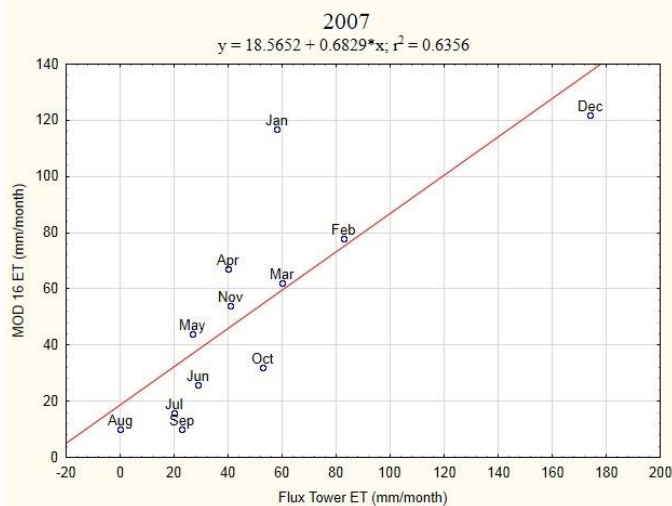
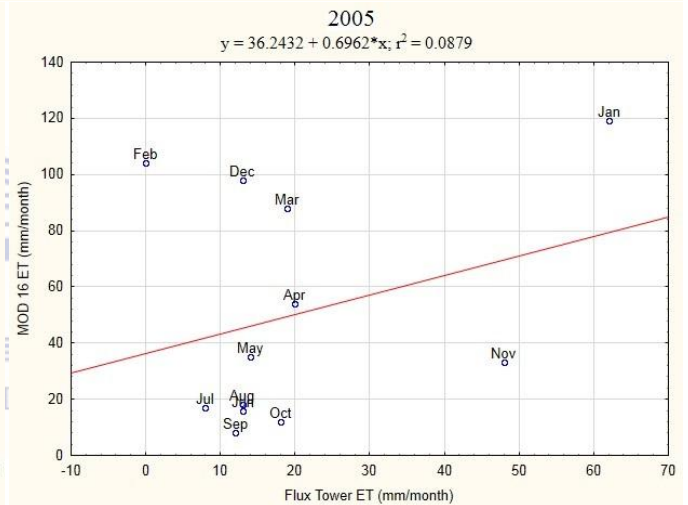
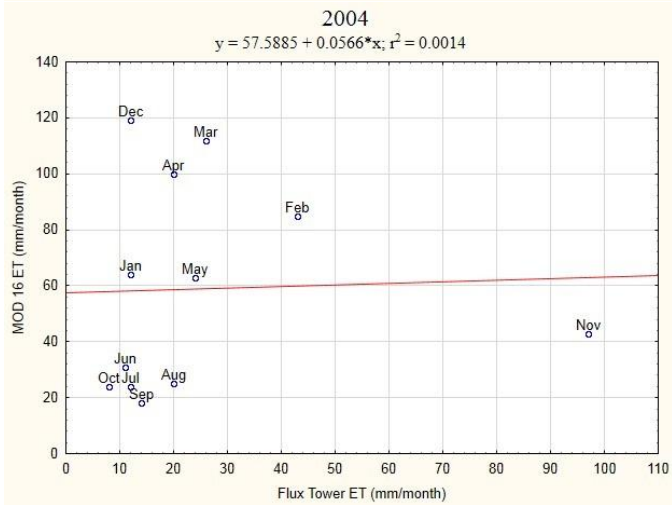
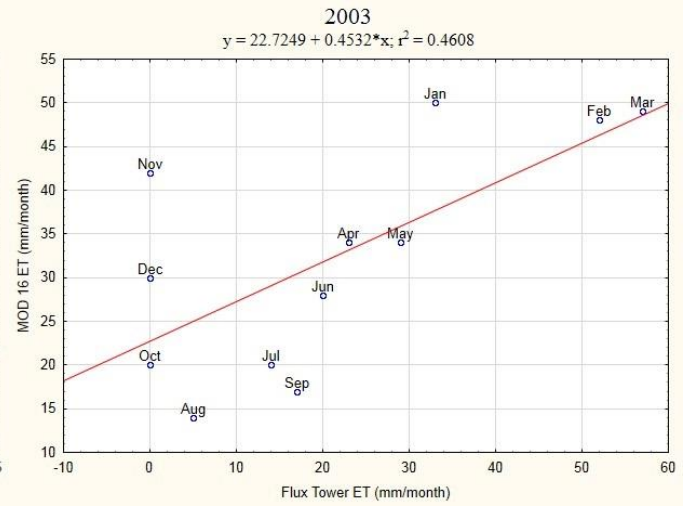
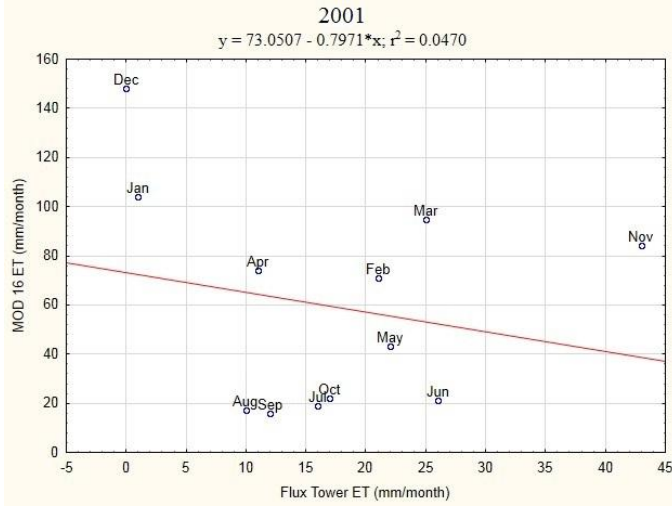
However wind speed was omitted in the comparison because of lack of sufficient wind data. The poor comparison of weather factors and MOD 16 ET and ET derived from flux towers is expected to cause substantial errors in predictions of ET.

#### 4.2.6 Relationship between Flux tower ET and MOD 16 ET at Skukuza

The flux tower ET was compared with MOD 16 ET from 2000-2012 (Figure 4.12). The comparison was done in years because the data obtained from CSIR was in years. The years 2000, 2002, 2006 and 2012 were excluded from analysis due to missing data. The results showed a varying comparison of the flux tower ET and MOD 16 ET over this period of time.

From 2000-2012, excluding 2000, 2002, 2006 and 2012, the lowest correlations were obtained in 2001, 2004 and 2005 achieving ( $R^2$  0.04, 0.001 and 0.08) between MOD 16 ET and actual ET derived from flux tower measurements. Based on RMSE, 2007 ( $R^2 = 0.64$ , RMSE = 2.49 mm/month), 2008 ( $R^2 = 0.64$ , RMSE = 3.24 mm/month), 2009 ( $R^2 = 0.65$ , RMSE = 3.53 mm/month), 2010 ( $R^2 = 0.89$ , RMSE = 6.8 mm/month) achieved the lowest values which indicates reasonable accuracy of the MOD 16 ET product. The inconsistency of the results may be due to change in land cover and land use types and change in climatic conditions over this period. In general, Skukuza results showed that there is an overestimation of MOD 16 ET from 2001-2011.

In 2001, 2003, 2004 and 2005 there was evidence of high overestimation of MOD 16 ET, while in 2007, 2008, 2009 and 2010 low bias and low PBias were obtained confirming the reasonable prediction of MOD 16 ET during these years. Flux tower measurements are mainly influenced by weather conditions. Flux tower sensors either record abnormal values or do not record any data during rainy and stormy days (Ramoelo *et al.*, 2014). This is noticeable in Skukuza, as MOD 16 ET values are higher than flux tower ET values particularly during summer wet months, typically for years with gaps in data. During years with almost complete data MOD 16 ET values are closely related to flux tower ET values, accepting a substantial accuracy in MOD 16 ET. Having full monthly flux tower data measurements was marked to be an advantage in 2010, as this year attained a good relationship between MOD 16 ET and flux tower ET.



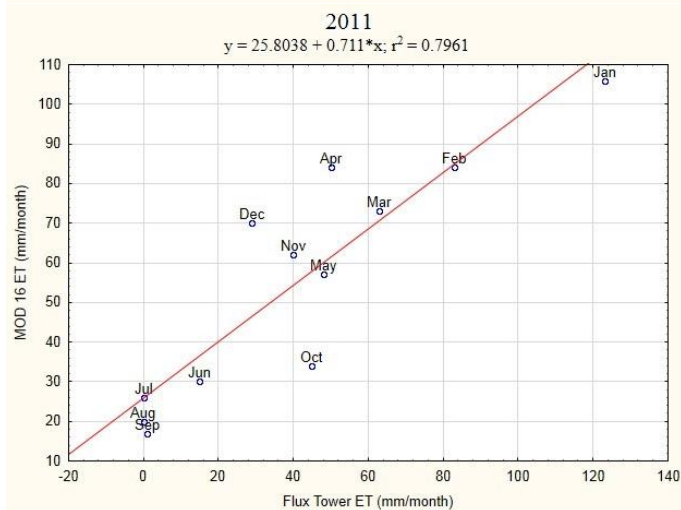
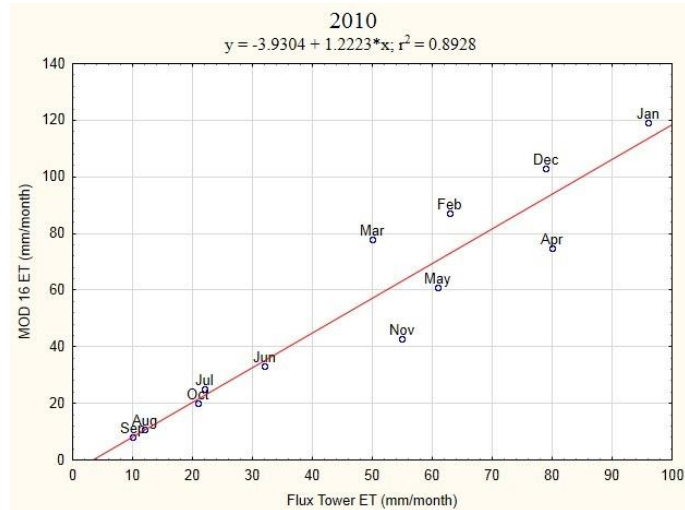
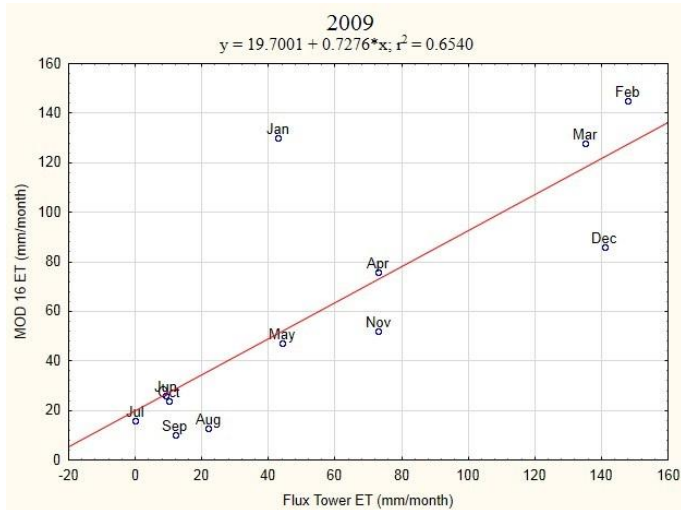


Figure 4.12: The relationship between flux tower ET and MOD 16 ET (mm/month) from 2001-2011 at Skukuza

A statistical t-test analysis was applied to examine the similarities between MOD 16 ET and ground based estimates of ET (Table 4.1, 4.2 and 4.3).

*Table 4.1: t-test variables used to test the similarities between MODIS and ground based estimates of ET at Malopeni site.*

<b>ET</b>	<b>Period</b>	<b>Sample mean</b>	<b>Standard dev.</b>	<b>Sample no.</b>	<b>sp</b>	<b>t</b>	<b>Critical value</b>
Flux tower ET	Mar 2009-Mar 2010	19	11.6	13	16.26	-1.41	2.06
MOD 16 ET	Mar 2009-Mar 2010	28	18.8	13			

The null hypothesis tested on this analysis stated that there is no difference between the average of flux tower ET and MOD 16 ET, was not rejected. Therefore these results suggest that there is no significant difference between the ET estimated using flux towers and MOD 16 ET.

*Table 4.2: t-test variables used to test the similarities between MOD 16 ET and ground based estimates of ET at Skukuza site.*

<b>ET</b>	<b>Period</b>	<b>Sample mean</b>	<b>Standard dev.</b>	<b>Sample no.</b>	<b>sp</b>	<b>t</b>	<b>Critical value</b>
Flux tower ET	2001-2011	36.56	29.80	9	35.24	-0.9	2.12
MOD 16 ET	2001-2011	53.11	36.32	9			

The null hypothesis tested on this analysis stated that there is no difference between the annual average of flux tower ET and MOD 16 ET, was not rejected. Therefore these results suggest that there is no significant difference between the annual averages of ET estimated using flux towers and MOD 16 ET.

*Table 4.3: t-test variables used to test the similarities between MOD 16 ET and ground based estimates of ET at Elandsberg site.*

<b>ET</b>	<b>Period</b>	<b>Sample mean</b>	<b>Standard dev.</b>	<b>Sample no.</b>	<b>sp</b>	<b>t</b>	<b>Critical value</b>
Scintillometer ET	Nov 2012- Nov 2013	57	30	12	22.59	3.04	2.07
MOD 16 ET	Nov 2012- Nov21- 2013	29	6	12			

The null hypothesis tested on this analysis stated that there is no difference between the average of scintillometer ET and MOD 16 ET, was rejected. Thus, the results support the alternative hypothesis that the ET derived from Scintillometer differs from MOD 16 ET.

According to the t-test analysis it was found that there is a difference between average of MOD 16 ET and average of ET derived from scintillometer in Elandsberg site, which means that MOD 16 underestimated ET in Mediterranean climate of the Western Cape. The t-test analysis also found that there is no meaningful variation between average of MOD 16 ET and average of ET derived from flux towers in Skukuza and Malopeni sites, which means that MOD 16 is reasonably accurate although slightly overestimated ET in Sub-tropical climate of the Limpopo province. Poor comparison of weather factors such as: wind speed, temperature and humidity with flux tower ET and MOD 16 ET in 2009 have an impact in underestimation and overestimation of ET in the Sub-tropical climate of the Limpopo Province. The different land cover types found in different parts of the catchment also possibly cause the underestimation and overestimation of ET. This is as a result of land cover types requiring different amount of water; some consume a lot of water such as forests and others such as cultivated dryland consume less water thus they have different ET rates.

### 4.3 Seasonal and interannual variation of MOD 16 ET

#### 4.3.1 Letaba catchment

The seasonal (wet and dry seasons) and interannual (year to year variation) variations of MOD 16 ET are examined in this section. To determine MOD 16 ET seasonal and interannual variations, monthly MOD 16 ET maps for 2000-2012 for the Letaba catchment were created (Appendix A). For all the 13 years analyzed, Jan to Jun are wet, and Jul to Dec are dry, except for 2000 (Figure 4.13), and 2003 (Figure 4.14). The year 2000 and 2003 were selected to be presented because 2000 (ET = 752 mm/year) was relatively wet and 2003 (ET = 396 mm/year) was relatively dry. The months Jan and Feb were selected to represent the wet season, Aug and Sep were selected to represent the dry season. These months were selected because the interest was generally on the rates of ET during wet and dry seasons respectively.

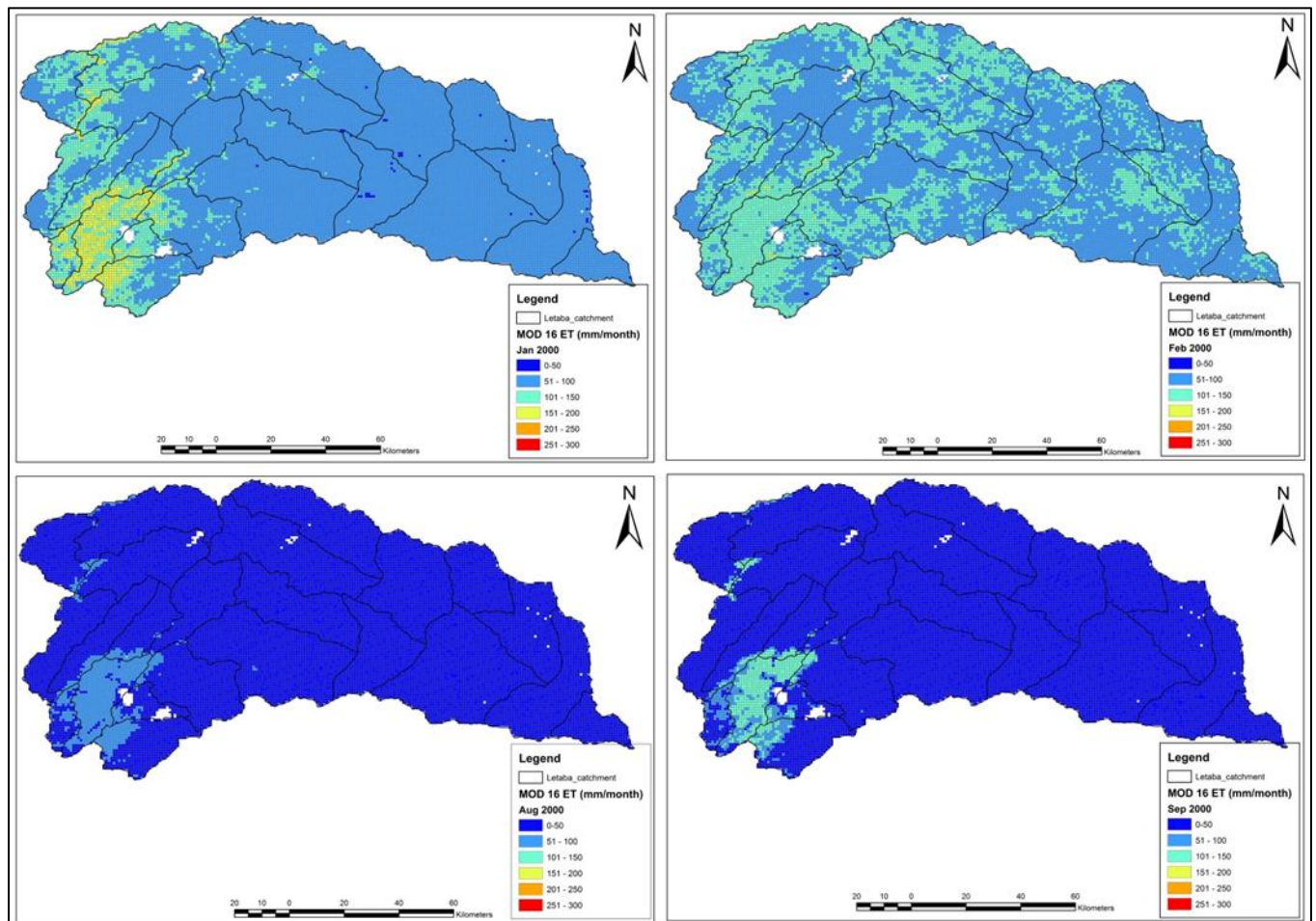


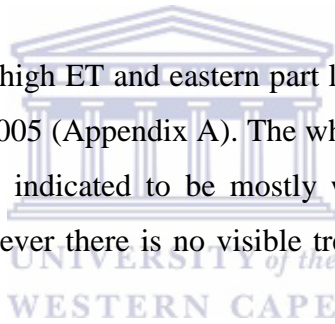
Figure 4.13: MOD 16 monthly evapotranspiration rates for Jan (top left), Feb (top right), Aug (bottom left) and Sep (bottom right) in 2000 for Letaba catchment at a pixel resolution of approximately 1 km.



High ET occurred in the western part of the catchment throughout the year (101-250 mm/month), and low ET occurred in the eastern part especially in dry season (0-50 mm/month and 51-100 mm/month). High ET occurs in summer because of availability of solar radiation and moisture. According to Xu & Singh (2005), soil moisture is the dominating factor controlling actual ET in warmer and drier months. Therefore, at the beginning of dry season the soil is moist thus the ET is high while in the mid dry season (Aug and Sep) the soil is dry, due to low availability of moisture hence the ET is low.

The land cover type map (Figure 3.8) shows the existence of irrigation and forest plantations in the western part of the catchment that utilizes high volumes of water; hence this part had relatively high ET in all years. The eastern part of the catchment has low lying plains which receive low rainfall. These areas have woodland, bush, and bush clumps which have adjusted to dry conditions and have low ET rates. Areas with free water surfaces (lakes) had very high rates of ET.

The same pattern (i.e western part high ET and eastern part low ET) is shown in all other part years, except in 2003 (Figure 4.14) and 2005 (Appendix A). The whole catchment was relatively dry in these years. Although other years indicated to be mostly wet during the rainfall season and mostly dry in the dry season, however there is no visible trend of how ET varies from year to year.



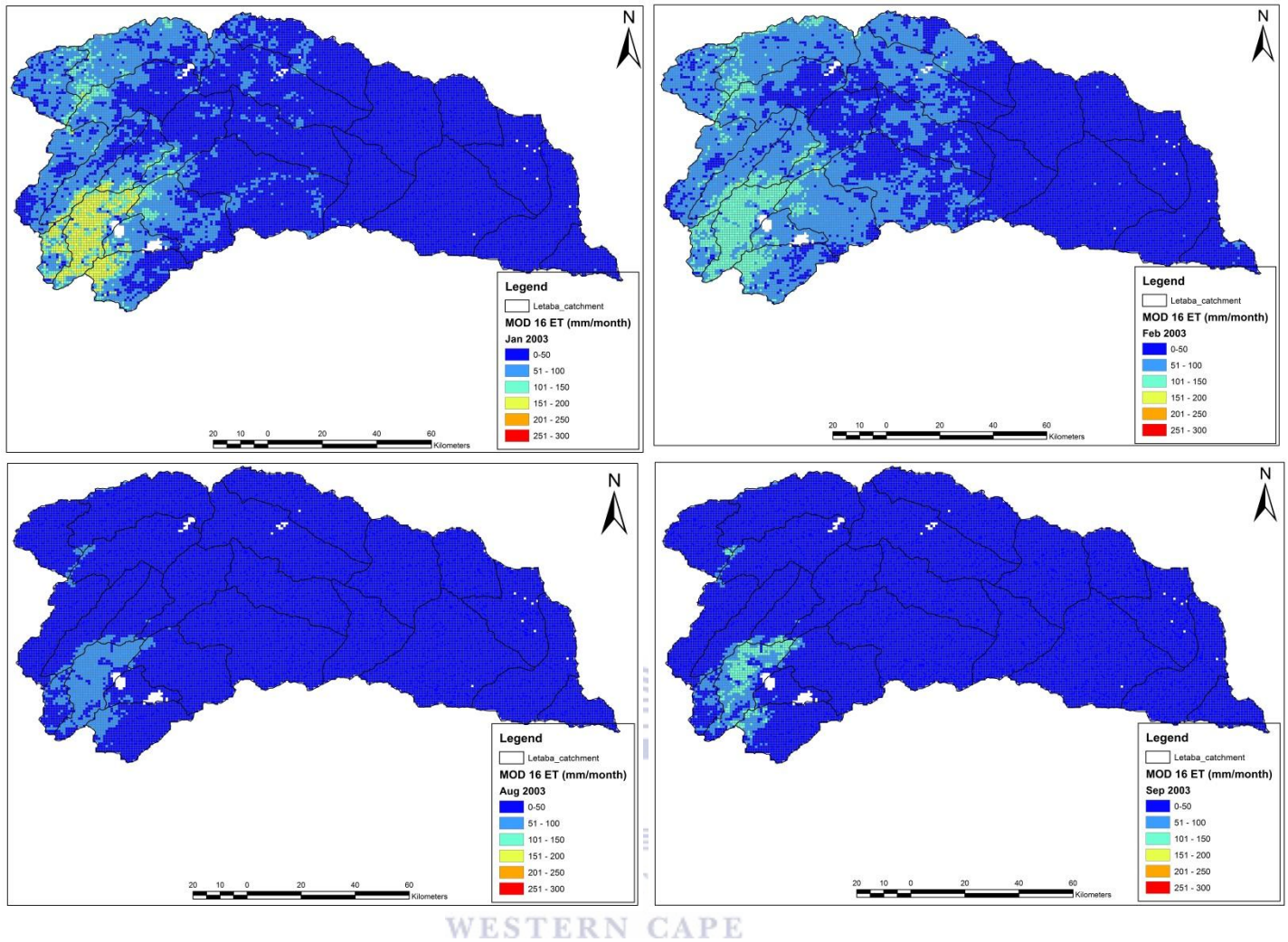


Figure 4.14: MOD 16 monthly evapotranspiration rates for Jan (top left), Feb (top right), Aug (bottom left) and Sep (bottom right) in 2003 for Letaba catchment at a pixel resolution of approximately 1 km.

The average of all pixel values were used to obtain the monthly ET estimates. The results in Figure 4.15 indicates that all the years follow a similar pattern, with relatively high monthly average ET in summer rainfall season (Jan- Apr) and low monthly average ET in winter season (May-Sep) and the monthly average ET slightly increases again in early summer (Oct- Dec). These results are rather expected in the Letaba catchment. The Letaba catchment receives rainfall during summer period and there is also high evaporative demand, thus high ET occurs. During winter period the catchment is relatively dry and the evaporative demand is low therefore low ET occurs. The variations in ET are mainly caused by weather factors such as rainfall, solar radiation, relative humidity and air temperature. The ET process is determined by the amount of energy available to vaporize water (Allen *et al.*, 1998). Therefore during summer when there is

high solar radiation the ET rates are high and during winter when there is less solar radiation the rates of ET decrease. Also in summer season when there are high temperatures, the loss of water by ET is greater than in winter season when there are low temperatures.

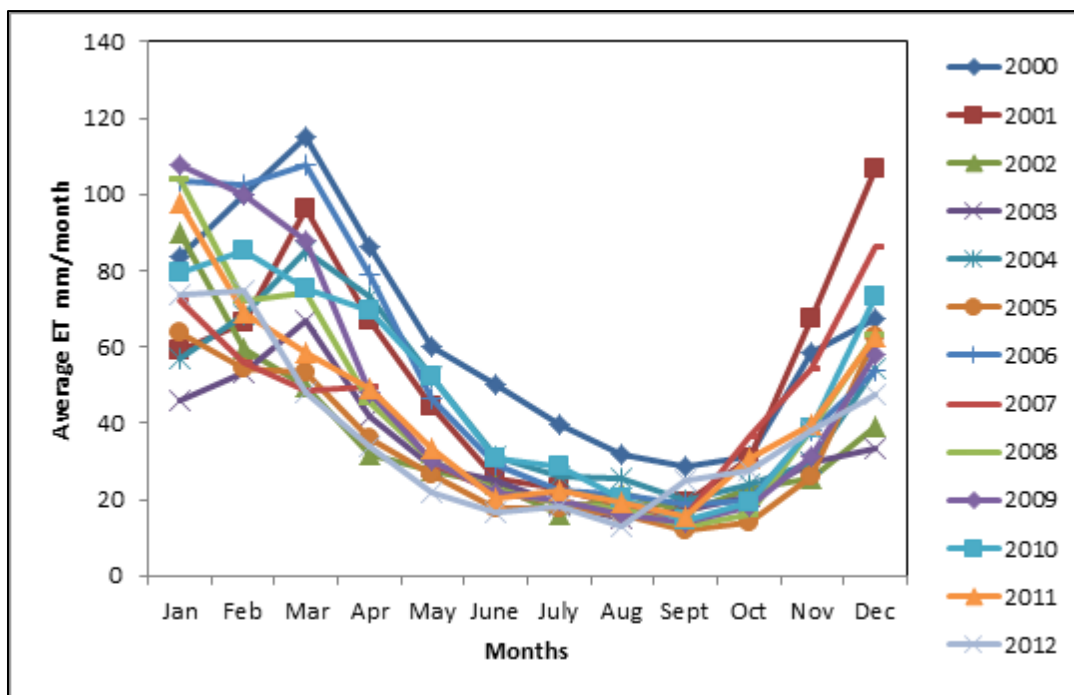


Figure 4.15: Monthly average evapotranspiration rates from 2000-2012 in the Letaba catchment estimated from MOD 16

The year 2000 was the wettest year while 2003 and 2005 were the driest years (Figure 4.16). There is a considerable variation of ET from year to year; some years had high ET and others had slightly low ET. Years with high rainfall had high ET and the years with low rainfall also had low ET. The maximum ET estimated ranges between 198.7-248.2 mm/year, and the minimum ET estimated ranges between 2.5- 7.9 mm/year (Table 4.4). The lowest minimum value was estimated in 2012 (2.5 mm/year) and the highest minimum value was estimated in 2000 (7.9 mm/year). This means there was a considerable spatial variability in rainfall received by the catchment in each year. The years that had relatively high maximum and minimum values also had higher median values than the years that had low maximum and minimum values. The standard deviations are relatively high for all the years, with the least one being 26.62 mm/year in 2003 and the highest on being 39.10 mm/year in 2006. This indicates that a wide range of values were observed in all years.

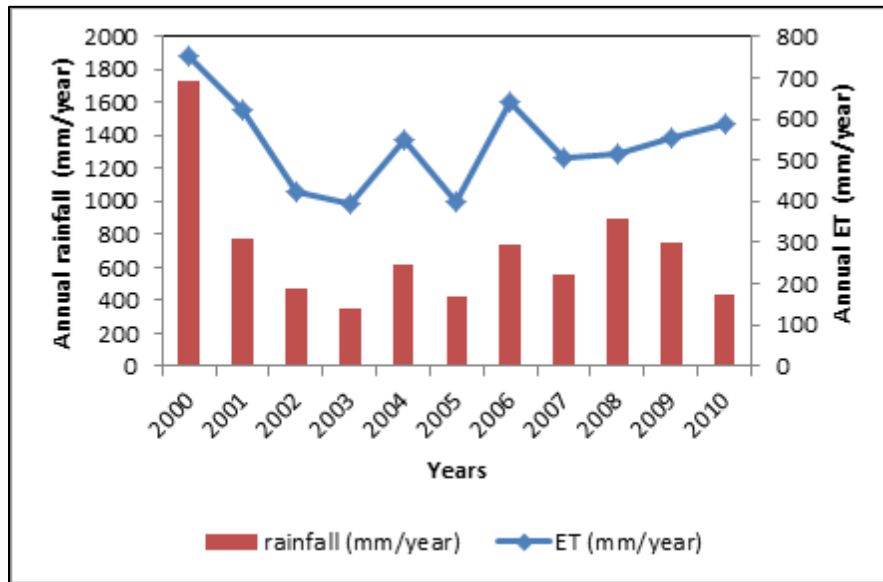


Figure 4.16: MOD 16 annual average evapotranspiration and annual rainfall from 2000-2012 in the Letaba catchment.

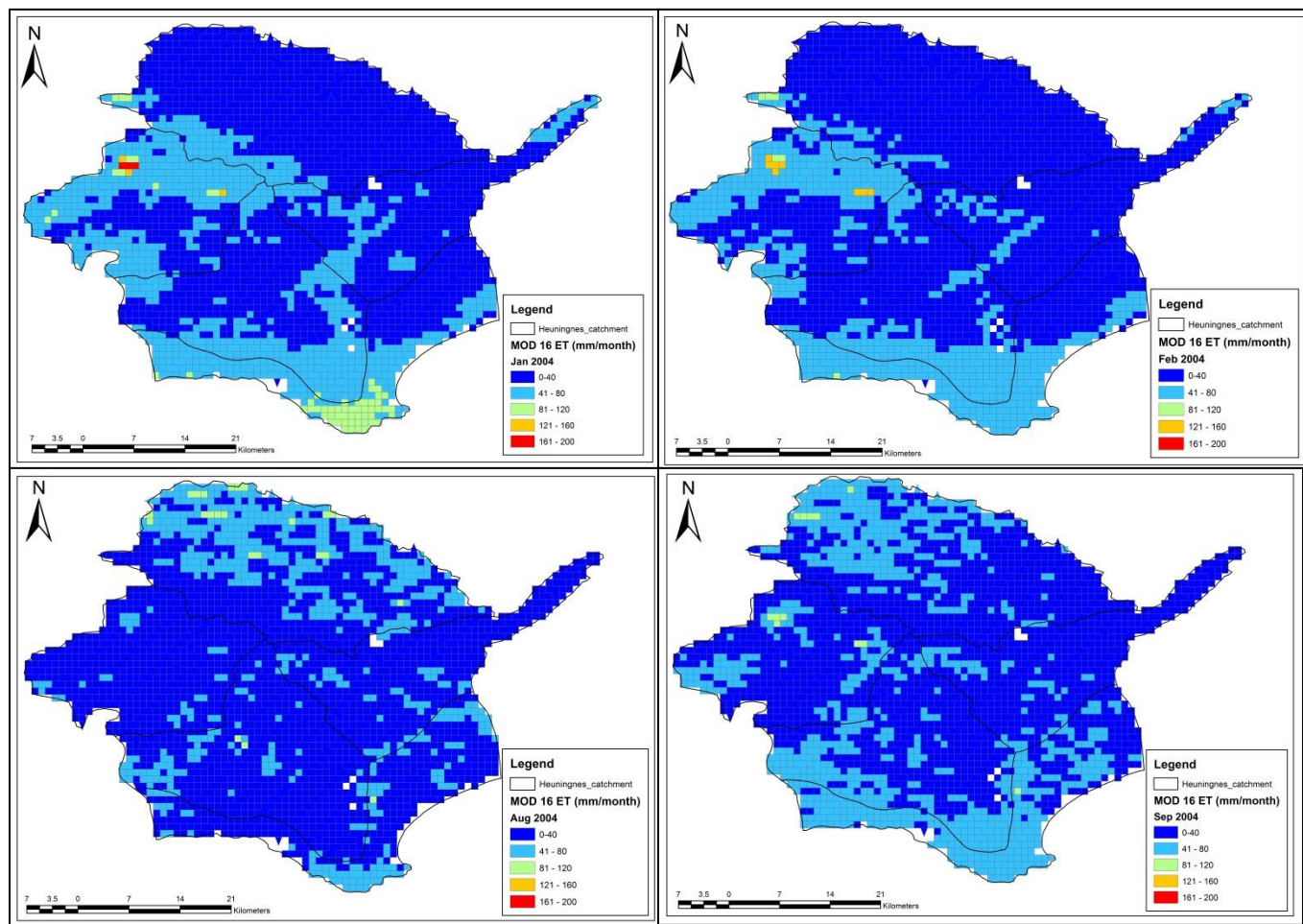
Table 4.4: Descriptive statistics of MOD 16 ET from 2000-2012 in the Letaba catchment

	Years												
Statistical parameters	2000	2001	2002	2003	2004	2005	2006	2007	2008	2009	2010	2011	2012
Maximum (mm/year)	229.3	248.2	254.8	198.7	201.4	217	237.9	238.2	213.4	248.8	231.8	240.1	217.2
Minimum (mm/year)	7.9	5.8	5	5.8	5.4	2.9	4.8	4.3	3.4	3.5	3.3	3.4	2.5
Median (mm/year)	55.4	46.1	22.7	23.3	37.4	22.2	38.3	34.8	28.8	27.3	45.3	32.4	24.7
Standard deviation (mm/year)	33.6	34.4	30.9	26.6	29.5	28.0	39.1	30.7	34.7	38.9	33.0	32.6	29.9

### 4.3.2 Heuningnes catchment

For all the 13 years analyzed (Appendix B), ET decreases from Jan to Jun and increases from Jul to Dec. The year 2004 (Figure 4.17) and 2008 (Figure 4.18) were selected because 2004 (ET = 403 mm/year) was relatively dry and 2008 (ET = 465 mm/year) was relatively wet. The months Jan and Feb were selected to represent the dry season, Aug and Sep were selected to represent the wet season. These months were selected because the interest was generally on the rates of ET during wet and dry seasons respectively.

In summer season the northern part had low ET (ranging from 0-40 mm/month) during all the years. This part of the catchment corresponds to dry land as shown in the land cover types map (Figure 3.5), thus low ET occurs. The southern part of the catchment which is a low land is always wet during summer season (range of ET from 81-160 mm/month). This part has wetlands and fynbos, hence there is high ET. In winter there is high spatial variability of ET across the whole catchment (range of ET 0-80 mm/month). There are few noticeable areas with high ET throughout the year, these areas coincide with the wetlands in the catchment. High ET occurs at the beginning of warm dry season, because the soil is relatively moist and there is high evaporative demand and low ET occurs in cold wet season; in this season there is high rainfall but less sunshine thus less evaporative demand.



UNIVERSITY of the  
WESTERN CAPE

Figure 4.17: MOD 16 monthly evapotranspiration rates for January (top left), February (top right), August (bottom left) and September (bottom right) in 2004 for the Heuningnes catchment at a pixel resolution of approximately 1 km.

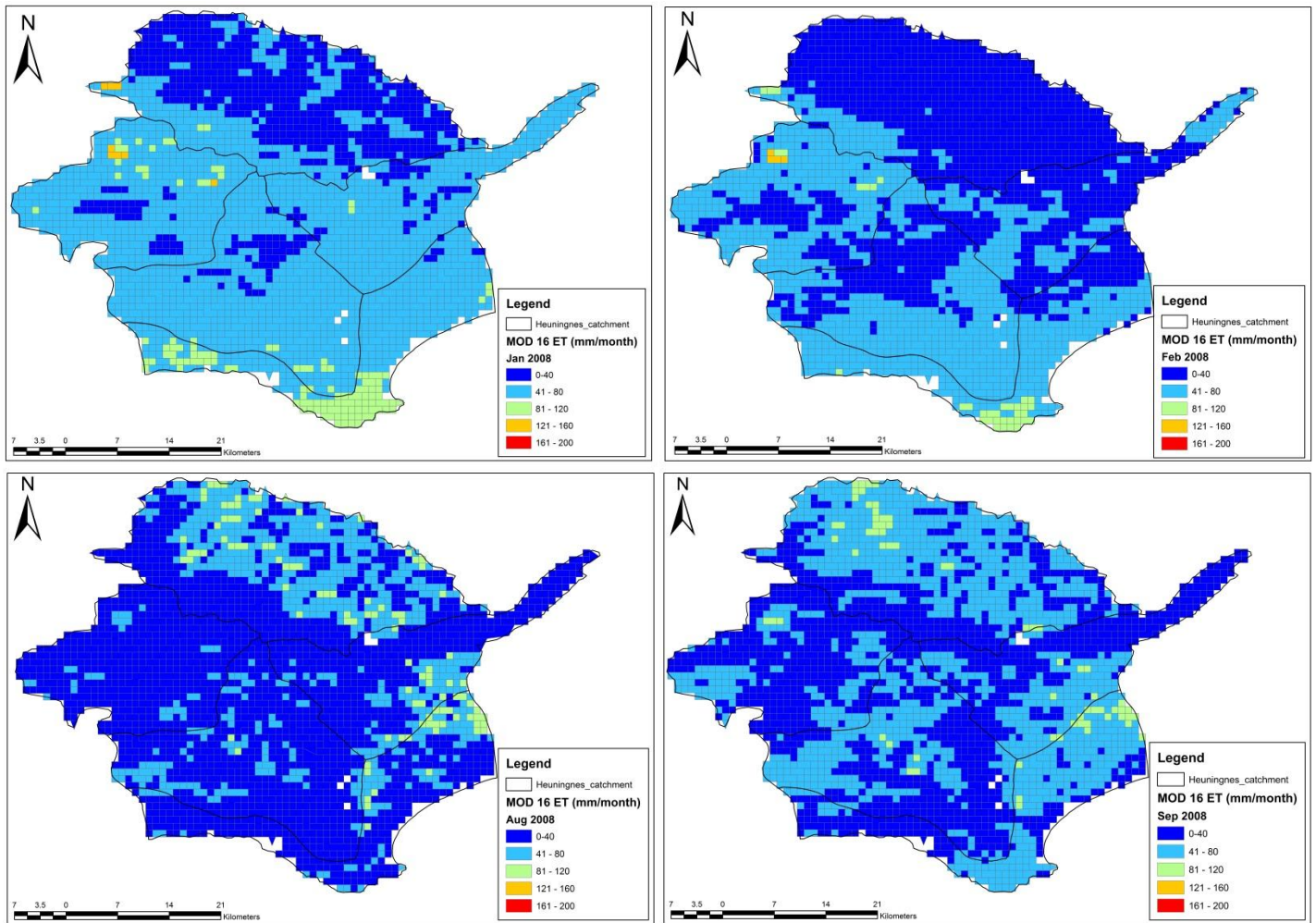


Figure 4.18: MOD 16 monthly evapotranspiration rates for January (top left), February (top right), August (bottom left) and September (bottom right) in 2008 for the Heuningnes catchment at a pixel resolution of approximately 1 km.

The average of all pixel values were used to obtain the monthly ET estimates. All the years follow a similar pattern with monthly average ET slightly decreasing in January until June (30 mm/month- 20 mm/month) and increasing from July until December (25 mm/month- 60 mm/month) (Figure 4.19). At the end of summer dry period, the ET is low because the soil is relatively dry. During winter wet season, the soil conditions are relatively moist allowing high ET to occur but there is low evaporative demand due to less energy coming from the solar radiation therefore a lot of water is stored and becomes evaporated at the beginning of summer dry season (October) when the temperatures are high and evaporative demand is high.

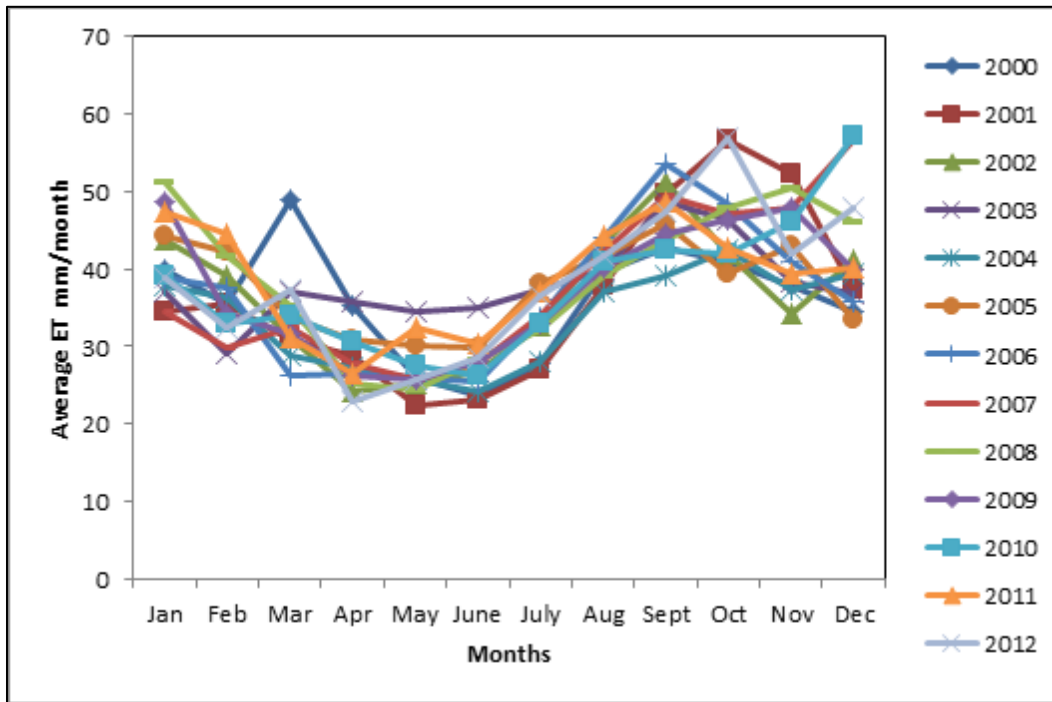


Figure 4.19: MOD16 monthly average evapotranspiration from 2000-2012 in the Heuningnes catchment

There are variations of ET over the years; some years had high ET and others had slightly low ET. Years with high rainfall had high ET and the years with low rainfall also had low ET (Figure 4.20). Generally it is apparent that MOD 16 ET is higher in the Letaba catchment (Sub-tropical region) compared to the Heuningnes catchment (Mediterranean region) in some years and lower in other years from 2000-2012. This observation is rather expected as a study by Jovanovic *et al.*, (2015), established that ET was higher in summer rainfall areas compared to winter rainfall areas in some years, and lower in other years, depending on rainfall pattern and distribution. The maximum ET estimated ranges from 140 to 172.8 mm/year and the minimum ET ranges from 15 to 19.6 mm/year (Table 4.5). This means there was a spatial variation of rainfall received in the catchment from year to year. The median values ranged between 30-35.7 mm/year throughout all the years. The standard deviations are relatively high for all the years ranging from 12- 15.76. This indicates that a range of values were observed from all years.



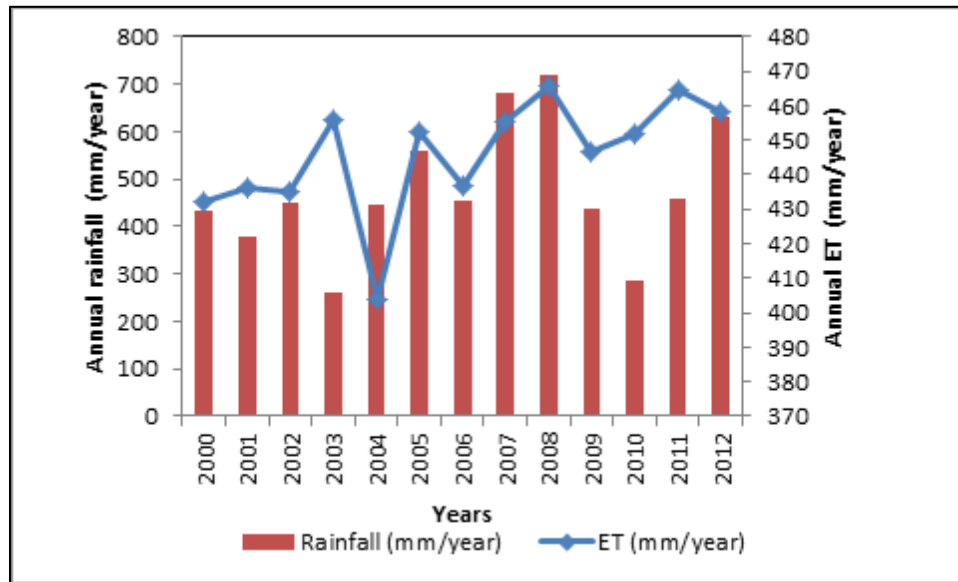


Figure 4.20: MOD 16 annual average evapotranspiration and annual average rainfall from 2000-2012 in the Heuningnes catchment

Table 4.5: Descriptive statistics of MOD 16 ET from 2000-2012 in the Heuningnes catchment

	Years												
Statistical parameters	2000	2001	2002	2003	2004	2005	2006	2007	2008	2009	2010	2011	2012
Maximum (mm/year)	140	156	150.3	164.7	164.2	161.1	154.2	163.5	169.8	163.4	150.1	159.7	172.8
Minimum (mm/year)	16.2	16.5	15	15.4	15.7	16.6	16.3	15.9	16	16.3	19.6	16.9	15.2
Median (mm/year)	33.4	31.8	32	35.1	30.8	34.4	32.1	33.7	35.7	33.2	33.6	34.3	33.5
Standard deviation (mm/year)	13.0	15.6	15.0	13.9	12.4	13.0	15.3	15.7	14.9	14.9	14.1	15.3	15.8

In comparison, the seasonal and interannual variations of MOD 16 ET differ between the Letaba and Heuningnes Catchments. The catchments have different climatic conditions. The Letaba catchment is characterized by summer rainfall, thus ET is high in summer and the Heuningnes catchment is characterized by winter rainfall, hence ET is high in winter. Highest ET was obtained in the western part of the Letaba catchment (range from 101-250 mm/month) and highest ET was obtained in the southern part of the Heuningnes catchment (range from 81-160 mm/month). These variations are due to the land cover and land use types that are found in these areas and the topography of these areas. The interannual variations of MOD 16 ET differed in these catchments; in Letaba ET had decreased over the 13 years period and had increased in the Heuningnes catchment. The years with high rainfall also had high ET in both catchments.



## Chapter 5: Variations of ET with land cover

### 5.1 Introduction

This chapter presents and discusses the second and third objectives. The objectives are: to examine whether ET rates estimated by MOD 16 capture the variation of actual ET with land cover and land use types in the selected catchments, and also to evaluate whether MOD 16 can be used to identify areas with shallow groundwater. The results of the spatial variation of MOD 16 ET in the Letaba and Heuningnes catchments are presented. Following those results, ground-truthing results are presented. Ground-truthing was done to check the vegetation, land cover and land use types in the areas with high spots of ET in the MOD 16 ET maps. Lastly shallow groundwater areas were mapped in both catchments. The purpose was to determine the spatial variation of ET and to evaluate whether MOD 16 ET can be used as a method to map shallow groundwater areas.

### 5.2 Spatial variation of MOD 16 ET in different land cover types

#### 5.2.1 Letaba catchment

Evapotranspiration varies in different land cover types, therefore MOD 16 ET rates captured by different land cover and land use types in the Letaba catchment were extracted using ArcGIS. Figure 5.1 presents MOD 16 evapotranspiration rates captured in different land cover types in 2000 wet year, 2003 dry year and 2004 average year. The years 2000, 2003, and 2004 were selected to be wet, dry, and average years respectively based on the amount of ET they obtained throughout the year. Year 2000 obtained the highest ET (752 mm/year), hence it was regarded as a wet year, 2003 obtained the lowest ET (396 mm/year) thus it was considered as a dry year, and 2004 obtained ET that is more or less the same as other years (547 mm/year), therefore it was used to represent average years.

There is a considerable variation of ET among different land cover types within the same year and between the years. The forest had the highest ET (1204 mm/year in 2000, 1070 mm/year in 2003 and 1130 mm/year in 2004) in both summer and winter seasons compared to all the other land cover types. Cultivated dry land (671 mm/year in 2000, 317 mm/year in 2003 and 437 mm/year in 2004) and urban land (653 mm/year in 2000, 330 mm/year in 2003 and 436 mm/year in 2004) exhibited the smallest ET in both summer and winter compared to all the other land cover types. Actual ET depends upon rainfall, soil properties, climatic conditions, land cover and land use, vegetation and topography which cause it to vary both spatially and temporally (Hafeez

*et al.*, no date). For example the land cover types that are situated in mountainous areas where there is a lot of rainfall reaching the surface the ET rates are likely to be high, whereas the land cover types situated in low land areas that receive low amount of rainfall the ET rates tend to be low.

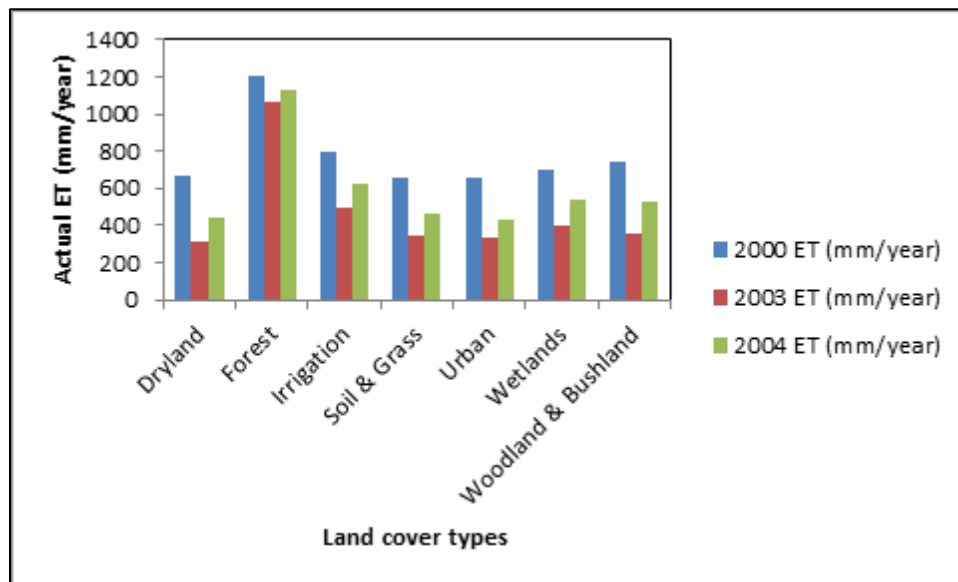


Figure 5.1: MOD 16 ET (mm/year) for different land cover types in 2000 (wet year), 2003 (dry year) and 2004 (average year) in the Letaba catchment

An ANOVA test was undertaken to determine if the actual ET rates for different land cover and land use types were significantly different. The null hypothesis stated that that MOD 16 cannot differentiate actual ET rates in different land cover types ( $\bar{x}_1 = \bar{x}_2 = \bar{x}_3 = \dots \bar{x}_n$ ). The alternative hypothesis stated that MOD 16 has the ability to distinguish differences in the actual ET rates in different land cover types. The test was done at the 5% significance level. The calculated F was greater than  $F_{crit}$  (2.10), therefore null hypothesis was rejected and the results showed that average ET rates differed significantly among the land cover types. These results rather match the results of other studies. Ibrahim *et al.*, (2016), used an ANOVA test to analyse the impact of land surface temperature on different land cover types. The results showed that there is a significant difference in the temperature variation in land cover types.

Furthermore the box and whiskers plots were used to determine the land cover types that have an average ET that differ from the others (Figure 5.2). The forest mean was found different from the means of other land cover types, which ascertains that MOD 16 can distinguish the actual ET rates in different land cover types. This variation is shown in all three years with forest having

the most distinct mean compared to other land cover types. A study by Weligepolage (2005), reported that the analysis of spatial variation in actual ET between different land cover types presented has revealed that the average ET over different land cover types are substantially different from each other. These findings rather match the results of the current study, as forest had ET rates that differed significantly from the other land cover types.

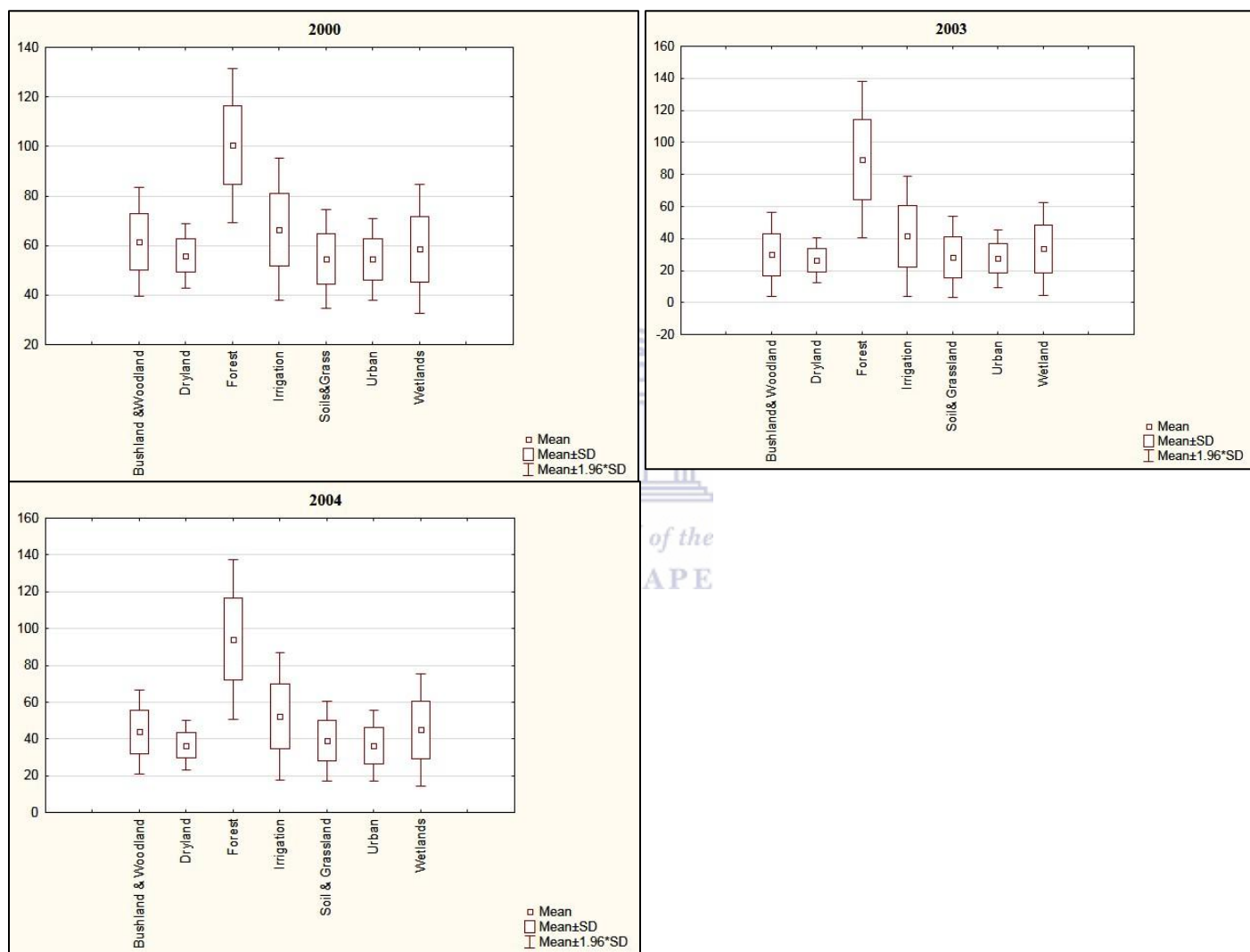


Figure 5.2: The box plots of MOD 16 ET data for different land cover types in 2000 (wet year), 2003 (dry year) and 2004 (average year) in the Letaba catchment

### 5.2.2 Heuningnes Catchment

There is considerable variation of ET in different land cover types within the same year and over the years. Forest had the highest ET in; 2004 (548 mm/year), 2008 (578 mm/year) and 2009 (603 mm/year) compared to all other land cover types (Figure 5.3). Cultivated dry land had relatively low ET in; 2004 (367 mm/year), 2008 (444 mm/year) and 2009 (423 mm/year). Forest plantations have long roots that can abstract water from groundwater, thus they always have high ET rates. The canopy of forest plantations have the holding capacity of water, hence they also play a substantial role in the rates of ET. Cultivated dryland on the other hand had low ET rates because of shallow roots.

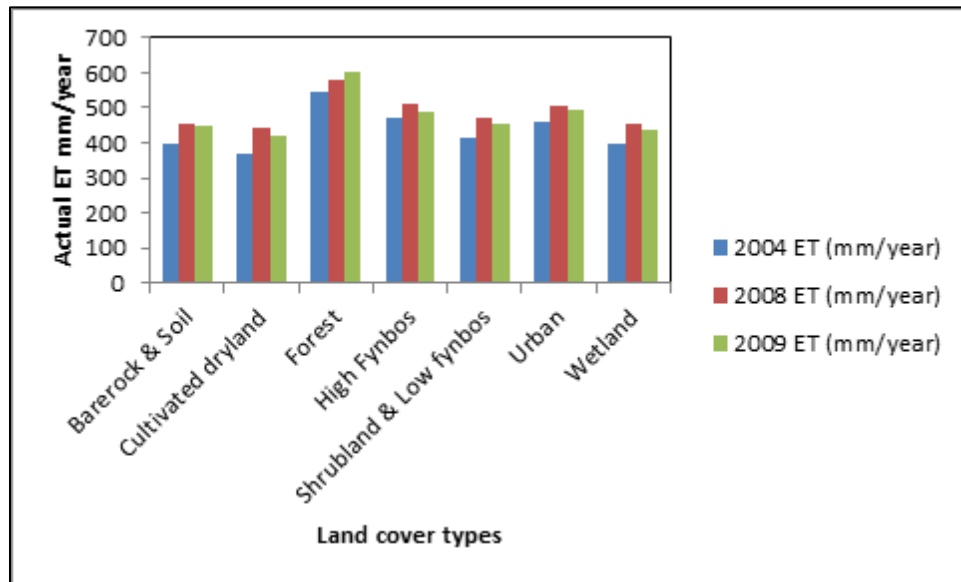


Figure 5.3: MOD 16 ET (mm/year) for different land cover types in 2008 (wet year), 2004 (dry year) and 2009 (average year) in the Heuningnes catchment

An ANOVA test was undertaken to determine if the actual ET rates for different land cover and land use types were significantly different. The null hypothesis stated that that MOD 16 cannot differentiate actual ET rates on different land cover types ( $\bar{x}_1 = \bar{x}_2 = \bar{x}_3 \dots = \bar{x}_n$ ). Where  $n$  is the number of different land cover types. The alternative hypothesis stated that MOD 16 has the ability to distinguish differences in the actual ET rates on different land cover types. The test was done at the 5% significance level. The calculated  $F$  was greater than  $F_{crit}$  (2.10), therefore null hypothesis was rejected and the results showed that average ET rates differed significantly among the land cover types.

Additionally, the box and whiskers plots were used to determine the land cover types that have an average ET differing from the others (Figure 5.4). The forest mean was found significantly different from the means of others. Thus MOD 16 can distinguish the actual ET rates of different land cover types. The variation is shown in all three years with forest having the most distinct mean compared to the other land cover types. There is also a variation in the means and standard deviations of different land cover types.

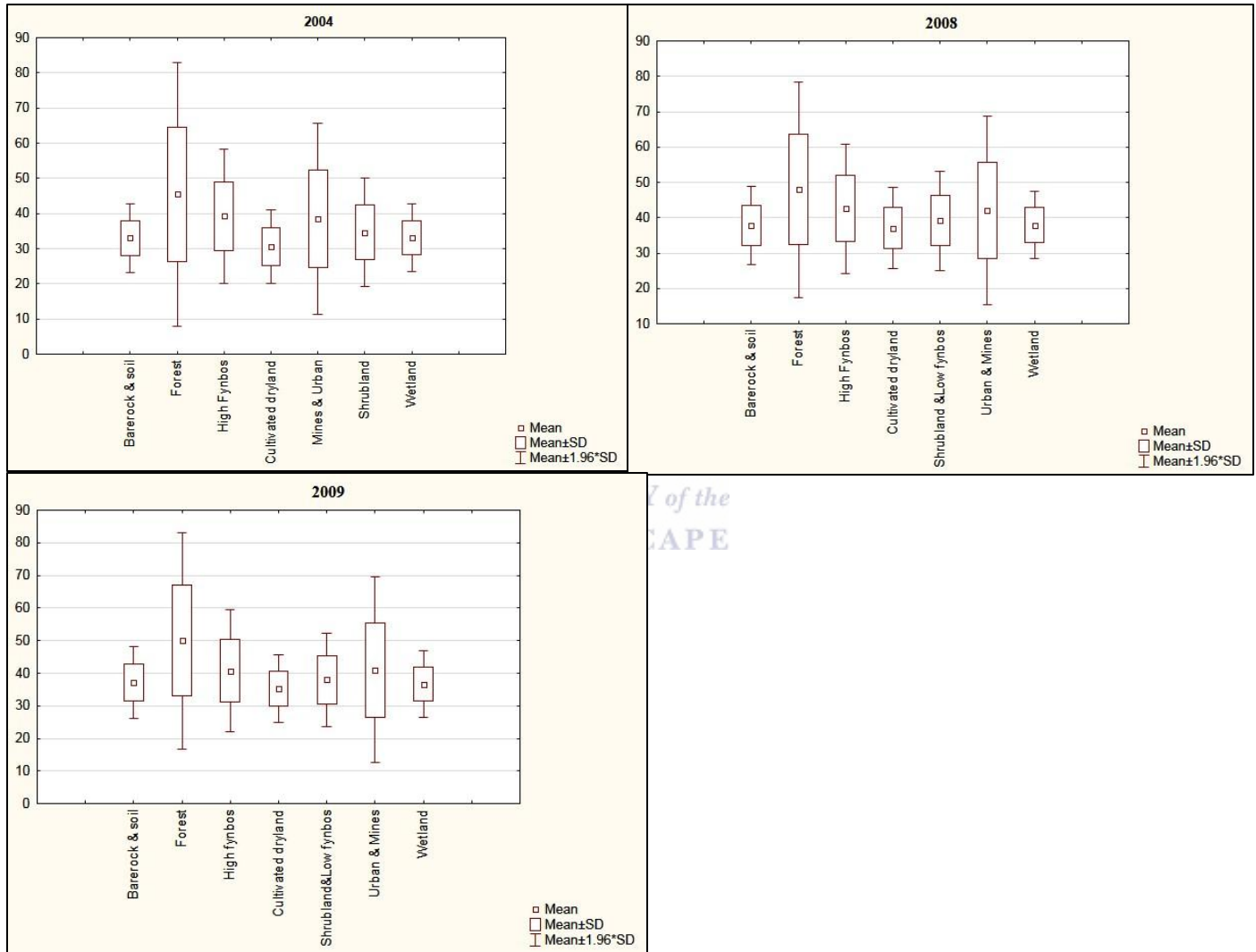


Figure 5.4: The box plots of MOD 16 ET data for different land cover types in 2004 (dry year), 2008 (wet year) and 2009 (average year) in the Heuningnes catchment

The Letaba catchment is relatively larger than the Heuningnes catchment; thus the Letaba catchment had more spatial variation of MOD 16 ET compared to the Heuningnes catchment. The standard deviations also indicated that there was less spatial variation in Heuningnes catchment compared to the Letaba catchment. The Letaba catchment had highest ET rates for different land cover types as compared to the Heuningnes catchment. The variation of ET rates in the same land cover types of contrasting catchments is as the result of difference in location of land cover types and difference in weather conditions of these catchments.

### **5.3 Ground-truthing and mapping of shallow groundwater areas**

#### **5.3.1 Ground-truthing in Letaba catchment**

The sites visited and recorded during the field trip are summarized in Figure 5.5. Photos taken at each of these sites are also presented in Appendix C.

The field trip started in the upper reaches at the source of the Molototsi River (Figure 5.5, and Appendix C). The presented pictures show areas that had high spots of ET and areas that had low ET rates. The Molototsi River originates in the vicinity of the village of Kgapane (Site 2). It flows through the village in the form of a narrow and deep valley (Site 3). Site 1 is in the northern adjacent catchment of the Brandboontjies River, a tributary of the Middle Letaba River. Site 5 is in the southern adjacent catchment of the Nwanedzi River, a tributary of the Greater Letaba River.

The upper reaches of the Molototsi River are characterized by hilly and mountainous areas, with densely populated areas in the valleys and forests at higher altitudes. Forests are both plantations and natural forests. An example of forest plantations was found at Site 4, which is at the watershed between the Molototsi and Tzaneen dam catchments. Sites 6 and 7 are representative of natural forests, in the neighborhood of the Modjadji Nature Reserve. Such landscape occurs down to the Modjadji Water Scheme (Site 8). The Modjadji Water Scheme earth dam is visible from Site 6 and it showed a fairly low water level during the field visit.

The landscape downstream of the Modjadji Water Scheme (Site 8) exhibits flatter and undulating hills, it is fairly densely populated, and it appears to be drier than the upper reaches. The vegetation is sparse and the land appears to be over-grazed. The Molototsi River is dry in these mid-reaches, however traces of shallow groundwater were found. For example, Site 9 is a site where sand mining appears to occur although no traces of water on the surface were observed.



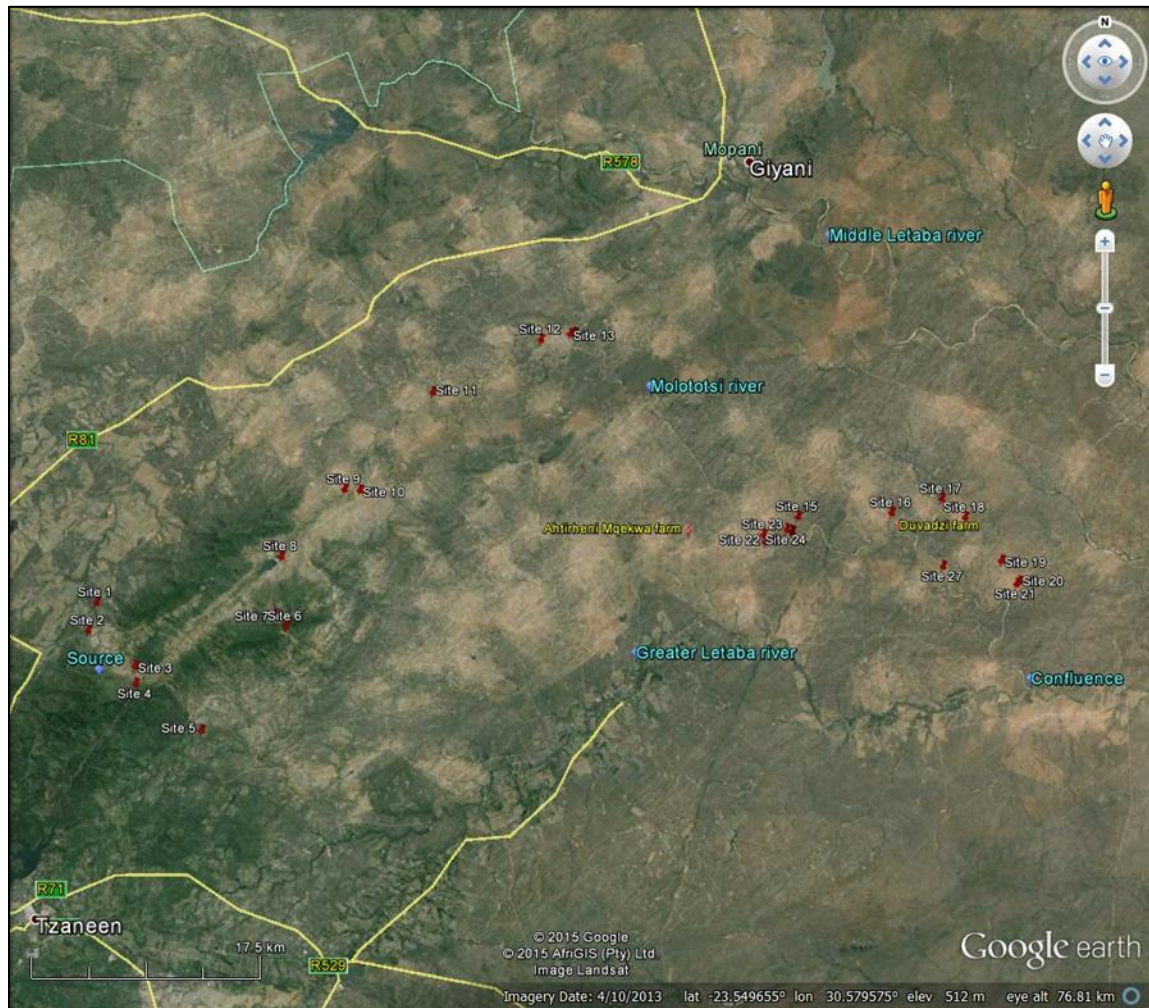


Figure 5.5: Sites visited during the recognisance trip in the Molototsi river catchment, starting from the East (source) to the West (confluence) on a Google Earth map. Source: ([www.google earth](http://www.google.com/earth), Date 04/10/2013)

Several perennial tributaries of the Molototsi river were observed, such as at Site 10 where water was ponding in the stream bed. Site 11 is the site of major earthworks. A sand dam was erected at this site to allow the construction of a new bridge. Excavations in the river bed indicated that a water table occurs at about 2 m depth overlying bedrock. This site could also be deemed suitable for the construction of barrage dams for water supply (populated villages and agriculture) and for the regulation of flow/floods upstream of the new bridge. Downstream of Site 11, the sand river bed of the Molototsi is remarkably exposed and this occurs down to its confluence in the Greater Letaba River. An example of the sand river bed appearance was evident at Site 12. A dug well was observed in the sand river bed at this site. The water table was about 1.5 m below the river bed, protected by thorn branches and a zinc sheet. The well was cased with a metal container (Appendix C).

A water sample was collected in the well. Site 13 occurs in an area where MOD16 ET indicates unusually high levels of evapotranspiration. It was observed that this is likely due to green and dense natural vegetation, which may be an indication of the occurrence of a shallow groundwater table. This area also includes a small irrigated vegetable farms. Tributaries of the Molototsi were observed, with sandy and rather stony river beds (Site 14) (Appendix C).

In the lower reaches of the Molototsi, the vegetation is predominantly natural and sparse bushveld with small trees and the population is sparse in villages. The density of the vegetation increases in the neighborhood of water courses, as evidenced at Sites 15, 16, 17 and 19, where torrential tributaries occur on the left banks of the Molototsi river. Due to the visibly drier landscape, earth dams for cattle have been built, such as at Sites 18 and 21. Occasionally, the density of natural vegetation becomes high depending on water availability, such as at Site 20. A similar landscape occurs on the right bank of the Molototsi river, as evidenced at Site 22 where a torrential tributary occurs in the neighborhood of Dzumeri village. In these lower reaches, the groundwater depth in the Molototsi river bed is between about 0.4 m and 2.5 m as measured at Site 23 and Site 24 during the field trip, respectively. Sites 25, 26 and 27 are locations where some boreholes were found. Site 27 is in the neighborhood of a perennial tributary and a concrete water reservoir (Appendix C).

### 5.3.2 Mapping of shallow groundwater areas in the Letaba catchment

In the Letaba catchment, a small catchment called Molototsi catchment was chosen for the mapping of shallow groundwater areas. Below are the steps that were taken to compile the map of shallow groundwater areas.

#### *Delineation of shallow groundwater based on borehole measurements*

The first step in the compilation of shallow groundwater maps was the delineation of shallow groundwater areas based on interpolated maps of groundwater depth, using data points obtained from the Groundwater Resource Information Project of the Limpopo Province (GRIP database; <http://griplimpopo.co.za/> accessed on 9 November 2015). The borehole measurements in the GRIP database include a large number of boreholes and these are shown in Figure 5.6 for the Molototsi catchment and adjacent catchments.

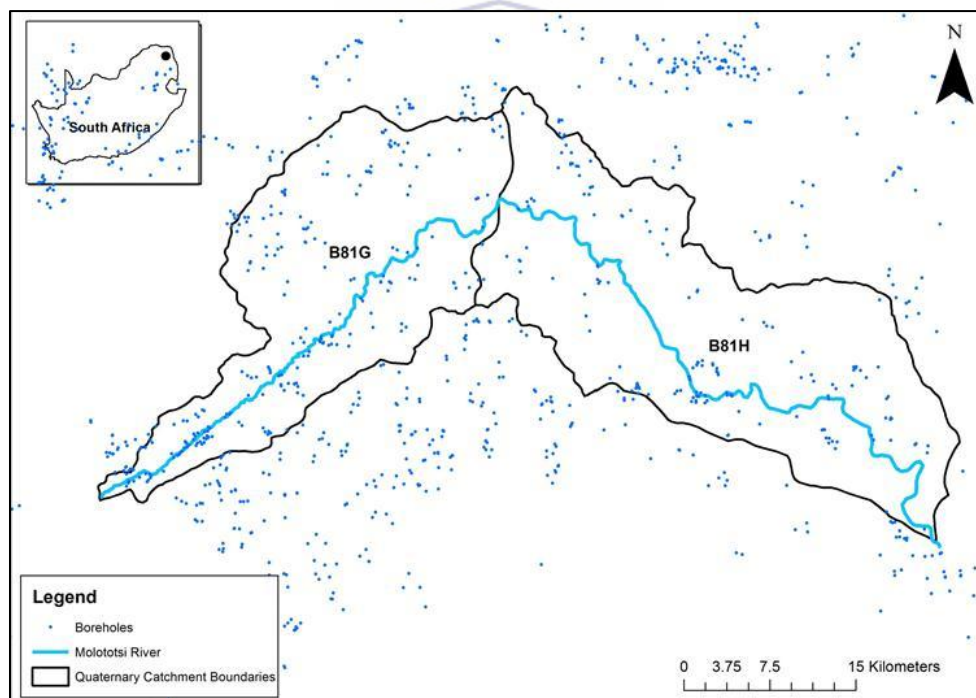


Figure 5.6: Groundwater monitoring points from GRIP database for the Molototsi river catchment.

Data for all boreholes shown in Figure 5.6 were used to interpolate groundwater depth. Groundwater depth was plotted in ArcGIS using default cell size and interpolation with inverse distance weighting (IDW) with power factors from 0.5 to 2. A power factor of 0.5 tends to smooth out the interpolated values, whilst a power factor of 2 separates the interpolated values

the least. The interpolated groundwater depths are shown in Figure 5.7. Almost the entire Molototsi catchment has a groundwater depth < 20 m and in many areas < 10 m. The map interpolated with IDW and power factor of 0.5 showed the smallest areas of shallow groundwater. This interpolation was carried forward in the process of shallow groundwater mapping.

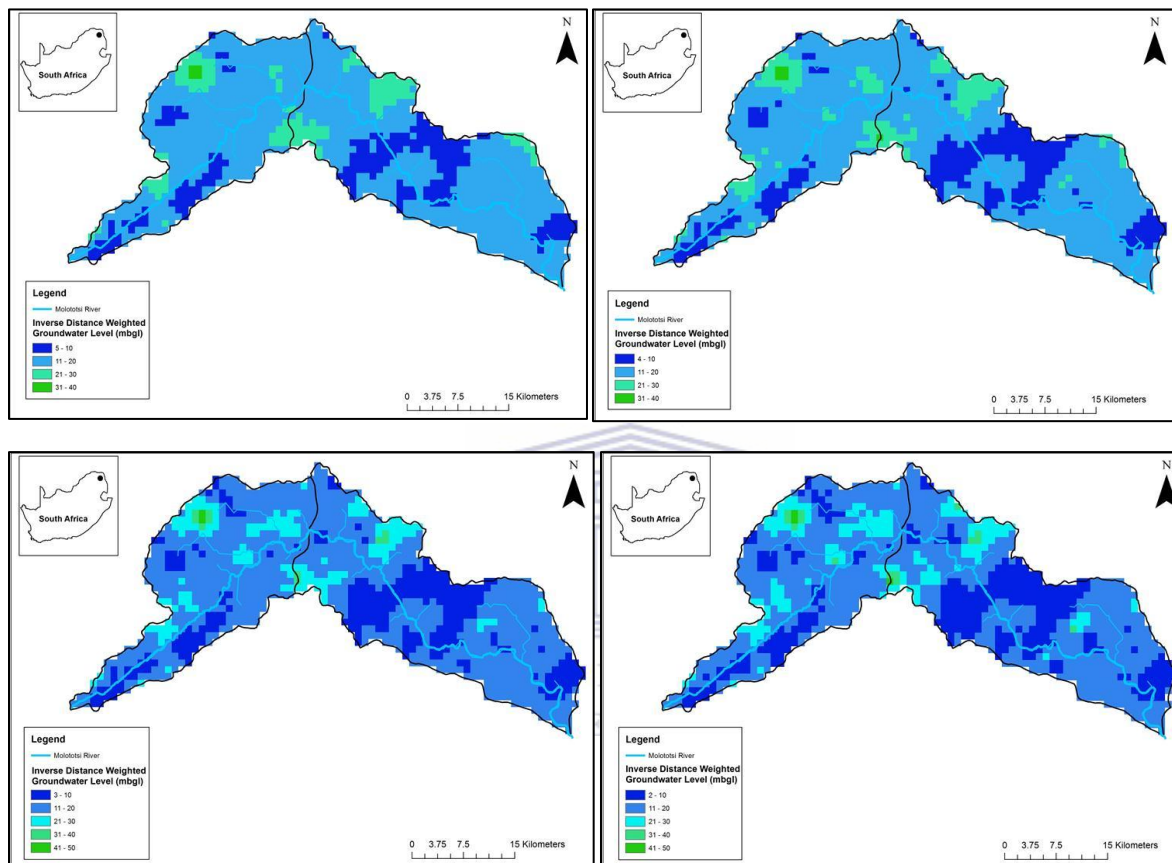


Figure 5.7: Groundwater depths interpolated with inverse distance weighting with a power factor of 0.5 (top left), 1 (top right), 1.5 (bottom left) and 2 (bottom right), all with default cell size.

### ***Delineation of shallow groundwater based on National Freshwater Ecosystem Priority Areas (NFEPA) wetland maps***

The second step in the compilation of shallow groundwater maps was the delineation of wetlands based on National Freshwater Ecosystem Priority Areas (NFEPA) wetland maps. The information used to map wetlands and the national wetland classification systems used in NFEPA were described by *Nel et al.*, (2011). An extract of this information is briefly summarized below.

### ***Information used to map wetlands***

South African National Biodiversity Institute (SANBI) classified the wetlands. A brief description of how the classification was done is summarized. To compile the national wetland map, SANBI's National Wetland Map 1 was used as the base GIS layer. This layer was derived from National Land Cover 2000 GIS layer, in which wetland polygons are described as wetland or waterbody. The waterbody category did not distinguish between natural and artificial waterbodies, therefore the National Wetland Map 1 was combined with the 1:50,000 inland water features to derive National Wetland Map 2 that was divided into 3 GIS layers: wetland (marsh vlei, swamp), natural waterbody (dry pan, lake, mudflats, pool, non-perennial and perennial pan) and artificial waterbody (dam, fish farm, large reservoir, water tank and purification plant). The wetland and natural waterbody GIS layers were then combined to produce a natural waterbody GIS layer. This was then combined with the artificial waterbody GIS layer to produce the National Wetland Map 3, in which wetland polygons have been described as either natural or artificial waterbodies. Finally, existing sub-national wetland locality maps from other biodiversity planning initiatives were added to the National Wetland Map 3 to derive the final NFEPA Wetland 3.

### ***Wetland ecosystem types***

Wetlands in the same wetland ecosystem type are expected to share similar broad functionalities and ecological characteristics. The diversity of wetland ecosystems was therefore represented using wetland ecosystem types according to the national wetland classification system (SANBI, 2010). The national wetland classification system is a hierarchical classification framework consisting of six levels, with each level requiring increasing levels of detail about a wetland:

- In level 1, wetlands are identified as estuaries or as inland wetland.
- Levels 2 to 4 identify broad groups of wetlands sharing similar regional context, type of landform (slopes, benches, valley floors and plains) and broad hydrology.
- Levels 5 and 6 describe site characteristics such as geology, hydro-period, substratum, vegetation, salinity, pH and naturalness.

### *Types of wetlands in Molototsi and their sources of water*

In the Molototsi river catchment, the following types of wetlands occur and they were mapped in NFEPA:

- a) Seep is a wetland area located on gently to steeply sloping land, which is dominated by the colluvial (gravity-driven), unidirectional movement of material down-slope. The source of water for this wetland is the subsurface flow that enters the wetland from an up-slope direction.
- b) Valleyhead seep is a gently-sloping, typically concave wetland area located on a valley floor at the head of drainage line. The source of water is mainly from subsurface flow although there is usually also a convergence of diffuse overland water flow in these areas during and after rainfall events.
- c) Depression is a landform with closed elevation contours that increases in depth from the perimeter to a central area of greatest depth and within which water typically accumulates. The dominant sources of water for this wetland are precipitation, groundwater discharge, interflow and overland flow.
- d) Channelled valley-bottom is a mostly flat wetland area on a valley floor that is dissected by, and typically elevated above a well-defined stream channel. The dominant source of water is the channel and also the adjacent valley-side slopes.
- e) Unchannelled valley-bottom is a mostly flat wetland area without a well-defined stream channel running through it, and it is characterized by an absence of distinct channel banks and the prevalence of diffuse flows, even during and after rainfall events. The source of water is from an upstream channel, as the flow becomes dispersed and from adjacent slopes.
- f) Flat is a near-level wetland area with little or no gradient, situated on a plain or a bench. The primary source of water is precipitation.
- g) Floodplain is the mostly flat or gently-sloping wetland area adjacent to and formed by a lowland or upland floodplain river, which is subject to periodic inundation by overtopping of the channel bank. The source of water is mainly via overspill from a river channel during flooding.

The wetlands in the Molototsi catchment according to NFEPA are shown in Figure 5.8. The variety and type of wetland can be easily linked to the position in the catchment. For comparative purpose, the digital elevation model (DEM) of the Molototsi catchment is shown in Figure 5.10 (Weepener *et al.*, 2011). It is interesting to note that the location of many wetlands coincided with measured shallow groundwater (Figure 5.7). The wetlands are defined as areas with shallow groundwater and these areas were added to the interpolated maps of borehole measurements (Figure 5.7) in the compilation of the shallow groundwater map.

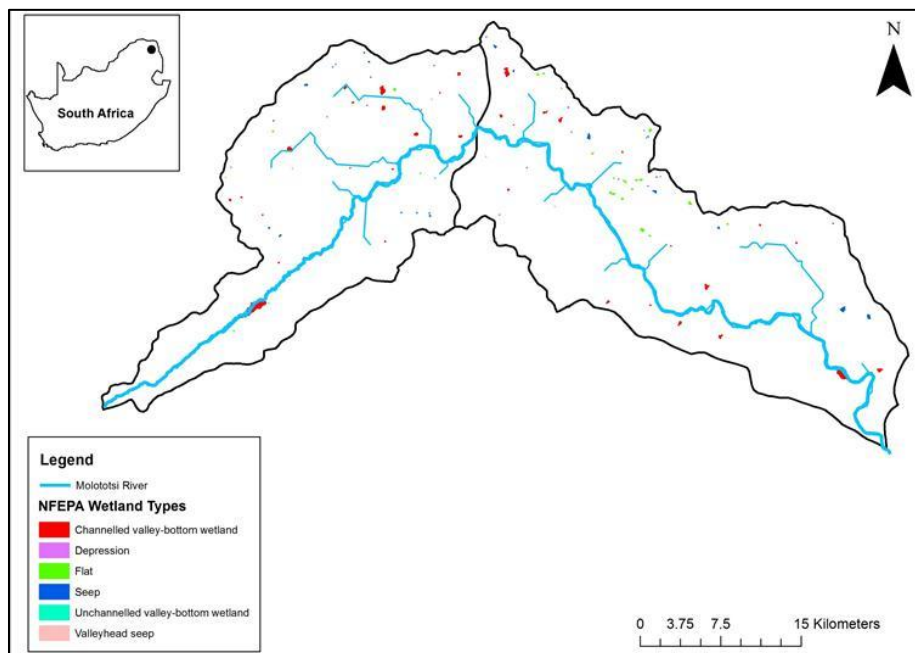


Figure 5.8: Wetland map for the Molototsi river catchment with categories and descriptions according to NFEPA (National Freshwater Ecosystem Priority Areas).

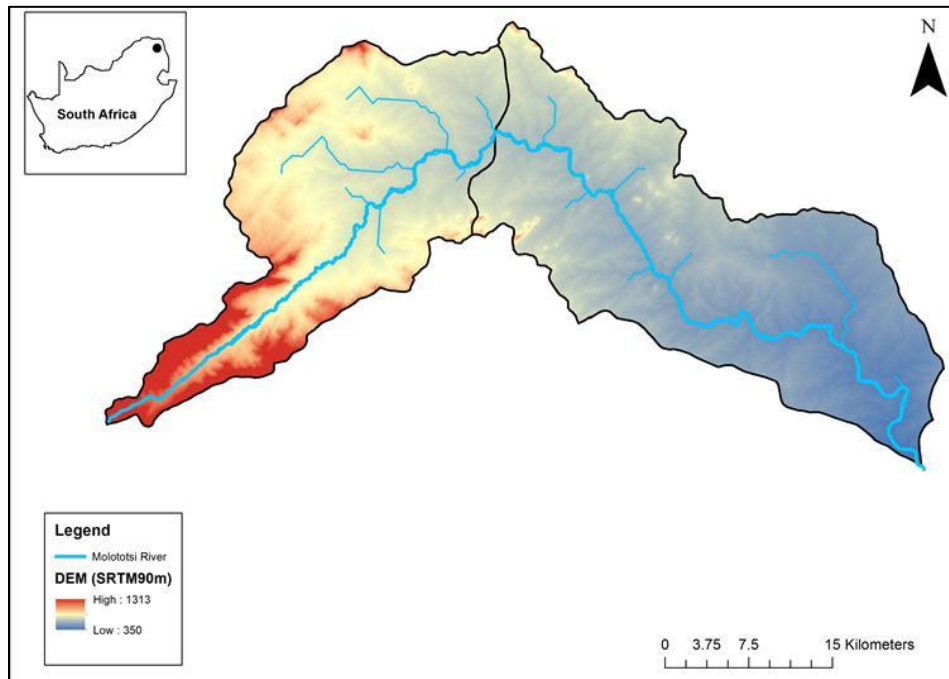


Figure 5.9: Digital elevation model (DEM) for the Molototsi river catchment.

### ***Delineation of areas with high evapotranspiration***

Areas with consistently high evapotranspiration (ET) may usually indicate the presence of shallow groundwater that provides a source of water to vegetation. Measurements of ET are generally resource and time-intensive, and representative of a restricted area (point measurements). In recent years, satellite imagery has provided the opportunity to overcome the problems linked to ground measurements and to obtain large scale spatial data of ET (Jovanovic *et al.*, 2014). In this instance, the MOD16 ET algorithm was used to identify areas with high evapotranspiration during the period 2000-2012. For the purpose of identifying areas where vegetation is possibly fed by shallow groundwater, we first selected a very dry year from the period 2000-2012. We used rainfall recorded by the network of weather stations of the Agricultural Research Council (ARC). Very few stations in Limpopo had a time series record as far back as 2000. Annual rainfall values from available weather stations (Citimba, Pietersburg, Brits-AGR, Lephalale, Dendron and Polokwane stations) for the period 2000-2012 are shown in Figure 5.10. Based on the data available, 2003 was a particularly dry year. The average rainfall for 2003 was about 350 mm/year. Any ET values substantially higher than rainfall (350 mm/year) would indicate the possible occurrence of shallow groundwater representing a water source for vegetation. Areas with  $ET > 350$  mm/year in 2003 were therefore extracted and added to the compilation of the shallow groundwater map for the Molototsi catchment.



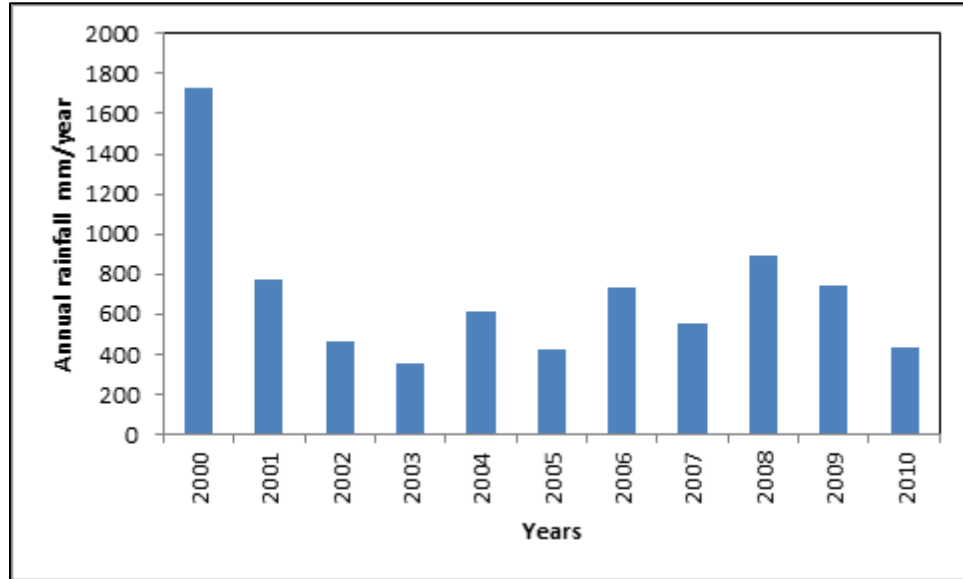


Figure 5.10: Annual average rainfall measured at weather stations of the Agricultural Research Council (ARC) in Limpopo.

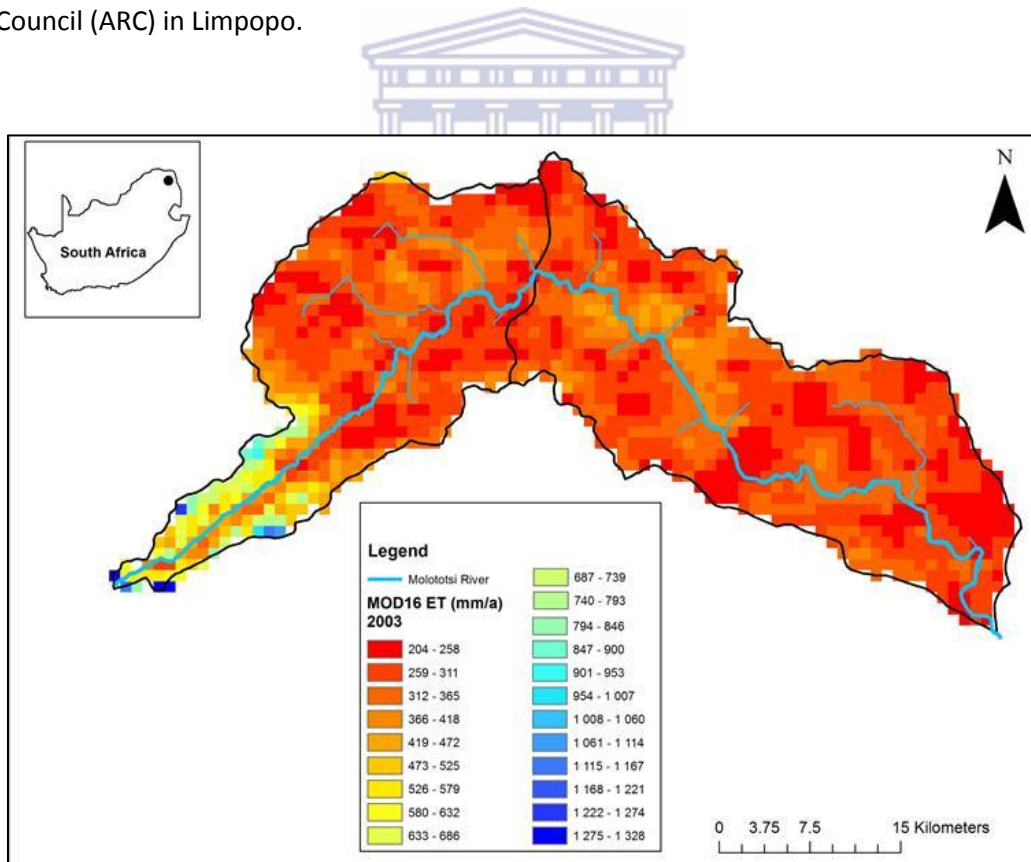


Figure 5.11: MOD16 annual evapotranspiration (ET) for the Molototsi river catchment during a dry year (2003).

### ***Interpretation of shallow groundwater areas***

The MOD16 ET for the Molototsi catchment in 2003 is shown in Figure 5.11. It is clear from the map that high ET values (>1,000 mm/year) occurred in the upper reaches in the western mountainous part of the catchment. This area corresponds to Sites 3, 4, 6 and 7 of the field trip (Appendix C), and it is likely that it receives more rainfall than the rest of the catchment through the orographic effect of the escarpment. The mountainous upper reach basically represents the main recharge area of the Molototsi River. The land uses and land cover were also checked against the National Land Cover (NLC) maps of 2009 (SANBI, 2009) and 2014 (GEOTERRAIMAGE, 2014). The land cover maps for the Molototsi catchment are shown in Figure 5.13. According to NLC 2009 by SANBI, the upper reaches of the river are represented by natural vegetation, forest plantations, urban areas and some cultivated areas. According to NLC 2014 (GEOTERRAIMAGE, 2014), these areas are represented by thicket/dense bush, urban areas and plantations. The ground-truthing during the field trip and the NLC maps description are consistent with the expected high ET values in the upper reaches of the Molototsi catchment, as indicated in the MOD 16 ET map (Figure 5.11).

From the Modjadji water scheme downstream (Site 8 of the field trip; Appendix C), MOD16 ET varied in the range between 200 and 500 mm in 2003. These areas in the mid- and lower reaches of the Molototsi River were classified predominantly as natural land, land under cultivation, urban areas (villages) with some degraded areas especially in the mid-reaches according to NLC 2009. According to NLC 2014, these areas are classified as a mixture of woodland/open bush, grassland, thicket/dense bush, cultivated areas for subsistence agriculture and urban areas (villages). It is also interesting to notice that many locations of high MOD16 ET in the mid- and lower reaches coincide with the occurrence of wetlands (Figure 5.8). There are no major irrigated areas in the catchment that would be larger than the pixel resolution of ~1 km of MOD16 ET.

In summary, the mountainous areas in the upper reaches of the Molototsi catchment are likely to receive more rainfall that sustains water use by natural forests and plantations. In the mid- and lower reaches of the catchment, there exist spots of high ET that often coincide with wetlands mapped by NFEPA and natural vegetation areas. These spots appear to be fed by seasonal

groundwater (soil water stored in the unsaturated zone, perched groundwater tables or fluctuating groundwater tables).

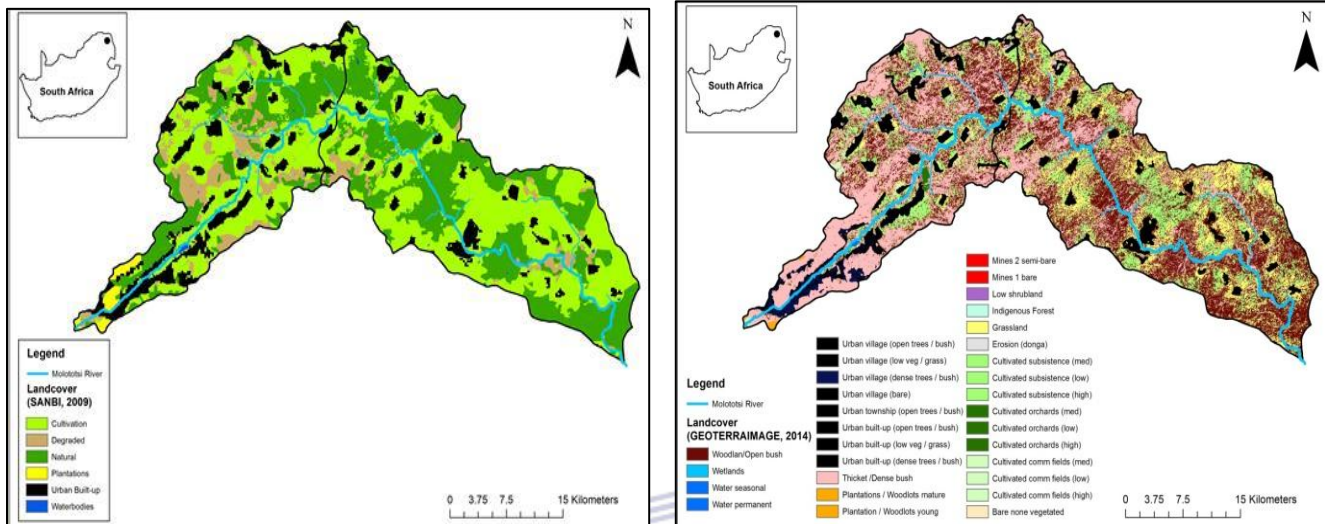
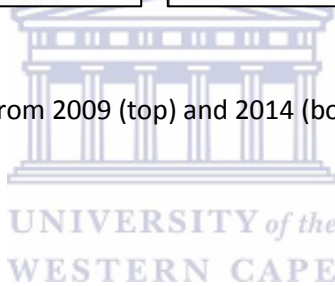


Figure 5.12: Land cover map from 2009 (top) and 2014 (bottom) for the Molototsi river catchment.



### ***Final shallow groundwater map***

The final shallow groundwater map for the Molototsi river catchment was produced by overlaying interpolated groundwater depths < 10 m, wetlands mapped by NFEPA and MOD16 pixels of high evapotranspiration ( $ET > 350 \text{ mm a}^{-1}$ ) estimated during a dry year (2003). The final shallow groundwater map is presented in Figure 5.13.

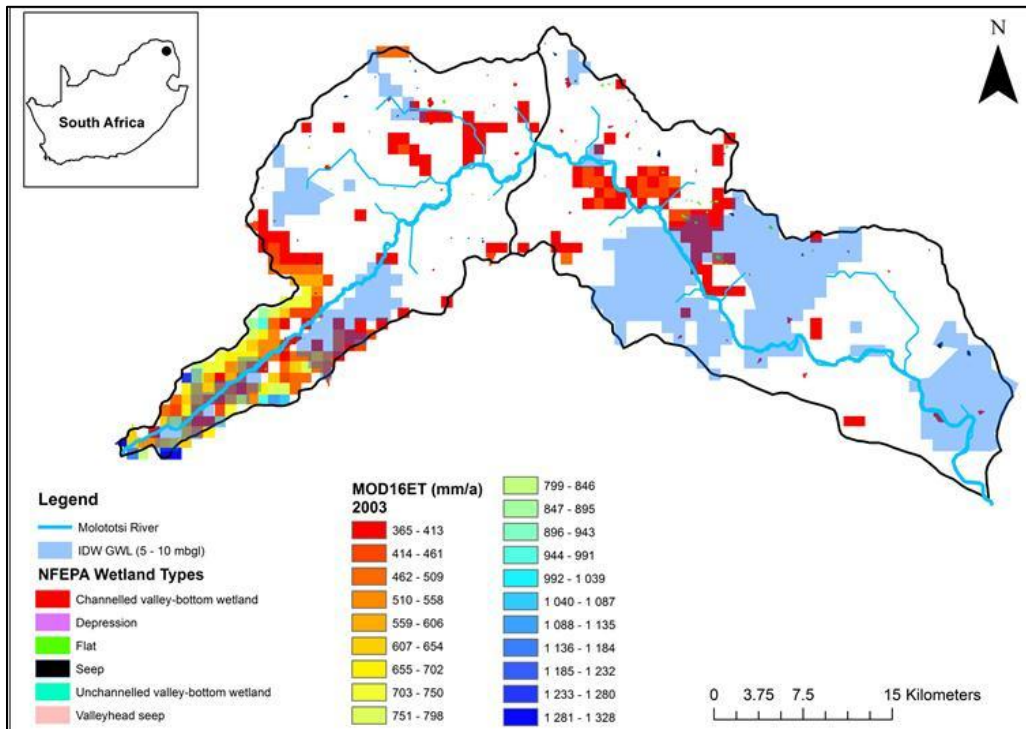


Figure 5.13: Final map of shallow groundwater for the Molototsi River overlaying interpolated groundwater depths with inverse distance weighting (IDW GWL), NFEPA wetlands and MOD16 pixels of high annual evapotranspiration (ET) during a dry year.

### 5.3.3 Ground-truthing in the Heuningnes catchment

The ground-truthing of land cover types and land uses from the Heuningnes catchment was done on 26 February 2016 and 20 sites were visited. The sites visited and recorded during the field trip are summarized in Figure 5.14. Photos taken at each of these sites are also presented in Appendix D.

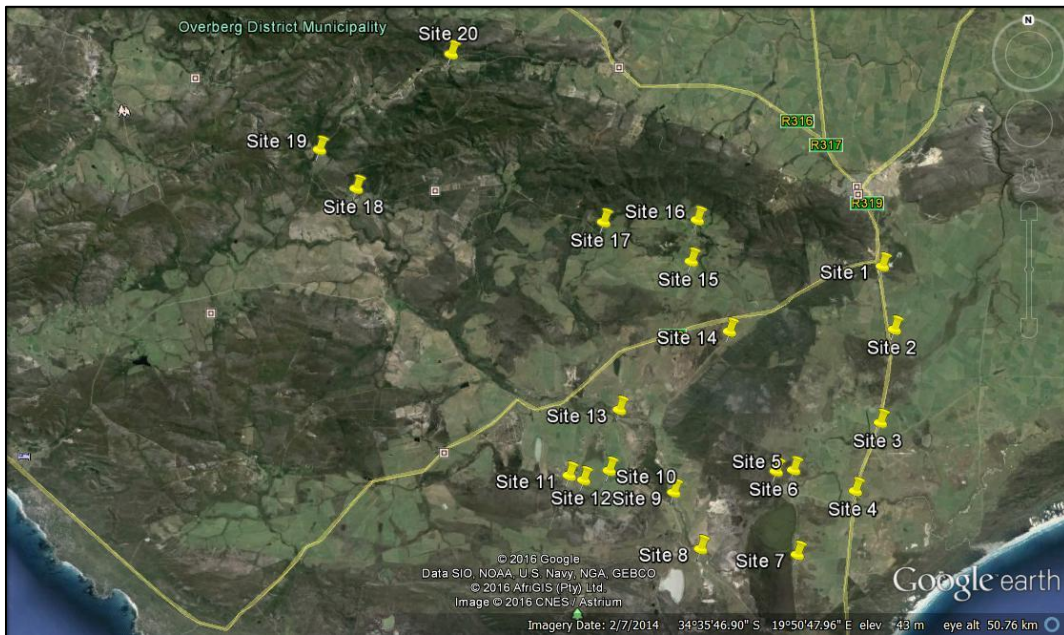


Figure 5.14: Sites visited in the Heuningnes catchment. Source: ([www.google](http://www.google.com) earth, Date 02/07/2014)

Site 1 is a lowland area and is characterized by dense alien vegetation (*Acacia saligna* and *Acacia mearnsii*). The *Acacia saligna* usually grows 2- 6 m tall but can reach up to 10 m in height. The *Acacia mearnsii* grows up to 15 m in height. Site 2 is an open dry land that is characterized by loam soil and with patches of grass and the area is lowland. There is short green grassland at site 3. Site 4 is the Heuningnes River characterized by dense tall reeds (*Phragmites australis*) in the riparian zones. The *Phragmites australis* typically grow to 2 m in height, but may reach 4 m. Site 5 is another part of the Heuningnes River in the Vissedrift, the stream is also characterized by tall reeds (*Phragmites australis*) in the riparian zones and within the stream. The stream is wider than the stream in site 4. There are also trees (*Acacia mearnsii*) in the surroundings of the stream (Appendix D).

At site 6 there is dense alien vegetation (*Acacia saligna* and *Acacia mearnsii*) and dry natural grass land and the area is lowland. The vegetation is in a good state, not overgrazed. Site 7 is Soetendalsvlei that is characterized by tall reeds (*Phragmites australis*) in its riparian zones. The Soetendalsvlei is a 3 km by 8 km lake that overflows into the Heuningnes River. Site 8 and 9 are dry land areas that are characterized by loam soil and small patches of grass. Site 10 is a cultivated bare land next to the Soetendalsvlei. At site 11 and 12 the areas are lowland with dense bush land (*Eucalyptus radiata*, *Acacia saligna* and *Acacia mearnsii*). *Eucalyptus radiata* is a medium to tall tree up to 30 m high (Appendix D).

Site 13 is a flowing stream with dense riparian vegetation (*Phragmites australis*) on the right bank and with small patches of grass on the left bank of the stream. The river flow is low as the river flow in the Heuningnes catchment is expected to be low during summer dry season and is expected to rise during winter wet season. At site 14 there is dense vegetation (*Acacia cyclops*) and dry land. The *Acacia cyclops* is an evergreen shrub or tree with a dense, untidy appearance and has an average height of 3 m, but it can reach a height of 8 m. Site 15 and 16 are characterized by mountainous areas with dense vegetation (*Acacia cyclops*) and cultivated bare land. Site 17, 18 and 19 are mountainous areas with dense vegetation (*Eucalyptus radiata*, *Acacia saligna*, *Acacia cyclops* and *Acacia mearnsii*). Site 20 is a mountainous area with dense vegetation (*Eucalyptus radiata* and *Acacia cyclops*) covering the slope and a grass land in the lower parts of the area. The mountainous areas are likely to receive more rainfall than the rest of the catchment through the orographic effect of the mountains. The dense alien vegetation also absorbs a lot of water and therefore is likely to have high ET rates (Appendix D).

### 5.3.4 Mapping of shallow groundwater areas in the Heuningnes catchment

#### *Delineation of shallow groundwater based on borehole measurements*

The first step in the compilation of shallow groundwater maps was the delineation of shallow groundwater areas based on interpolated maps of groundwater depth, using data points obtained from measurements taken during the field trip on 26 February 2016. The boreholes and piezometers are only in quaternary catchment G50 C as shown in Figure 5.15. There were no other borehole data found in the catchment.

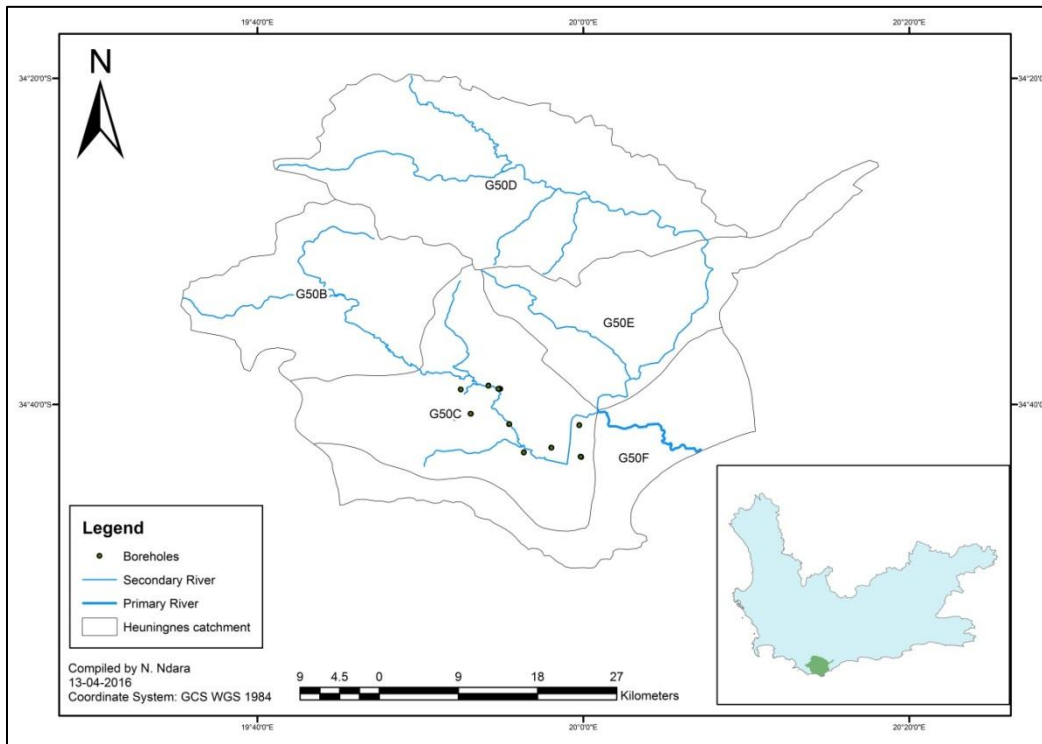
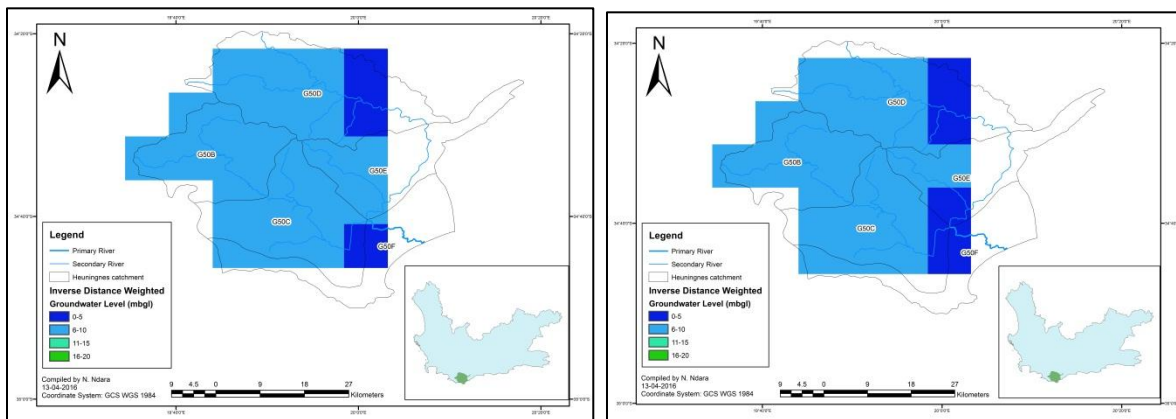


Figure 5.15: Groundwater monitoring points for the Heuningnes catchment.

Data for boreholes shown in Figure 5.15 were used to interpolate groundwater depth. Groundwater depth was plotted in ArcGIS using default cell size and interpolation with inverse distance weighting (IDW) with power factors from 0.5 to 2. The interpolated groundwater depths are shown in Figure 5.16. There were few points with measurements; therefore the entire Heuningnes catchment has a groundwater depth < 10 m and in few areas < 5 m.



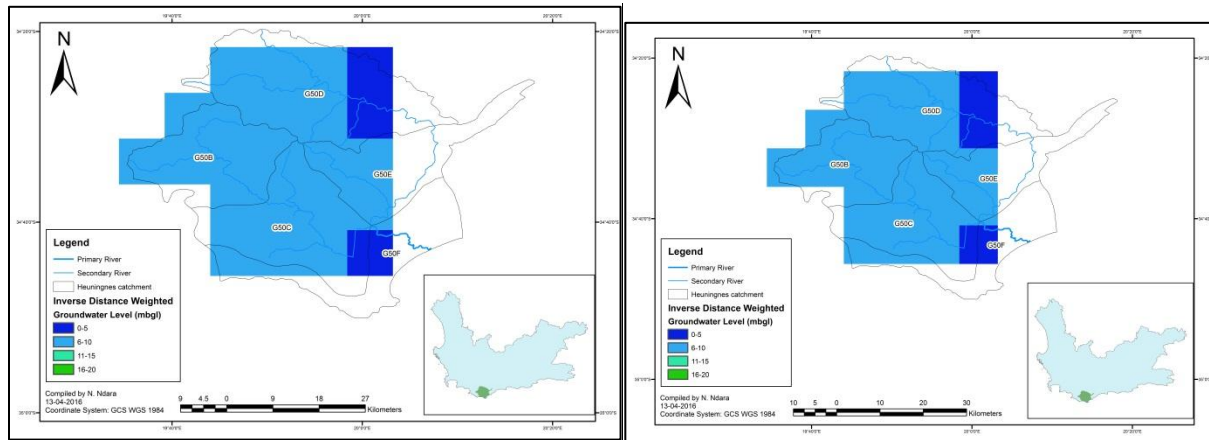


Figure 5.16: Groundwater depths interpolated with inverse distance weighting with a power factor of 0.5 (top left), 1 (top right), 1.5 (bottom left) and 2 (bottom right), all with default cell size.

### ***Delineation of shallow groundwater based on National Freshwater Ecosystem Priority Areas (NFEPA) wetland maps***

The second step in the compilation of shallow groundwater maps was the delineation of wetlands based on NFEPA wetland maps. The information used to map wetlands and the national wetland classification system used in NFEPA was described by *Nel et al.*, (2011). An extract of this information is briefly summarized above (under mapping of shallow groundwater areas in the Molototsi catchment)

The wetlands in the Heuningnes catchment according to NFEPA are shown in Figure 5.17. The variety and type of wetland can be easily associated to the position in the catchment. For comparative purpose, the digital elevation model (DEM) of the Heuningnes catchment is shown in Figure 3.3. The location of many wetlands matched with measured shallow groundwater (Figure 5.16). The wetlands are defined as areas with shallow groundwater and these areas were added to the interpolated maps of borehole measurements (Figure 5.16) in the compilation of the shallow groundwater map.



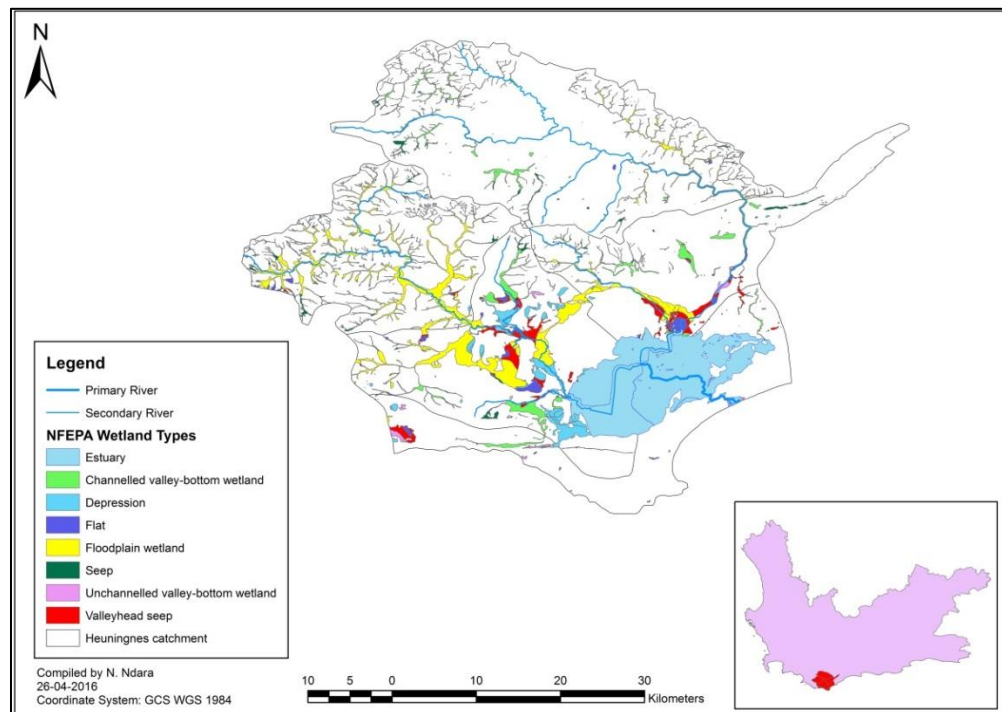


Figure 5.17: Wetland map for the Heuningnes catchment with categories and descriptions according to NFEPA (National Freshwater Ecosystem Priority Areas).

### *Delineation of areas with high evapotranspiration*

Areas with continually high evapotranspiration (ET) may usually indicate the presence of shallow groundwater that provides a source of water to vegetation. For the purpose of identifying areas where vegetation is possibly fed by shallow groundwater, we first selected a very dry year from the period 2000-2012 according to ET (Figure 5.19). The annual average rainfall values from available weather stations (Prinskraal and Agulhas stations) for the period 2000-2012 of the whole Heuningnes Catchment are shown in Figure 5.18, but because there is missing data in each weather station the rainfall data is not reliable, which makes it no feasible to choose a dry year based on rainfall. A 450 mm/year was assumed to be generally the annual average rainfall in the Heuningnes Catchment. Therefore any ET values substantially higher than this annual average rainfall (450 mm/year) would indicate the possible occurrence of shallow groundwater representing a water source for vegetation. Areas with  $ET > 450$  mm/year in 2004 were therefore extracted and added to the compilation of the shallow groundwater map for the Heuningnes catchment.

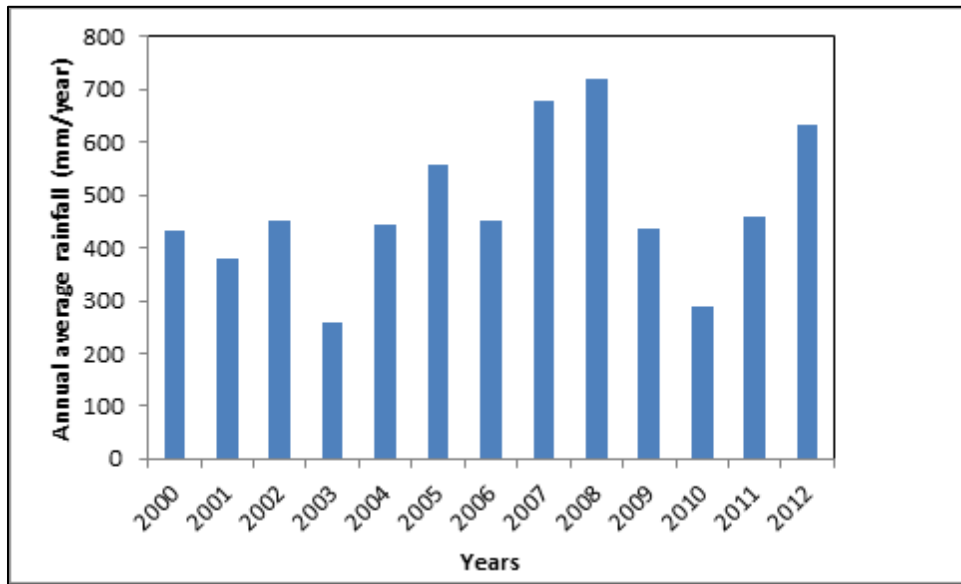


Figure 5.18: Annual average rainfall measured at weather stations (Prinskraal and Agulhas) in the Heuningnes Catchment.

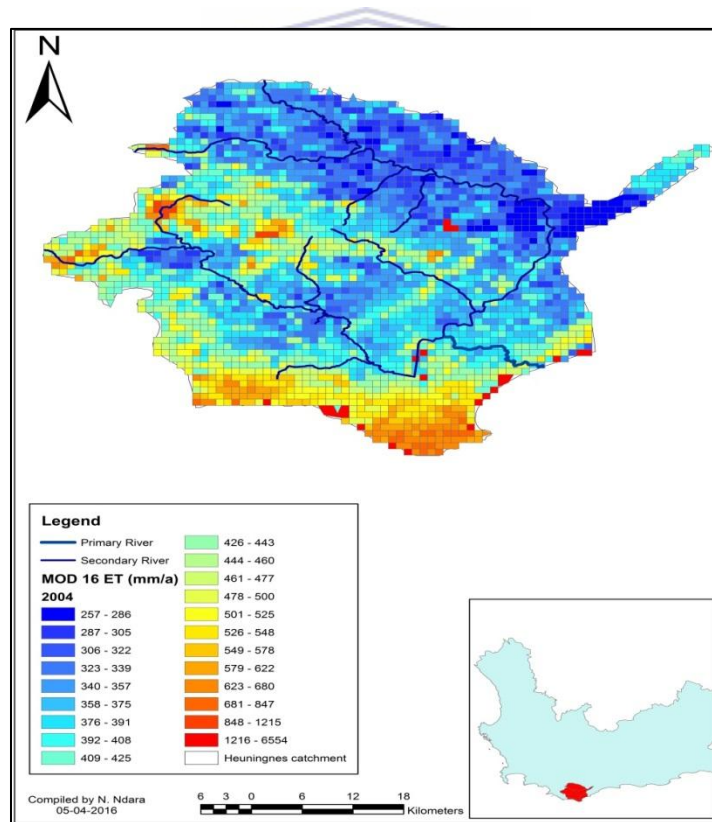


Figure 5.19: MOD16 annual evapotranspiration (ET) for the Heuningnes catchment during an average rainfall year (2004).

### ***Interpretation of shallow groundwater areas***

The MOD16 ET for the Heuningnes catchment in 2004 is shown in Figure 5.19. It is clear from the map that high ET values (>680 mm/year) occurred in the lower reaches in the south part of the catchment. This area is likely to receive more rainfall than the rest of the catchment and is close to the coast. The land cover and land use were also checked against the National Land Cover (NLC) map of 2014 (SANBI, 2014). The land cover map for the Heuningnes catchment is shown in Figure 3.5. According to NLC 2014 by SANBI, the lower reaches of the catchment are represented by shrubland and low fynbos, thicket bushland, bush clumps, high fynbos and cultivated temporary commercial dryland. These land cover types are likely to consume a lot of water. It is also interesting to notice that many locations of high MOD16 ET in the mid- and lower reaches match with the occurrence of wetlands (Figure 5.17) and others match with the Soetendalsvlei (Site 7 in the field trip) and tributaries of the Heuningnes River. The mid reaches with high MOD 16 ET correspond to Sites 16, 17, 18 and 19 of the field trip (Figure 5.14), and they are likely to receive more rainfall during winter wet season. This is a mountainous area according to the DEM shown in Figure 3.3.

In summary, the lowland areas in the south part of the Heuningnes catchment are likely to receive more rainfall that sustains water use by cultivation, shrubland and fynbos. In the mid- and lower reaches of the catchment, there exist spots of high ET that often match with wetlands mapped by NFEPA and natural vegetation areas. These spots appear to be fed by seasonal groundwater (soil water stored in the unsaturated zone, perched groundwater tables or fluctuating groundwater tables).

### ***Final shallow groundwater map***

The final shallow groundwater map for the Heuningnes catchment was produced by overlaying interpolated groundwater depths < 10 m, wetlands mapped by NFEPA and MOD16 pixels of high evapotranspiration ( $ET > 450 \text{ mm a}^{-1}$ ) estimated during an average rainfall year (2004). The final shallow groundwater map is presented in Figure 5.20.

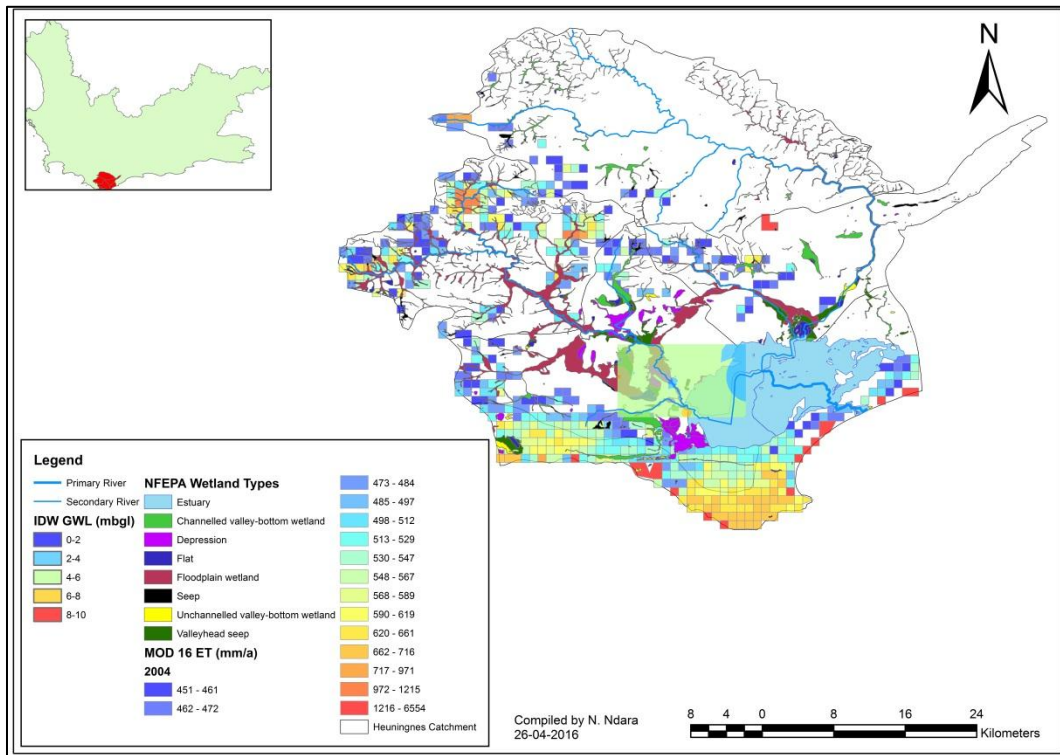


Figure 5.20: Final map of shallow groundwater for the Heuningnes catchment overlaying interpolated groundwater depths with inverse distance weighting (IDW GWL), NFEPA wetlands and MOD16 pixels of high annual evapotranspiration (ET) during an average rainfall year.

## Chapter 6: Conclusion and Recommendations

In this study the seasonal and spatial variation of MOD 16 ET for a period of 13 years (2000-2012) in the Letaba catchment and Heuningnes catchment was investigated. The following was concluded based on the analysis of the monthly MOD 16 ET maps that were plotted to determine the seasonal variation of ET in these catchments. MOD 16 is able to determine the temporal variation of ET; however it is not accurate at predicting the absolute value of ET. According to the plotted monthly MOD 16 ET maps, it is evident that during the 2000-2012 period ET has varied in the Letaba catchment (438-753 mm/year) and in the Heuningnes catchment (432-458 mm/year).

Validation of MOD 16 ET was done in Elandsberg (Mediterranean region), Skukuza (Sub-tropical region) and Malopeni sites (Sub-tropical region). From the results obtained, the null hypothesis which stated that there is no difference between averages of MOD 16 ET and ET derived from scintillometer and ET derived from flux towers was rejected in Elandsberg site and it was concluded that the average of ET derived from scintillometer differ from average of MOD 16 ET. However in Skukuza and Malopeni sites the null hypothesis was not rejected, thus it was concluded that there was no meaningful variation between averages of ET derived from flux towers and average of MOD 16 ET. It is indicated that MOD 16 has uncertainty in the prediction of absolute values of ET in different climatic regions as it is shown to underestimate ET in Mediterranean region and slightly overestimate in Sub-tropical region. The main sources of poor performance of MOD 16 in these regions are likely to be the poor comparison of predicted ET with some weather factors and different land cover types. Although the weather factors had some missing data in some days, the temperature, solar radiation and relative humidity generally had a moderate relationship when compared with the ET derived from scintillometer and flux tower. This means these weather factors should be fairly considered when estimating actual ET.

According to the statistical analysis and separation of ET in different land cover types, it is evident that MOD 16 has the ability to distinguish the spatial variation of ET in different land cover types. Furthermore, MOD 16 ET was found to be applicable in applications like mapping shallow groundwater areas, as it was successfully used to map areas with shallow groundwater in the Heuningnes catchment and Molototsi in the Letaba catchment.

Validation of MOD 16 ET in many sites within the Mediterranean region and Sub-tropical region is recommended, as it will further improve the conclusions about the accuracy of MOD 16 in these regions. The weather factors had missing data in some days, which makes it difficult to draw proper conclusions about their effect in estimating actual ET. Therefore further comparison of these weather factors is recommended to improve the conclusions about them. Ground measured ET data needs to be collected in the Heuningnes catchment and Letaba catchment for further studies to do validation of MOD 16 in these catchments.



## List of References

- Alemaw, B. F., Chaoka, T. R., and Matenge, O. (no date), Spatial and temporal variability of the Limpopo River basin water budget from a GIS-based Limpopo water balance LIMWAB model, *Geology Department, University of Botswana, Gaborone, Botswana*, pp. 1-12
- Allen, R.G., Pereira, L.S., Raes, D., and Smith, M. (1998). Crop evapotranspiration Guidelines for computing crop water requirements- FAO Irrigation and drainage paper: 56, pp 3
- Allen, R.G., Tasumi, M., Morse, A., and Trezza, R. (2007) Satellite-Based Energy Balance for Mapping Evapotranspiration with Internalized Calibration (METRIC)- Model. *Journal of Irrigation and Drainage Engineering*: 133 (4), pp 380-393
- Allen, R.G., Tasumi, M., Morse, A., Trezza, R., Wright, J., Bastiaan, W., Kramber, W., Lorite, I., and Robison, C. (2007) Satellite-Based Energy Balance for Mapping Evapotranspiration with Internalized Calibration (METRIC)- Application. *Journal of Irrigation and Drainage Engineering*: 133 (4), pp 395-406
- Azpurua, M., and Dos Ramos, K. (2010). A comparison of spatial interpolation methods for estimation of average electromagnetic field magnitude. *Progress in Electromagnetics Research M*: 14, pp 135-145
- Bala, A., Singh, R. K., and Gayathri, V. (2013). Review on different Surface Energy Balance algorithms for Estimation of Evapotranspiration through Remote Sensing. *International Journal of Emerging Technology and Advanced Engineering*, 3 (7), pp. 582-588, ISSN 2250-2459, 150 9001
- Baldocchi, D. (2003), Assessing the eddy covariance technique for evaluating carbon dioxide exchange rates of ecosystems: Past, present and future, *Global Change Biology*: 9 (4), pp. 479-492
- Bastiaanssen, W.G.M., Menenti, M., Feddes, R.A., and Holtslag, A.A.M. (1998) A remote sensing surface energy balance algorithm for land (SEBAL). *Journal of Hydrology*, pp 199-202
- Brown, P. (2000) Basics of Evaporation and Evapotranspiration. Cooperative Extension. The University of Arizona, College of Agriculture and Life Sciences, Tucson, Arizona 85721, pp 2-3

- Chen, J.M., Chen, X., Ju, W., and Geng, X. (2005) Distributed hydrological model for mapping evapotranspiration using remote sensing inputs. *Journal of Hydrology*: 305, pp 17-18
- Childs, C. (2004). Interpolating surfaces in ArcGIS Spatial Analyst, ESRI Education Services
- Cleugh, H.A., Leuning, R., Mu, Q., and Running, S.W. (2007). Regional evaporation estimates from flux tower and MODIS satellite data. *Remote Sensing of Environment*: 106, pp 285-304
- Courault, D., Seguin, B., and Olioso, A. (2005) Review on estimation of evapotranspiration from remote sensing data: From empirical to numerical modeling approaches. *Irrigation and Drainage Systems*: 19, pp 224-231
- Department of Water Affairs (DWA: 2004, First Edition): River System Annual Operating Analysis
- Department of Water Affairs and Forestry (DWAF: 2001) State of the Rivers Report, Letaba and Luvuvhu River Systems, pp 10-23
- Department of Water Affairs and Forestry, South Africa. 2004. Luvuvhu/Letaba Water Management Area: Internal Strategic Perspective. Prepared by Goba Moahloli Keeve Steyn (Pty) Ltd in association with Tlou and Matji, Golder Associates Africa and BKS on behalf of the Directorate: National Water Resource Planning.
- Diallo, Y., Hu, G., and Wen, X. (2009) Applications of Remote Sensing in Land use/ Land cover change detection in Puer and Simao Counties, Yunnan Province. *Journal of American Science*: 5 (4), pp 157-158
- Ding, R., Kang, S., Li, F., Zhang, Y., Tong, L., and Sun, Q. (2010). Evaluating eddy covariance method by large-scale weighing lysimeter in a maize field of northwest China. *Agricultural Water Management*: 98, pp. 87-95
- Douglas, A. F., and Inouye, R. S. (1994), Temporal Variation in Actual Evapotranspiration of Terrestrial Ecosystems: Patterns and Ecological Implications, *Journal of Biogeography*: 21 (4), pp. 401-411
- Eckel, S. (2008). Linear Regression Approach, Assumptions and Diagnostics, pp 1-42



Fisher, J.B., Tu, K.P., and Baldocchi, D.D. (2008). Global estimates of the land-atmosphere water flux based on monthly AVHRR and ISLSCP-II data, validated at 16 FLUXNET sites. *Remote sensing of Environment* (112), pp 903-906

GEOTERRAIMAGE (2014) 2013 - 2014 South African National Land Data. Geoterraimage for the Department of Environmental Affairs, Pretoria, South Africa.

Hafeez, M., Khan, S., Song, K., and Rabbani, U. (no date). Spatial Mapping of Actual Evapotranspiration and Soil Moisture in the Murrumbidgee Catchment: Examples from National Airborne field experimentation: pp 2611-2617

Heydorn, A.E.F. and Grindley, J.R. (1984) Estuaries of the Cape. Council for Scientific and Industrial Research National Research Institute for Oceanology Estuarine and Coastal Research Unit- ECRU, Heuningnes (CSW.19), Report No. 25, pp 3-8

Hoekstra, T., and Waller, L. (2014) Description and context of De Mond Nature Reserve Complex. De Mond Nature Reserve Complex. Western Cape, South Africa, pp 40-42

Hoffmann, J.P. (2010). Linear Regression Analysis: Applications and Assumptions, Second Edition. Department of Sociology. Brigham Young University, pp 1-285

Ibrahim, I., Abu Samah, A., Fauzi, R., and Noor, N. M. (2016). The Land Surface temperature impact to Land cover types. The International Archives of the Photogrammetry, Remote Sensing and Spatial Information Sciences, Volume XLI-B3, XXIII ISPRS Congress, Prague, Czech Republic, pp. 871-876

Johnson, T., and Odin, H. (1978). Measurements of evapotranspiration using a dynamic lysimeter. The Swedish University of Agricultural Sciences, College of Forestry, pp 5-7

Jovanovic, N., Dzikiti, S., Le Maitre, D., Roberts, W., Ramoelo, A., and Majozi, N. (2013). Monitoring of water availability using geo-spatial data and earth observations - Technical report, pp. 45-50

Jovanovic, N., Dzikiti, S., Masiyandima, M., and Gush, M. (2011) Remote sensing applications in water resources management- contributions to scoping study and review document. PG Progress Report. CSIR/ NRE/ ECOS/ IR/ 2011/ 0097/ A

- Jovanovic, N., Garcia, C.L, Bugan, R.D.H., Teich, I., and Rodriguez, C.M.G. (2014) Validation of remotely-sensed evapotranspiration and NDWI using ground measurements at Riverlands, South Africa. *Water SA Journal*: 40 (2), pp 211-212
- Jovanovic, N., and Israel, S. (2012) Critical review of methods for the estimation of actual evapotranspiration in hydrological models. In A. Irmak (Ed.) *Evapotranspiration- Remote Sensing and Modeling*, ISBN 978-953-307-808-3, InTech, Croatia, pp 330-332
- Jovanovic, N., Mu, Q., Bugan, R.D.H., and Zhao, M. (2015) Dynamics of MODIS evapotranspiration in South Africa. *Water SA Journal*: 41 (1), ISBN 1816-7950, pp 79-81
- Kim, H.W., Hwang, K., Mu, Q., Lee, S.O., and Choi, M. (2012). Validation of MODIS 16 Global Terrestrial Evapotranspiration Products in Various Climates and Land cover types in Asia. *Journal of Civil Engineering* 16 (2), pp 231-235
- Kim, H.W., Hwang, K., Mu, Q., Lee, S.O., and Choi, M. (2011). Validation of MODIS 16 Global Terrestrial Evapotranspiration Products in Various Climates and Land cover types in Asia. *Journal of Civil Engineering* 16 (2), pp. 229-238. DOI 10.1007/S 12205-012-0006-1
- Kirton, A., and Scholes, R. J. (2012). Site characterization of the Malopeni flux site, Kruger National Park, South Africa, web source ([http://www.carboafrika.net/downloads/ws/accra/6-Posters/Malopeni](http://www.carboafrika.net/downloads/ws/accra/6-Posters/Malopeni%20Site%20Characterization.pdf) Site Characterization.pdf, accessed on 22 September 2016)
- Kustas, W.P., and Norman, J.M. (1996) Use of remote sensing for evapotranspiration monitoring over land surfaces. *Hydrological Sciences Journal*: 41 (4), pp 496-497
- Lanthaler, C. (2004). Lysimeter Stations and Soil Hydrology Measuring Sites in Europe- Purpose, Equipment, Research Results, Future Developments. A diploma thesis. Department for Water Resources Management Hydrogeology and Geophysics, pp 54-57
- Liou, Y.A., and Kar, S.K. (2014). Evapotranspiration Estimation with remote sensing and various surface energy balance algorithms- Review. *Energies* (7), pp 2823-2835
- Matano, A., Kanangire, C. K., Anyona, D. N., Abuom, P. O., Gelder, F. B., Dida, G. O., Owuor, P. O., and Ofulla, A. V. O. (2015). Effects of Land use change on Land Degradation Reflected by Soil Properties along Mara River, Kenya and Tanzania. *Open Journal of Soil Science*, 5, pp. 20-38

Mausser, W., and Schadlich, S. (1998) Modeling the spatial distribution of evapotranspiration on different scales using remote sensing data. *Journal of Hydrology*, pp 250-252

McMahon, T.A., Peel, M.C., Lowel, L., Srikanthan, R., and McVicar, T. R. (2013) Estimating actual, potential, reference crop and pan evaporation using standard meteorological data: a pragmatic synthesis. *Hydrology and Earth System Sciences*: 17, pp 1332-1334

Mkhwanazi, M.M., and Chaves, J.L. (2013). Mapping evapotranspiration with the remote sensing ET algorithms METRIC and SEBAL under advective and non-advective conditions: accuracy determination with weighing lysimeters. Hydrology Days, Civil and Environmental Engineering Department, Colorado State University, pp 67-71

Mu, Q., Heinsch, F.A., Zhao, M., and Running, S.W. (2007) Development of a global evapotranspiration algorithm based on MODIS and global meteorology data. *Remote Sensing of Environment*: 111, pp 519-525

Mu, Q., Zhao, M., and Running, S.W. (2011) Improvements to a MODIS global terrestrial evapotranspiration algorithm. *Remote Sensing of Environment*: 115, pp 1781-1783

Mu, Q., Zhao, M., and Running, S.W. (2013). MODIS Global Terrestrial Evapotranspiration (ET) product (NASA MOD 16 A2/A3). Algorithm Theoretical Basis Document, Collections, Numerical Terradynamic Simulation Group, College of Forestry and Conservation, The University of Montana Missoula, pp 8-38

Nel, J.L., Murray, K.M., Maherry, A.M., Petersen, C.P., Roux, D.J., Driver, A., Hill, L., Van Deventer, H., Funke, N., Swartz, E.R., Smith-Adao, L.B., Mbona, N., Downsborough, L., and Nienaber, S. (2011) Technical Report for the National Freshwater Ecosystem Priority Areas project. WRC Report No. K5/1801, Water Research Commission, Pretoria, South Africa.

Overberg District Municipality (ODM). (2004). Overberg Spatial Development Framework pp. 1-30

Petropoulos, G.P., Carlson, T.N., and Griffiths, H.M. (2013) Turbulent Fluxes of Heat and Moisture at the Earth's Land Surface: Importance, Controlling Parameters, and Conventional Measurement Techniques. *Remote Sensing of Energy Fluxes and Soil Moisture Content*. CRC Press Taylor and Francis Group 6000 Broken Sound Parkway NW, Suite 300 Boca Raton, FL 33487-2742

- Ramoelo, A., Majazi, N., Mathieu, R., Jovanovic, N., Niclless, A., and Dzikiti, S. (2014). Validation of Global Evapotranspiration Product (MOD 16) using Flux Tower Data in the African Savanna, South Africa. *Remote Sensing*: 6, pp 7406-7423
- Rebelo, A. G., Boucher, C., Helme, N., Mucina, L., and Rutherford, M. (2006). Fynbos Biome. In: Mucina, L. and Rutherford, M.C. (eds). The vegetation of South Africa, Lesotho and Swaziland. *Strelitzia* 19, pp. 53-219. South African National Biodiversity Institute, Pretoria
- SANBI (2009) Updating National Land Cover. South African National Biodiversity Institute, Pretoria, South Africa.
- SANBI (2010) Updating National Land Cover. South African National Biodiversity Institute, Pretoria, South Africa.
- Savage, M.J., Odhiambo, G.O., Mengistu, M.G., Everson, C.S., and Jarman, C. (2010). Measurement of grassland evaporation using a surface-layer scintillometer. *Water South Africa*: 36 (1), pp. 1-8
- Scholes, R. J., Gureja, N., Giannecchini, M., Dovie, D., Wilson, B., Davidson, N., Piggott, K., McLoughlin, C., van der Velde, K., Freeman, A., Bradley, S., Smart, R., and Ndala, S. (2001). The environmental and vegetation of the flux measurement site near Skukuza, Kruger National Park. *Koedoe* 44(1), pp. 73-83
- Scott, R.L. (2010). Using watershed water balance to evaluate the accuracy of eddy covariance evaporation measurements for three semiarid ecosystems. *Agricultural and Forest Meteorology*: 150, pp. 219-225
- Senay, G.B., Leake, S., Nagler, P.L., Artan, G., Dickinson, J., Cordova, J.T., and Glenn, E.P. (2011). Estimating basin scale evapotranspiration (ET) by water balance and remote sensing methods. *Hydrological Processes*: 25, pp 4037-4049
- Seyfried, M. S., Hanson, C. L., Murdock, M. D., and VanVactor, S. (2001). Long-term lysimeter database, Reynolds Creek Experimental Watershed, Idaho, United States. *Water Resources Research*: 37 (11), pp. 2853-2854

Siebert, F., Eckhardt, H. C., and Siebert, S.J. (2010). The vegetation and floristics of the Letaba enclosures, Kruger National Park, South Africa, *Koedoe* 52 (1), Act. No 777, 12 pages. DOI: 10.4102/koedoe.V52i1.777

Singh, V., and Dubey, A. (2012) Land use Mapping using remote sensing and GIS Techniques in Naina-Gorma basin, Part of Rewa District, M. P., India. *International Journal of Emerging Technology and Advanced Engineering*: 2 (11), ISSN 2250-2459, PP 151-153

Su, Z. (2002). The Surface Energy Balance System (SEBS) for Estimation of Turbulent Heat Fluxes. *Hydrology and Earth Systems Sciences*: 6, pp. 85-99

Sun, Z., Wang, Q., Ouyang, Z., Watanabe, M., Matsushita, B., and Fukushima, T. (2007). Evaluation of MOD 16 algorithm using MODIS and ground observational data in winter wheat field in North China Plain. *Hydrological processes*: 21, pp 1196-1205

Verbesselt, J., Hyndman, R., Zeileis, A., and Culvenor, D. (2010). Phenological Change Detection while Accounting for Abrupt and Gradual Trends in Satellite Image Time Series. *Remote Sensing of Environment*: 114 (12), pp. 2970-2980

Wackerly, D.D., Mendenhall III, W., and Scheaffer, R.L. (2008). *Mathematical Statistics with Applications*, Seventh Edition. Thomson Higher Education. 10 Davis Drive, Belmont, CA 94002-3098, USA, ISBN-13:978-0-495-38508-0, PP 1-939

Weepener, H.L., Van Den Berg, H.M., Metz, M., and Hamandawana, H. (2011) The development of a hydrologically improved Digital Elevation Model and derived products for South Africa based on the SRTM DEM. WRC Report no. K5/1908, Water Research Commission, Pretoria, South Africa.

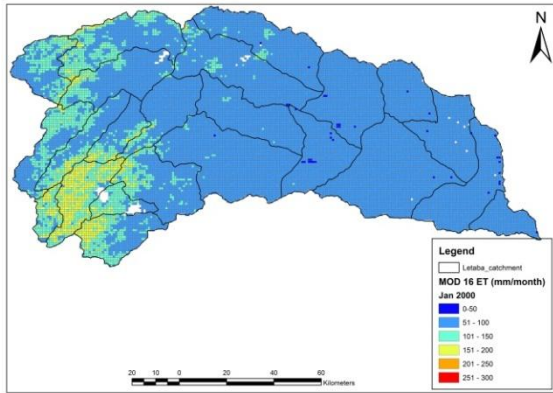
Weligepolage, K. (2005). Estimation of Spatial and temporal distribution of evapotranspiration by satellite remote sensing: A case study in Hupselse Beek, The Netherlands: MSc, Geoinformation Science and Earth Observation in Water Resources and Environmental Management programme specialisation: Watershed Management, Conservation and River Basin Planning

Xu, C. Y., and Singh, V. P. (2005). Evaluation of three complementary relationship evapotranspiration models by water balance approach to estimate actual regional evapotranspiration in different climatic regions. *Journal of Hydrology*: 308, pp 105-121

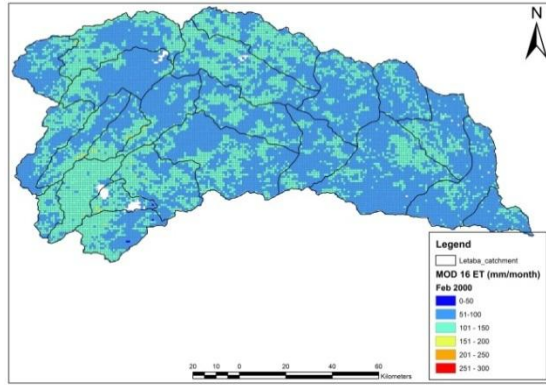
Appendices

Appendix A: Monthly MOD 16 ET in the Letaba catchment

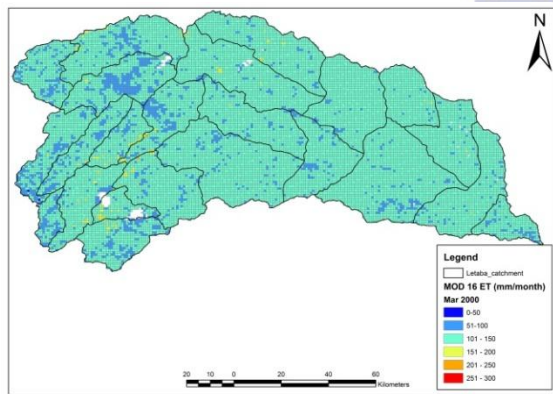
January 2000



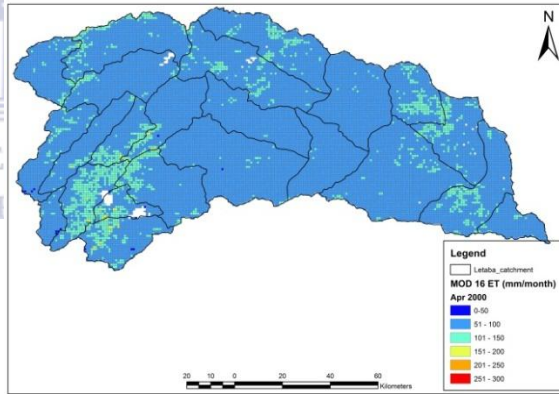
February 2000



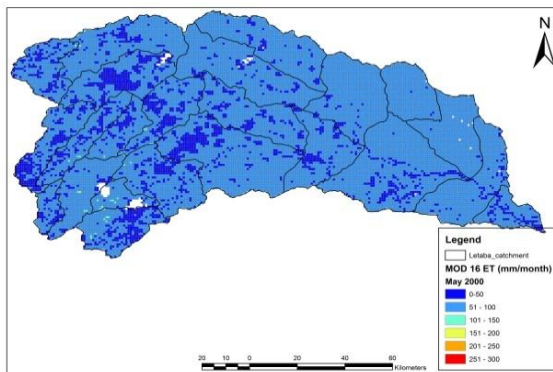
March 2000



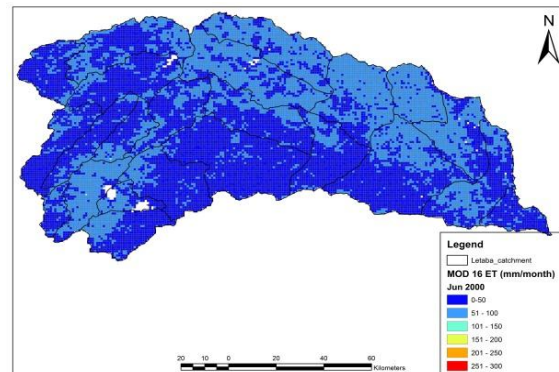
April 2000



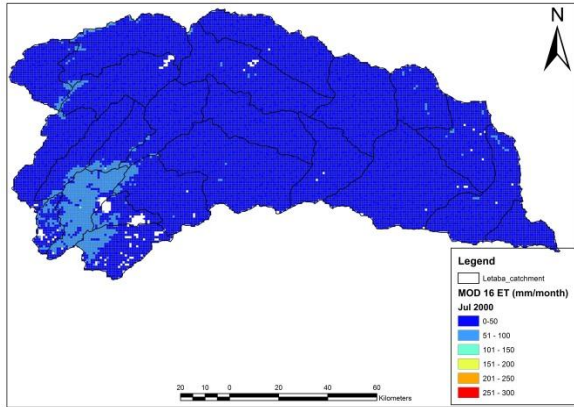
May 2000



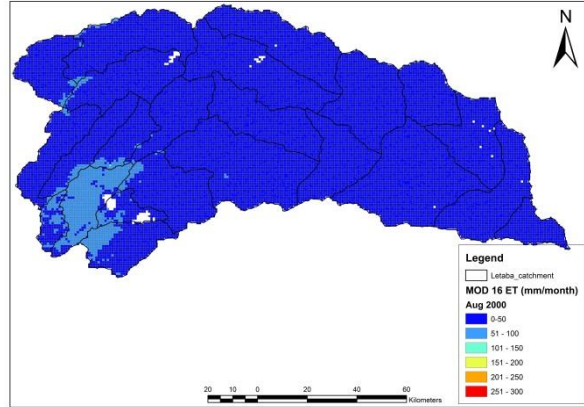
June 2000



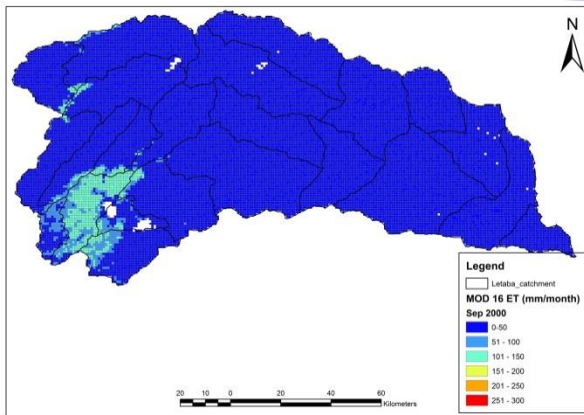
July 2000



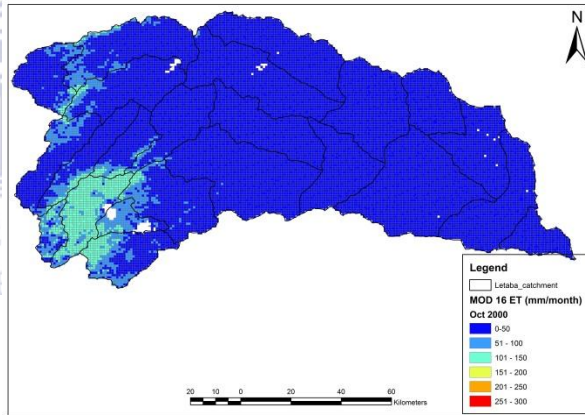
August 2000



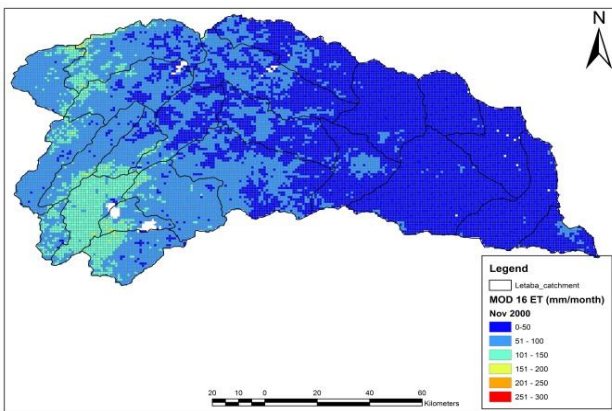
September 2000



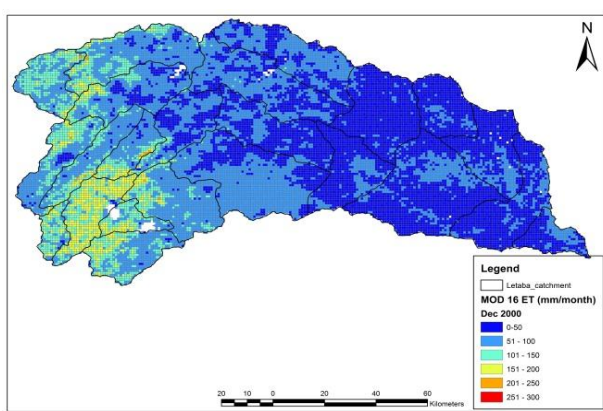
October 2000



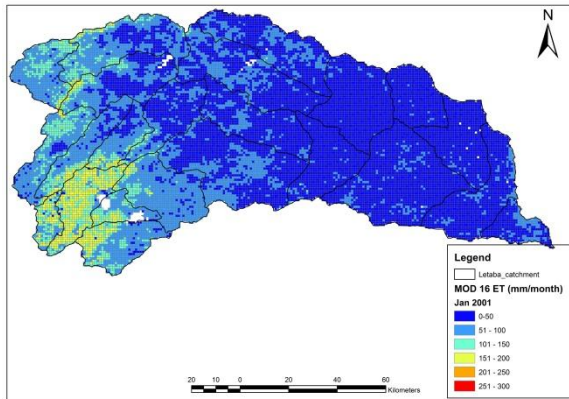
November 2000



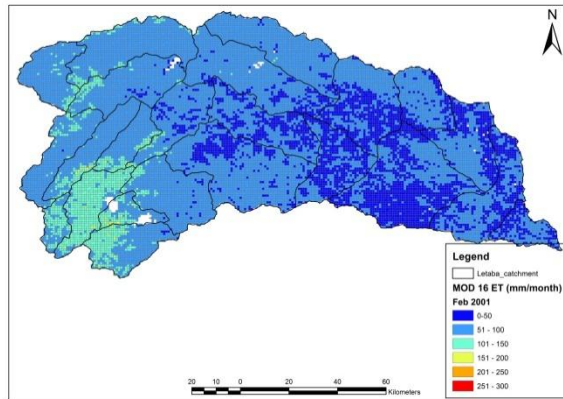
December 2000



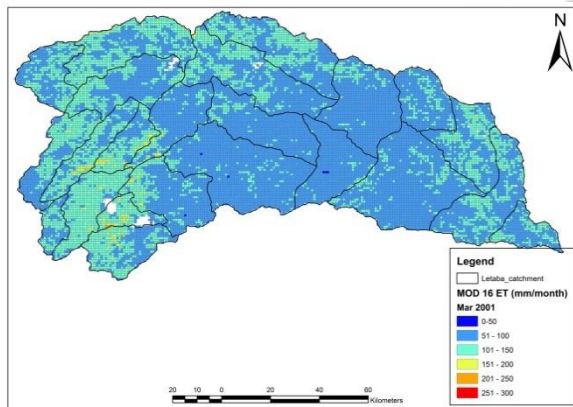
January 2001



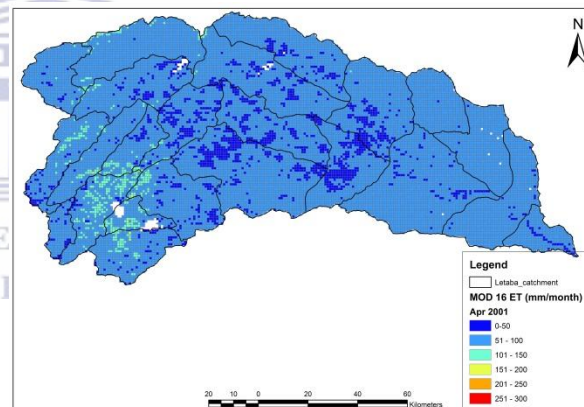
February 2001



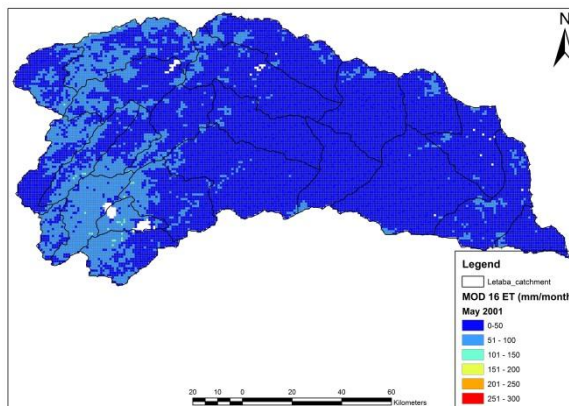
March 2001



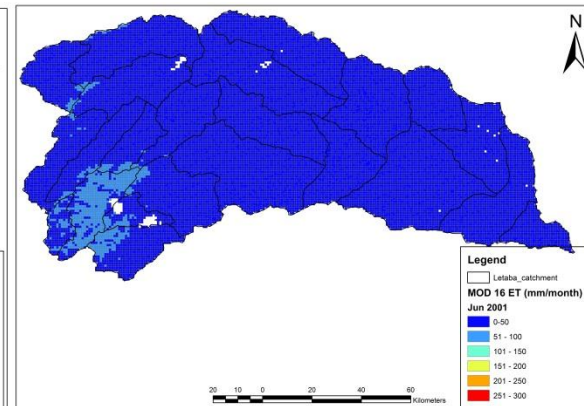
April 2001



May 2001

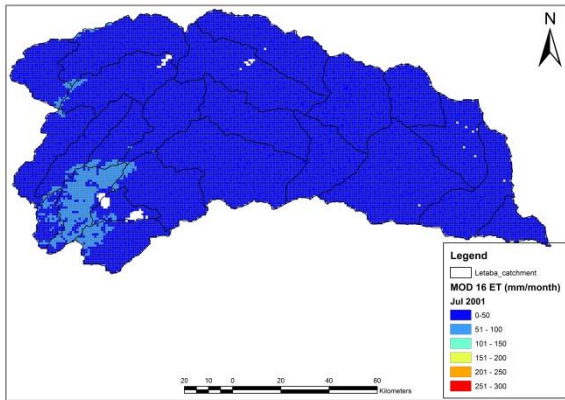


June 2001

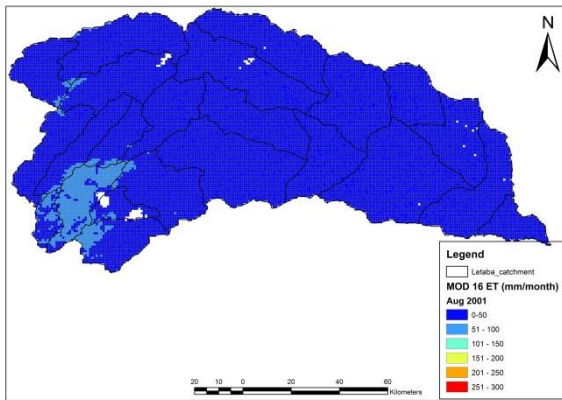




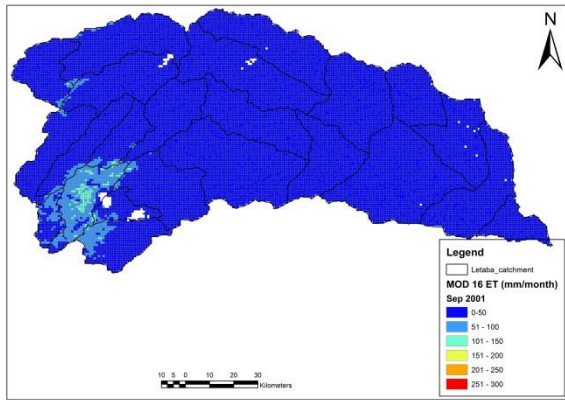
July 2001



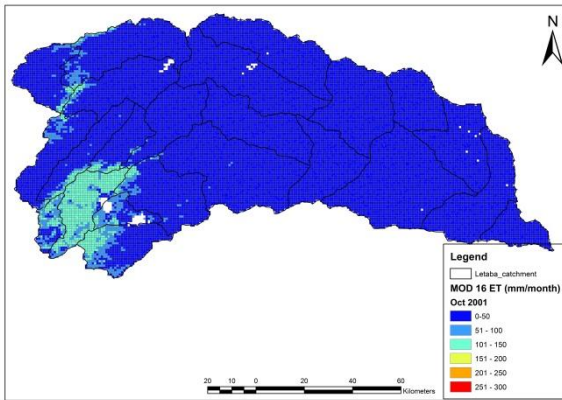
August 2001



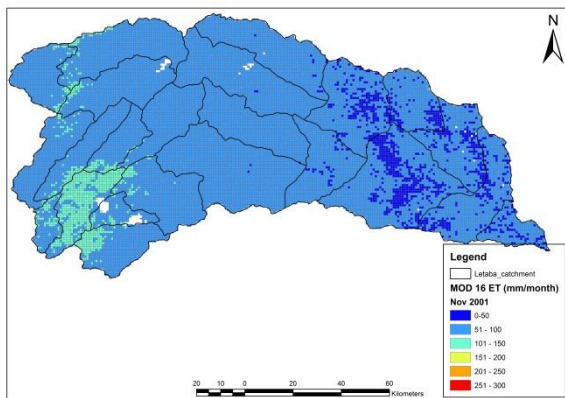
September 2001



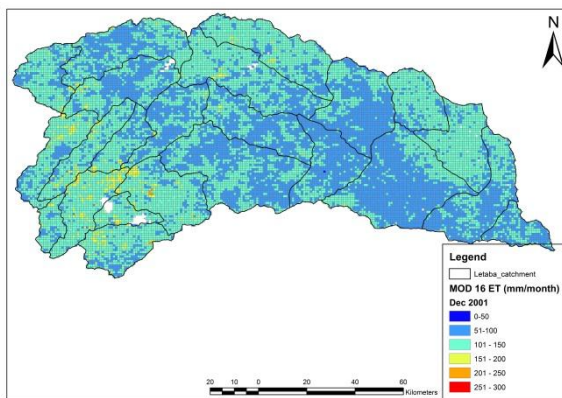
October 2001



November 2001

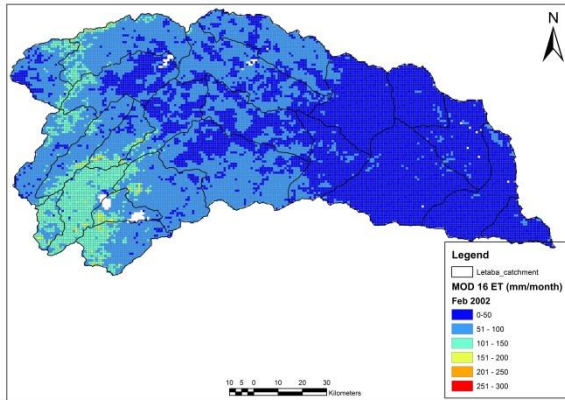
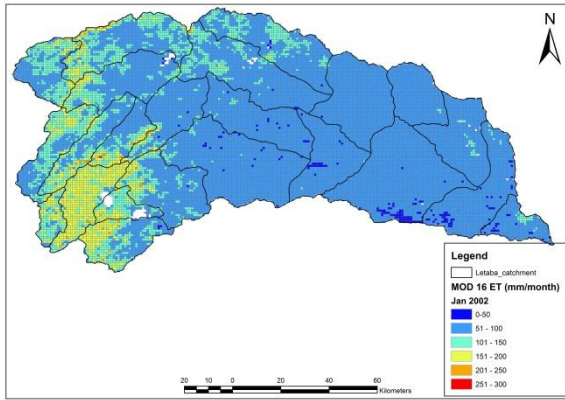


December 2001



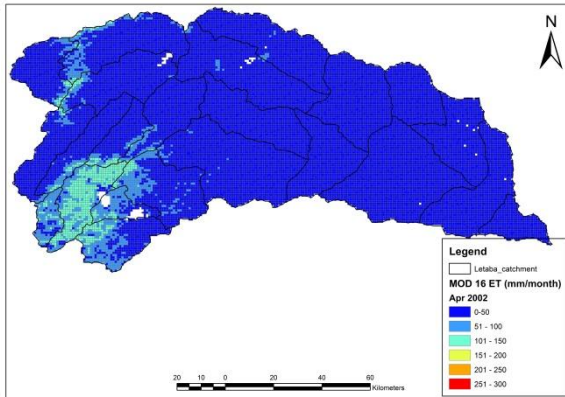
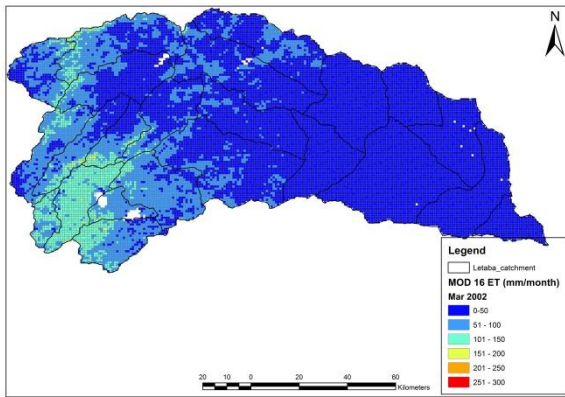
January 2002

February 2002



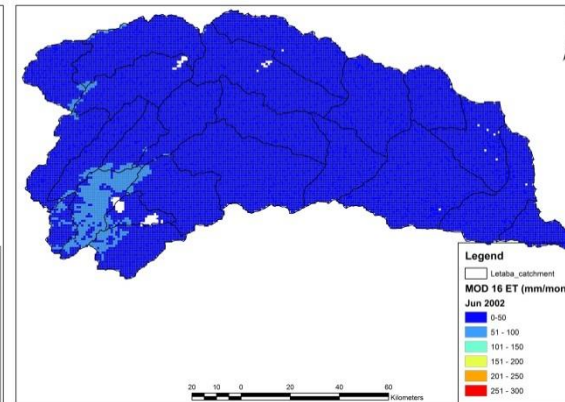
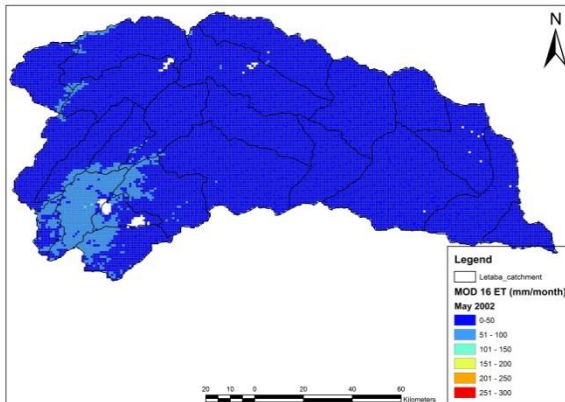
March 2002

April 2002

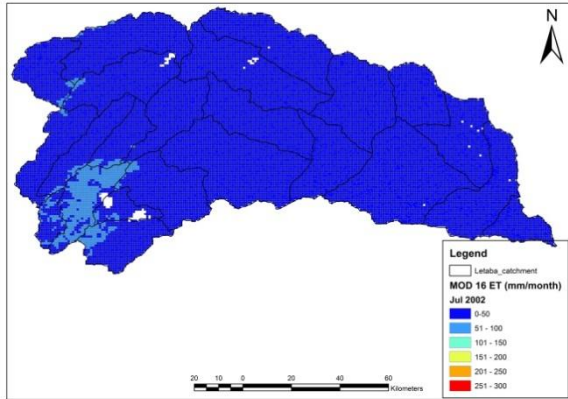


May 2002

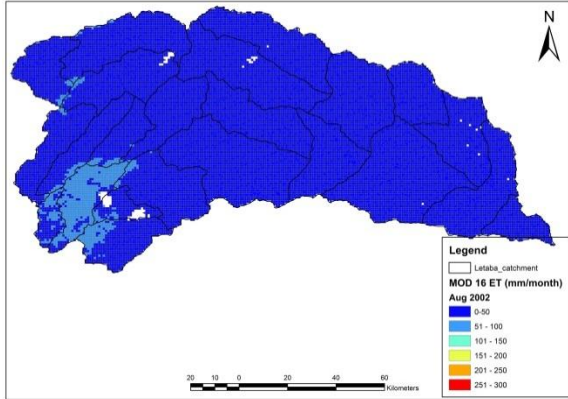
June 2002



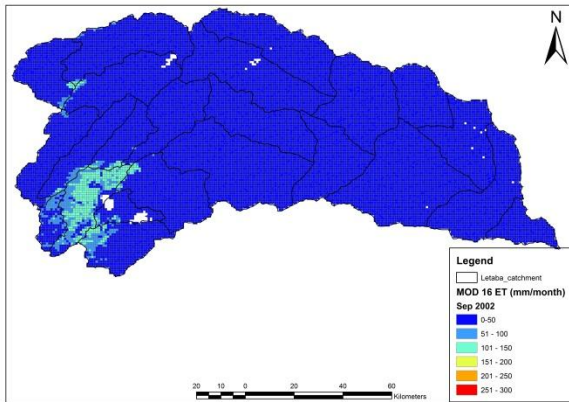
July 2002



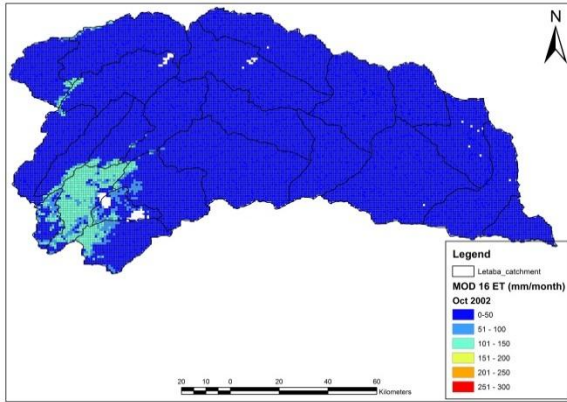
August 2002



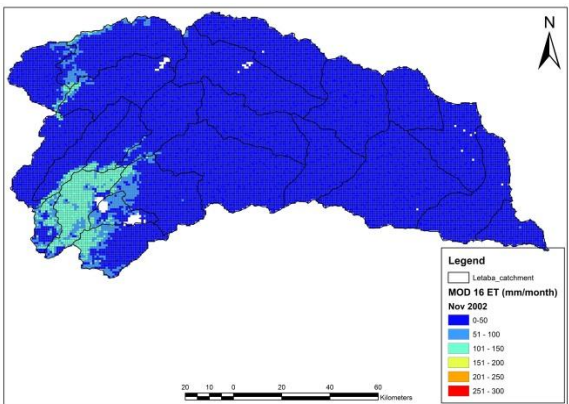
September 2002



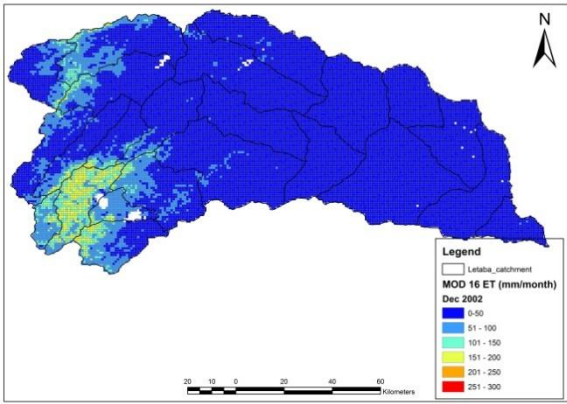
October 2002



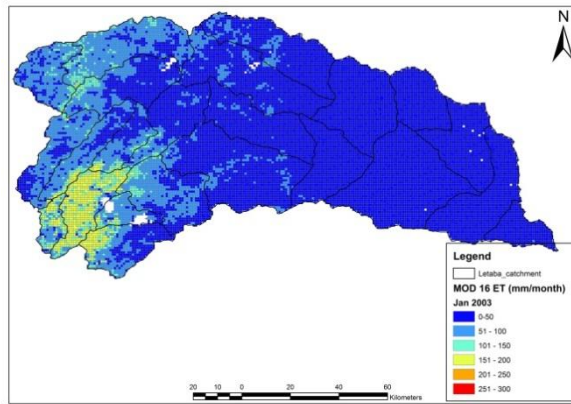
November 2002



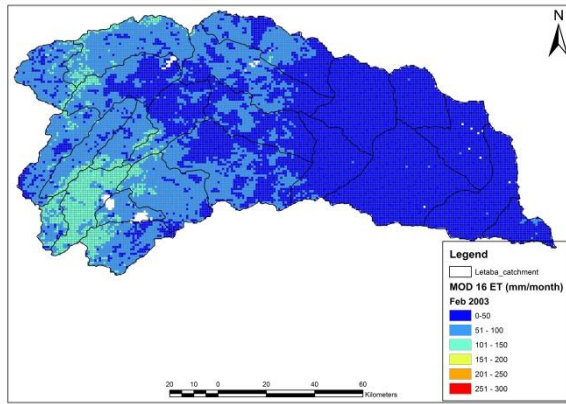
December 2002



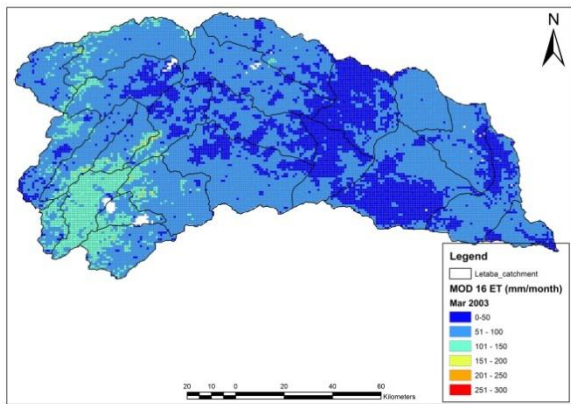
January 2003



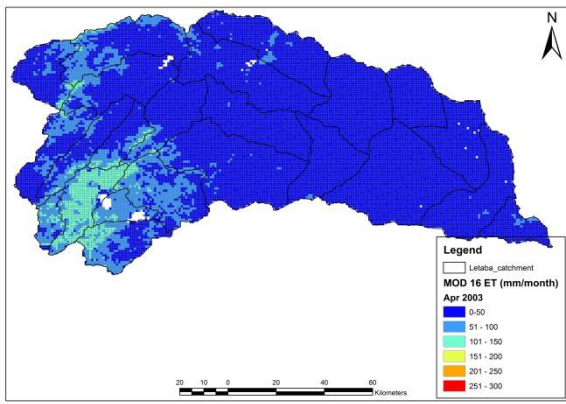
February 2003



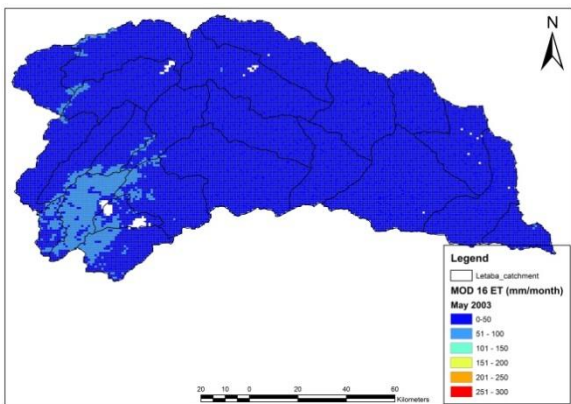
March 2003



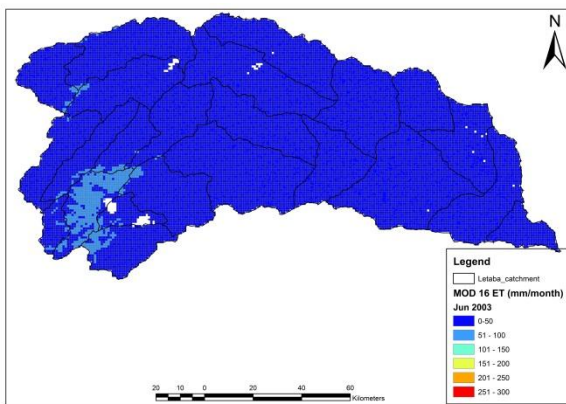
April 2003



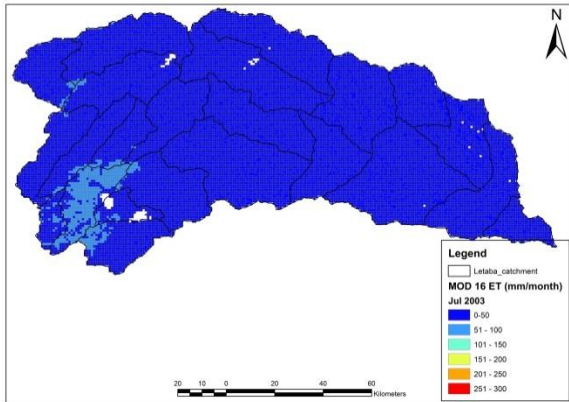
May 2003



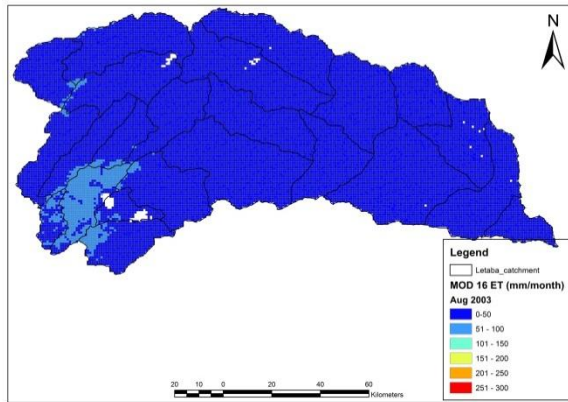
June 2003



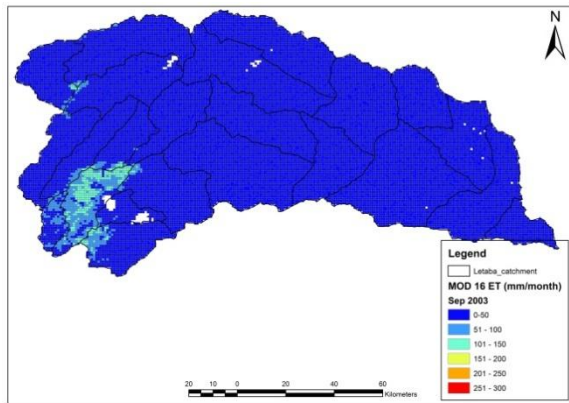
July 2003



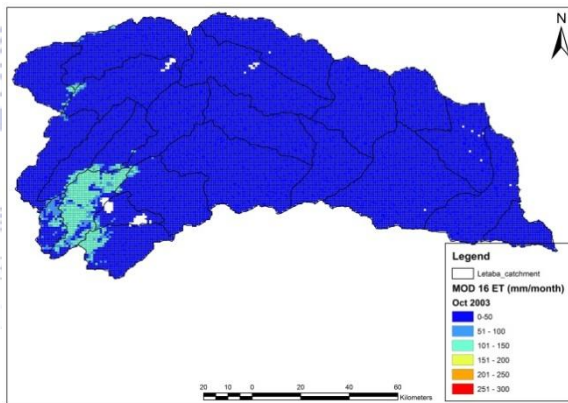
August 2003



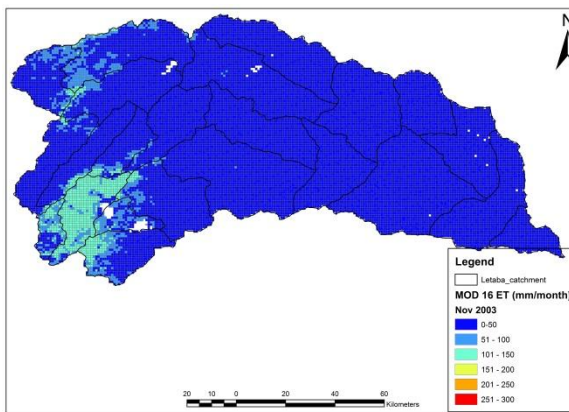
September 2003



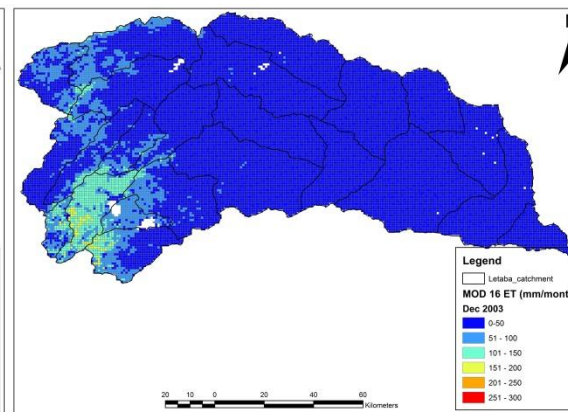
October 2003



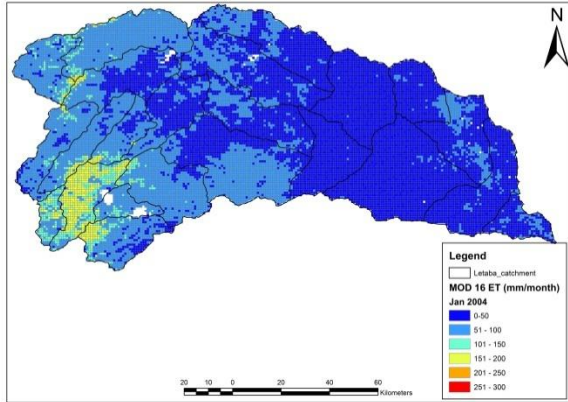
November 2003



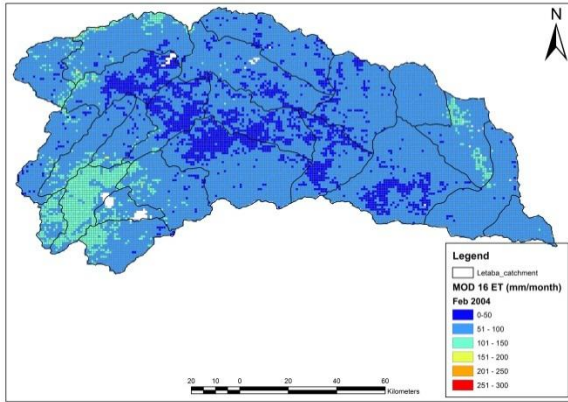
December 2003



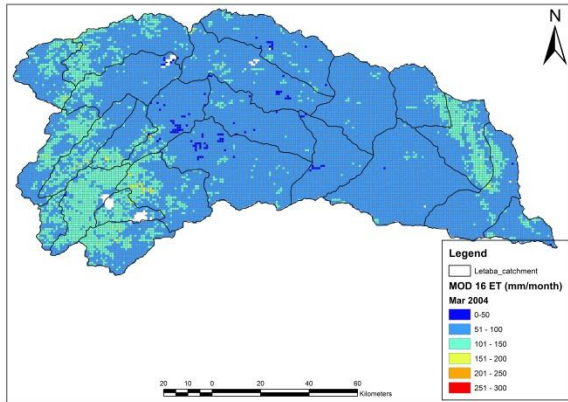
January 2004



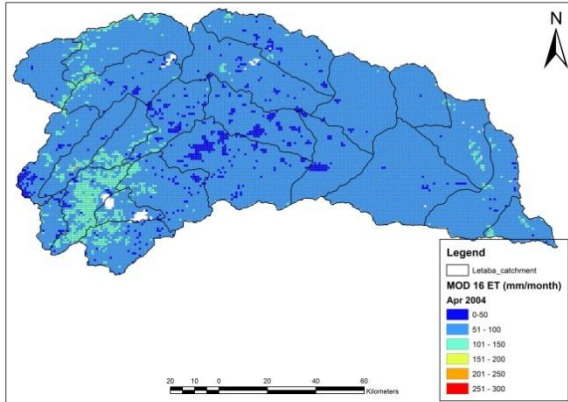
February 2004



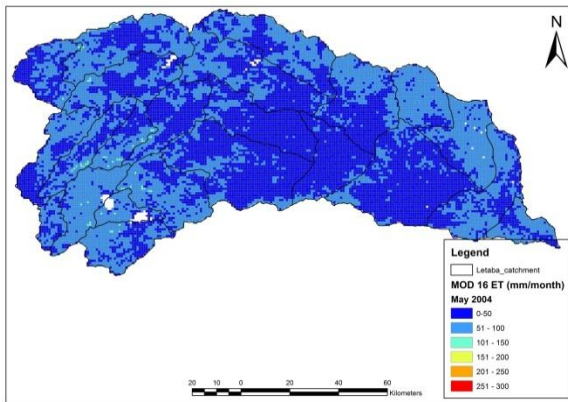
March 2004



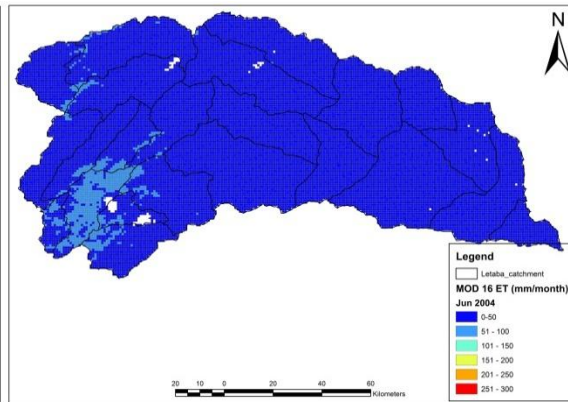
April 2004



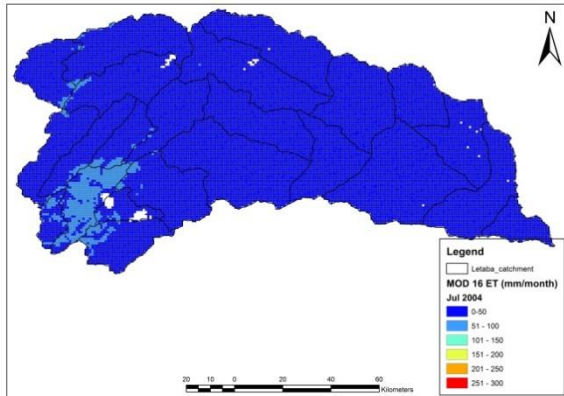
May 2004



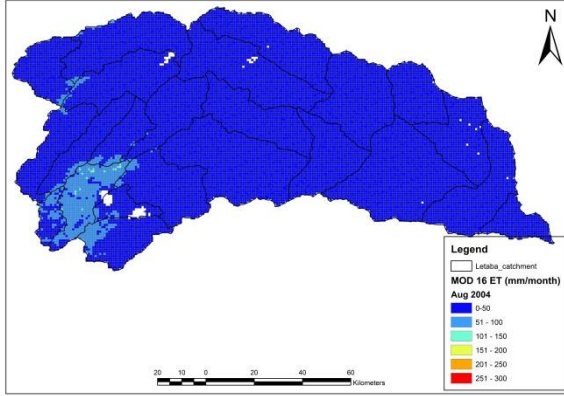
June 2004



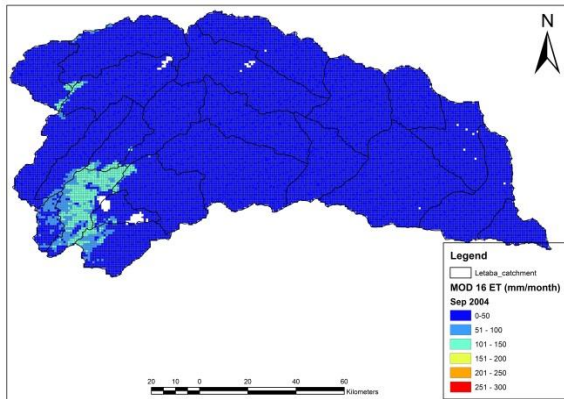
July 2004



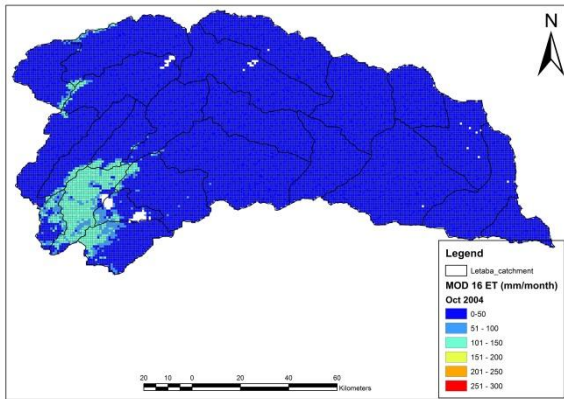
August 2004



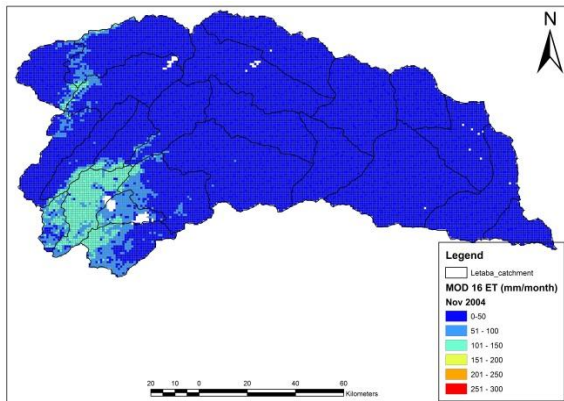
September 2004



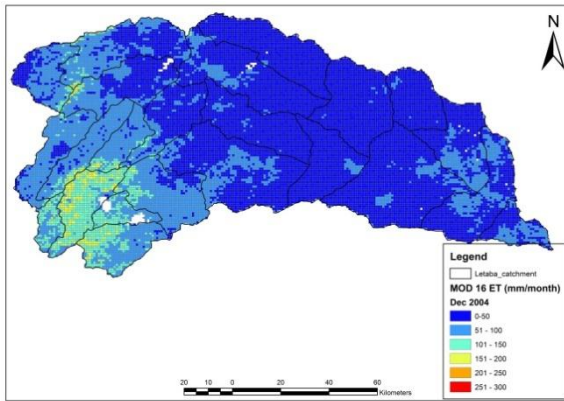
October 2004



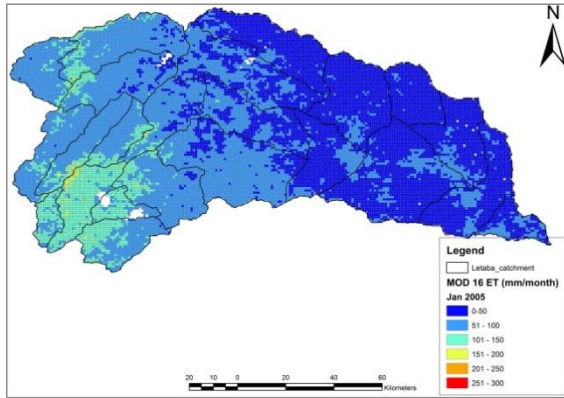
November 2004



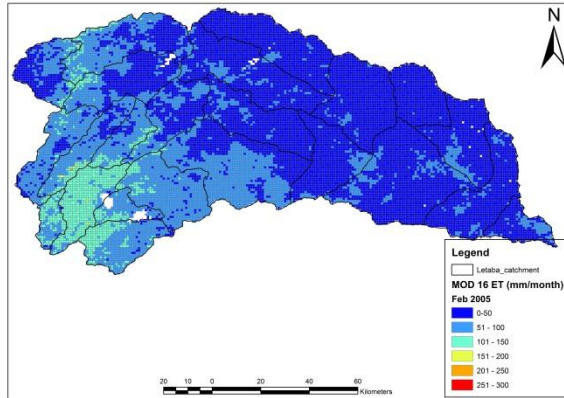
December 2004



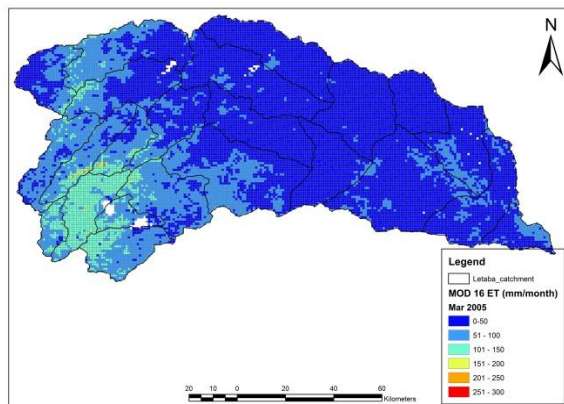
January 2005



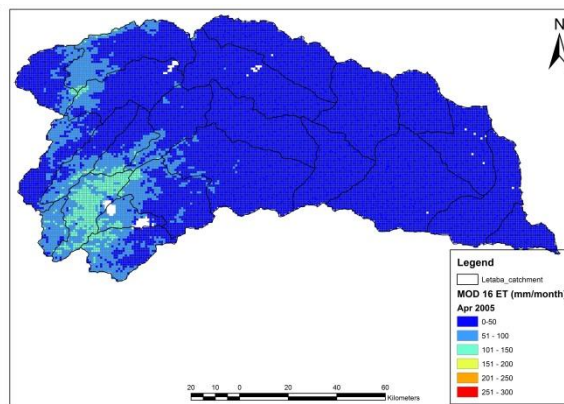
February 2005



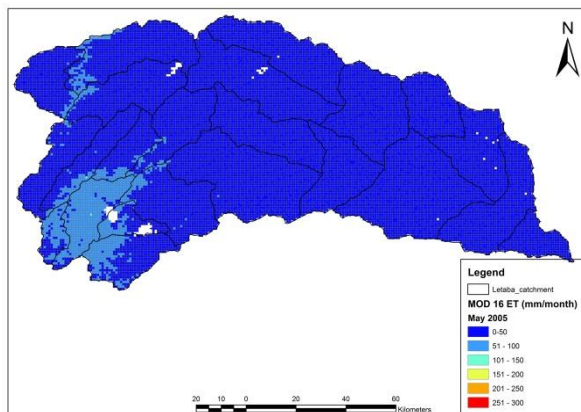
March 2005



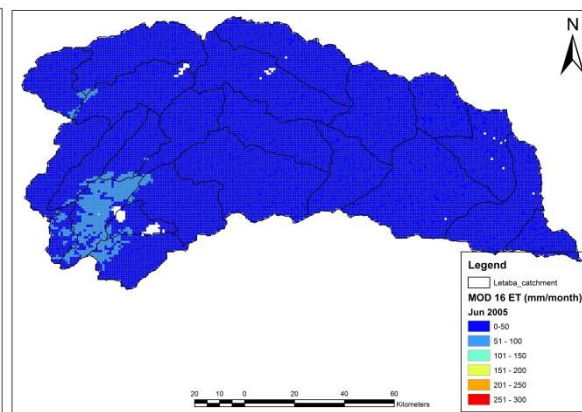
April 2005



May 2005

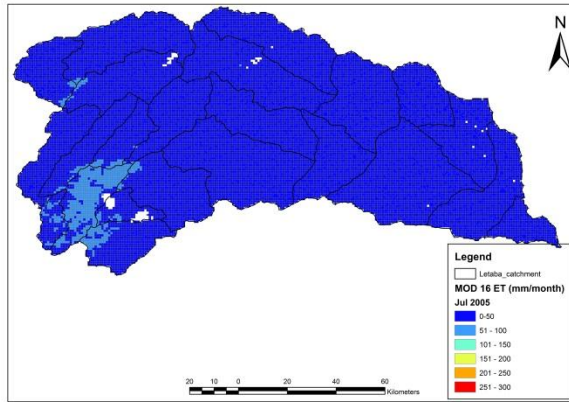


June 2005

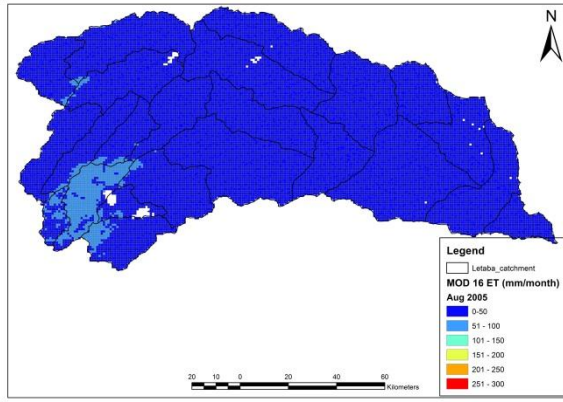




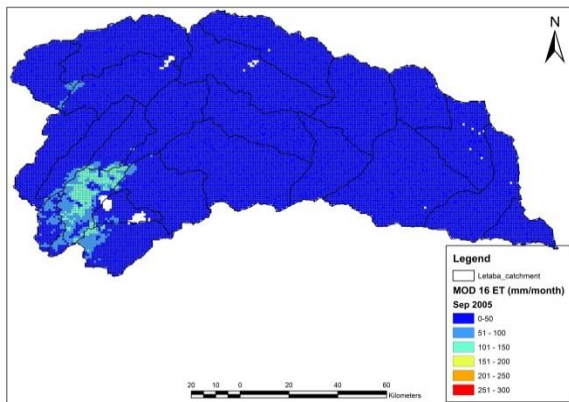
July 2005



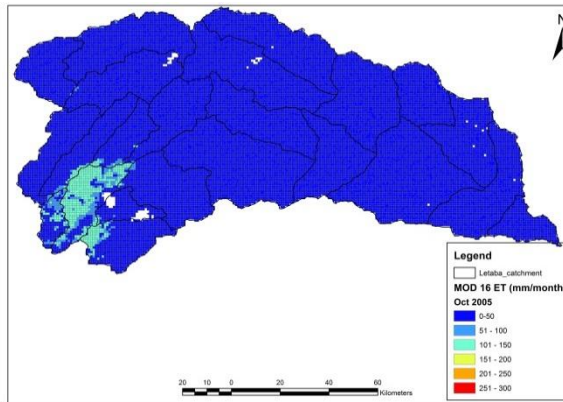
August 2005



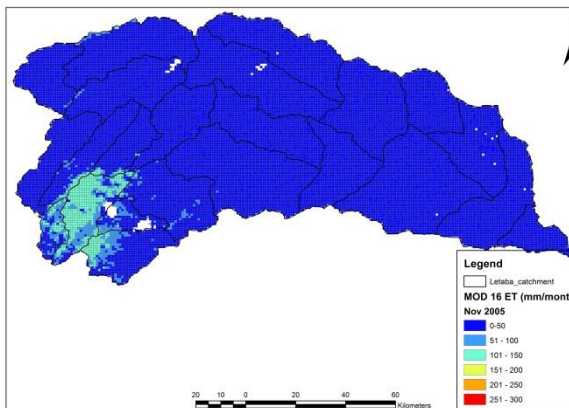
September 2005



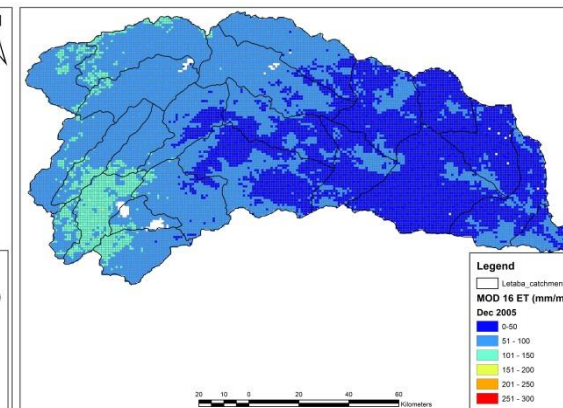
October 2005



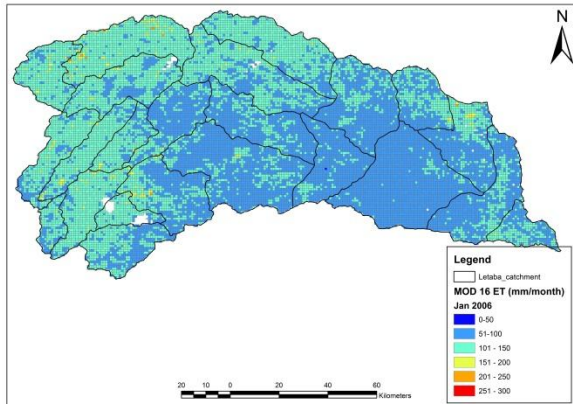
November 2005



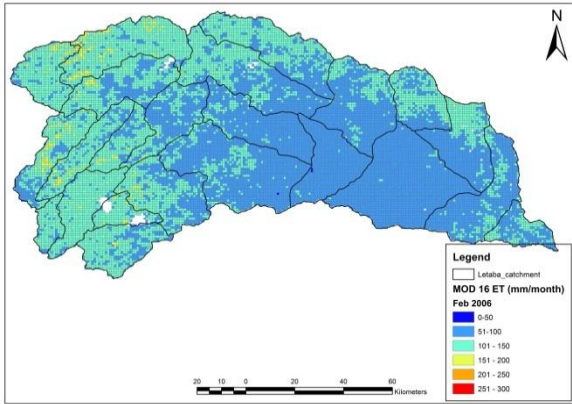
December 2005



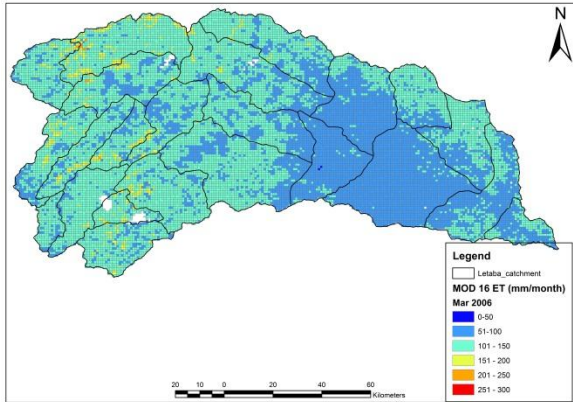
January 2006



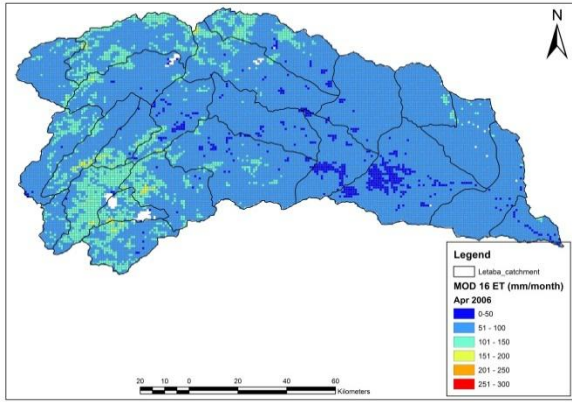
February 2006



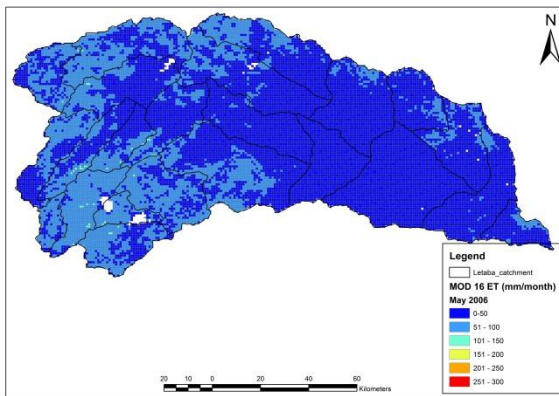
March 2006



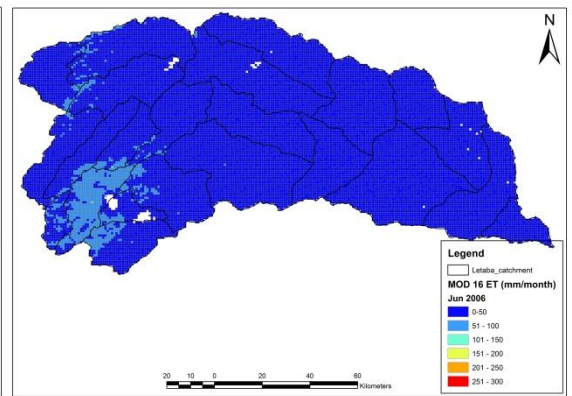
April 2006



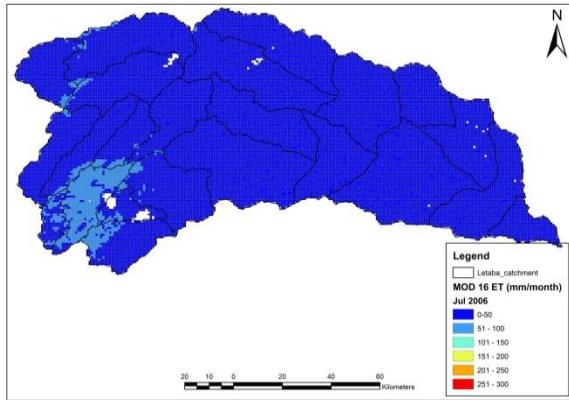
May 2006



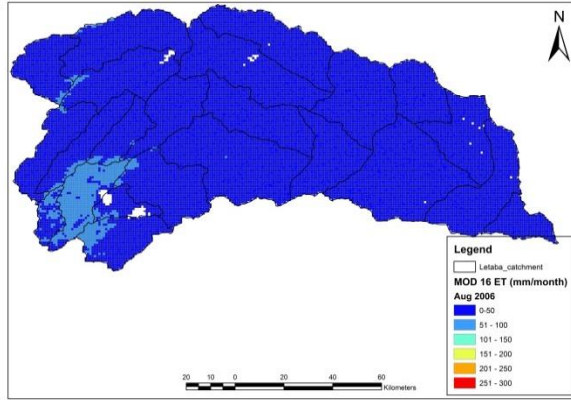
June 2006



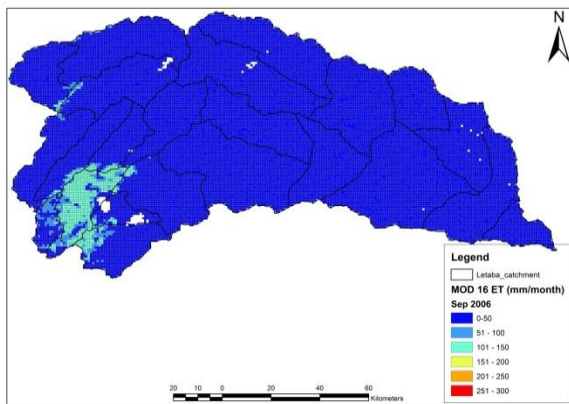
July 2006



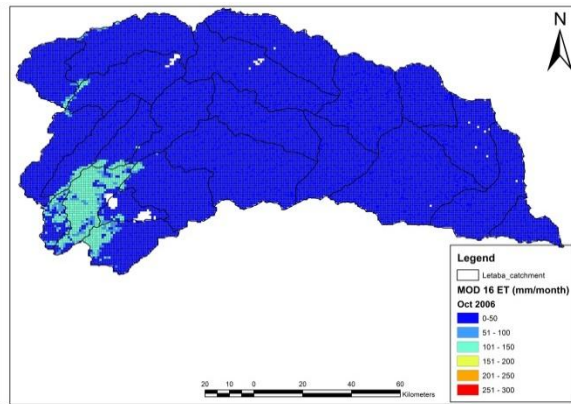
August 2006



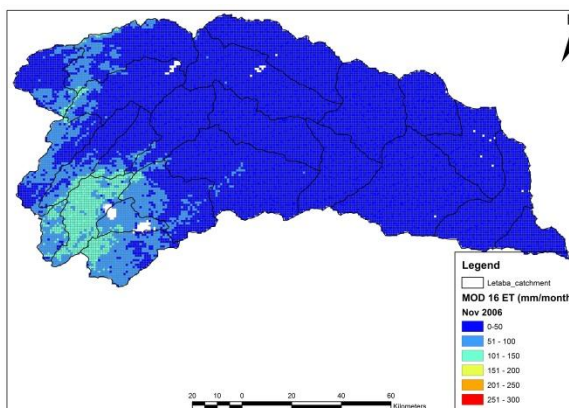
September 2006



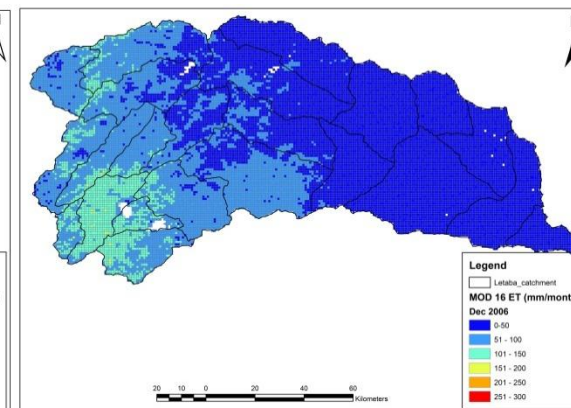
October 2006



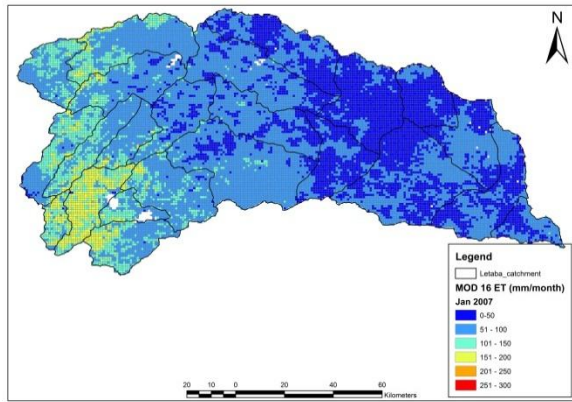
November 2006



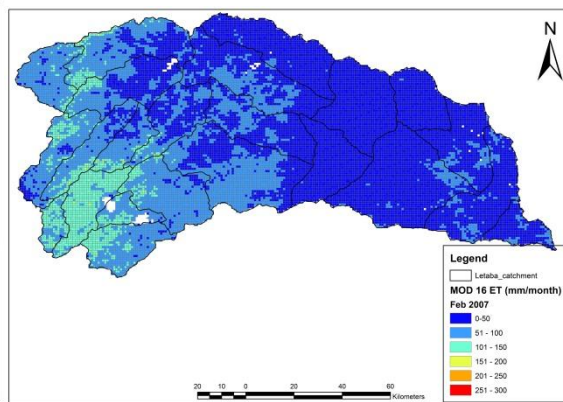
December 2006



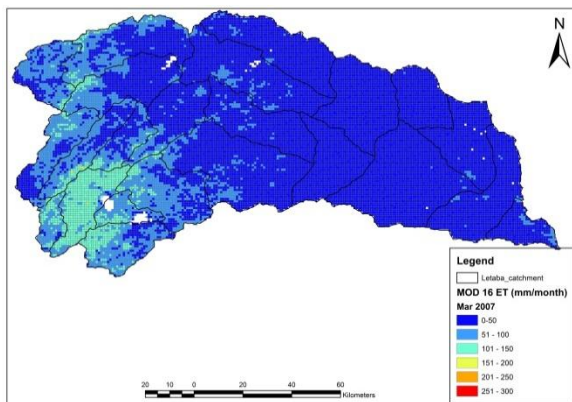
January 2007



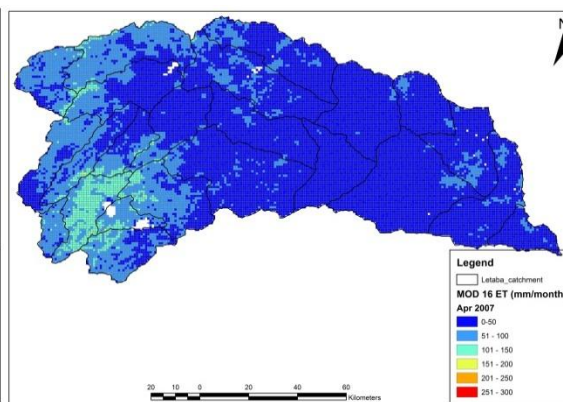
February 2007



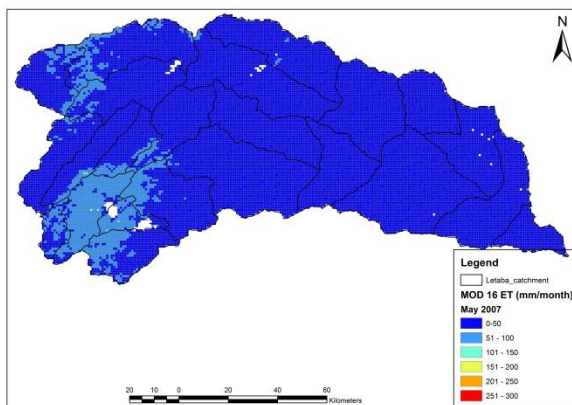
March 2007



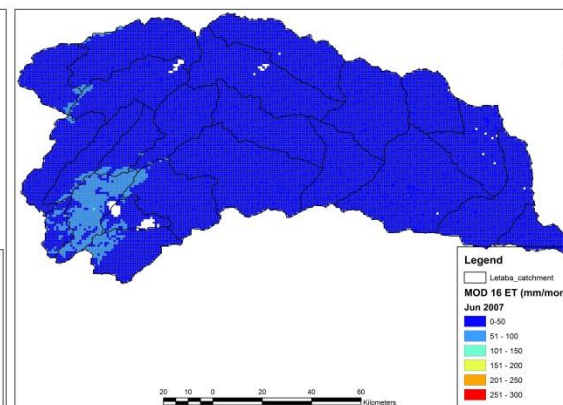
April 2007



May 2007

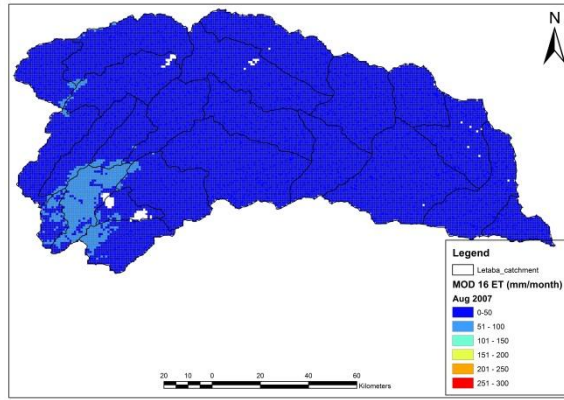
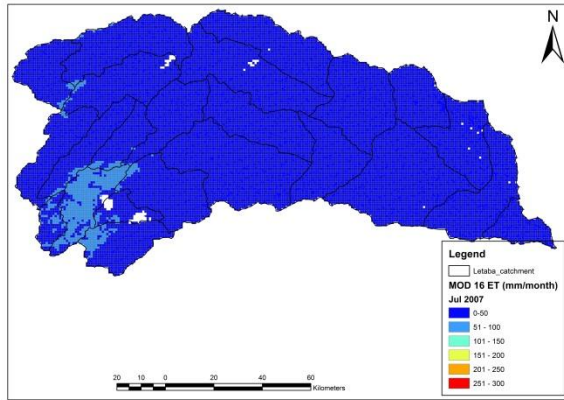


June 2007



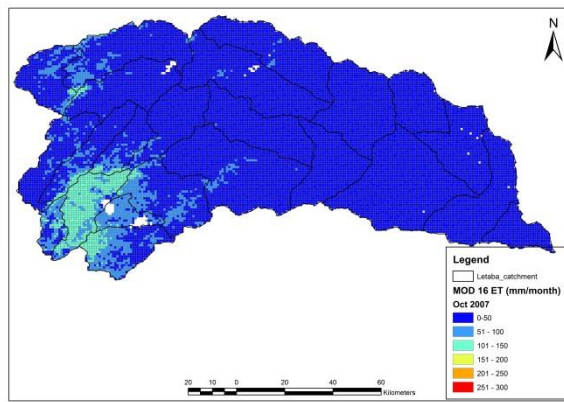
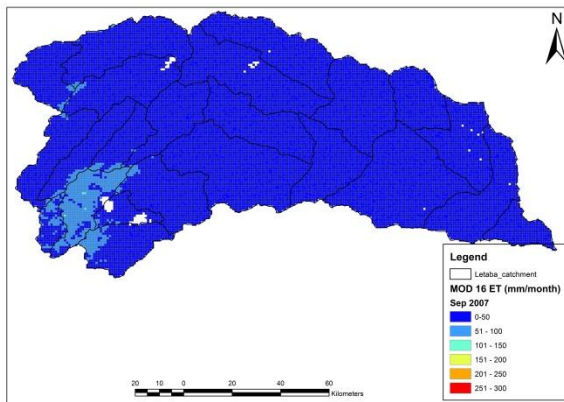
July 2007

August 2007



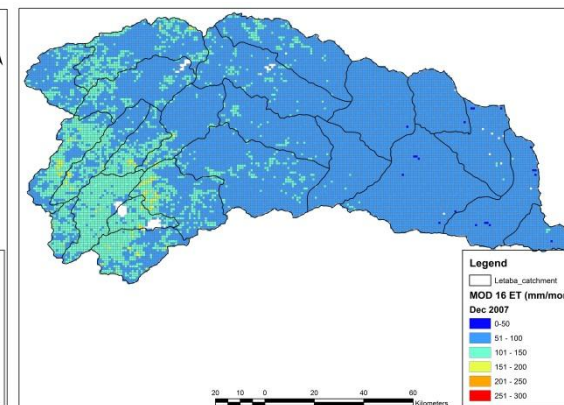
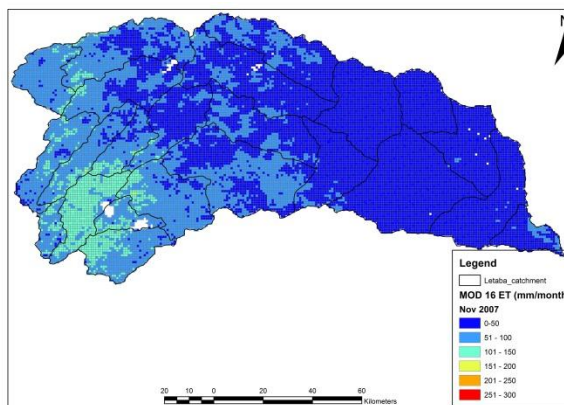
September 2007

October 2007

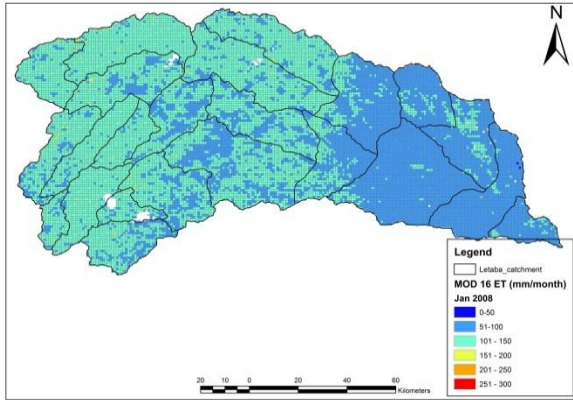


November 2007

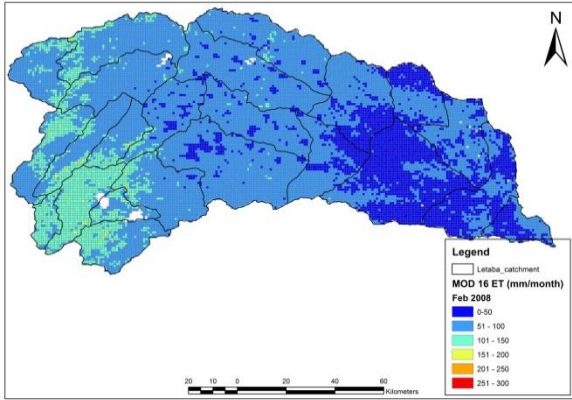
December 2007



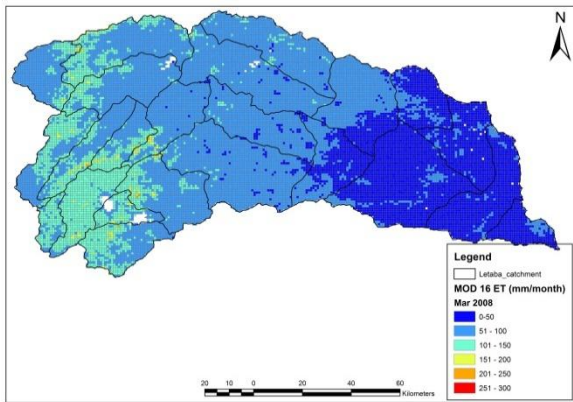
January 2008



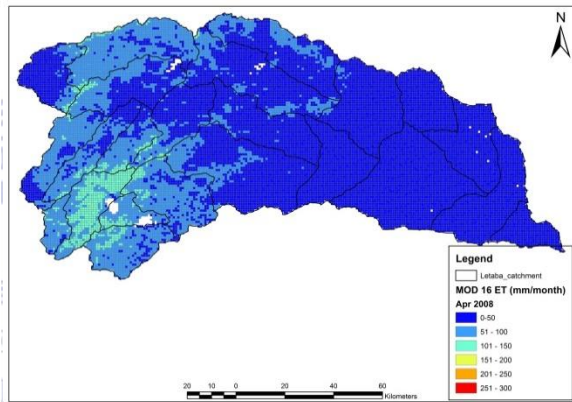
February 2008



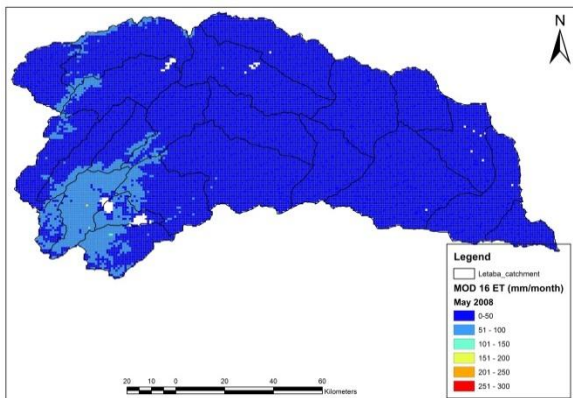
March 2008



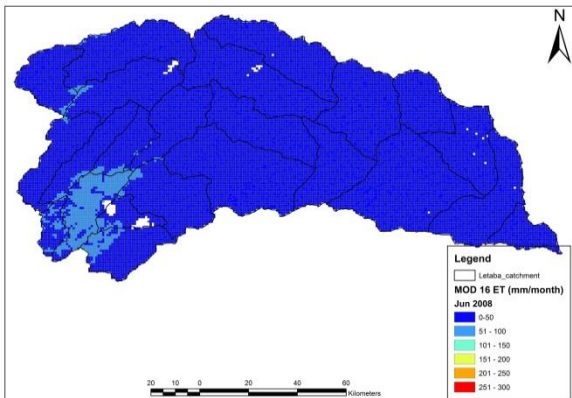
April 2008



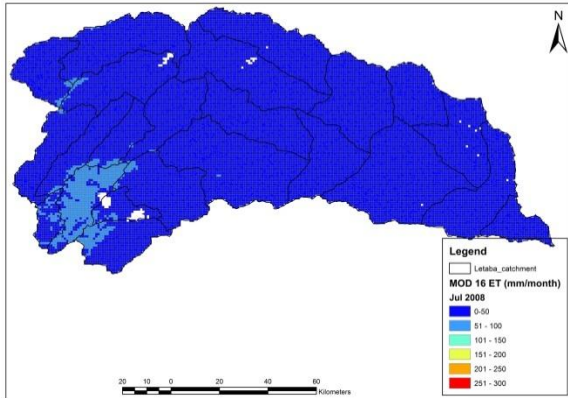
May 2008



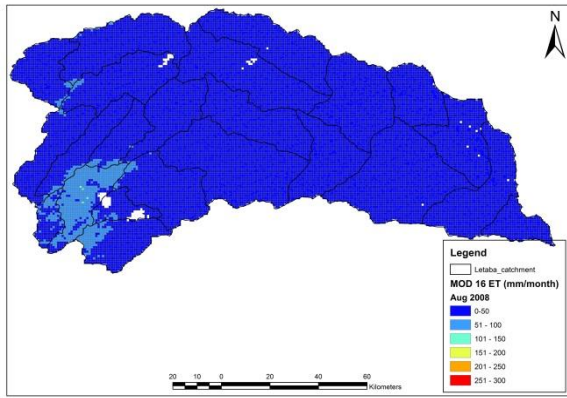
June 2008



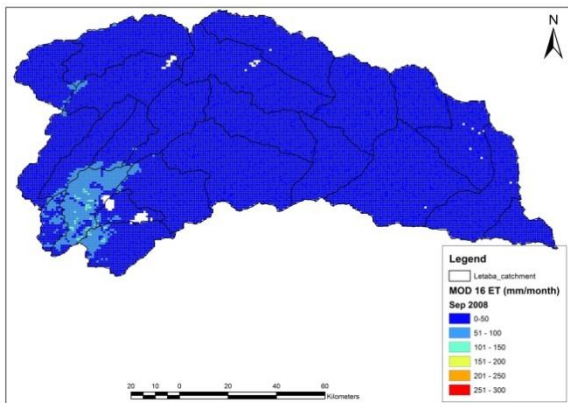
July 2008



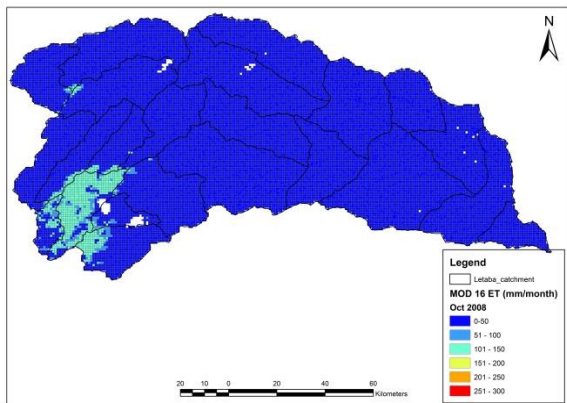
August 2008



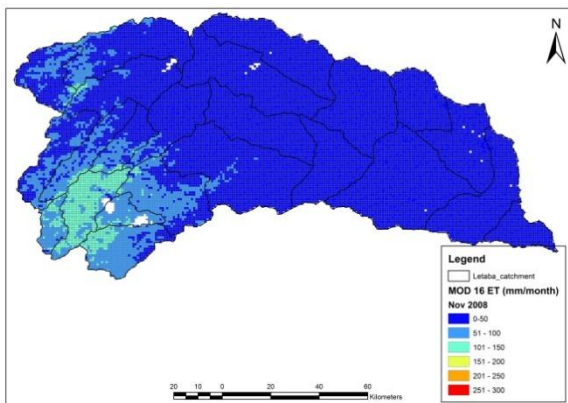
September 2008



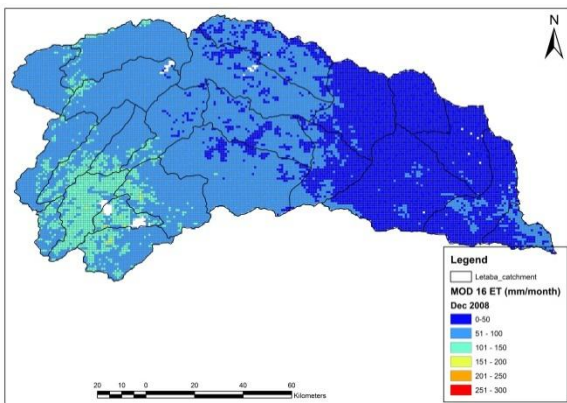
October 2008



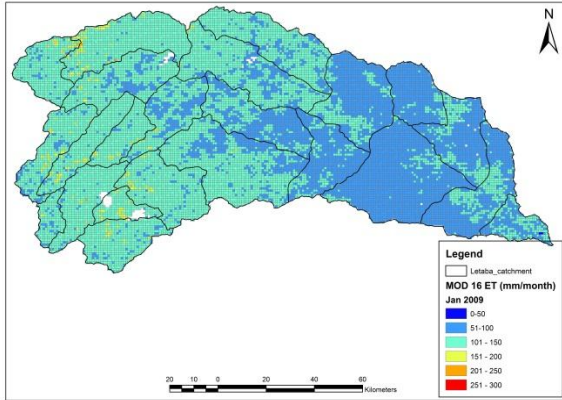
November 2008



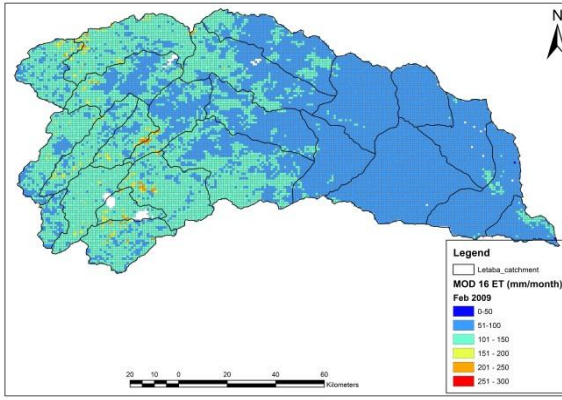
December 2008



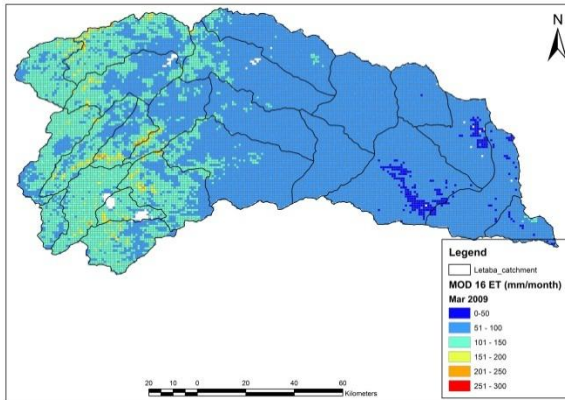
January 2009



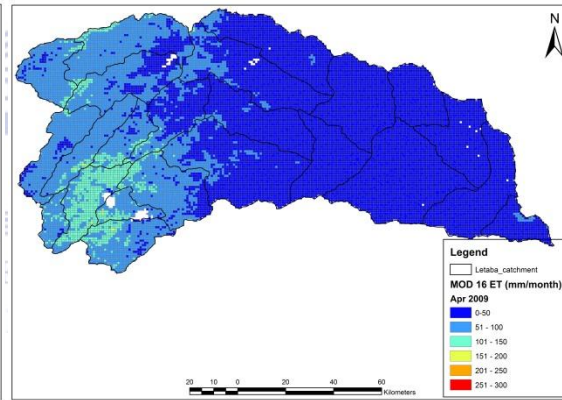
February 2009



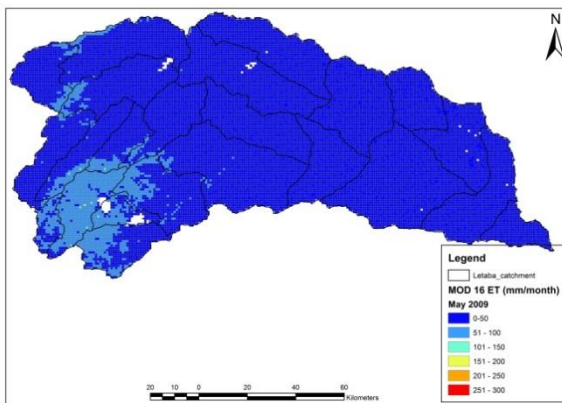
March 2009



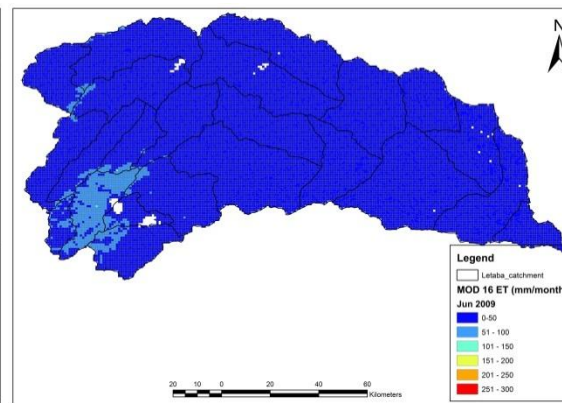
April 2009



May 2009



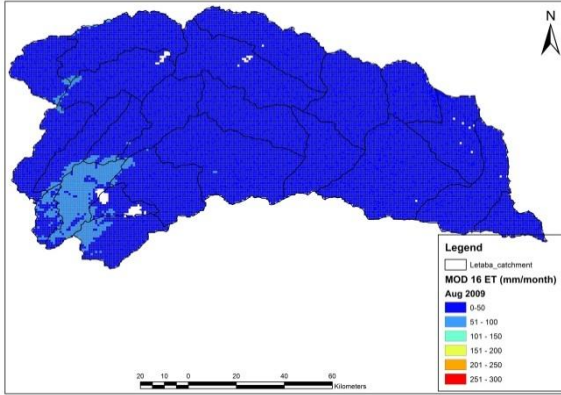
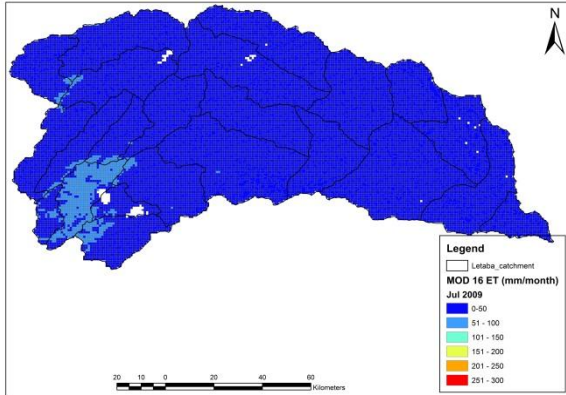
June 2009





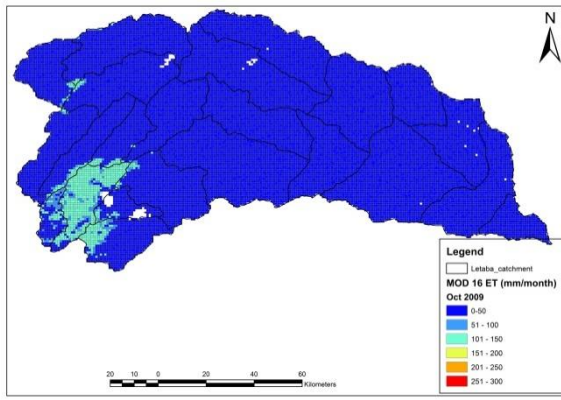
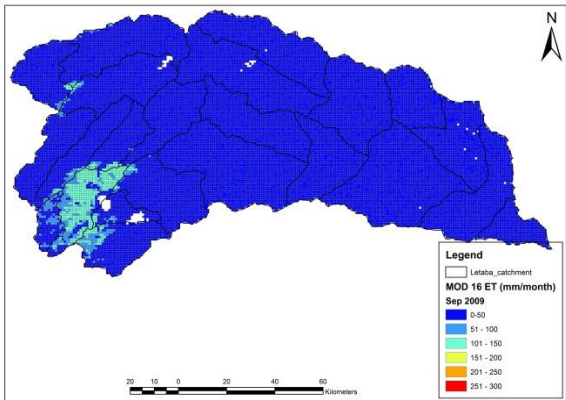
July 2009

August 2009



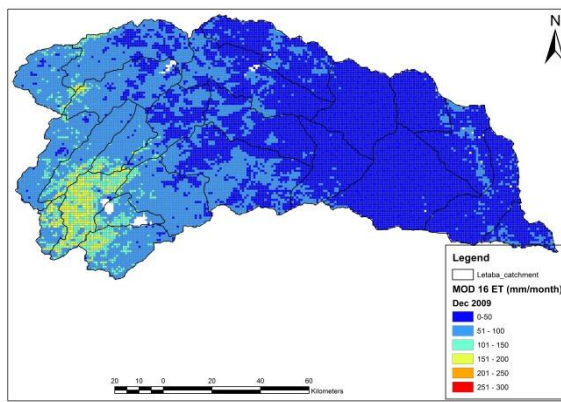
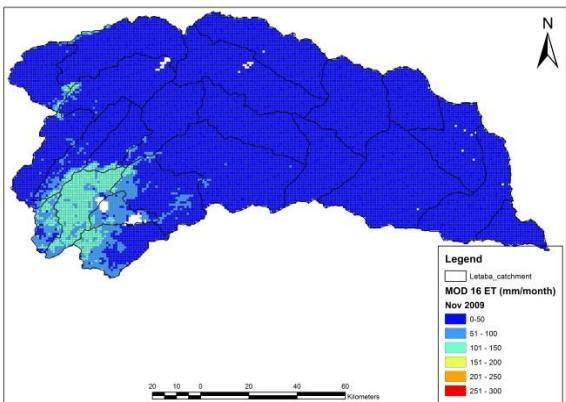
September 2009

October 2009



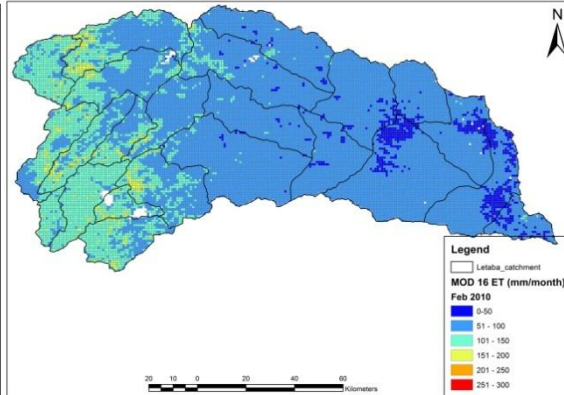
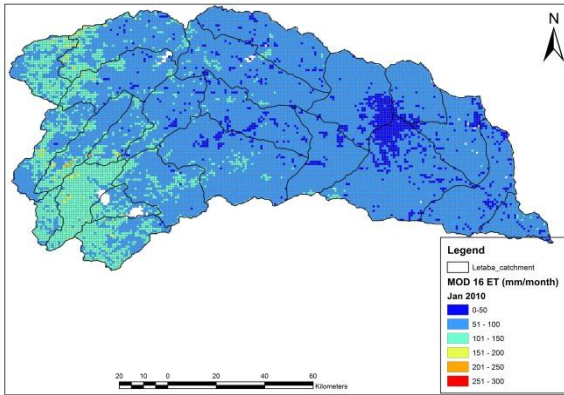
November 2009

December 2009



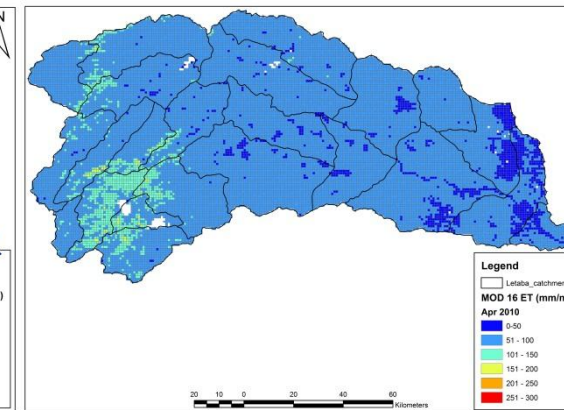
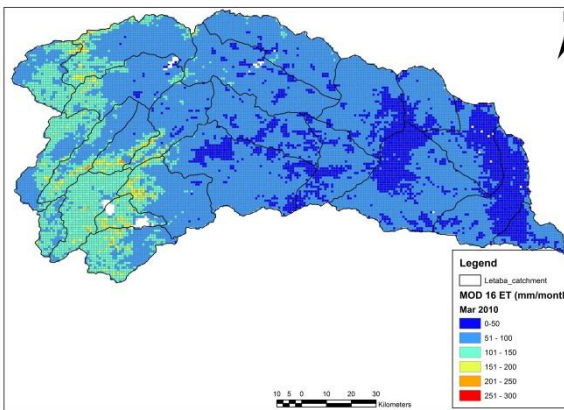
January 2010

February 2010



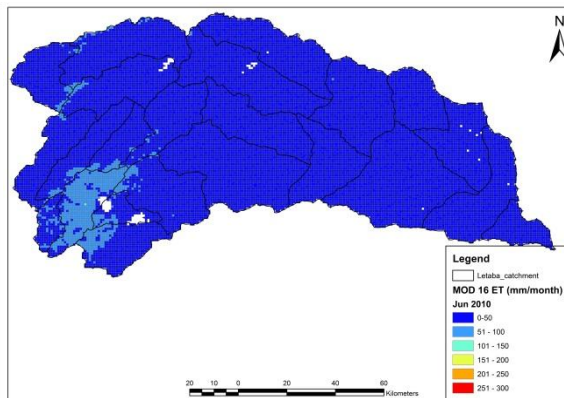
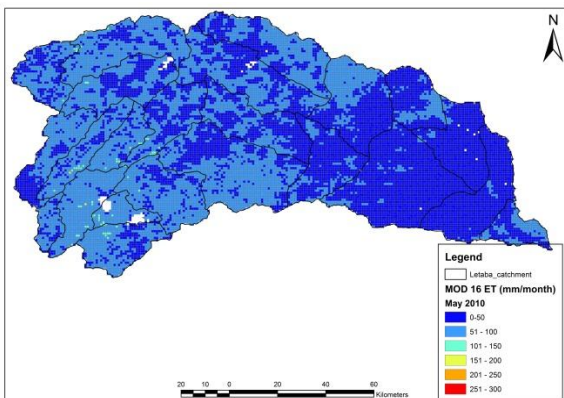
March 2010

April 2010

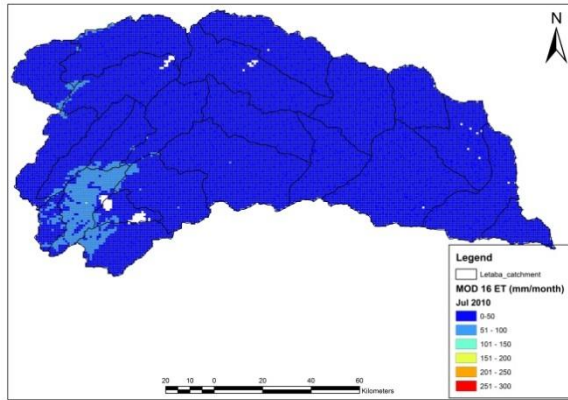


May 2010

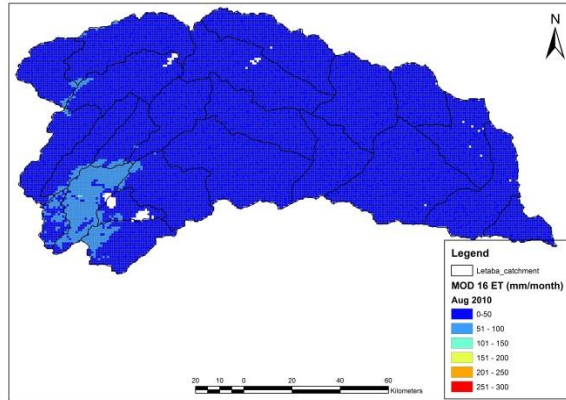
June 2010



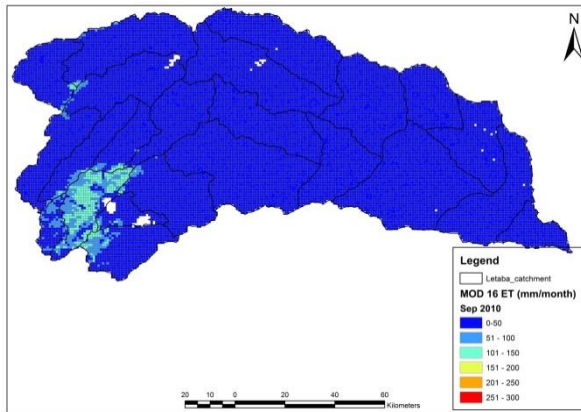
July 2010



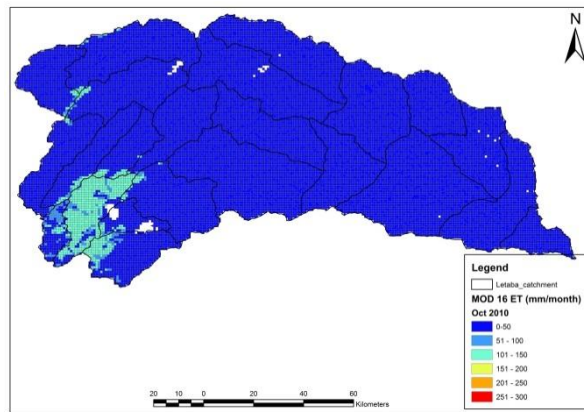
August 2010



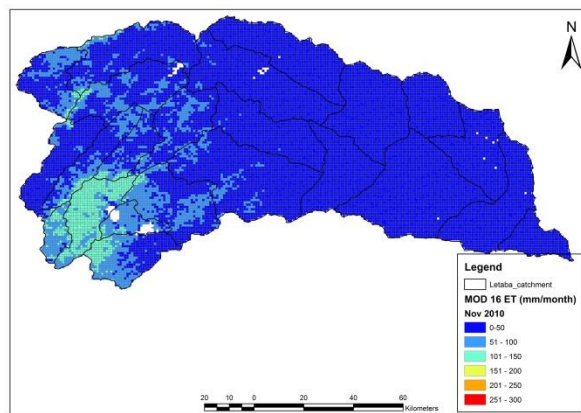
September 2010



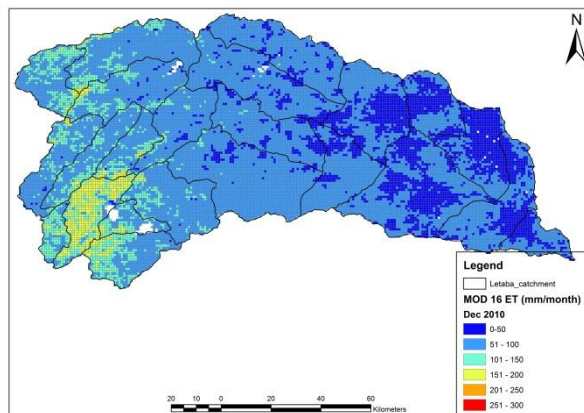
October 2010



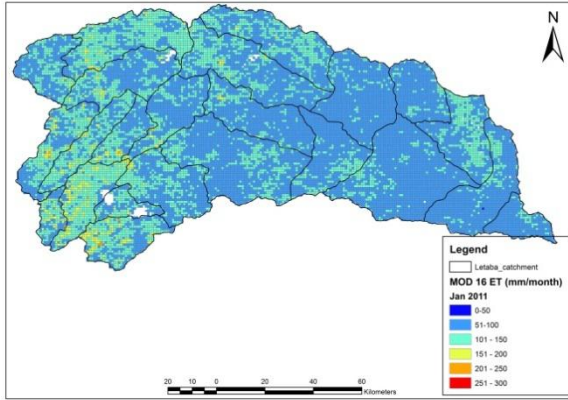
November 2010



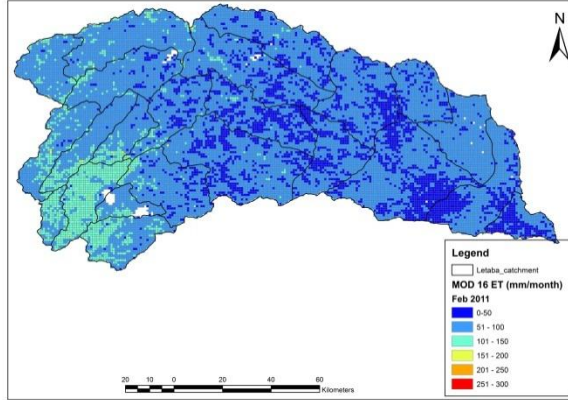
December 2010



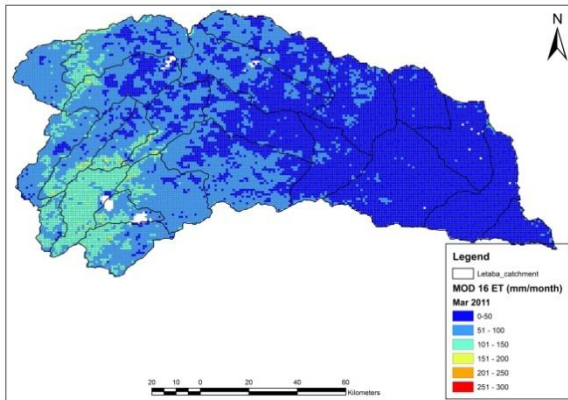
January 2011



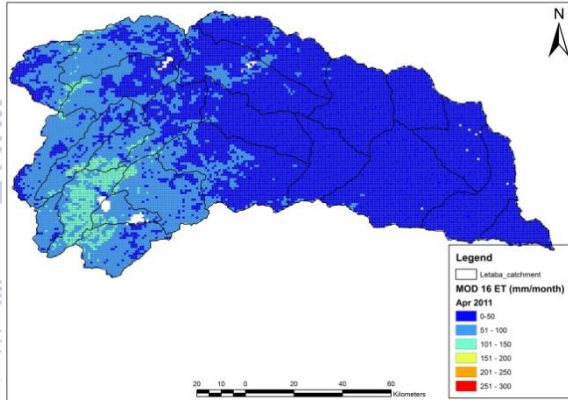
February 2011



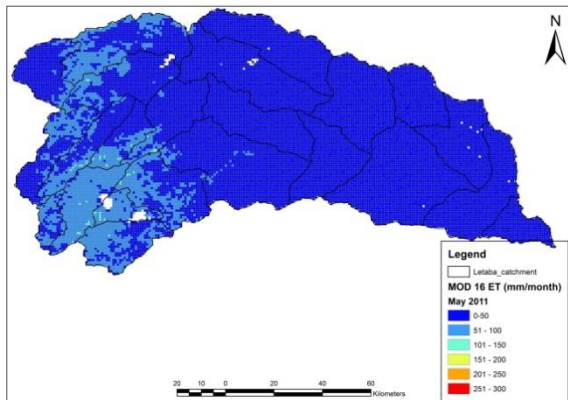
March 2011



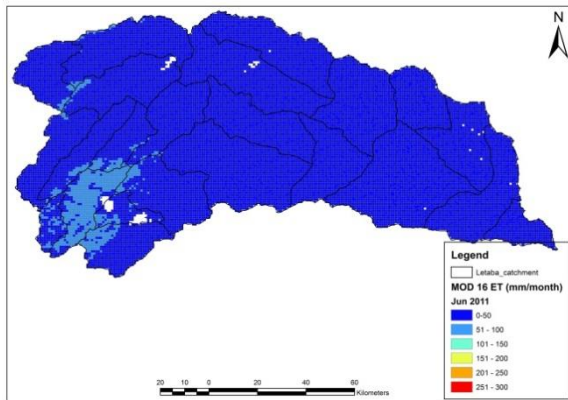
April 2011



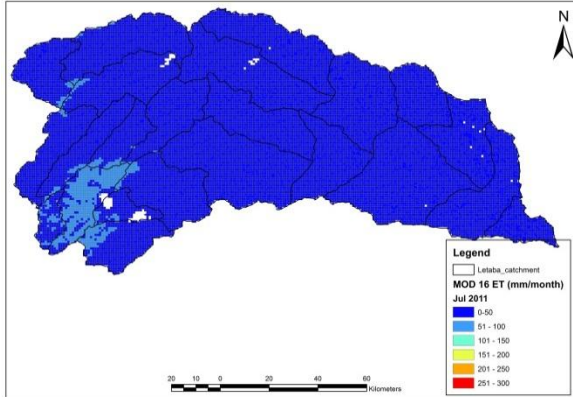
May 2011



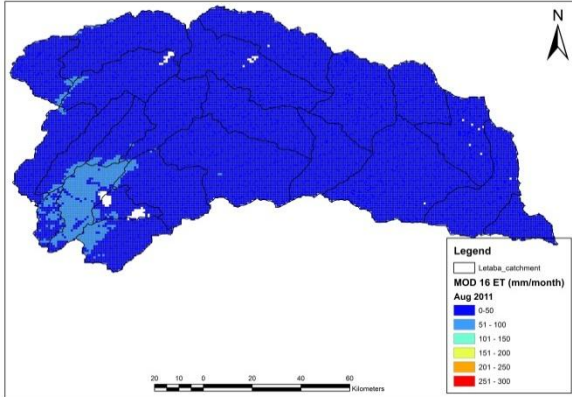
June 2011



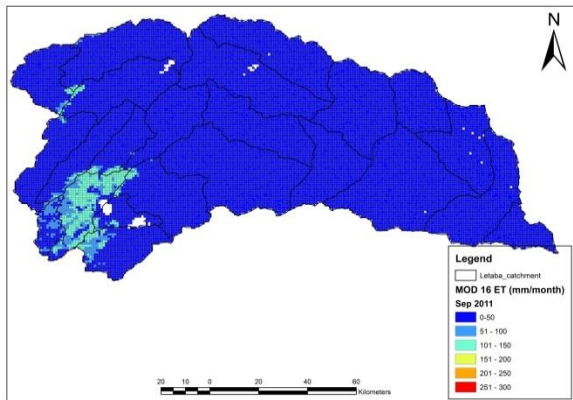
July 2011



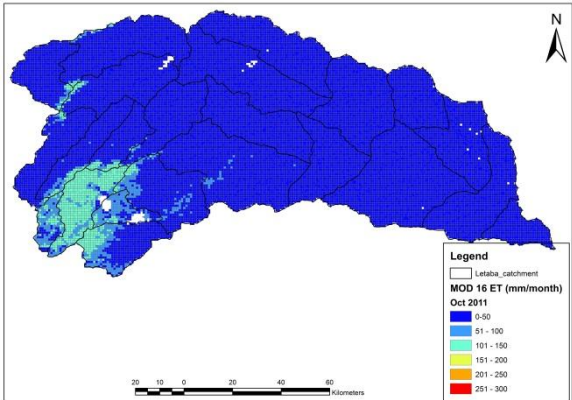
August 2011



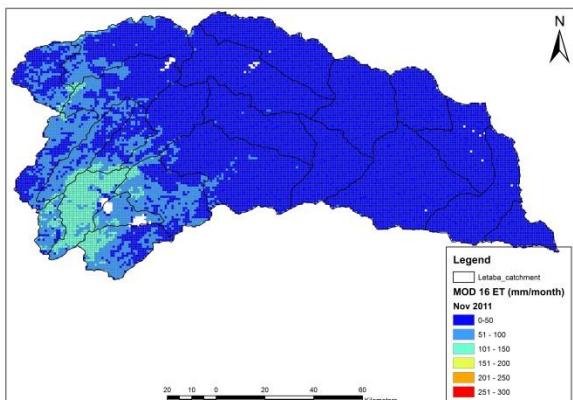
September 2011



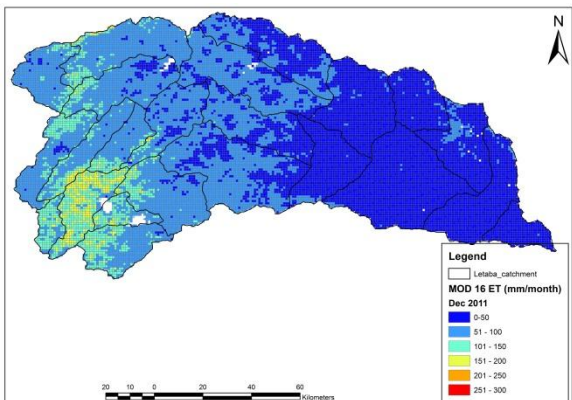
October 2011



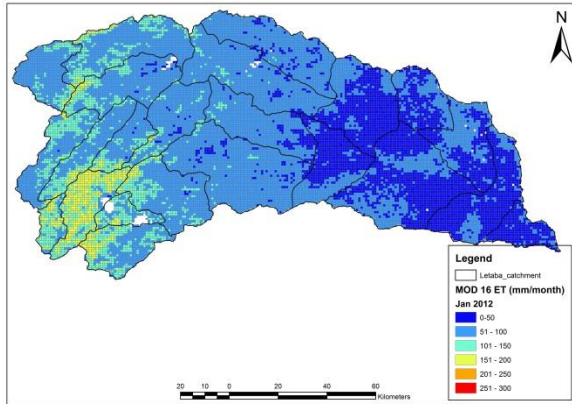
November 2011



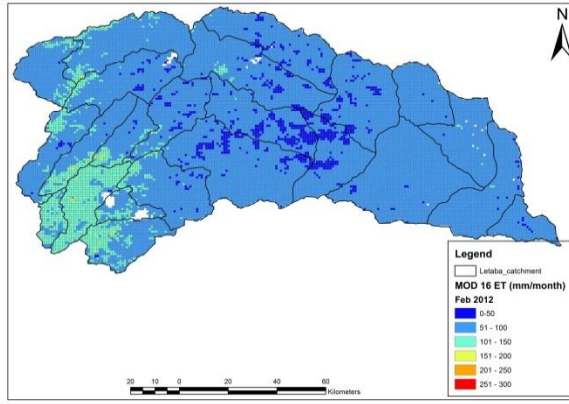
December 2011



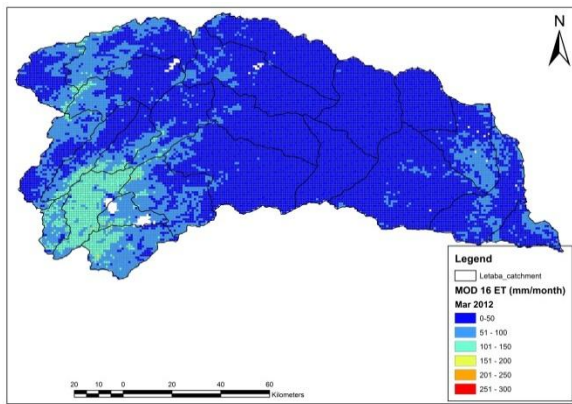
January 2012



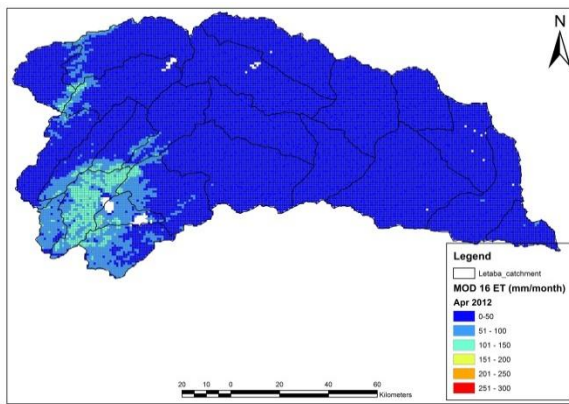
February 2012



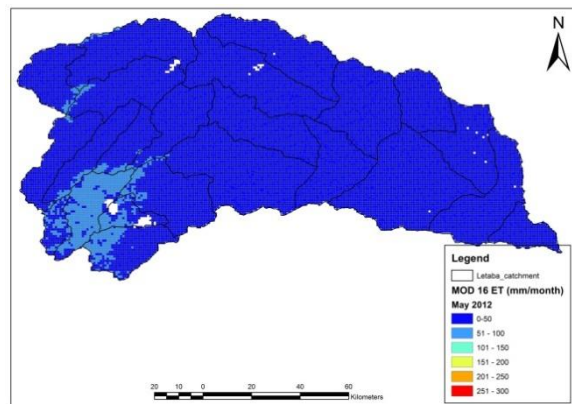
March 2012



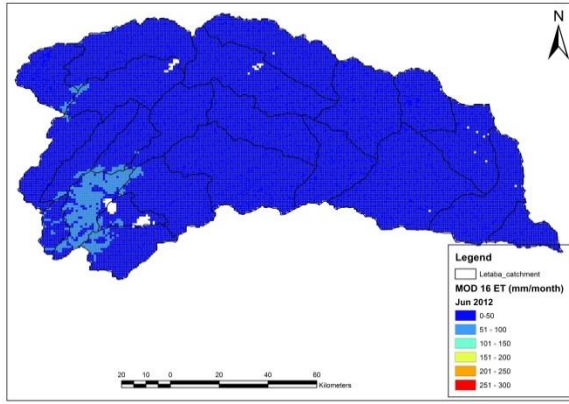
April 2012



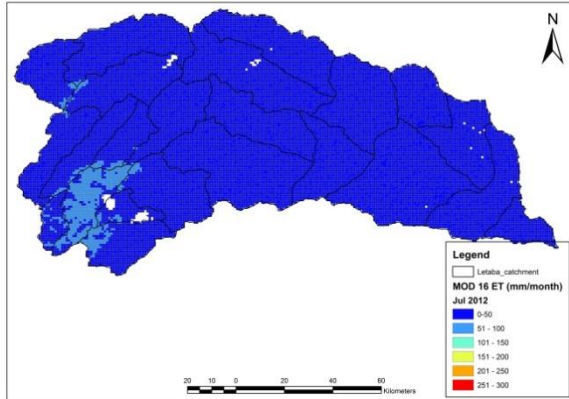
May 2012



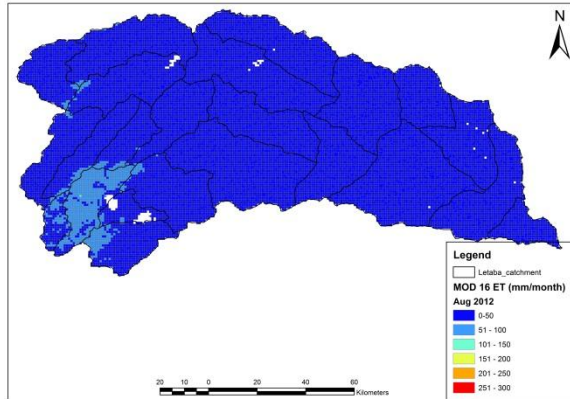
June 2012



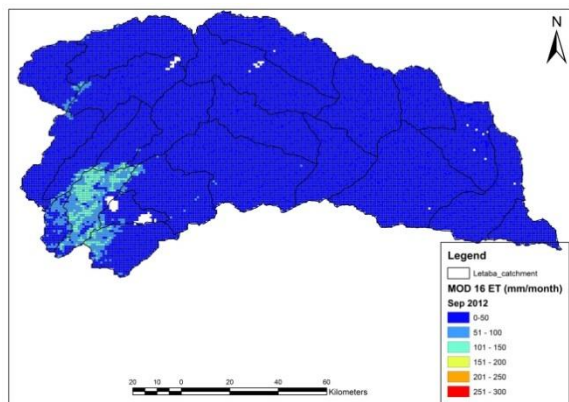
July 2012



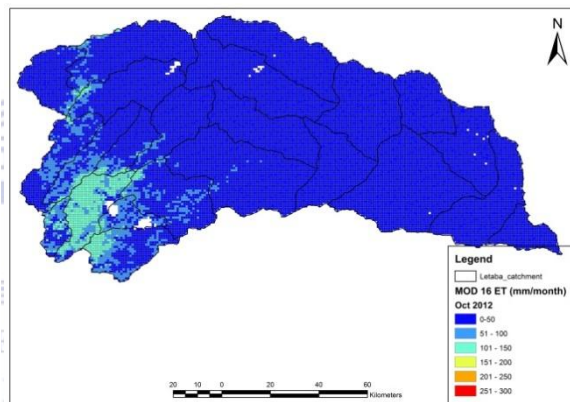
August 2012



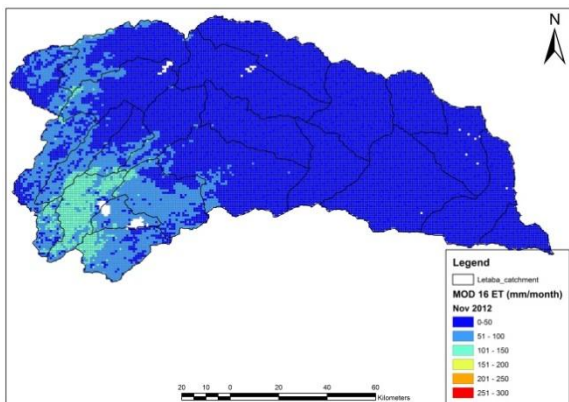
September 2012



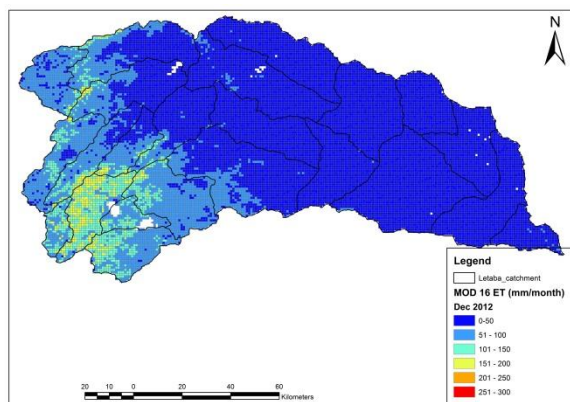
October 2012



November 2012



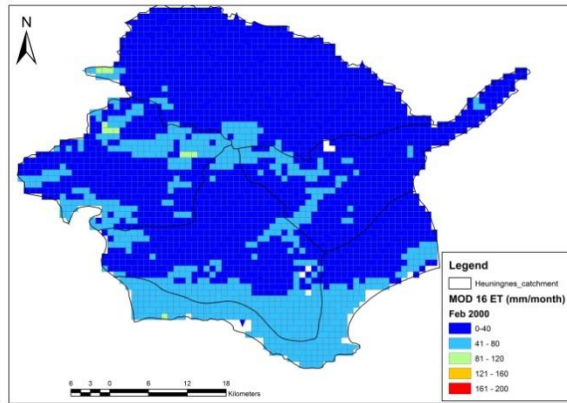
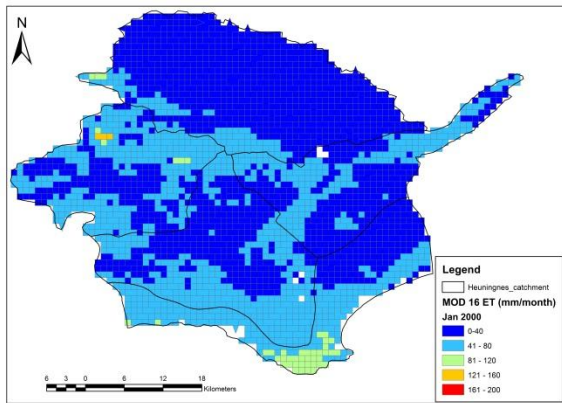
December 2012



## Appendix B: Monthly MOD 16 ET in the Heuningnes catchment

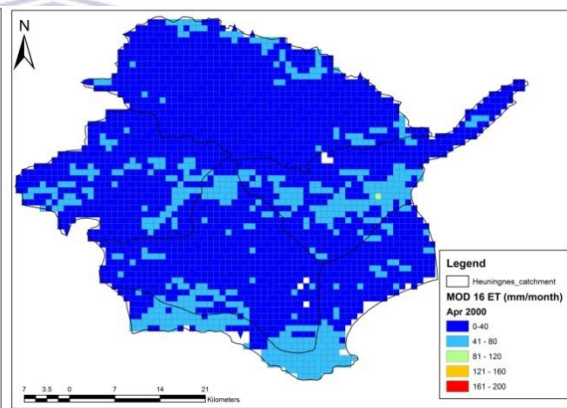
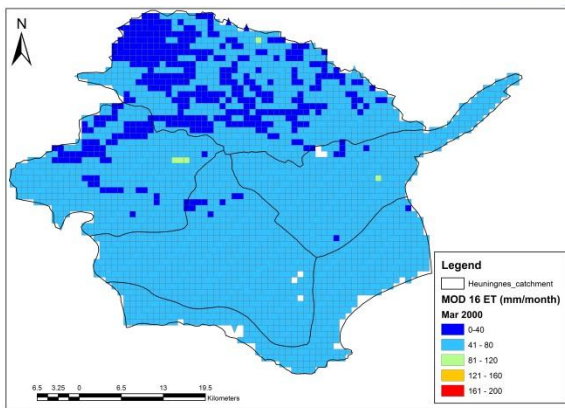
January 2000

February 2000



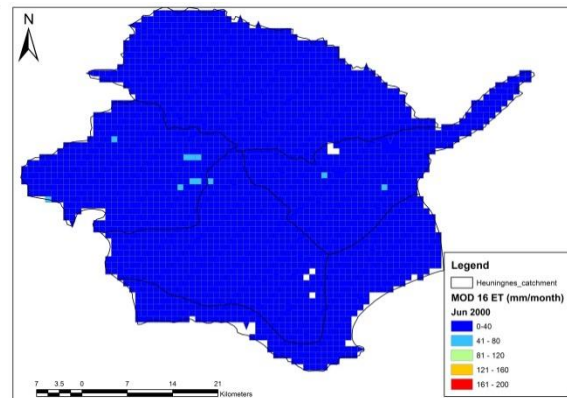
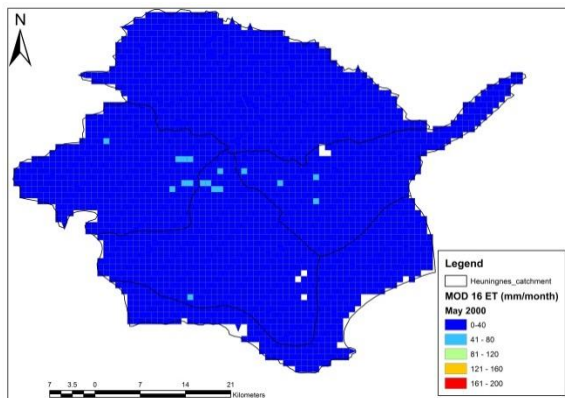
March 2000

April 2000



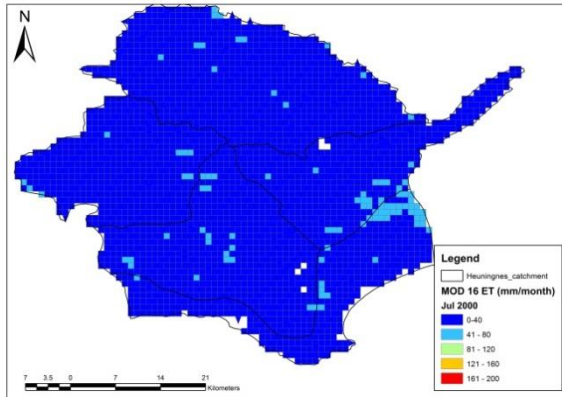
May 2000

June 2000

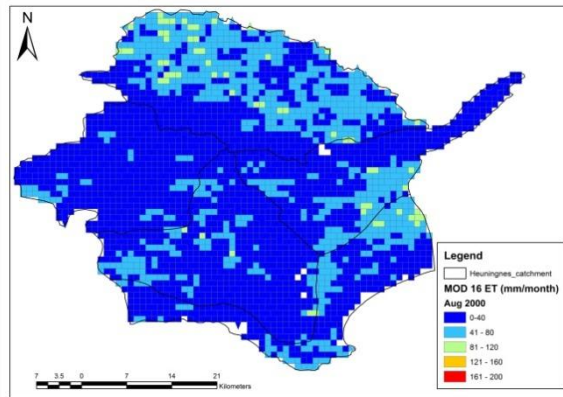




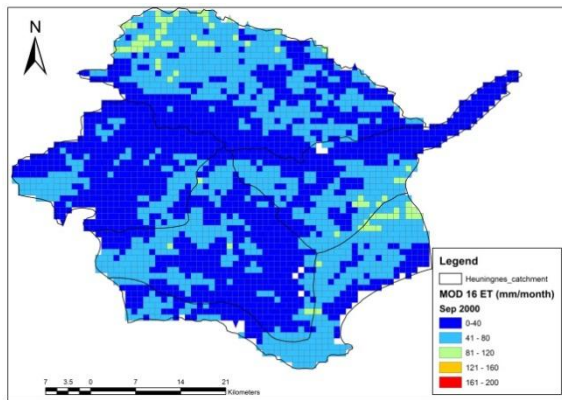
July 2000



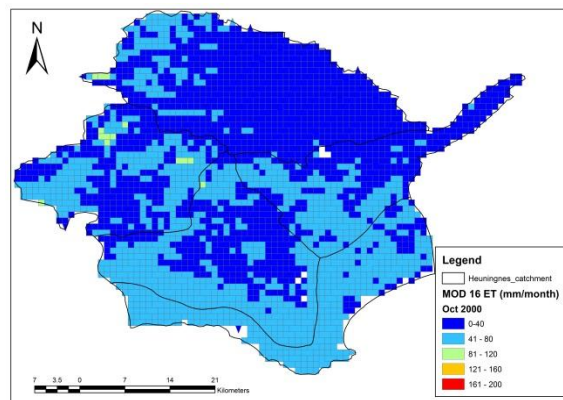
August 2000



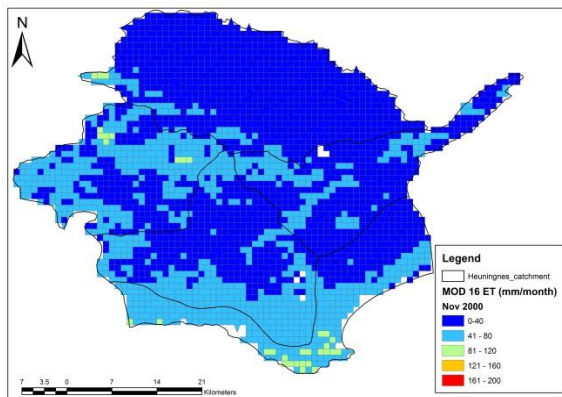
September 2000



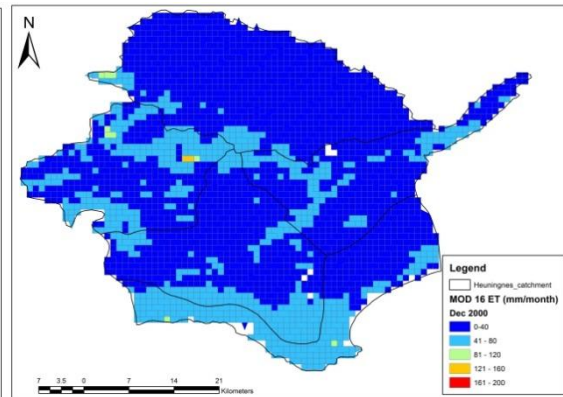
October 2000



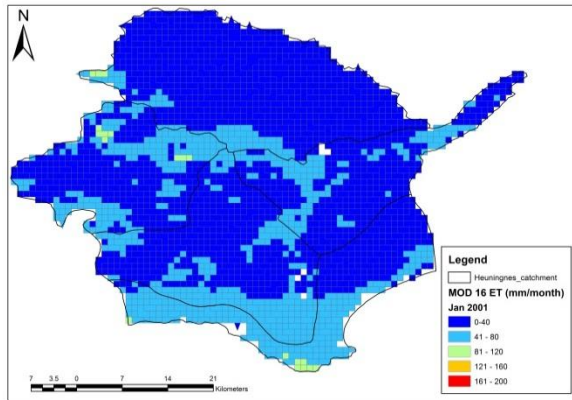
November 2000



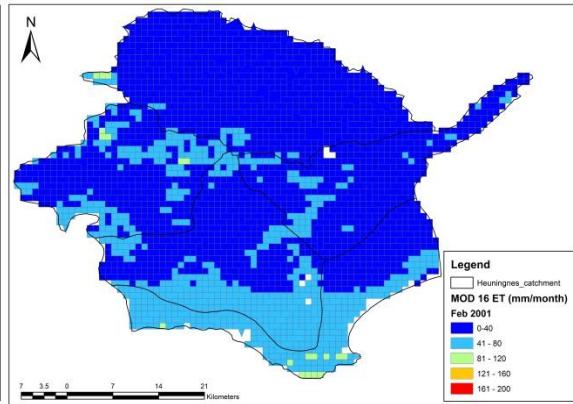
December 2000



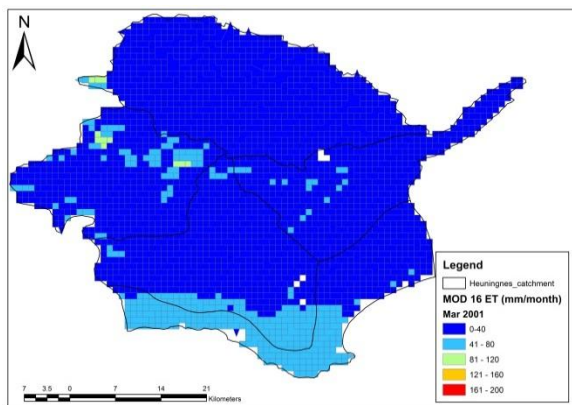
January 2001



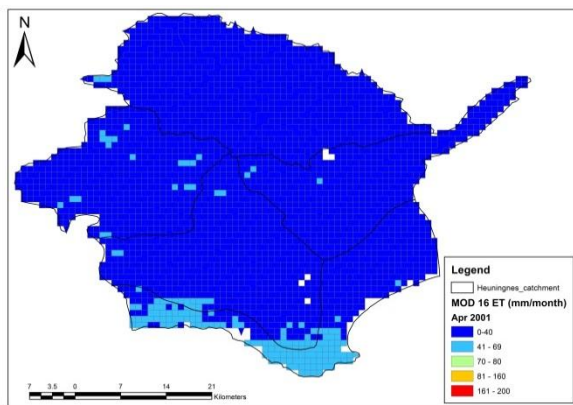
February 2001



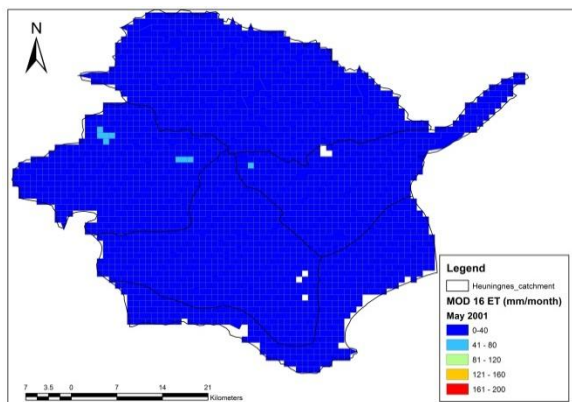
March 2001



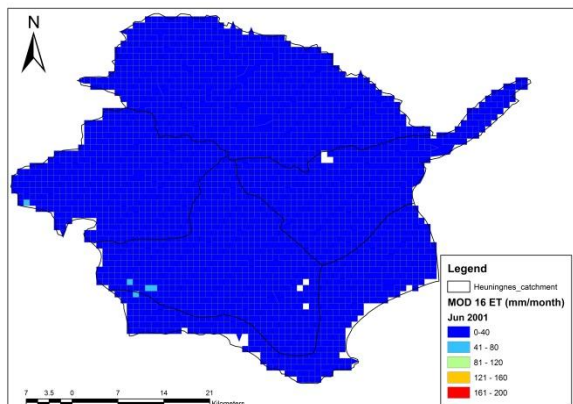
April 2001



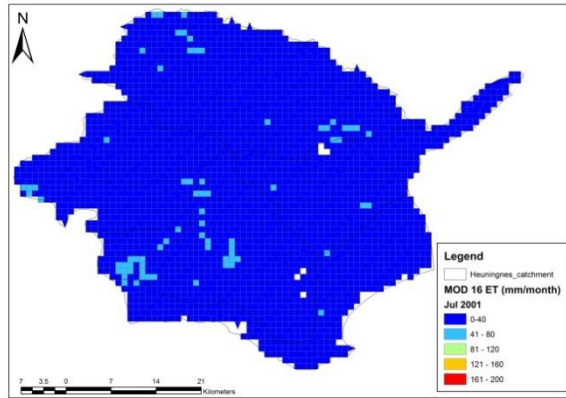
May 2001



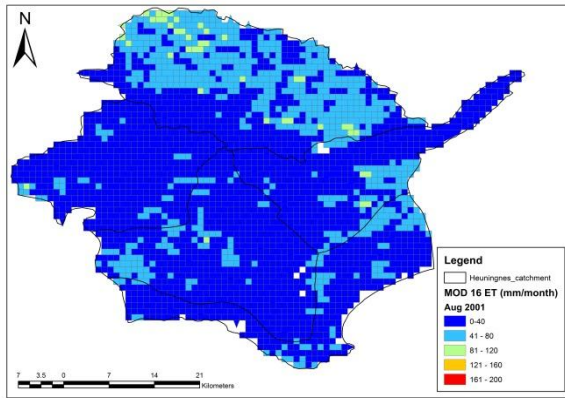
June 2001



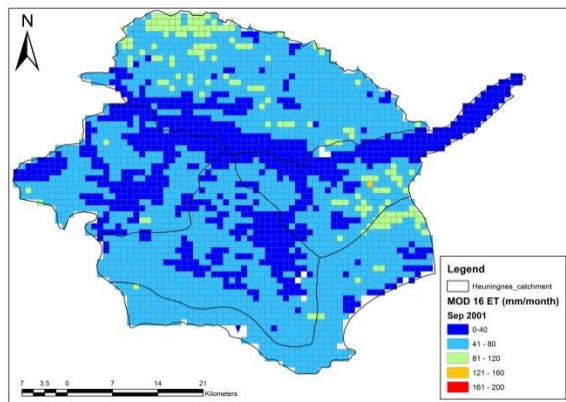
July 2001



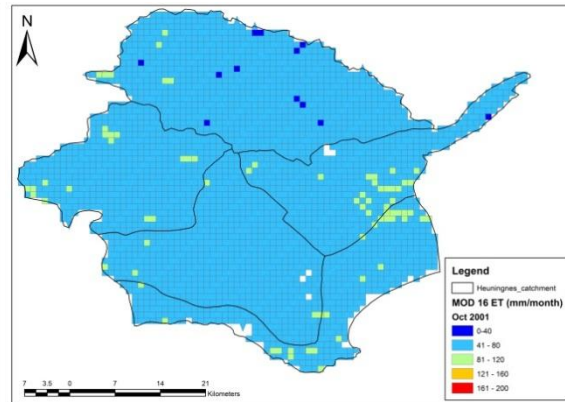
August 2001



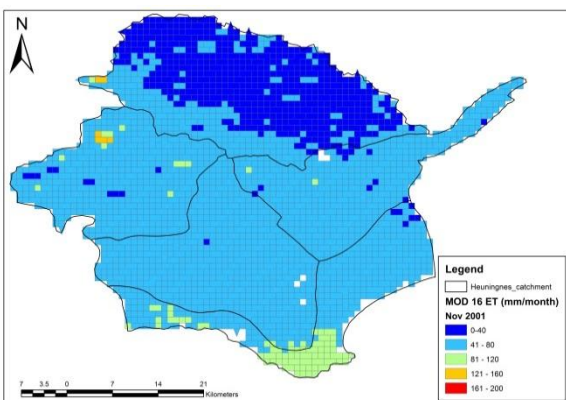
September 2001



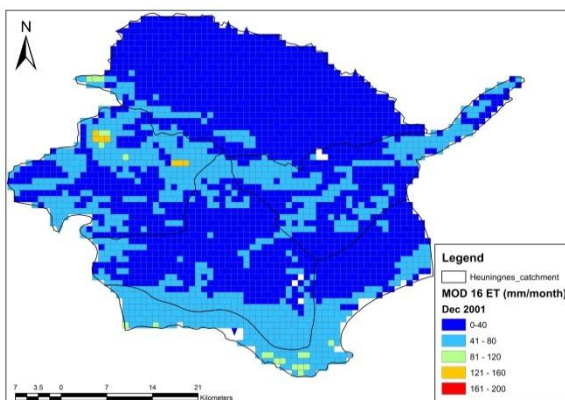
October 2001



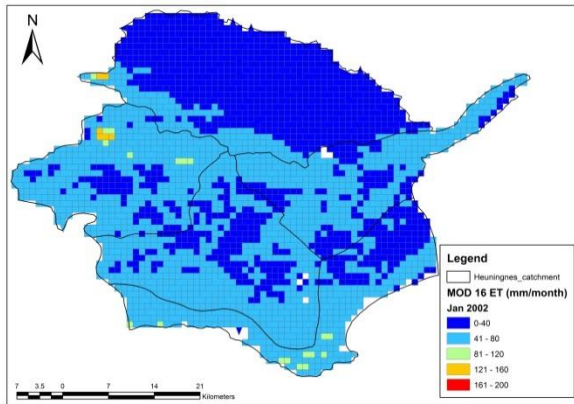
November 2001



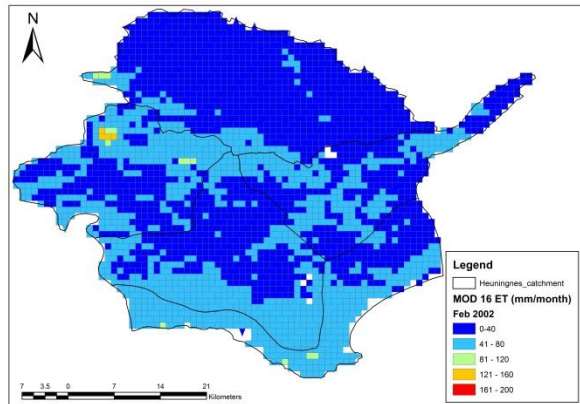
December 2001



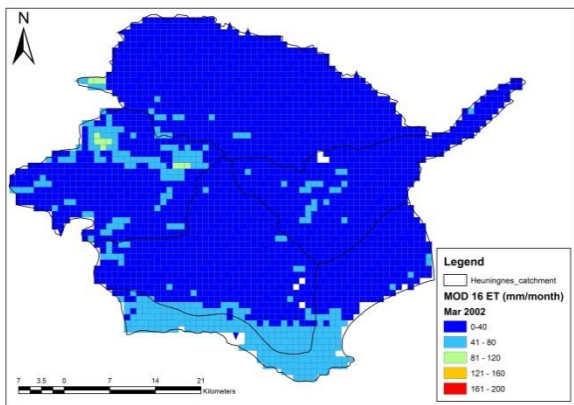
January 2002



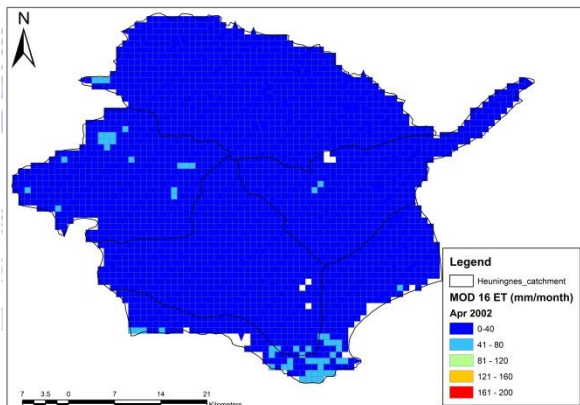
February 2002



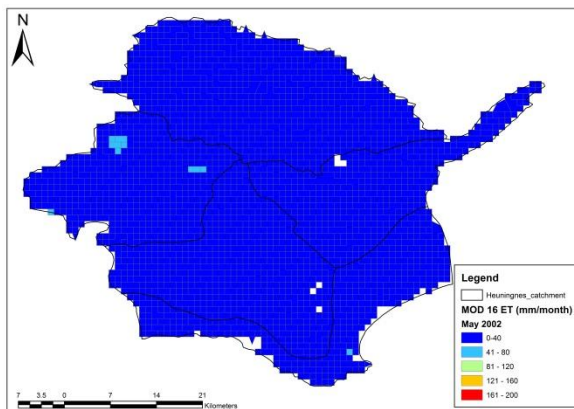
March 2002



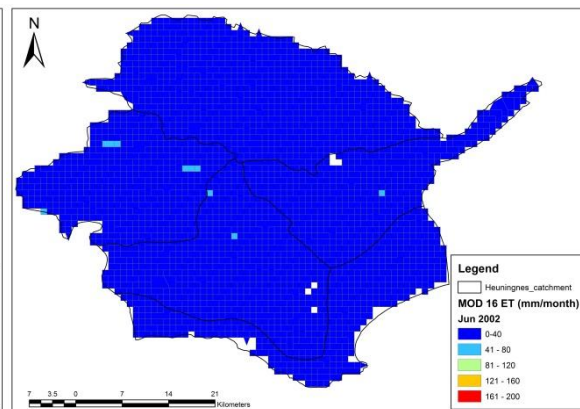
April 2002



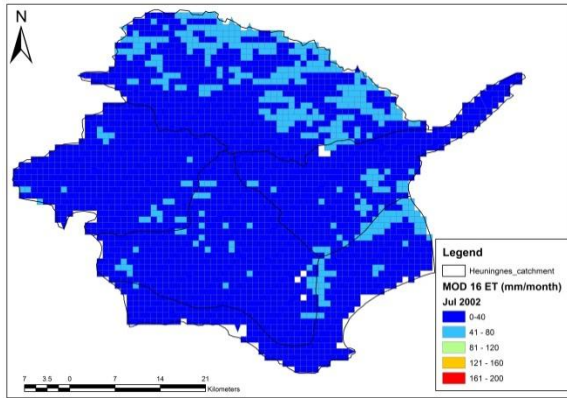
May 2002



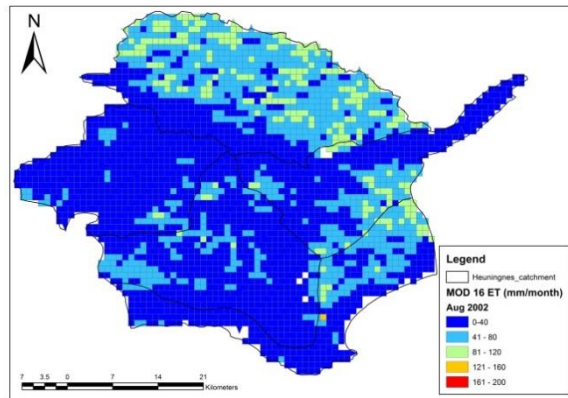
June 2002



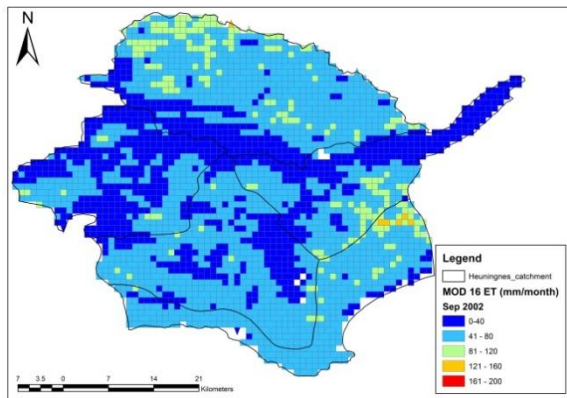
July 2002



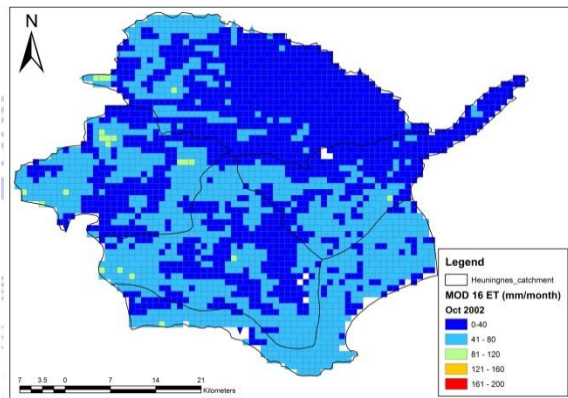
August 2002



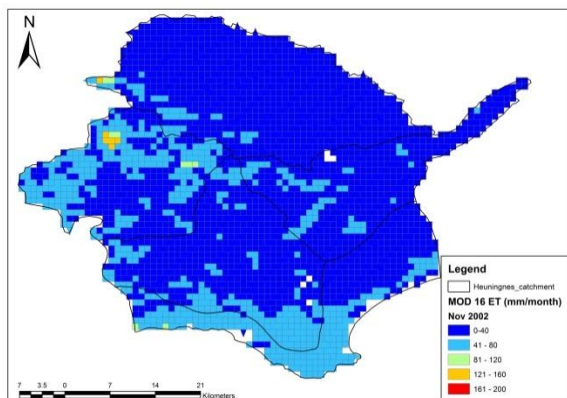
September 2002



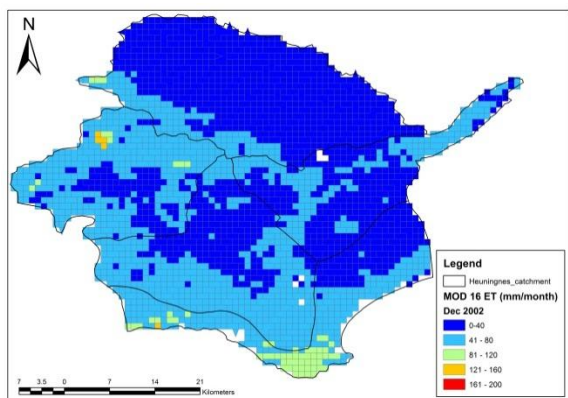
October 2002



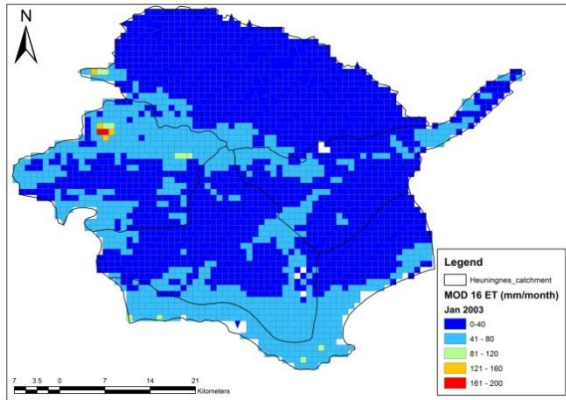
November 2002



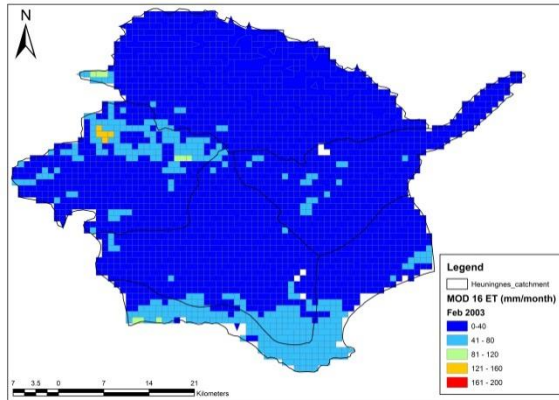
December 2002



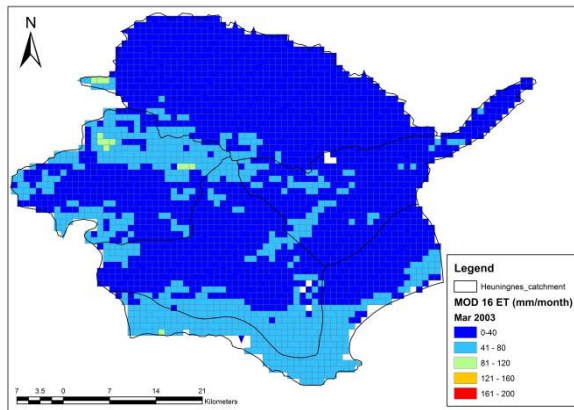
January 2003



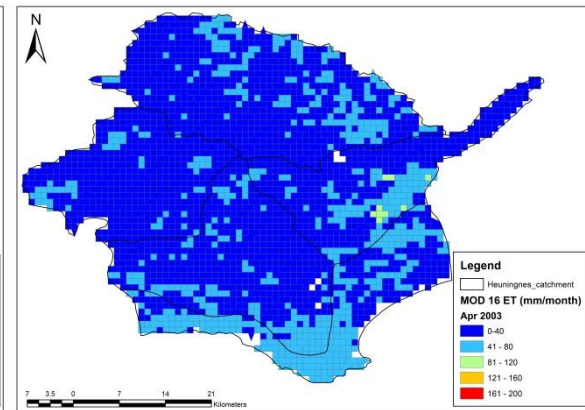
February 2003



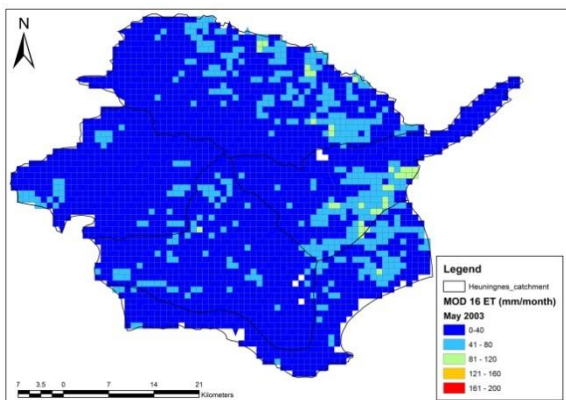
March 2003



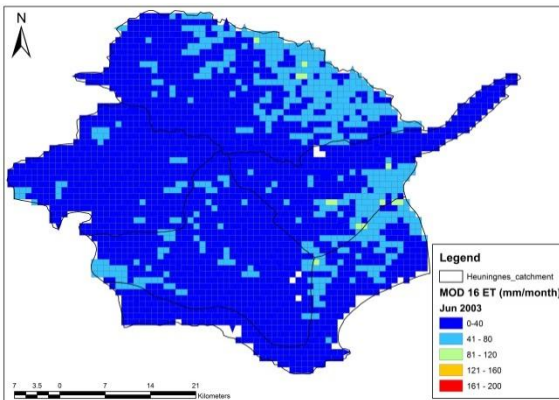
April 2003



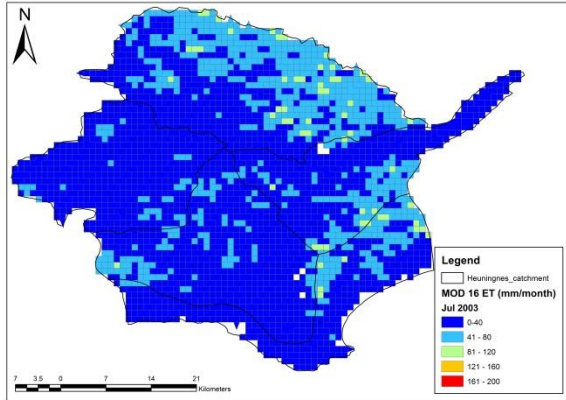
May 2003



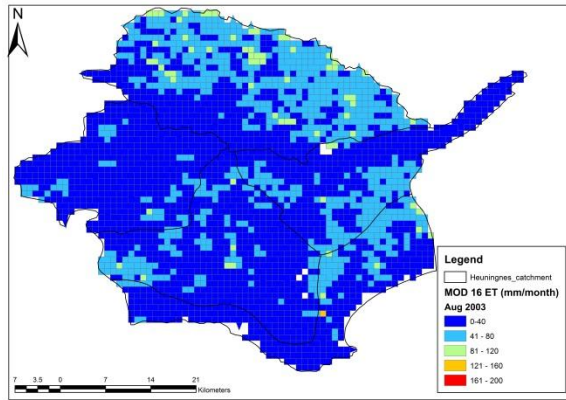
June 2003



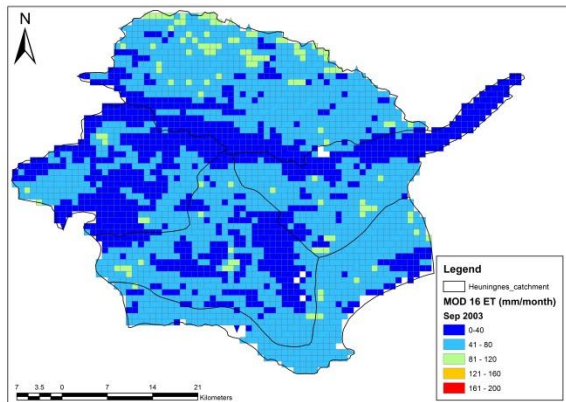
July 2003



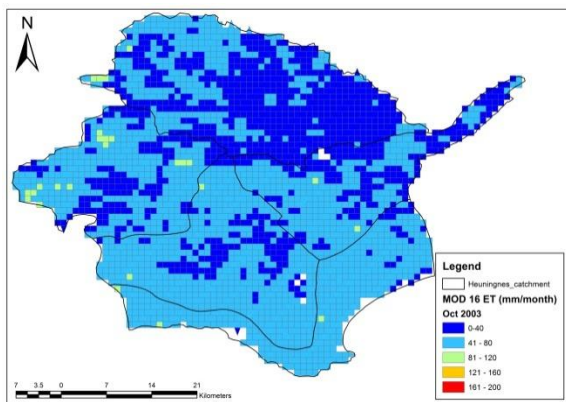
August 2003



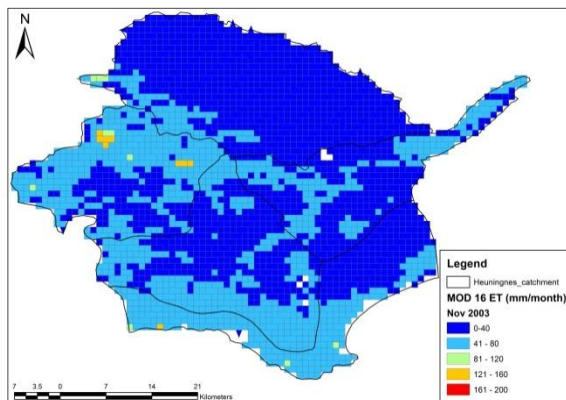
September 2003



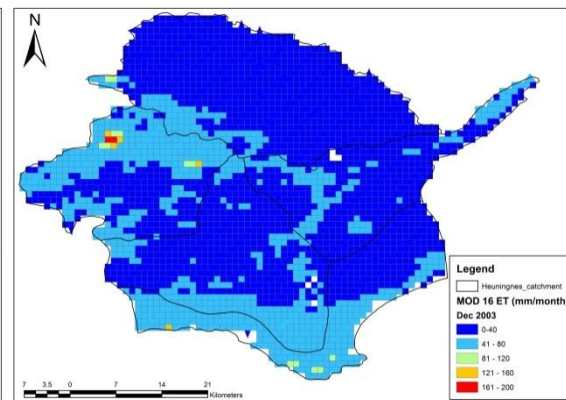
October 2003



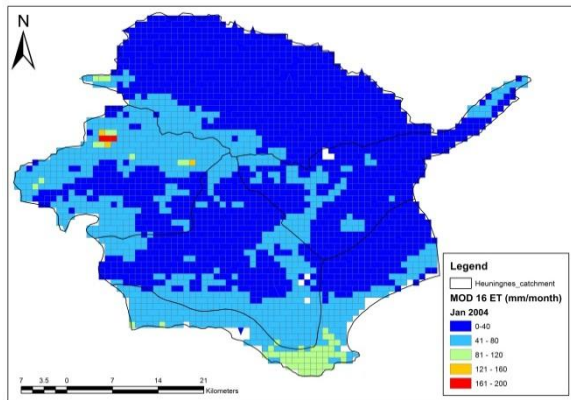
November 2003



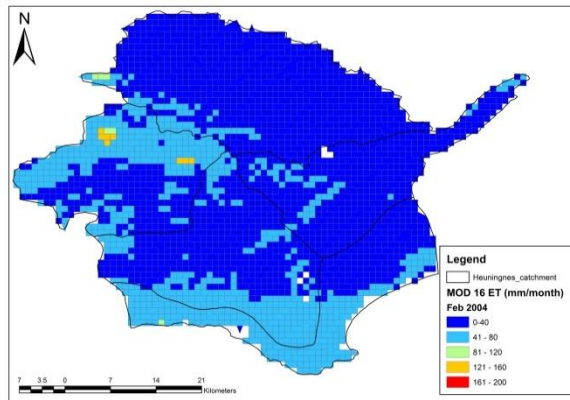
December 2003



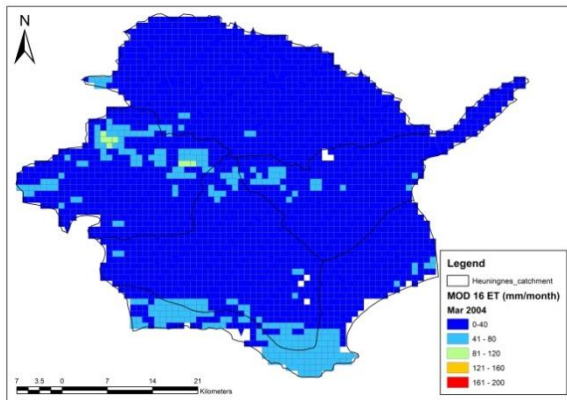
January 2004



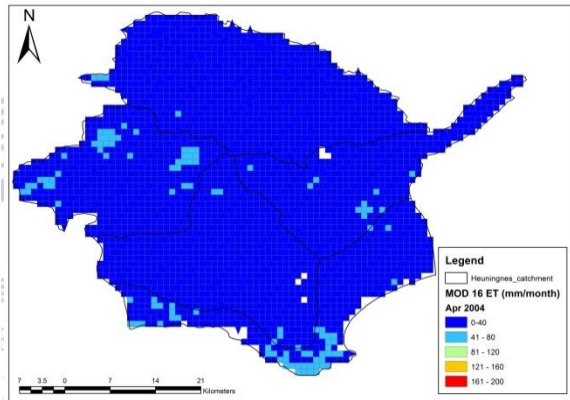
February 2004



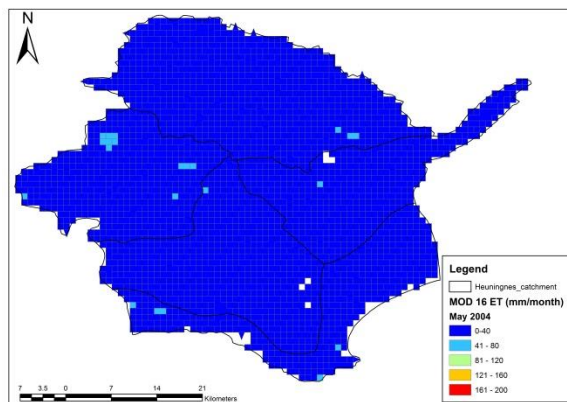
March 2004



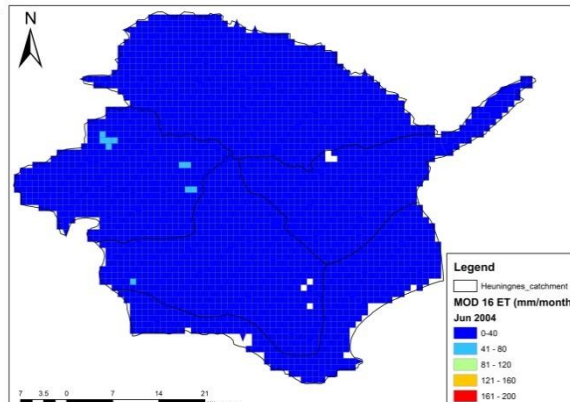
April 2004



May 2004

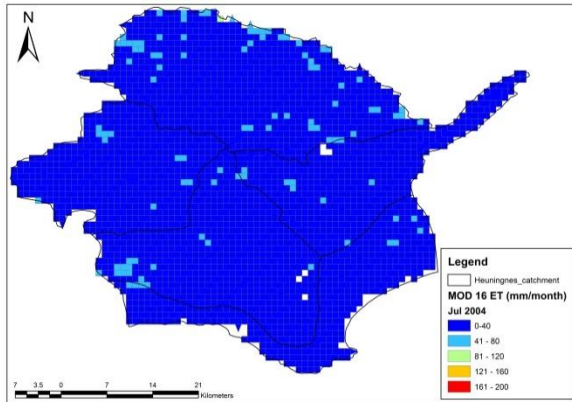


June 2004

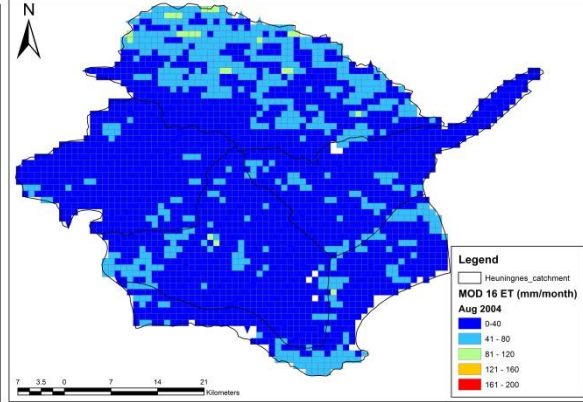




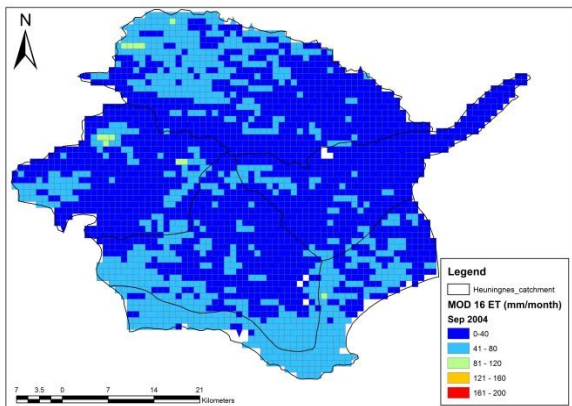
July 2004



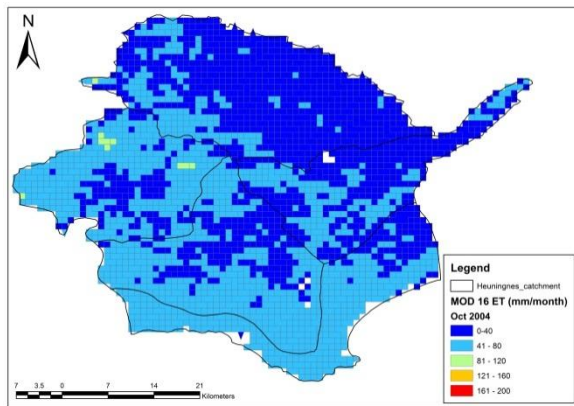
August 2004



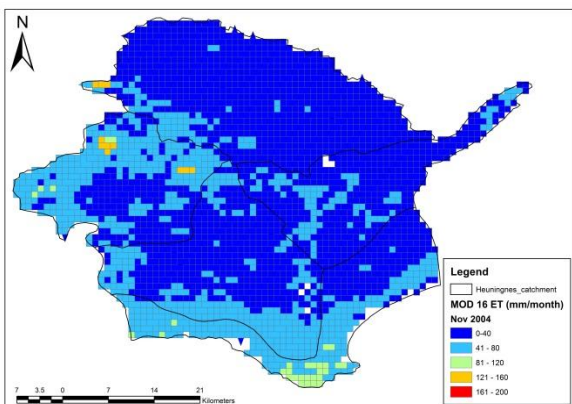
September 2004



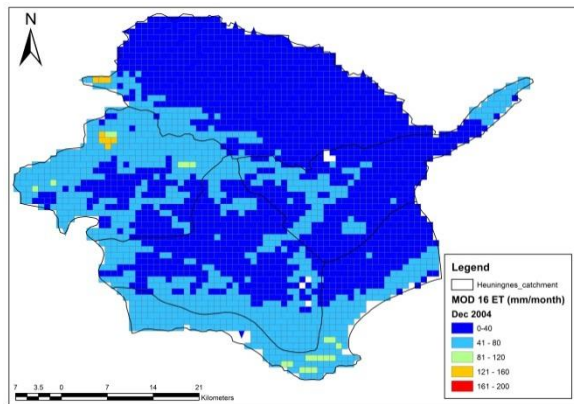
October 2004



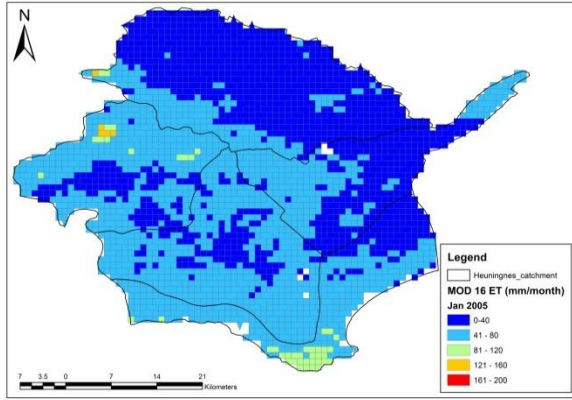
November 2004



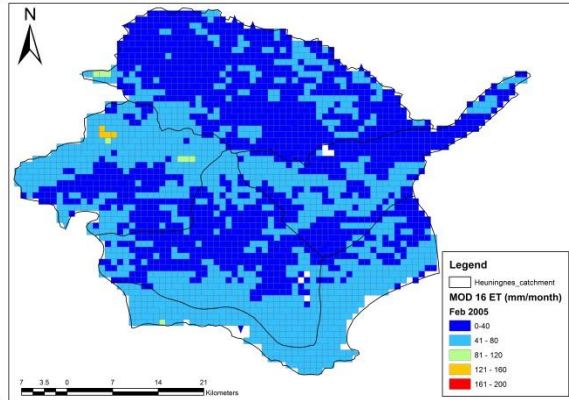
December 2004



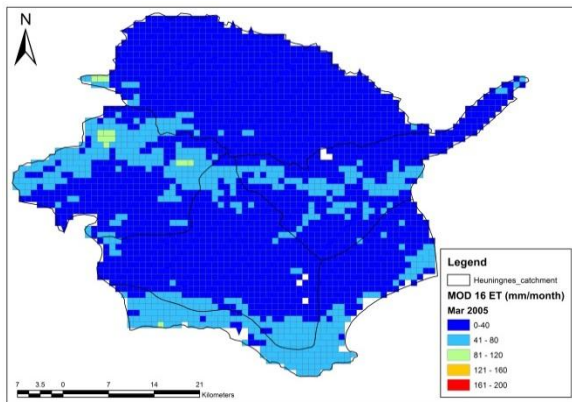
January 2005



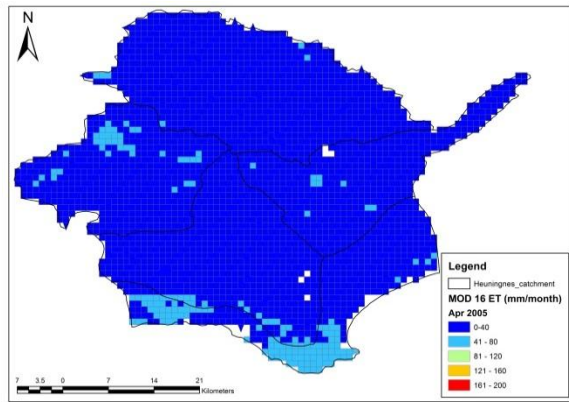
February 2005



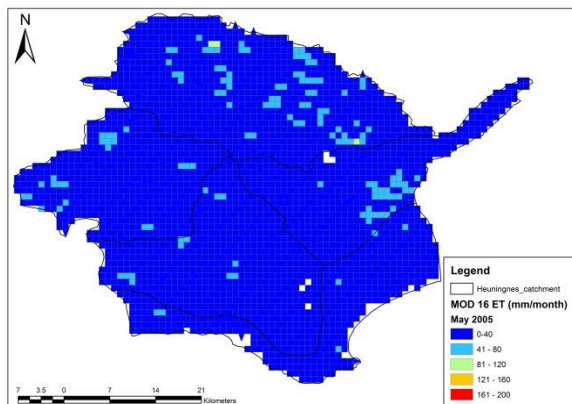
March 2005



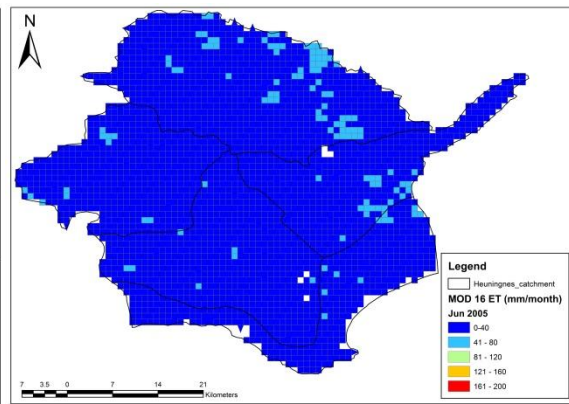
April 2005



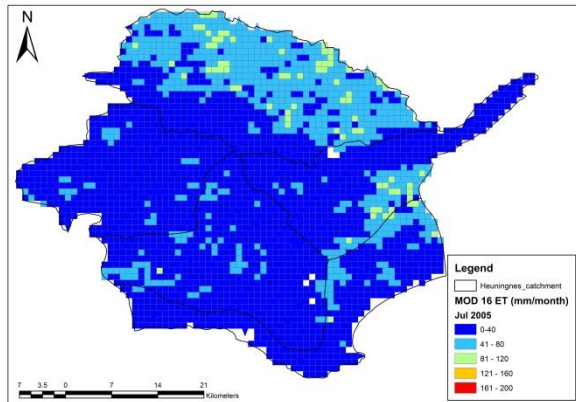
May 2005



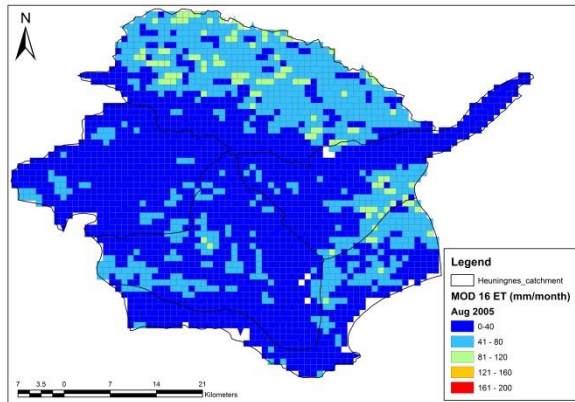
June 2005



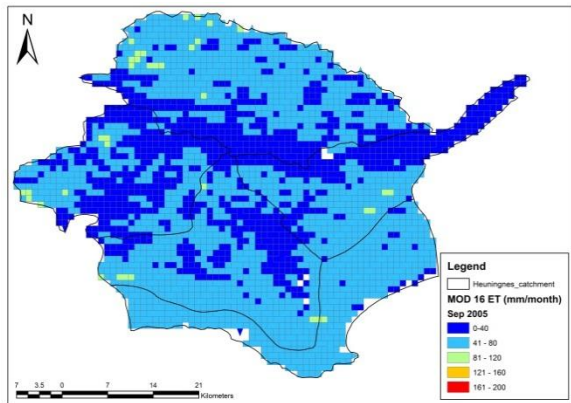
July 2005



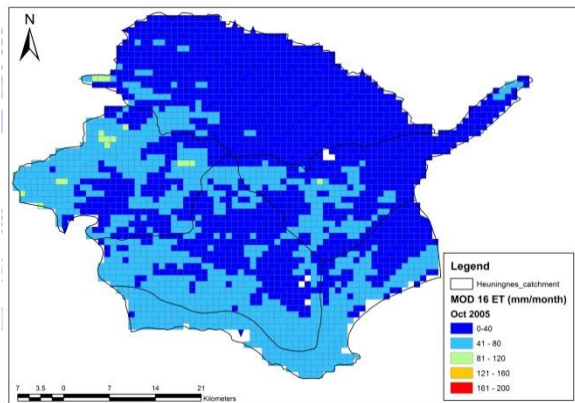
August 2005



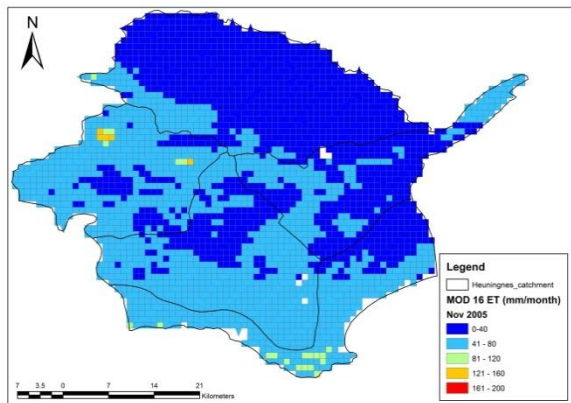
September 2005



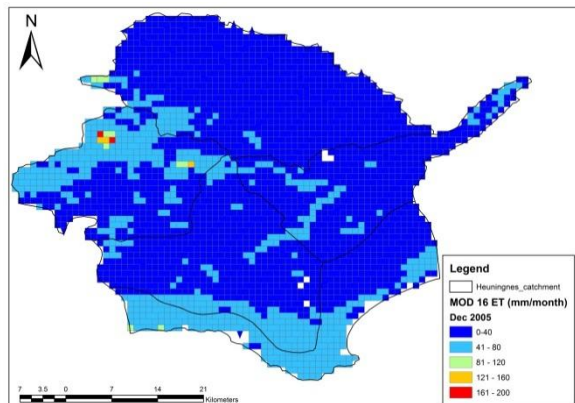
October 2005



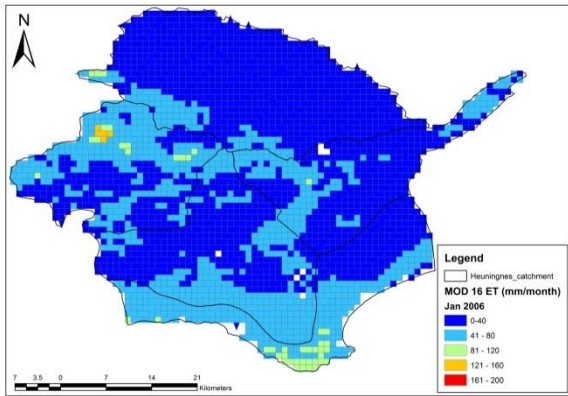
November 2005



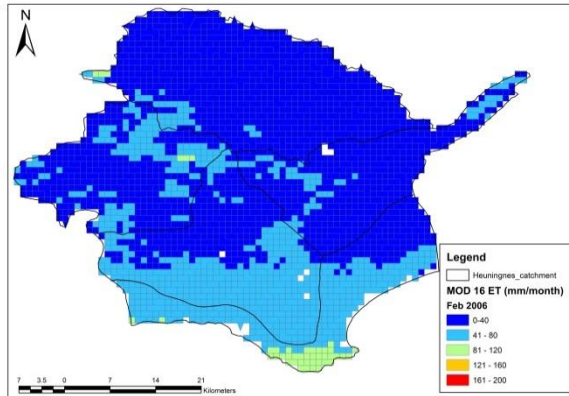
December 2005



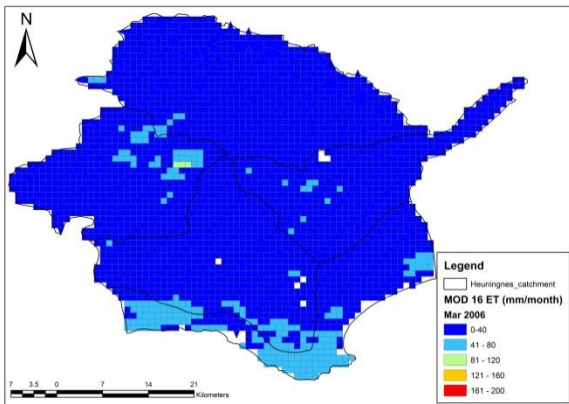
January 2006



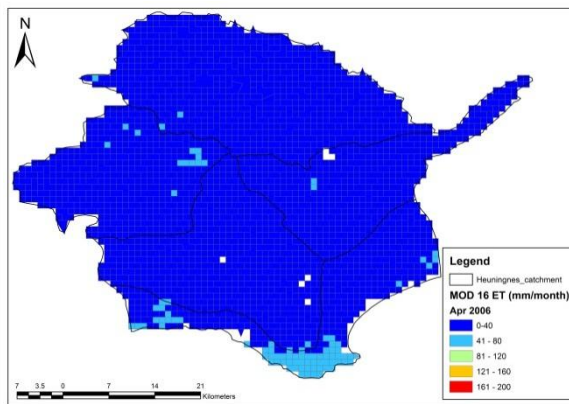
February 2006



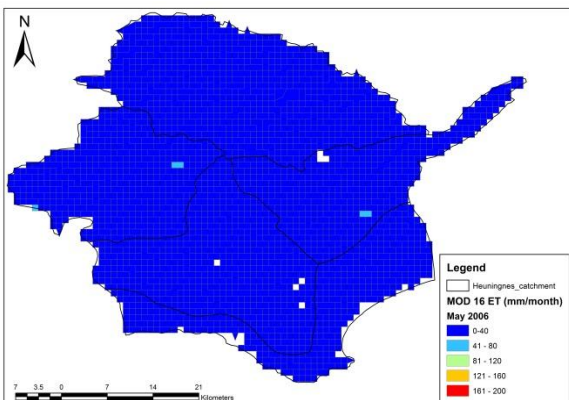
March 2006



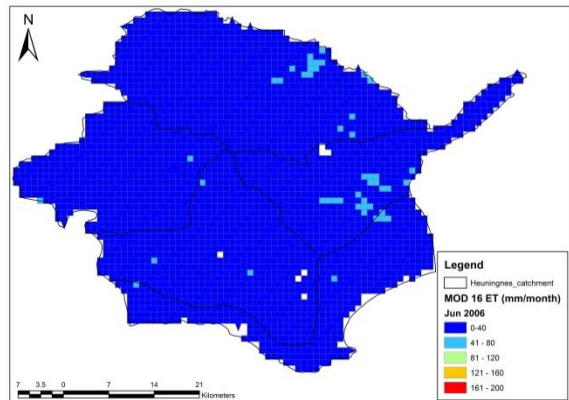
April 2006



May 2006

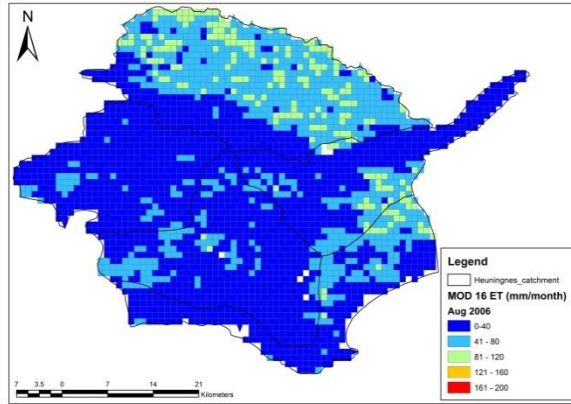
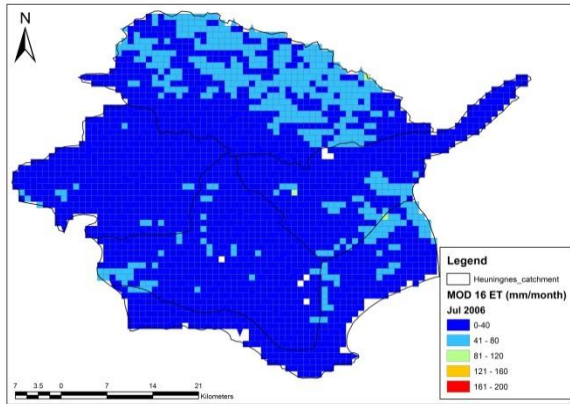


June 2006



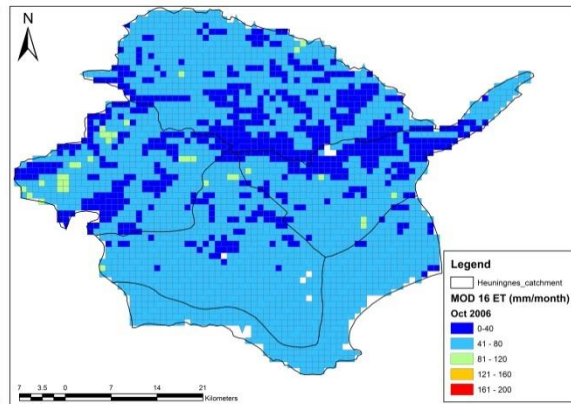
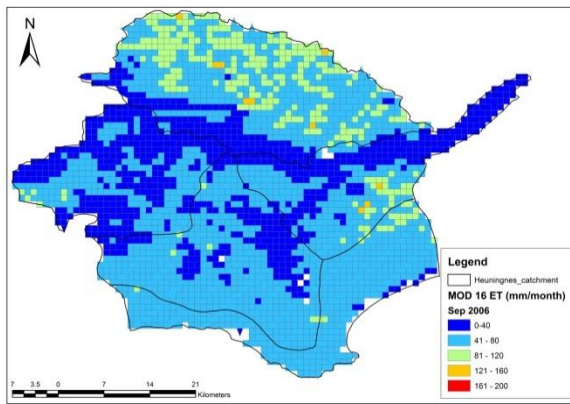
July 2006

August 2006



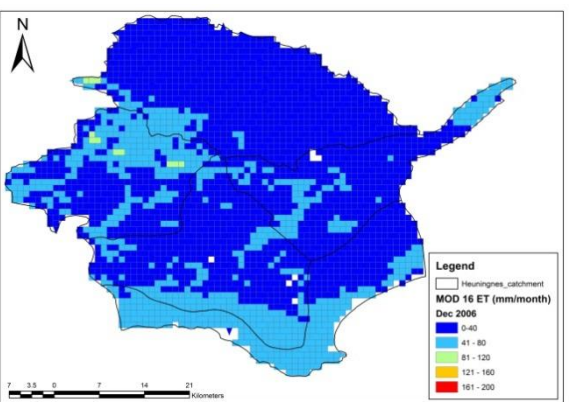
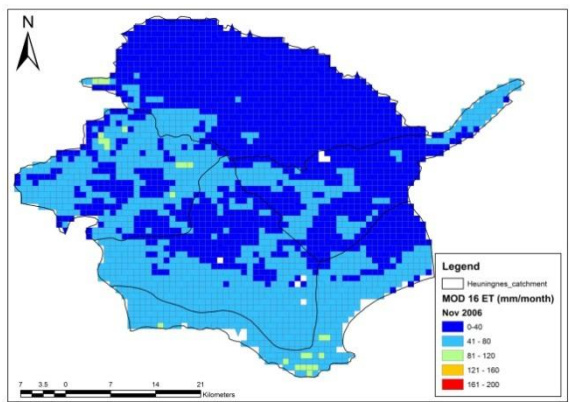
September 2006

October 2006

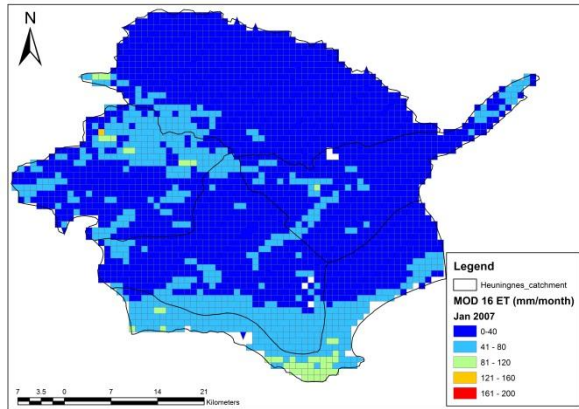


November 2006

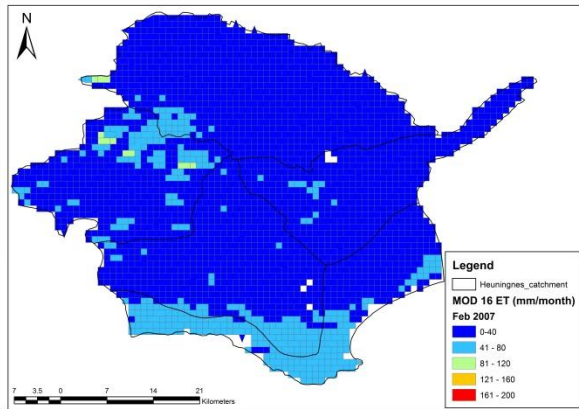
December 2006



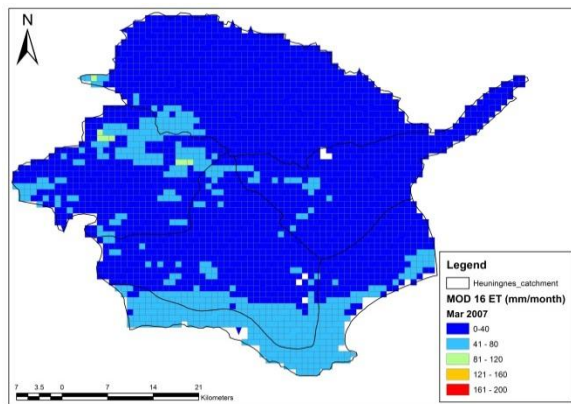
January 2007



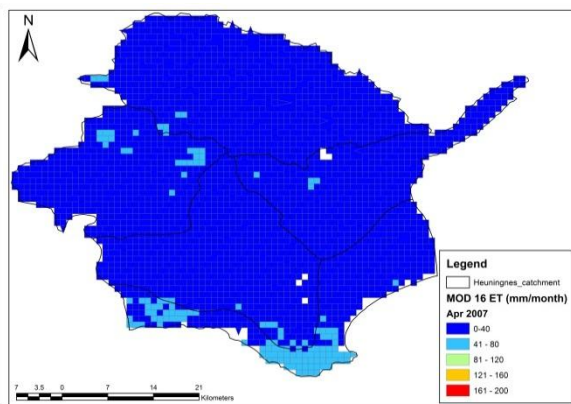
February 2007



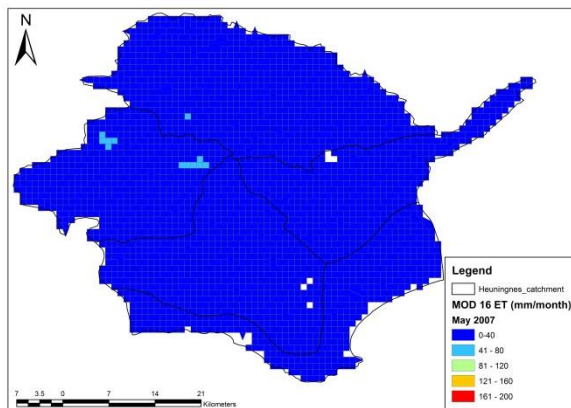
March 2007



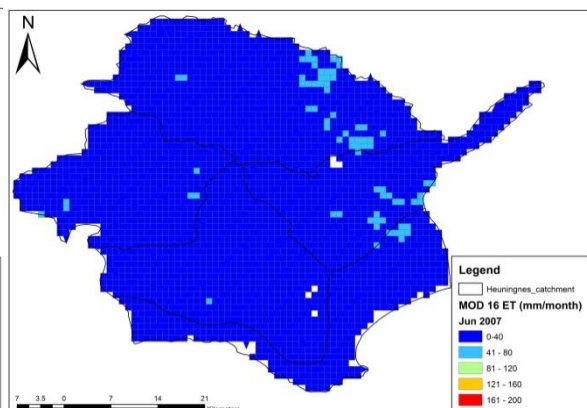
April 2007



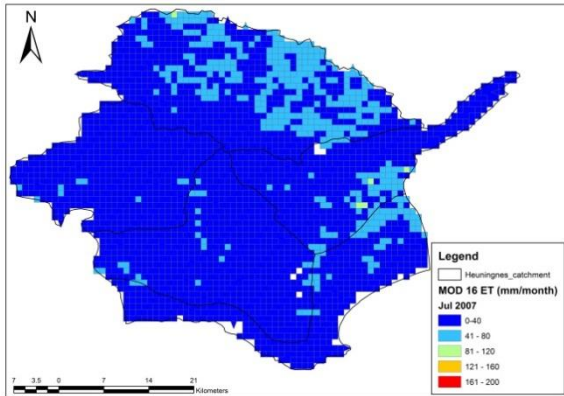
May 2007



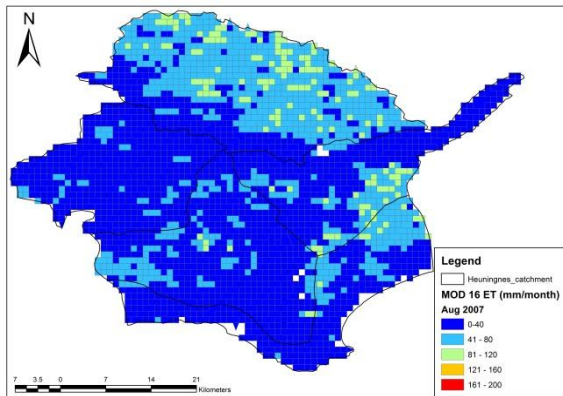
June 2007



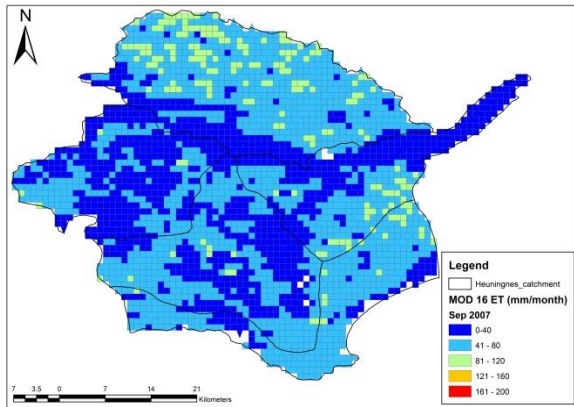
July 2007



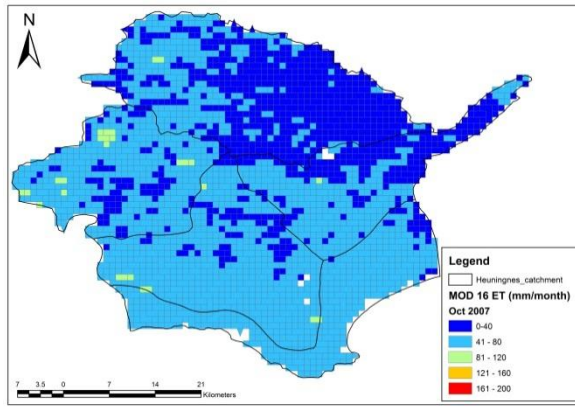
August 2007



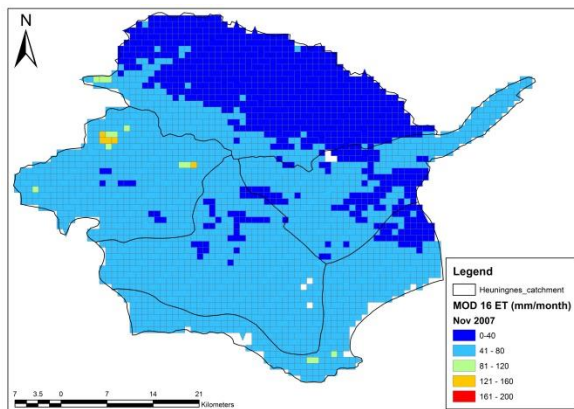
September 2007



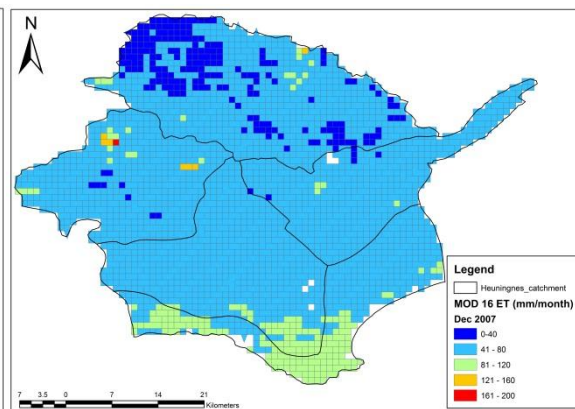
October 2007



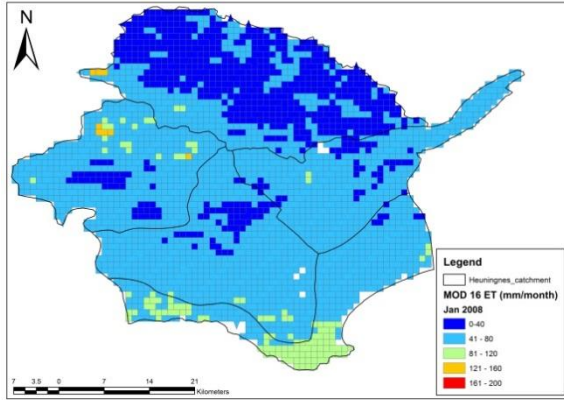
November 2007



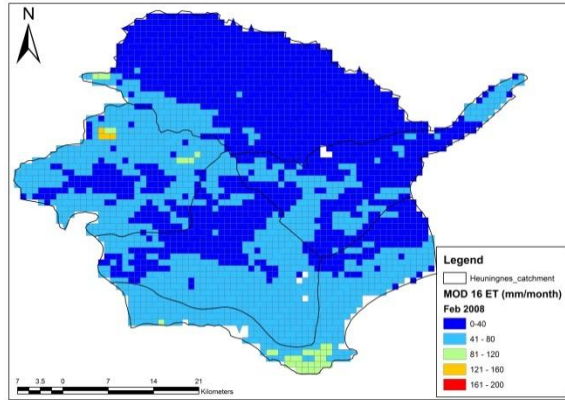
December 2007



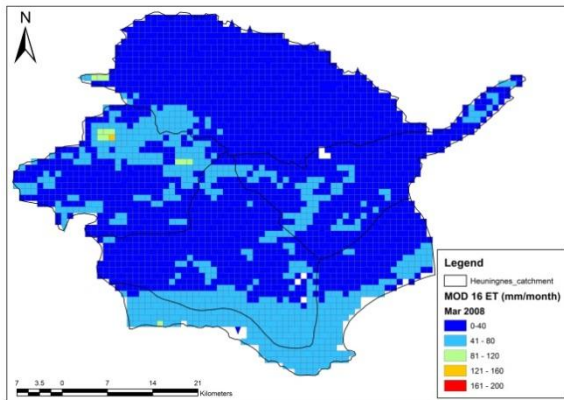
January 2008



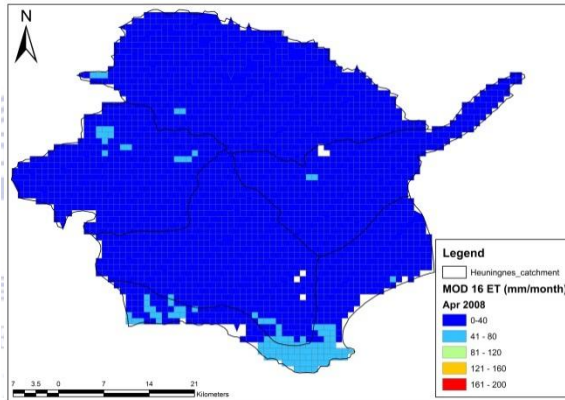
February 2008



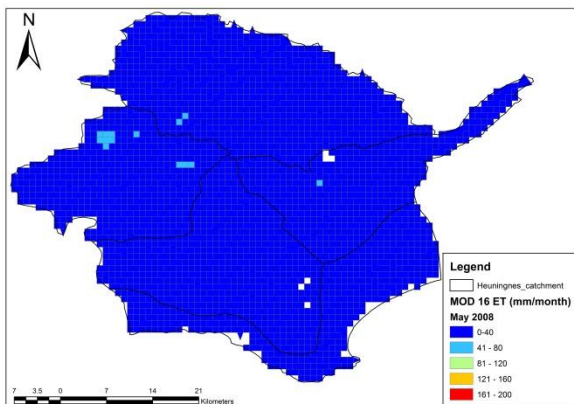
March 2008



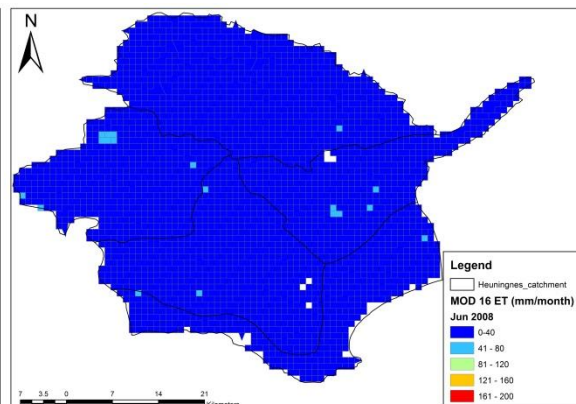
April 2008



May 2008

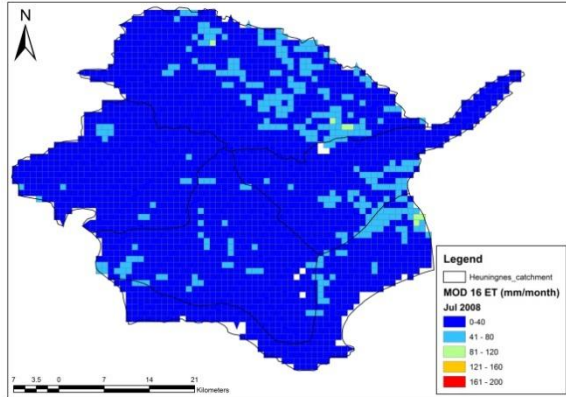


June 2008

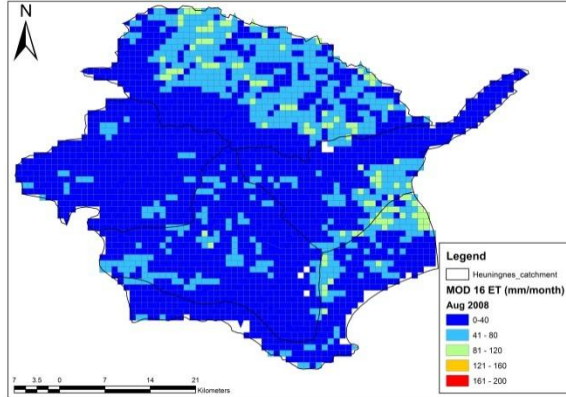




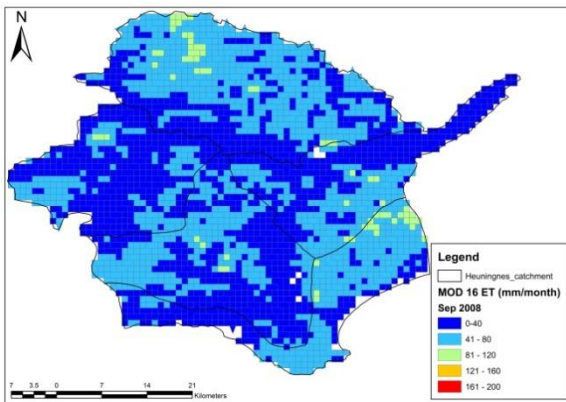
July 2008



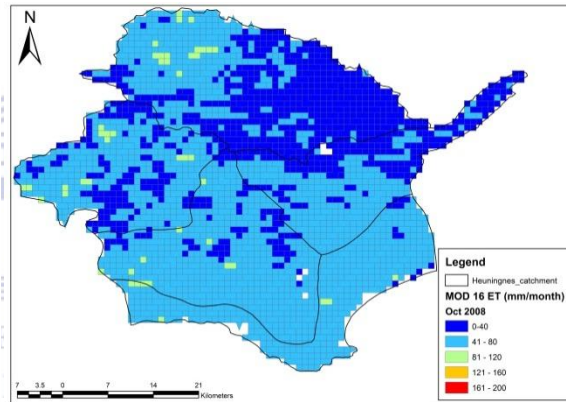
August 2008



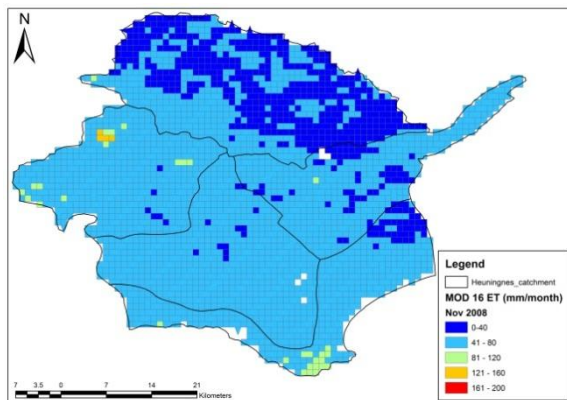
September 2008



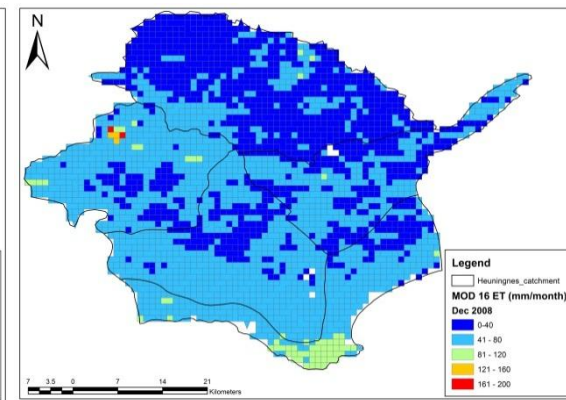
October 2008



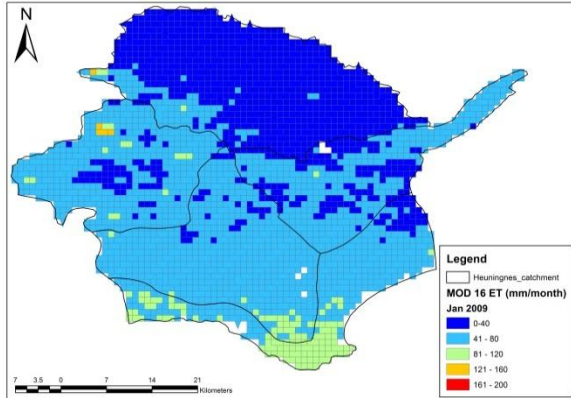
November 2008



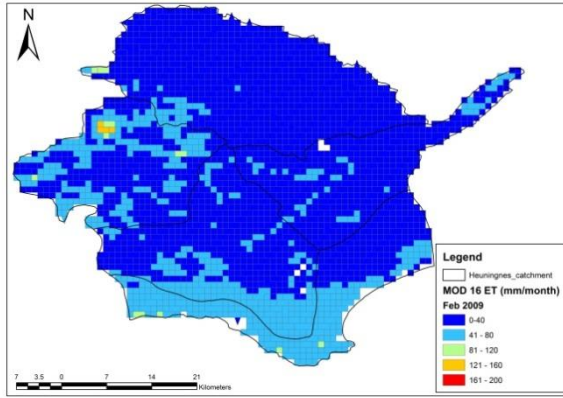
December 2008



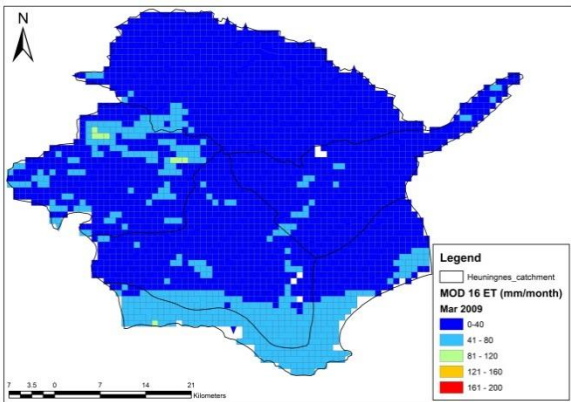
January 2009



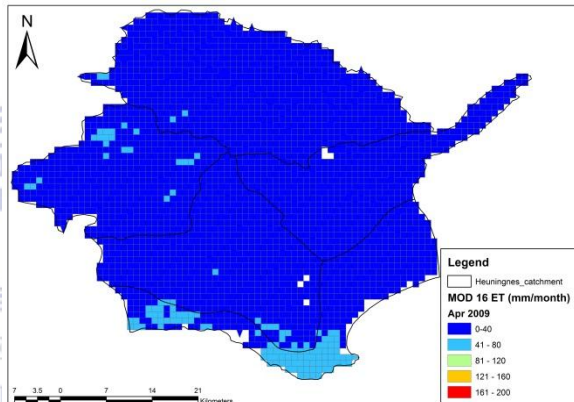
February 2009



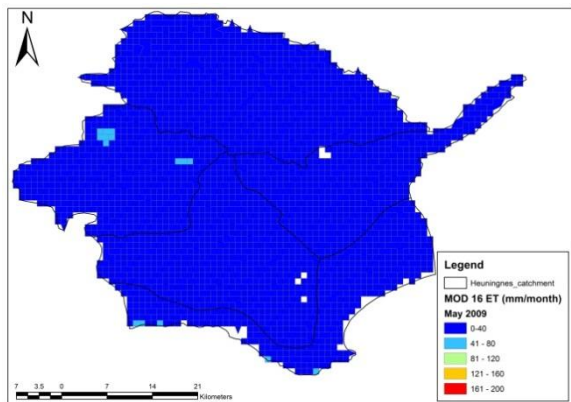
March 2009



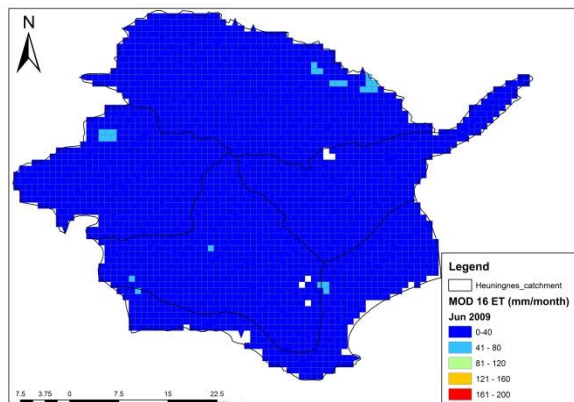
April 2009



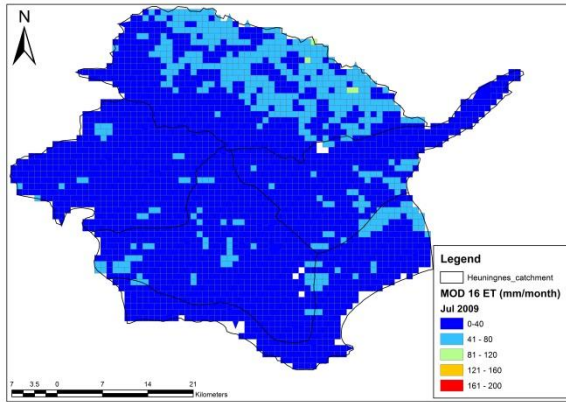
May 2009



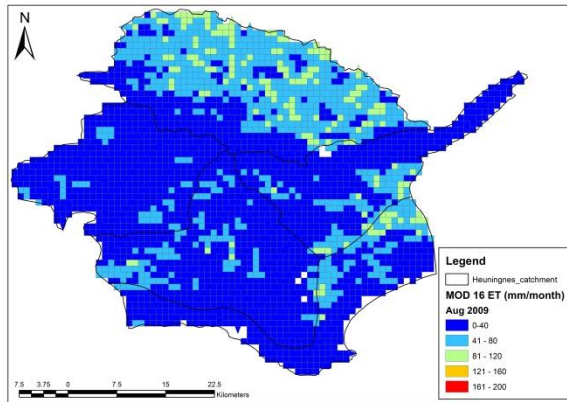
June 2009



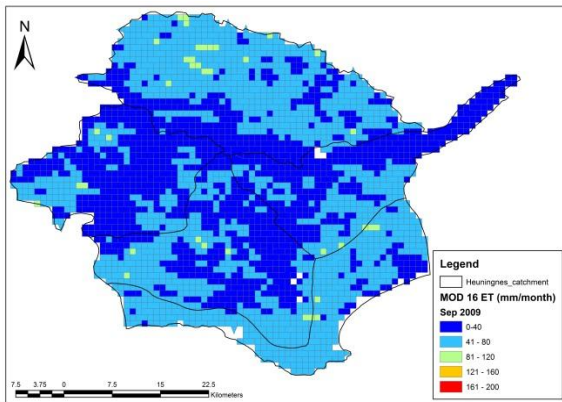
July 2009



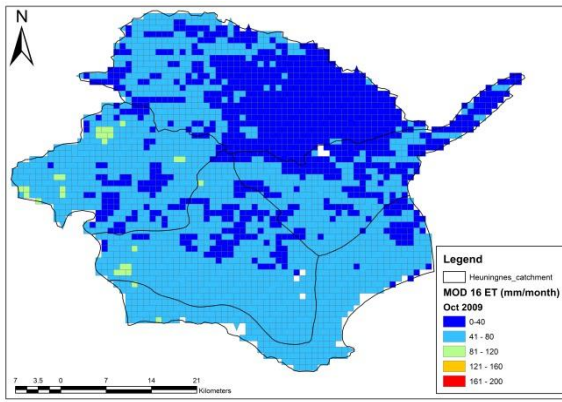
August 2009



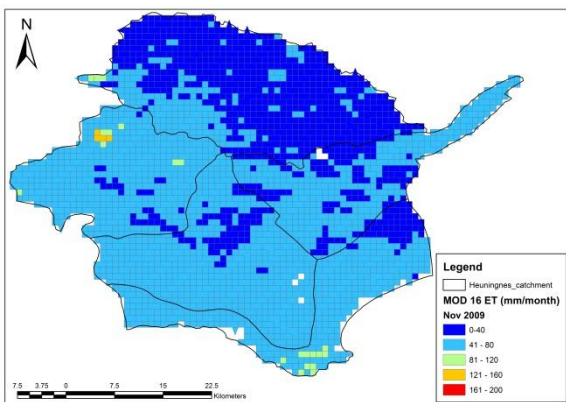
September 2009



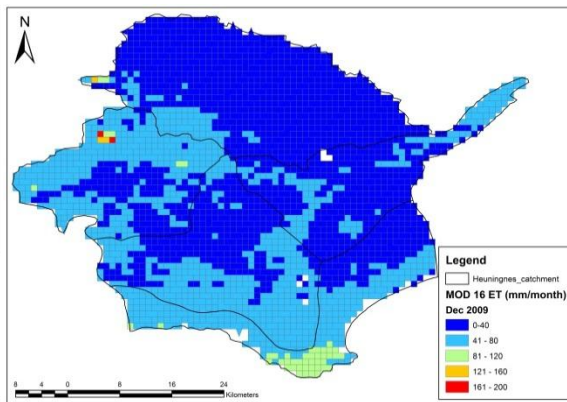
October 2009



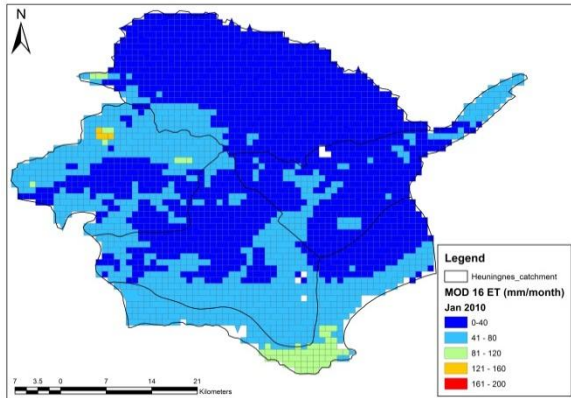
November 2009



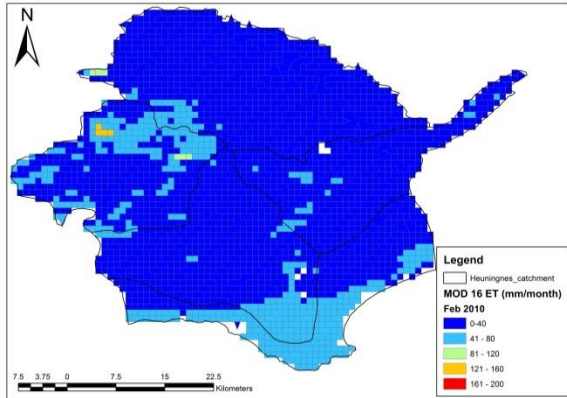
December 2009



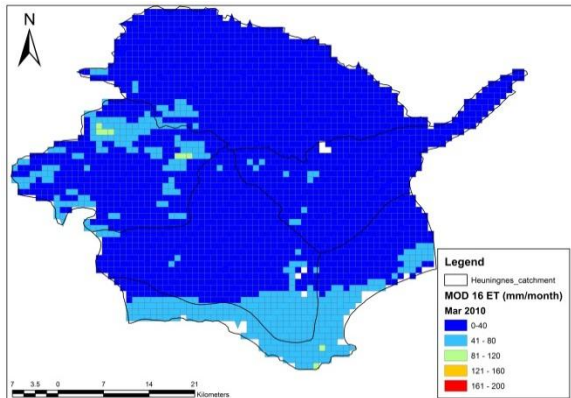
January 2010



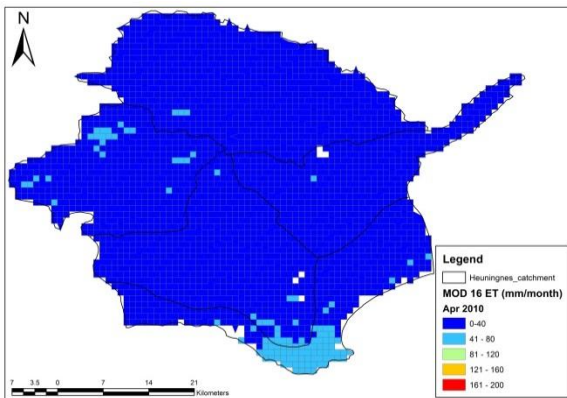
February 2010



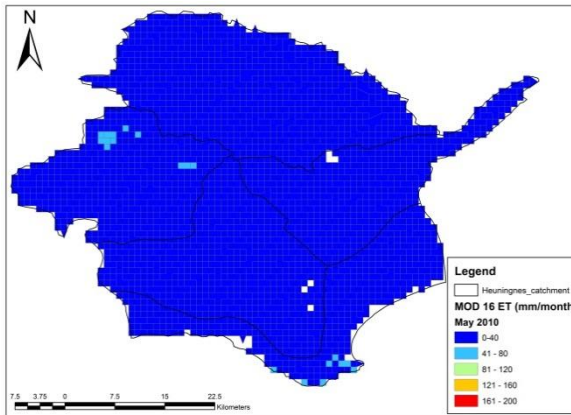
March 2010



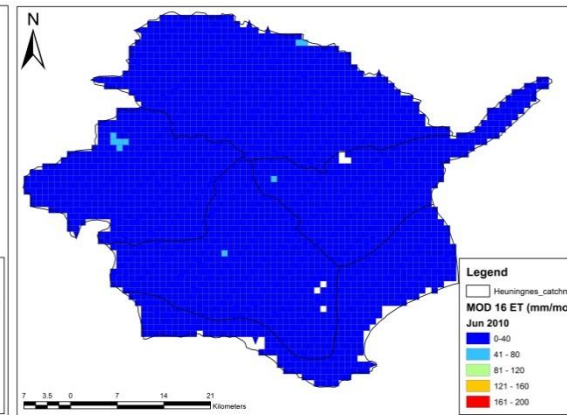
April 2010



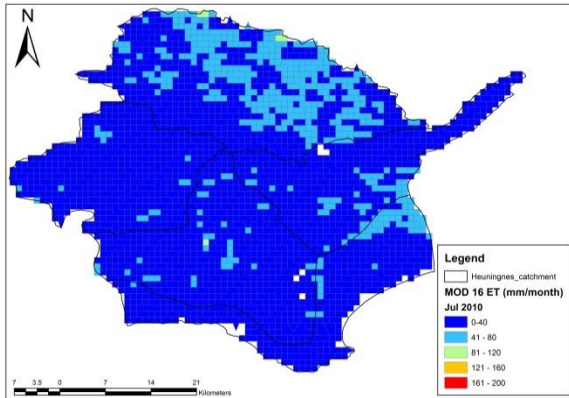
May 2010



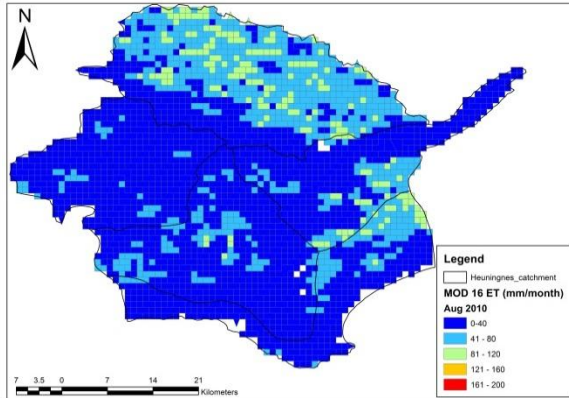
June 2010



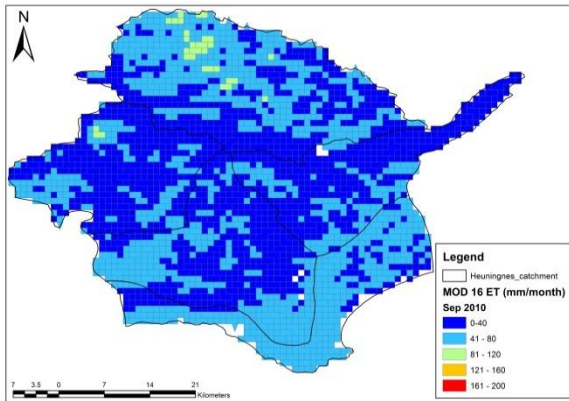
July 2010



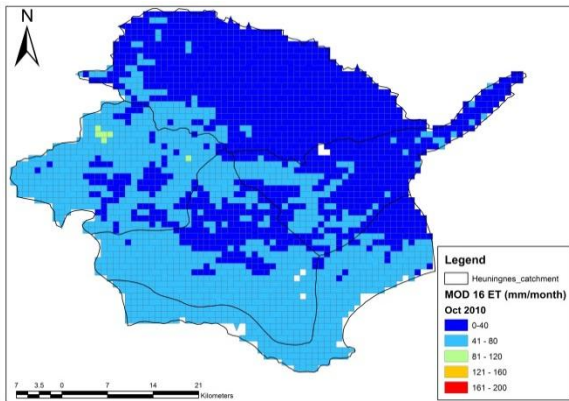
August 2010



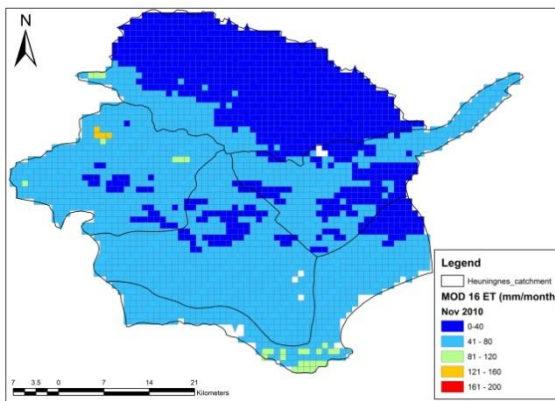
September 2010



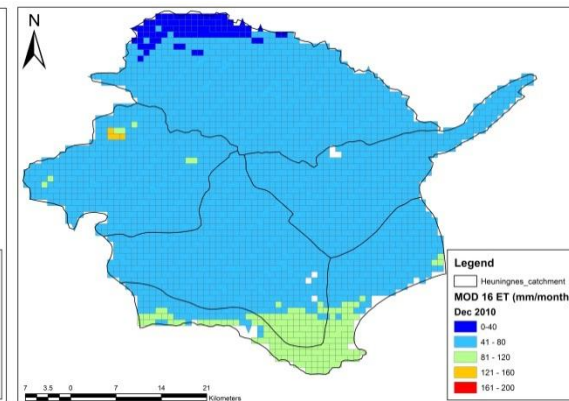
October 2010



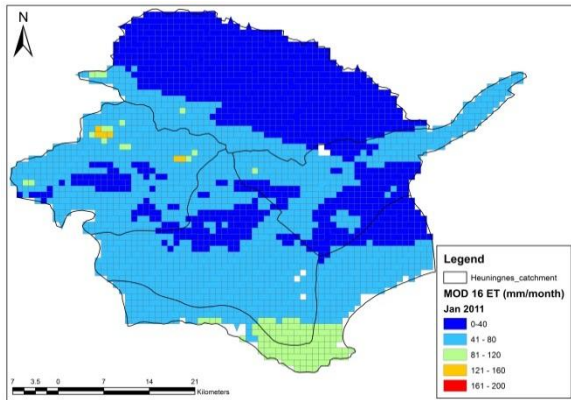
November 2010



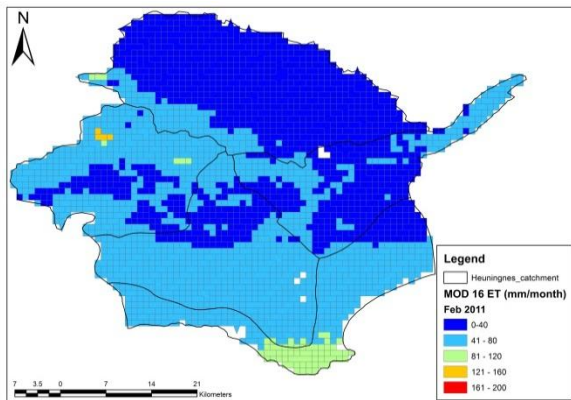
December 2010



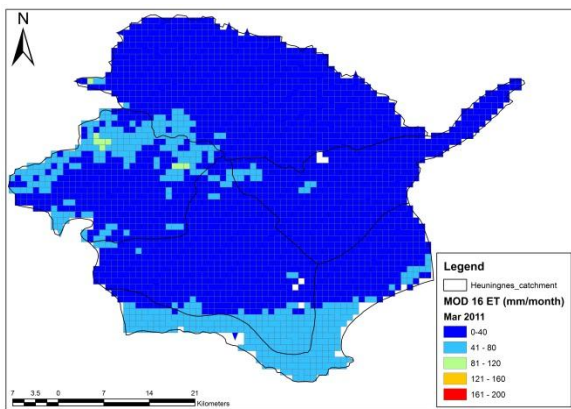
January 2011



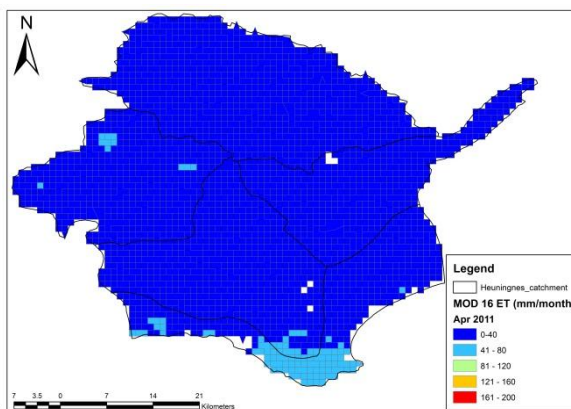
February 2011



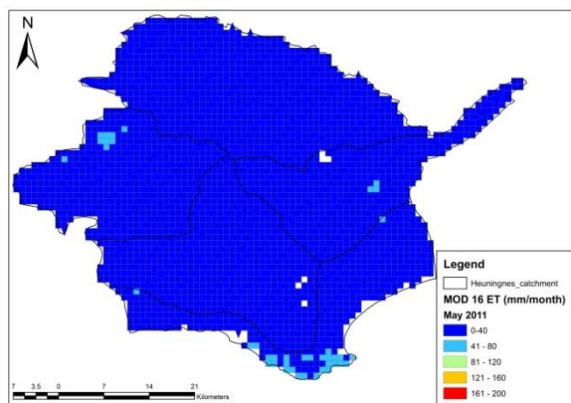
March 2011



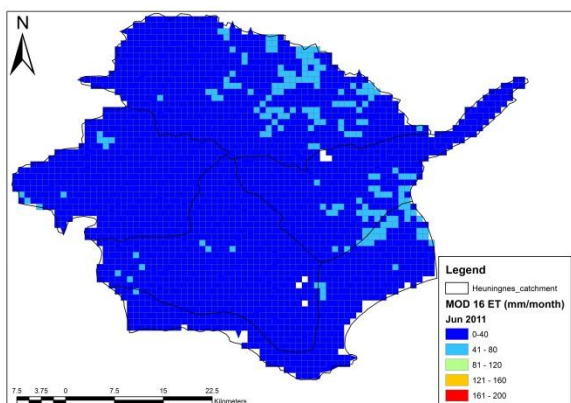
April 2011



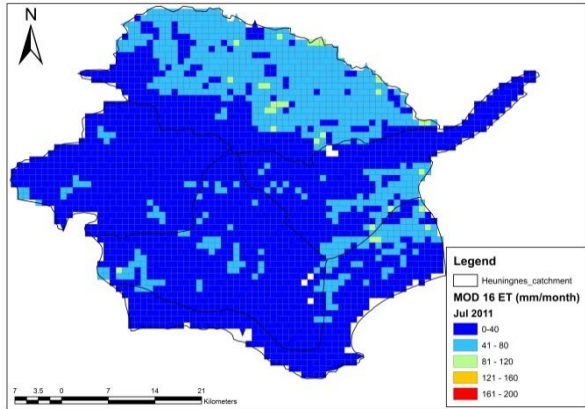
May 2011



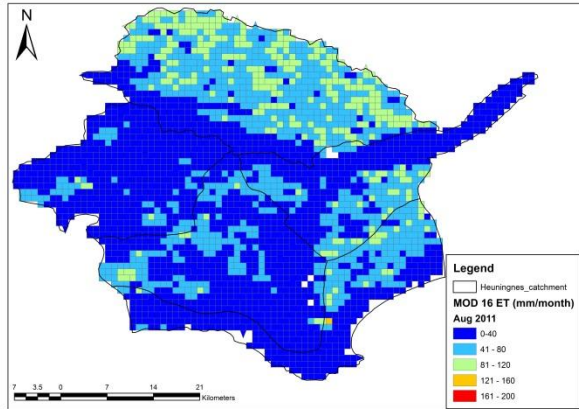
June 2011



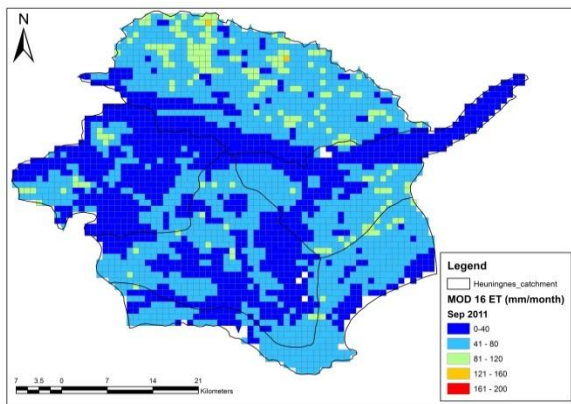
July 2011



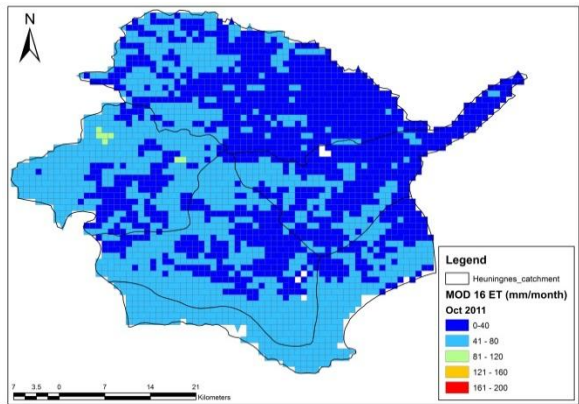
August 2011



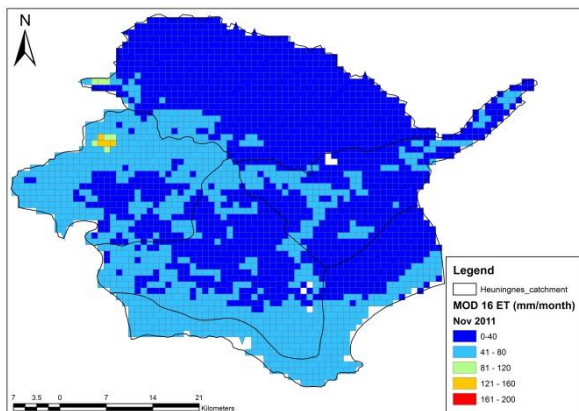
September 2011



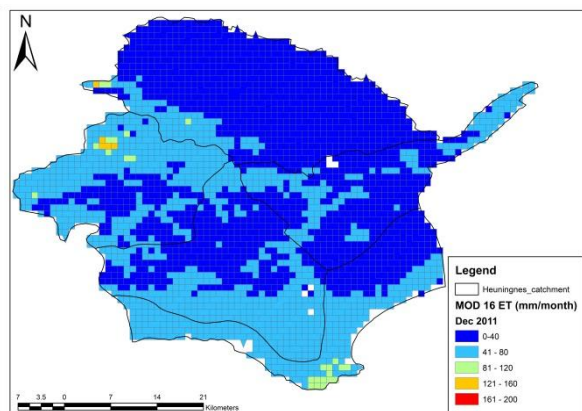
October 2011



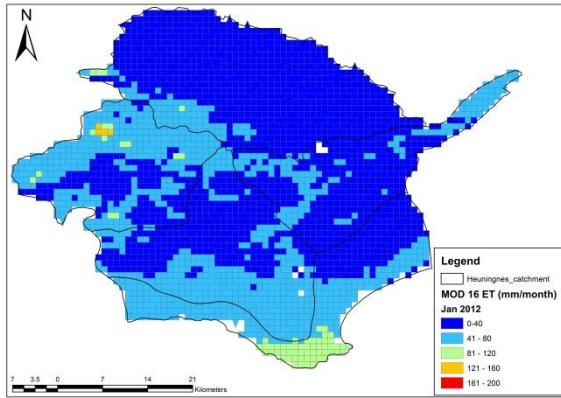
November 2011



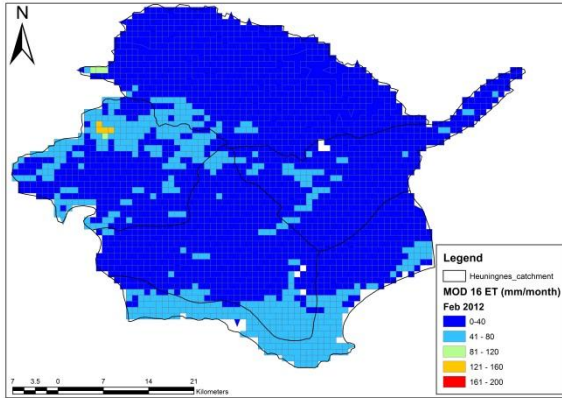
December 2011



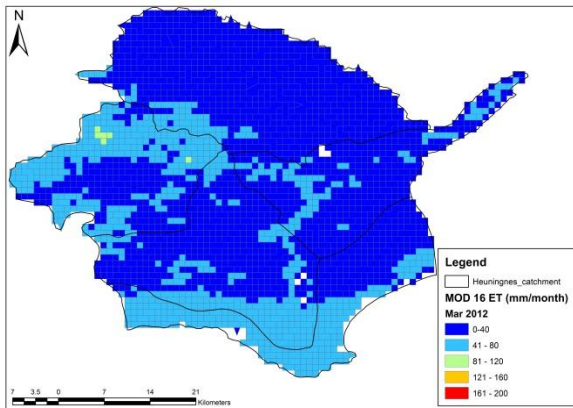
January 2012



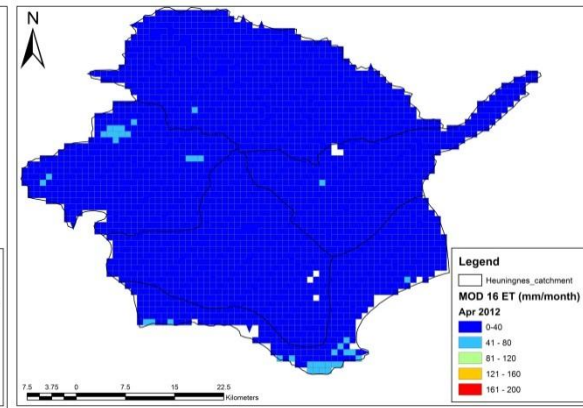
February 2012



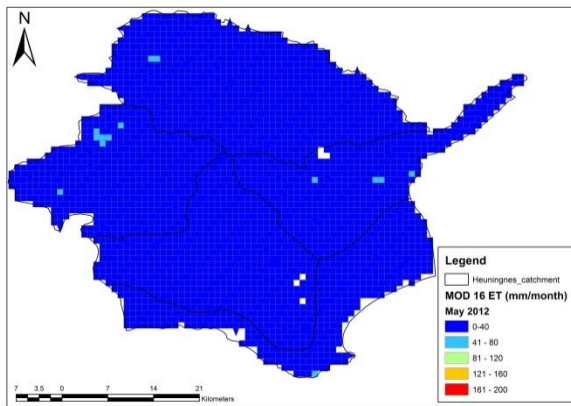
March 2012



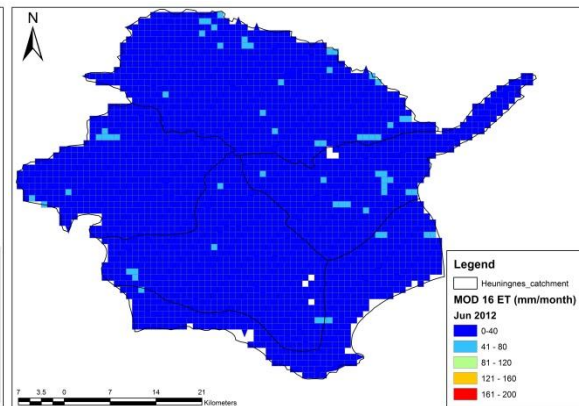
April 2012



May 2012

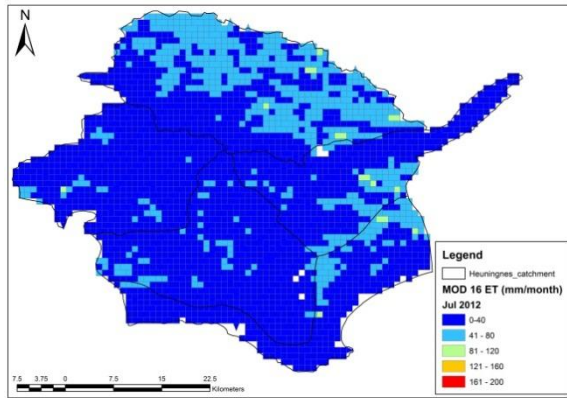


June 2012

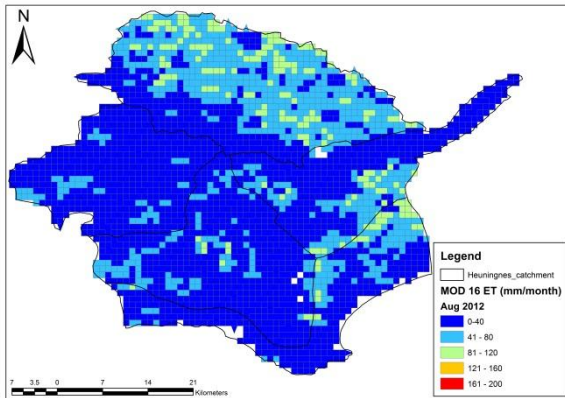




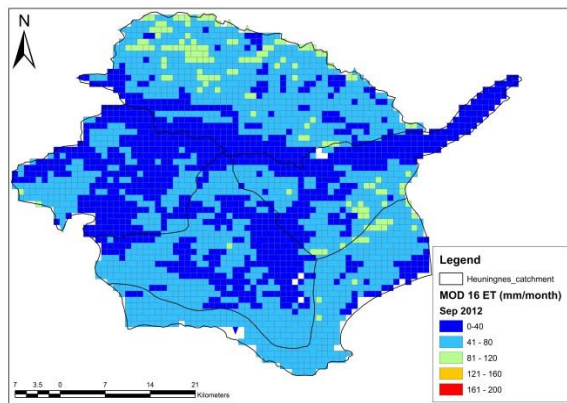
July 2012



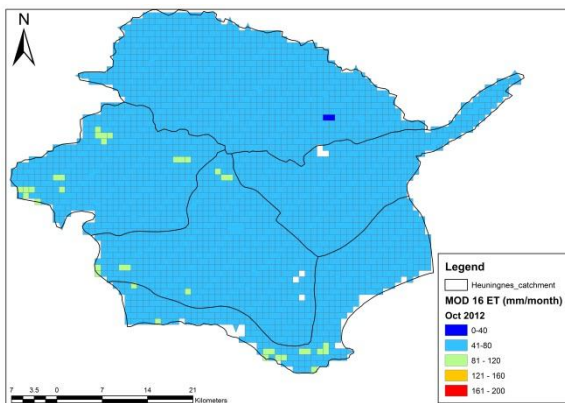
August 2012



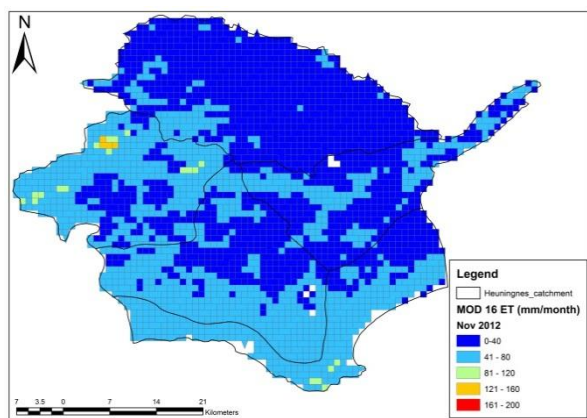
September 2012



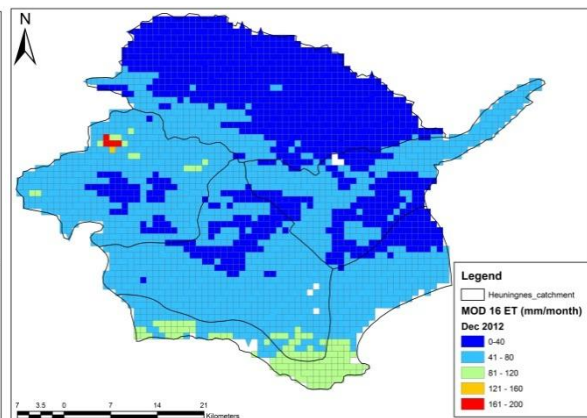
October 2012



November 2012



December 2012



Appendix C: The sites visited during the recognisance trip in October 2015 in the Molototsi catchment

Site 1



Site 2



**Site 3**



**Site 4**



Site 5



Site 6



Site 7



Site 8



Site 9



Site 10



Site 11



Site 12



Site 13



Site 14



**Site 15**



**Site 16**



**Site 17**



**Site 18**





**Site 19**



**Site 20**



**Site 21**



Site 22



Site 23



lxxx

**Site 24**






**Sites 25 and 26**



Site 27



**Appendix D: The sites visited during the field trip on 26 February 2016 in the Heuningnes catchment**

<p>Site 1</p>  A photograph of a field with tall, green and brown grass. A utility pole stands in the middle ground. The background shows a line of trees under a cloudy sky.	<p>Site 2</p>  A wide-angle photograph of a flat, open field with dry, yellowish-brown grass. The horizon is low, and the sky is filled with large, grey clouds.
<p>Site 3</p>  A photograph of a green field with a utility pole in the foreground. The sky is overcast with grey clouds.	<p>Site 4</p>  A photograph of a narrow, winding water channel or stream flowing through a green field. The water is dark and reflects the sky.
<p>Site 5</p>  A photograph of a water channel with tall reeds in the foreground. The water is calm and reflects the sky.	<p>Site 6</p>  A photograph of a field with low, scrubby vegetation. The sky is overcast and grey.
<p>Site 7</p>	<p>Site 8</p>



Site 9



Site 10



Site 11



Site 12

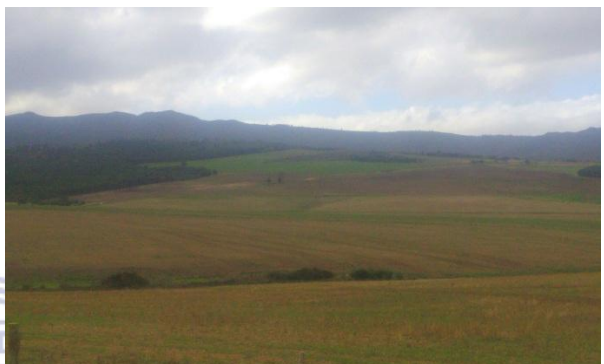


Site 13



Site 14

Site 15



Site 16

Site 17



Site 18



Site 19

Site 20

